Investigating the Wnt/β-catenin Pathway in Conventional Dendritic cells in Obesity-Induced Tissue Inflammation and Insulin Resistance

Claire Elizabeth Macdougall

Submitted in partial fulfilment of the requirements of the Degree of Doctor of Philosophy

William Harvey Research Institute,
Queen Mary University of London.

March 2019

Dedicated in memory of my grandmother Pat Macdougall,
who inspired me to never stop wondering and always ask why.

Acknowledgements

I am thankful to the many people who have supported me on my PhD journey. Firstly, I would like to express my sincere gratitude to my supervisor Dr. Paula Longhi for her continued guidance throughout the last few years. I will always appreciate the generous opportunity she gave me to complete my PhD. I thank Paula for the time, patience and motivation she gave both to me and the project, to drive the best science. Without her help and advice, I would definitely not be the scientist I am today. My gratitude also extends to my second supervisor Prof. Federica Marelli-Berg. I thank Federica for her unwavering enthusiasm and encouragement and will always be grateful for her continued support during my time in her lab.

A huge thanks to my lab colleagues past and present, for all their help both in and out of the lab. Everyone has played a part in making my PhD experience what it has been. I really appreciate their technical help and personal support, especially all the laughs and morale-boosting moments over the years. Special thanks to Liz Wood and Dr. Suchita Nadkarni for all their helpful advice and for always having a listening ear for me. I am grateful for scientific discussions and input from Dr. Marika Charalambous, Dr. Antonia Solomou and George Elia. Thanks also to my fellow PhD students Eleanor, Grace, Harriet, Anna and Eithne, I am so glad we have shared this experience (and many bottles of wine!) and will always hold fond memories of our PhD time together.

Thank you to all my friends and family who have helped me throughout my PhD years. It really has been a journey and their endless encouragement, kindness and care has, no doubt made it easier. I appreciate all the support from my sister, Kate, her advice and gifts have been a great help along the way. A final thank you to my parents, who have always told me anything is possible, I am so grateful for their constant love, guidance and belief in me.

Statement of Originality

I, Claire Elizabeth Macdougall, confirm that the research included within this thesis is my own work or that where it has been carried out in collaboration with, or supported by others, that this is duly acknowledged below and my contribution indicated. Previously published material is also acknowledged below.

I attest that I have exercised reasonable care to ensure that the work is original and does not to the best of my knowledge break any UK law, infringe any third party's copyright or other Intellectual Property Right, or contain any confidential material.

I accept that the College has the right to use plagiarism detection software to check the electronic version of the thesis.

I confirm that this thesis has not been previously submitted for the award of a degree by this or any other university.

Signature: 

Date: 07 March 2019

Details of collaborations and publications:

Immunohistochemistry staining was carried out by Histopathology core services, QMUL (Figure 3.20A&C, Figure 4.1C&D, Figure 4.2C&E and Figure 4.7D).

Micelles for targeted delivery experiments were generated by Dr. Remzi Becer, School of Engineering and Materials Science, QMUL (Figure 5.9).

Macdougall, C.E., Wood, E.G., Loschko, J., Scagliotti, V., Cassidy, F.C., Robinson, M.E., Feldhahn, N., Castellano, L., Voisin, M.B., Marelli-Berg, F., Gaston-Massuet, C., Charalambous, M., Longhi, M.P. Visceral Adipose Tissue Immune Homeostasis Is Regulated by the Crosstalk between Adipocytes and Dendritic Cell Subsets. *Cell Metabolism*. 2018;27,588-601.

Abstract

Chronic low-grade inflammation in visceral adipose tissue (VAT) is a key feature of obesity and crucial in the development of insulin resistance (IR) and type 2 diabetes mellitus (T2DM). VAT harbours resident immune cells including conventional dendritic cells (cDC), that work in cooperation to regulate metabolic homeostasis. Modulation of the immune system has the potential to ameliorate disease progression. VAT-cDCs are characterised by the activation of the Wnt/β-catenin pathway, which is known to modulate cDC function and promote T cell immune tolerance. Impaired Wnt/β-catenin pathway activity in VAT-cDCs is observed during obesity. The aim of this thesis was to investigate the effect of sustained activation of Wnt/β-catenin signalling in cDCs in obese VAT, with the hypothesis that this could revert the development of VAT inflammation and IR. The immune and metabolic phenotype was characterised in mice with constitutively active β-catenin in cDCs, referred to as gain-of-function (GOF), in a model of diet-induced VAT inflammation.

Increased tolerogenic responses of VAT-cDCs in the GOF mice was able to revert the development of VAT inflammation in part, altering T cell recruitment and inducing a more T cell immunosuppressive phenotype, but not sufficient to improve insulin sensitivity. Improvement of whole-body glucose homeostasis in the GOF mice was explained by increased insulin production from the islets. Reduced islet inflammation and expansion of islets, provided a greater insulin reserve in the GOF mice, improving β-cell insulin compensation in response to obesity-induced IR.

Enhanced levels of adiponectin and reduced secretion of CCL17 in the GOF mice, prompted the investigation of atherogenic development in *Ldlr*$^{-/-}$ GOF chimera mice. Constitutive activation of β-catenin in cDCs was not sufficient to decrease aortic lesion density.

Collectively these results indicate the significance of systemically modulating Wnt/β-catenin pathway in cDCs, with the potential to control the development of VAT inflammation and metabolic dysfunction in obesity.

Table of Contents

List of Tables

List of Figures

Abbreviations

A	APC	Antigen Presenting Cell
	AT	White Adipose Tissue
	ATM	Adipose Tissue Macrophages
B	BMDC	Bone Marrow Dendritic Cells
	BMI	Body Mass Index
	BSA	Bovine Serum Albumin
C	CCR/L	-CC- Motif Receptor / Ligand
	CD	Cluster of differentiation
	cDC	Conventional Dendritic Cell
	cDNA	Complementary Deoxyribonucleic Acid
	CFSE	Carboxyfluorescein Succinimidyl Ester
	Ctnnb	β-catenin gene
	CXCR/L	-CXC- Motif Receptor / Ligand
D	DAMP	Danger Associated Molecular Pattern
	DAPI	4',6-diamidino-2-phenylindole
	DC	Dendritic Cell
	DNA	Deoxyribonucleic Acid

	dNTP	Deoxynucleotide triphosphate
E	EDTA	Ethylenediaminetetraacetic Acid
	ELISA	Enzyme-linked Immunosorbent Assay
	ER	Endoplasmic Reticulum
F	FACS	Fluorescent Associated Cell Sorting
	FALC	Fat- Associated Lymphoid Cluster
	FBS	Foetal Bovine Serum
	FFA	Free Fatty Acid
	FITC	Fluorescein Isothiocyanate
	FLT_3L	Fms-Like Tyrosine kinase 3 Ligand
	FOXP3	Forkhead Box P3
	FZD	Frizzled receptor
G	GLA	Glucopyranosyl Lipid A
	GLP-1	Glucagon-Like Peptide
	GM-CSF	Granulocyte Macrophage-Colony Stimulating Factor
	GOF	Gain- of- Function model
	GSK3β	Glycogen synthase kinase-3β
	GTT	Glucose Tolerance Test

	GWAS	Genome-Wide Association Study
H	HDL	High-Density Lipoprotein
	HFD	High Fat Diet
	HIF1α	Hypoxia Inducible Factor-1α
I	IF	Immunofluorescence
	IFN	Interferon
	Ig	Immunoglobulin
	IHC	Immunohistochemistry
	IL	Interleukin
	IR	Insulin Resistance
	IRF	Interferon Regulatory Factor
	ITT	Insulin Tolerance Test
L	LD	Lipid Droplet
	LDL	Low-Density Lipoprotein
	Ldlr	Low-Density Lipoprotein Receptor gene
	LDL-R	Low-Density Lipoprotein Receptor
	LEF	Lymphoid Enhancing Factor
	LPS	Lipopolysaccharide

	LRP	Low-Density Lipoprotein Receptor-related Protein
	LYVE	Lymphatic Vessel Endothelial Hyaluronan Receptor
M	MFI	Mean Fluorescent Intensity
	MHC	Major Histocompatibility Complex
	MMP	Matrix Metalloproteinases
	mRNA	Messenger Ribonucleic Acid
N	ND	Normal chow Diet
	NFκB	Nuclear Factor κ B
O	OVA	Ovalbumin
P	PAMP	Pathogen Associated Molecular Pattern
	PAT	Perinodal Adipose Tissue
	PBS	Phosphate Buffered Saline
	PCR	Polymerase Chain Reaction
	pDC	Plasmacytoid Dendritic Cell
	PE	Phycoerythrin
	PECAM	Platelet Endothelial Cell Adhesion Molecule
	PMA	Phorbol 12-myristate 13-acetate
	PPAR	Peroxisome Proliferator- Activated Receptor

	PRR	Pattern Recognition Receptor
Q	qRT- PCR	Quantitative Reverse Transcription Polymerase Chain Reaction
R	RNA	Ribonucleic Acid
	ROS	Reactive Oxygen Species
	RT	Room Temperature
S	SAT	Subcutaneous Adipose Tissue
	SD	Standard Deviation
	SDS	Sodium Dodecyl Sulphate
	SDS-PAGE	Sodium Dodecyl Sulphate - Polyacrylamide Gel Electrophoresis
	SEM	Standard Error of the Mean
	SVF	Stromal Vascular Fraction
T	TCF	T Cell Factor
	TCR	T Cell Receptor
	TG	Triglycerides
	TGF-β	Transforming Growth Factor β
	Th1	T Helper 1 Cell
	Th17	T Helper 17 Cell

	Th2	T Helper 2 Cell
	TLR	Toll Like Receptor
	TMB	3,3',5,5'-Tetramethylbenzidine
	TNFα	Tumour Necrosis Factor α
	T reg	T Regulatory Cell
	T1DM	Type 1 Diabetes Mellitus
	T2DM	Type 2 Diabetes Mellitus
U	UT	Untreated
V	VAT	Visceral Adipose Tissue
	VEGF	Vascular Endothelial Growth Factor
	VLDL	Very Low-Density Lipoprotein
W	WD	Western Diet
	WT	Wild Type

Chapter 1 Introduction

1.1 Obesity

Obesity is the accumulation of excess body fat which confers negative effects on human health. It is currently a global epidemic, with the number of adults classified with a body mass index (BMI) ≥ 30 kg/m^2 increasing in prevalence every year (1). The obesity crisis is now the most serious public health problem worldwide causing a huge economic impact on healthcare providers (2). Increased BMI is associated with significantly higher risks of developing cardiovascular diseases, diabetes, cancers, osteoarthritis, depression and non-alcoholic fatty liver disease, as well as an increased mortality rate. The World Health Organisation has established obesity as the leading preventable cause of death worldwide (3).

1.1.1 Aetiology

The aetiology of obesity is multifactorial, involving complex interactions between the environment and genetics. The principle cause of excessive fat deposition is an energy imbalance which has arisen from environmental and socioeconomic changes in diet and physical activity. A sedentary lifestyle and the over-consumption of high-energy dense foods promotes a disequilibrium between energy intake and expenditure. The increased storage of excess energy predominately occurs in white adipose tissue, whereby fat mass expands over time. Specifically, the development of visceral adiposity results in obesity. In contrast to brown adipose tissue which is specialised in heat production (thermogenesis), the function of white adipose tissue is much broader and is the focus of this thesis, hence forth referred to as AT.

Although societal and behavioural changes are fundamental in the development of obesity, biological factors are also known to regulate energy balance. A genetic component has been linked to obesity, with a high rate of heritability identified (4). Rare monogenic forms of obesity have been recognised, including mutations

involved in appetite regulation such as melanocortin receptor *MC4R* and *Lep* leptin genes (5). Genomewide association studies (GWAS) have identified over 300 loci associated with common polygenic obesity. The most prominent discovery has been the cluster of variants at the *FTO* locus, which has demonstrated increased body weight with risk alleles (6). Epigenetic processes such as DNA methylation and histone modifications are emerging as risk factors for obesity (7). Interestingly, prenatal and postnatal exposures are suggested to influence metabolic health outcomes including the development of obesity. Physiological mechanisms that regulate energy balance through the brain-gut axis, cause excess fat deposition. Gastrointestinal hormones communicate with the central nervous system to control food intake and energy homeostasis. The role of microbiota has recently been implicated in the development of obesity (8). A number of acquired neuroendocrine conditions are also known to cause weight gain, including Cushing syndrome, hypothyroidism and polycystic ovary syndrome. In addition medication can have obesogenic effects, specifically psychoactive drugs which have a propensity to induce weight gain. These biological factors that contribute to the aetiology of obesity are exacerbated by environmental and behavioural influences which interplay to instigate excessive adiposity.

1.1.2 Pathophysiology

Chronic nutrition overload results in excessive adiposity and the dysregulation of lipid and glucose metabolism. The metabolic dysfunction in obesity is a central factor in metabolic syndrome and is involved in the pathophysiology of many obesity-associated diseases (9). In obesity the levels of lipids including triglycerides (TG) and cholesterol are elevated in the blood (dyslipidaemia), while free fatty acids (FFA) are released from adipocytes causing ectopic lipid deposition and lipotoxicity in other cell types. Blood glucose levels increase during obesity in the development of insulin resistance. Additionally, increased adiposity dysregulates adipokine release from AT which has significant implications in tissue dysfunction. Insulin resistance and adipocyte dysfunction are further discussed in section 1.2.2 and 1.3.3 respectively.

An important connection between obesity and chronic low-grade inflammation has been recognised over the last two decades. Inflammation develops as a

consequence of a complex network of cell and humoral responses, that defend the body from stimuli such as infection and tissue damage, in order to resolve homeostasis. Low-grade chronic inflammation in obesity exerts profound effects on whole-body lipid and glucose metabolism. A first key finding for the causal relationship was the increased expression of the pro-inflammatory cytokine tumour necrosis factor α (TNFα) in the AT of obese animals (10). Loss of TNFα improved glucose homeostasis resulting in increased insulin sensitivity, confirming the role of obesity-induced AT inflammation (11) (12). Other pro-inflammatory cytokines, chemokines and cells have since been implicated in the pathogenesis of obesity. In view of this, obese AT and in particular visceral adipose tissue (VAT), have shown to mimic an active local inflammation site with detrimental effects on AT homeostasis. This is further discussed in section 1.4.

1.1.3 Metabolic syndrome

Metabolic abnormalities caused by visceral obesity and inflammation, have direct pathological consequences. It has been observed that endothelial dysfunction, oxidative stress, elevated blood pressure and pro-thrombotic state are, in part, the consequence of altered FFA metabolism and differential release of adipokines in obesity (13). The interaction between risk factors of metabolic susceptibility such as age and stress, and underlying metabolic changes including excess adiposity, insulin resistance and dyslipidaemia, perpetuates chronic vascular inflammation and ultimately results in atherogenic processes (14) (15). Metabolic dysfunction underlies the pathology of atherosclerosis and hypertension. This cluster of interconnected metabolic features is now diagnosed as metabolic syndrome, which develops over time into a multiple risk factor syndrome conferring a two-fold increase in the risk of developing atherosclerotic cardiovascular disease (ASCVD) and a five-fold increase in the risk of developing type 2 diabetes mellitus (T2DM) (Figure 1.1) (16). The core risk factors of the metabolic syndrome are atherogenic dyslipidaemia, elevated blood pressure, elevated plasma glucose, a pro-thrombotic state and a pro-inflammatory state which are exacerbated by the development of visceral obesity.

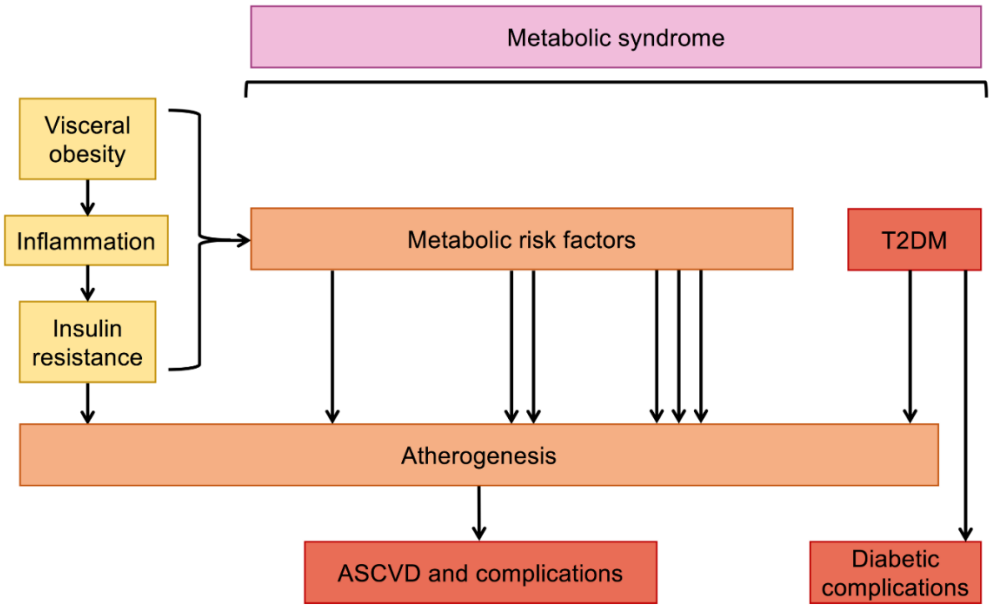

Figure 1.1 Development of Metabolic syndrome
Atherosclerotic cardiovascular disease (ASCVD) and other cardiovascular complications are the consequence of persistent atherogenesis. This is the result of metabolic risk factors which build up over time, exacerbated by visceral obesity. Metabolic syndrome results in type 2 diabetes mellitus (T2DM) and further increases the risk of ASCVD. Adapted from Grundy, 2006 (17).

1.2 Type 2 diabetes mellitus

The prevalence of type 2 diabetes mellitus (T2DM) is significantly increasing each year, becoming an expanding global health problem closely linked with the obesity epidemic (18). The diagnosis of T2DM is based on impaired glucose tolerance or elevated glycated haemoglobin A1c levels (19). As the most common form of diabetes, T2DM individuals have a high risk of developing vascular complications, such as retinopathy, nephropathy, neuropathy and cardiovascular disease. The chronic increase of blood glucose levels reduces vessel function and increases risk of cardiovascular morbidity and mortality (20) (21). As a multifactorial disorder involving the dysregulation of glucose, lipid and protein metabolism, T2DM is a complex chronic heterogeneous disease. Insulin resistance (IR) of peripheral tissues and impaired insulin secretion are critical in the development of T2DM. This pathophysiology results predominately from environmental factors such as obesity, however polygenic defects have additionally been identified by GWAS analysis in the T2DM population (22).

1.2.1 Glucose homeostasis

Glucose is critical for cellular function as it is required as fuel for glycolysis. The concentration of glucose circulating in the blood is carefully regulated in the body by negative feedback. There are many mechanisms which monitor blood glucose levels, however the response from the pancreas is the most well understood. The hormone insulin is produced from β-cells in the islets of the pancreas and released in response to high blood glucose levels (hyperglycaemia), whereas another hormone, glucagon, is secreted by α-cells in the islets of the pancreas when blood glucose levels are too low (hypoglycaemia). Insulin decreases blood glucose concentration by converting glucose into glycogen for storage (glycogenesis) (23), while glucagon exerts the opposite reaction releasing glucose from glycogen store (glycogenolysis), to increase blood glucose levels. Glycogenesis and glycogenolysis predominately occur in the muscle and liver. Another major metabolic effect of insulin is to increase the cellular glucose uptake primarily in muscle and AT, by upregulating glucose transporters (GLUT) which facilitate the diffusion of glucose into the cell. As soon as the glucose enters the cell, it is immediately phosphorylated into glucose-6-phosphate to preserve the concentration gradient, increasing glucose uptake and hence decreasing blood glucose levels. Insulin also inhibits the generation of glucose from non-carbohydrate substrates such as lactate, glycerol and glucogenic amino acids in the cell (gluconeogenesis) (23). Although insulin and glucagon have been well characterised, many other hormones have been discovered which play roles in the regulation of glucose homeostasis, including amylin, somatostatin, epinephrine and glucagon-like peptide (GLP)-1 (24). Glucose homeostasis is critical for the body's physiological function. However the metabolic control of glucose can become dysregulated. Diminished insulin production and sensitivity leads to subsequent hyperglycaemia, which have major systemic implications and promote the development of diabetes mellitus. Type 1 diabetes mellitus (T1DM) is a well characterised autoimmune disease, whereby β-cells are targeted for destruction by self-reactive immune cells, preventing the pancreas from producing insulin. T1DM is currently treated by administering exogenous insulin. While T2DM develops from IR and the insufficient production of insulin. The extent of IR and β-cell dysfunction varies amongst the T2DM population indicating a heterogeneous disorder.

1.2.2 Insulin resistance

Insulin resistance (IR) is defined as the failure of cells to respond to insulin, which therefore prevents the lowering of blood glucose levels. Hyperglycaemia can result in vessel and organ damage. The absence of insulin sensitivity can be observed in most tissues in the body, predominantly in the muscle and liver, and precedes T2DM by many years (25). IR is caused by several factors that impair insulin signalling including excess lipids and other metabolic fuels, enhanced inflammatory signalling and activation of endoplasmic reticulum (ER) stress pathways. The phosphorylation of serine residues of insulin receptor substrate (IRS) inhibits insulin signalling through the phosphatidylinositol 3-kinase (PI3K)/Akt pathway (Figure 1.2) (26). Ectopic lipid accumulation during obesity results in increased FFA which can activate serine kinases such as c-Jun N-terminal kinase (JNK) and IκB kinase (IKK) or through the generation of diacylglycerol (DAG) that activates protein kinase C (PKC) to induce serine phosphorylation of IRS (27). Obesity induces mitochondrial dysfunction increasing reactive oxygen species (ROS) and ER stress, which further activates PKC (19). Inflammation is a well established contributor to IR. The increased production of pro-inflammatory cytokines such as IL-6 and TNFα can activate JNK and IKK pathways and stimulate the production of suppressor of cytokine signalling (SOCS), which inhibits IRS action through ubiquination targeted degradation (28).

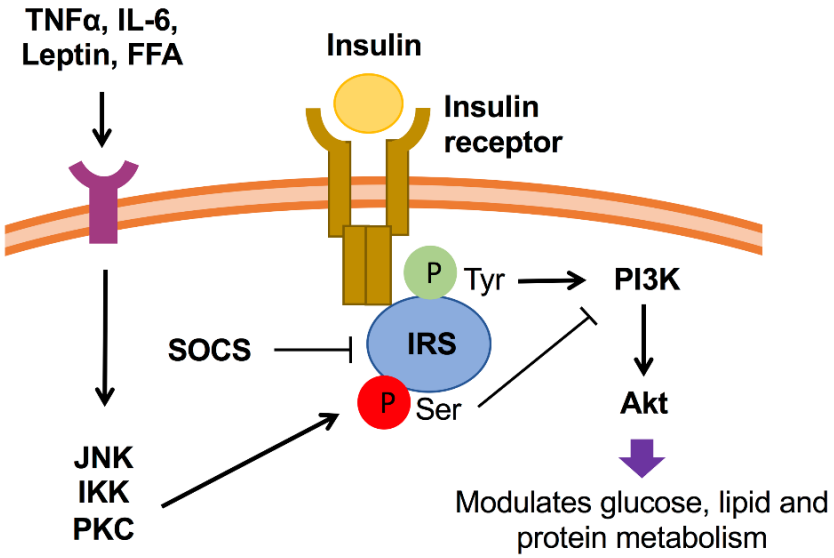

Figure 1.2 Disrupted insulin signalling causes insulin resistance
Activation of the insulin receptor leads to tyrosine phosphorylation of insulin receptor substrate (IRS), initiating signal transduction through the PI3K/Akt pathway. Akt modulates glucose uptake by upregulating glucose transporters to the cell surface, increases glycogenesis and supresses gluconeogenesis. Akt inhibits the breakdown and promotes the synthesis of lipids and proteins. IRS can be alternatively phosphorylated on serine 307 reside, which diminishes its downstream signalling ability inhibiting the PI3K/ Akt pathway. Serine kinases such as c-Jun N-terminal kinase (JNK), IκB kinase (IKK) and protein kinase C (PKC) are activated by external stimuli such as cytokines and free fatty acids (FFA), which result in the serine phosphorylation of IRS. Inflammation induced suppressor of cytokine signalling (SOCS) promotes IRS degradation.

1.2.3 β-cell dysfunction

T2DM does not develop solely through IR; impairment of insulin secretion due to β-cell dysfunction must also occur. Pancreatic islets consist of endocrine cells that secrete specific hormones to regulate glucose metabolism, including insulin-secreting β-cells (29). β-cells fill a predominant proportion of the islets and can situate in subclusters or hubs to form functional connectivity through gap junctions (30). The β-cell response to blood glucose levels by insulin synthesis and release, is critical to manage changes in nutrient load. Indeed, in obesity, there is a dramatic increase in compensatory β-cell mass. An acute expansion of β-cell mass occurs in response to the onset of diet-induced obesity to fulfil the systemic insulin requirement (31). However in T2DM, β-cells cannot secrete sufficient amounts of insulin to compensate for the increased IR of the peripheral tissues (32). This is represented by a reduction in β-cell mass and loss of β-cell function resulting in β-cell failure (Figure 1.3) (19). Although interventions have been developed to improve β-cell function, advances are being made to find

strategies to drive human β-cell proliferation and regeneration for the treatment of T2DM (33).

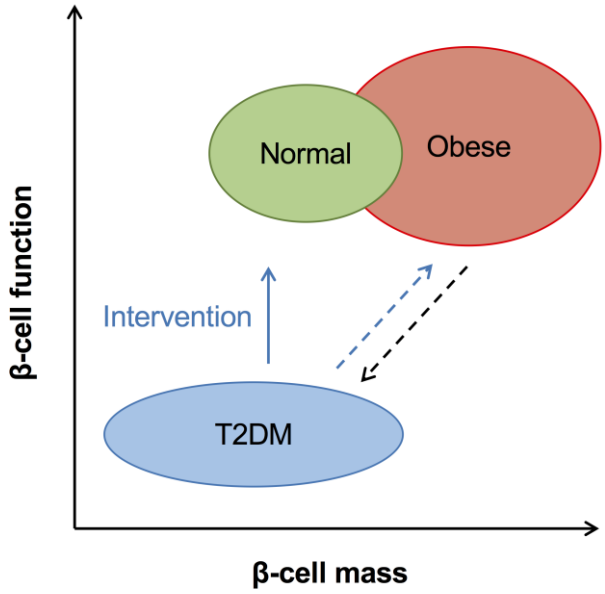

Figure 1.3 Relationship between β-cell mass and function
β-cell mass increases in obesity, while β-cell function remains unchanged. In T2DM, β-cell mass and function significantly decreases leading to β-cell failure. Interventions such as weight loss or anti-diabetic drugs aim to improve β-cell function, although it is unclear how β-cell mass changes. Restoring β-cell mass in T2DM by interventions may revert to a compensatory phenotype observed in obesity.

Multiple factors contribute to β-cell failure in T2DM, including ageing, genetic variants, resistance to GLP-1 and activation of ROS (32). Metabolic insults, such as glucotoxicity, lipotoxicity and ER stress, which are associated with the pathology of IR, are widely thought to be the main cause of damage to β-cells (34). However, it has recently emerged that activation of inflammatory pathways are also contributory factors in β-cell dysfunction (35). Characterisation of islet inflammation in T2DM has begun to reveal that immune cells affect β-cell insulin secretion. Increased numbers of leukocyte and pro-inflammatory mediators have been identified in islets of T2DM individuals (36). The roles of macrophage infiltration and interleukin (IL)-1β have been well described in promoting islet inflammation with deleterious effects on β-cell insulin secretion (37) (38). While the expression of cytokines and chemokines in transcriptomic analysis of islets has shown heterogeneity in T2DM individuals, it is widely accepted that they a play a role in exacerbating islet inflammation (39). Interestingly, β-cell hub structures which are necessary for insulin secretion, are adapted in response to inflammation and metabolic changes. Pro-inflammatory cytokines or exposure to

glucotoxicity or lipotoxicity results in β-cell dysfunction and impaired insulin production (40). Thus, it may be possible to envisage that immune cells play a role in maintaining proper connections in the islet hubs to prevent the disruption of β-cell function.

1.2.4 Other pathophysiological mechanisms

The dysfunction of glucose homeostasis in T2DM is mainly attributable to IR and impaired insulin secretion, leading to hyperglycaemia and dyslipidaemia. Other pathophysiological mechanisms in T2DM that contribute to hyperglycaemia have been identified (19). Increased glucagon levels in T2DM elevates glucose production by the liver (41). IR of adipocytes causes higher rates of the breakdown of lipids (lipolysis) and increased release of plasma FFA, which exacerbates IR (42). Additionally, increased intestinal and renal glucose absorption in T2DM promotes hyperglycaemia (43) (44). Furthermore, the dysregulation of neurotransmitters and resistance to appetite-suppressive factors such as leptin, contributes to increased nutrient overload, leading to increased IR (45) (46).

1.2.5 Treatment

Lifestyle modifications including changes to diet and physical activity can revert T2DM. Reducing excess adiposity has a significant impact on reducing IR and improving glucose tolerance (47) (48). However, interventions with pharmacological agents may be required to maintain normoglycaemia and reduce cardiovascular disease risk. Therapies summarised in Table 1.1, are often used in combination to treat multiple pathophysiological defects in T2DM. Although effective, many of these drugs have unwanted side effects and because of the heterogeneous nature of the T2DM population, can provide varying clinical response (49). Long-term normalisation of blood glucose levels in T2DM, depends on delaying or reversing β-cell failure to ensure appropriate insulin secretion (Figure 1.3).

Drug	Mechanism of action
Metformin	Supresses hepatic glucose production
Sulfonylureas	Increases insulin secretion
Meglitinides	Short-acting insulin secretagogues (aiding insulin secretion)
Thiazolidinediones	Insulin-sensitising agents, increase β-cell function
DPP4 inhibitors	Prolongs half-life of GLP-1 in plasma, increasing insulin
GLP-1 receptor agonist	Increases in plasma GLP-1 levels, increasing insulin
α-glucosidase inhibitors	Reduces intestinal glucose absorption, increases GLP-1
Sodium/ glucose co-transporter 2 inhibitors	Blocks renal glucose absorption

Table 1.1 Therapeutics to treat T2DM
Summary of anti-diabetic drugs and their mechanism of action. DPP4; Dipeptidyl peptidase-4, GLP-1; glucagon-like peptide 1.

The deleterious effect of inflammation on β-cell function highlights the potential of immune modulation in the treatment of T2DM. Clinical studies have shown that modulation of the immune system, for example by IL-1 antagonism, can have beneficial effects on blood glucose levels, β-cell secretory function and insulin sensitivity (50) (51). In addition, supressing the pro-inflammatory transcription factor nuclear factor κB (NFκB), through administration of salicylates, improved glucose metabolism in patients with T2DM (52). A further strategy that has improved insulin secretion is the targeting of chemokines involved in macrophage infiltration, specifically CCR2 antagonism inhibiting monocyte chemoattractant protein (MCP)-1 (53). However, the possible benefits of modulating adaptive immune responses are less clear. These findings suggest that modulation of the immune system has the potential to ameliorate T2DM progression.

1.3 Adipose tissue

White adipose tissue (AT) is one of the body's connective tissues, comprised mainly of adipocytes but also contains pre-adipocytes, mesenchymal stem cells and immune cells. In contrast to brown adipose tissue, which is present at birth and decreases in ageing adult humans, AT is widely distributed over the body in specific adipose depots; subcutaneous AT (SAT) is located beneath the skin, visceral AT (VAT) surrounds the internal organs and AT is further found in the bone marrow and within muscles (54) (55). Physiologically AT acts as an insulating layer with a protective function, but most importantly, is a reserve of energy, providing metabolic support to the body. Excess energy is stored as TG in adipocytes and can be mobilised through lipolysis to be released as FFA into the circulation when required. AT is critical for maintaining lipid balance in response to changes in nutrition intake. However, despite being considered in the past as a passive inert energy store, AT has recently been recognised as a highly active metabolic and endocrine organ (56).

1.3.1 Adipokines

Mature adipocytes secrete cytokines, hormones and growth factors which are collectively known as adipokines. Adipokines act in an autocrine, paracrine, or endocrine manner to regulate food intake, AT homeostasis, immunity, vasculogenesis and energy metabolism (57). Differences in adipokine production have been reported from varying AT depots, with VAT generating a more active adipokine profile. The main adipokines secreted from VAT and their functions are outlined in Table 1.2.

Adipokine	Physiological role	Effect on metabolism and cardiovascular system	Response to obesity
Adiponectin	AMPK activator	Insulin sensitiser, anti-inflammatory, reduces gluconeogenesis and increases fatty acid oxidation in the liver	Decreases
Leptin	Satiety factor	Inhibits appetite, decreases insulin-mediated glucose uptake, pro-inflammatory and VEGF secretagogue	Increases
Resistin	Inflammatory mediator	Regulation of inflammation, decreases insulin secretion and sensitivity, induces endothelial dysfunction and pro-atherosclerotic	Increases
TNFα	Cytokine	Decreases insulin sensitivity, pro-atherosclerotic, pro-inflammatory	Increases
IL-6	Cytokine	Inhibits gene transcription of IRS, limits β-cell regeneration, pro-angiogenesis and pro-inflammatory	Increases
MCP1	Transcription factor/ chemokine	Decreased insulin transcription, increased β-cell apoptosis, pro-angiogenesis, pro-inflammatory	Increases
Visfatin	NAD biosynthesis	Insulin-mimetic effects	Increases
IL-1β	Cytokine	Decreased insulin secretion, pro-inflammatory and pro-atherosclerotic	Increases
IL-10	Cytokine	Anti-inflammatory	Decreases
VEGF	Growth factor	Pro-angiogenesis	Increases

Table 1.2 Function of key adipokines
Summary of main adipokines secreted from VAT, their effect on metabolism and cardiovascular disease and response to obesity. AMPK; 5' adenosine monophosphate-activated protein kinase, VEGF; vascular endothelial growth factor, MCP1; monocyte chemoattractant protein, NAD; nicotinamide adenine dinucleotide.

1.3.2 Adipose tissue homeostasis

During changes in nutrient intake, AT responds rapidly and dynamically through a tightly regulated process of adipocyte expansion (hypertrophy) and adipogenesis where pre-adipocytes differentiate into mature adipocytes (hyperplasia). This enables AT to increase storage requirements and conversely provide energy through lipolysis when necessary. Adipocytes uptake excess lipids, whereby esterification and synthesis of TG (lipogenesis) occurs for storage in the lipid droplet (LD). This results in AT expansion and prevents ectopic lipid deposition and lipotoxicity in other cell types. Lipid balance is central to AT response to metabolic demand, linking the cell biology of the adipocyte and AT physiology to whole-body metabolism.

A number of adipogenic factors regulate healthy AT expansion, which are critical for maintaining tissue homeostasis (Figure 1.4). The nuclear receptor peroxisome proliferator-activated receptor-γ (PPARγ) is a master transcriptional regulator of adipogenic gene program. Activation of PPARγ promotes adipocyte lipid uptake, hypertrophy of mature adipocytes and induces adipogenesis, increasing the number of insulin sensitive adipocytes (58). Interestingly, reduced adipose mass was observed in PPARγ knockout mice (59) (60). PPARγ also maintains AT homeostasis by promoting beneficial adiponectin secretion from adipocytes, antagonizing pro-inflammatory transcription factors such as NFκB to halt inflammatory responses. Furthermore, PPARγ agonists are potent insulin sensitisers, preventing the development of IR (61). Another transcription factor family CCAAT/enhancer-binding proteins (C/EBP) also play a role in inducing adipocyte differentiation, confirmed by the absence of AT in C/EBPα$^{-/-}$ mice (62). C/EBPα and PPARγ cooperate to induce adipocyte differentiation through direct activation of multiple genes of terminally differentiated adipocytes (63). Their expression is sustained by a positive feedback loop which serves to maintain the phenotype of the mature adipocyte (63). Signalling proteins have also been implicated in regulating adipogenesis by activating C/EBPα and PPARγ. Wnt proteins which activate β-catenin signalling, are known to inhibit the differentiation of pre-adipocytes, specifically Wnt10b, to limit hyperplasia (64). Activation of the β-catenin pathway in transgenic mice over-expressing Wnt10b in adipocytes, prevents high-fat-diet-induced adipose tissue accumulation (65). ER signalling is

required for healthy AT function (66), including the X-box binding protein 1 (Xbp1) pathway which promotes adipogenesis and increases insulin sensitivity (67) (68).

1.3.3 Adipose tissue dysfunction

Chronic overnutrition results in aberrant adipocyte hypertrophy and impaired adipogenesis (Figure 1.4). Excess adiposity and subsequent AT dysfunction are central in the pathophysiology of obesity. AT dysfunction is characterised by oxidative stress, increased FFA release, dysregulation of adipokine release, ER and mitochondrial stress, hypoxia, extracellular matrix remodelling and the establishment of local pro-inflammatory environment (69). The dysfunction of AT contributes to metabolic dysregulation and the development of IR in obesity (42).

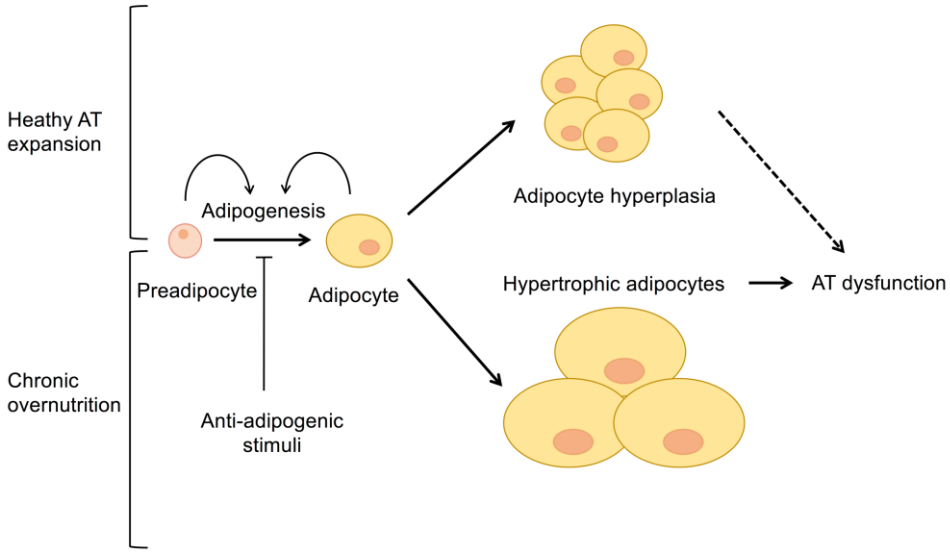

Figure 1.4 Adipose tissue expansion
Local factors regulate adipogenesis in positive energy balance, to induce adipocyte hyperplasia. Local signalling networks are impaired during chronic overnutrition which results in excessive adipocyte hyperplasia and aberrant adipocyte hypertrophy contributing to AT dysfunction.

The unhealthy AT expansion in obesity is linked to the rapid induction of dense pro-fibrotic extracellular matrix (70). Interactions of adipocytes with the fibrous matrix have been identified as potential cues for driving AT dysfunction (66). Hypoxic conditions develop during aberrant AT expansion due to a decrease in interstitial oxygen tension and an increased need for tissue vascularisation. Hypoxia stabilises the transcription factor hypoxia inducible factor (HIF)-1α. Accumulation of HIF1α is observed in hypertrophic adipocytes, inducing a change

in gene expression and a cellular metabolic switch promoting glycolysis and supressing fatty acid oxidation (71). HIF1α plays an essential role in mediating adaptive changes of cell metabolism during hypoxia to balance oxygen demand and supply. Inhibition of adipocyte specific HIF1α activation attenuates AT expansion and inhibits diet-induced tissue inflammation and the development of IR (72) (73). Furthermore, hypoxia has been suggested to drive the dysregulation of adipokines in obesity (74).

The modulation of adipokines released from adipocytes is well reported during obesity, detailed in Table 1.2. A decrease in the level of adiponectin and IL-10 secreted from healthy adipocytes, perturbs the anti-inflammatory milieu and insulin sensitive state in healthy AT (75). However the majority of adipokines increase during obesity exacerbating AT dysfunction (76). Hypertrophic adipocytes produce increased levels of pro-inflammatory cytokines including IL-6, IL-1β, TNFα and MCP1, to promote the development of AT inflammation and drive the initiation of IR. In addition, the adipocyte-derived hormones leptin and resistin become elevated in obesity (57). Leptin participates in the regulation of food intake and energy expenditure, involving pathways in the central nervous system. However during chronic overnutrition, peripheral leptin sensitivity decreases which results in the failure to control satiety. Additionally, leptin has pro-inflammatory actions, further increasing the production of IL-6 and TNFα and polarising T cell responses (77). Resistin also disrupts AT function by promoting aberrant inflammatory responses, such as increasing the expression of vascular adhesion molecule expression enhancing leukocyte entry into AT (78). The imbalance of pro- and anti-inflammatory adipokines in obesity alters tissue immune responses, promoting AT inflammation which contributes to tissue dysfunction (79).

1.4 Immune cells in adipose tissue

AT harbours a variety of immune cells in both healthy and pathological conditions, that work in cooperation with adipocytes to regulate metabolic homeostasis (80). Resident immune cells fulfil important house-keeping functions to maintain an anti-inflammatory milieu in the tissue. The tolerogenic state of lean AT provides

systemic metabolic control of glucose homeostasis and insulin sensitivity. However excess adiposity leads to substantial changes in the abundance and function of immune cells (81). The release of pro-inflammatory adipokines from hypertrophic adipocytes promotes immune cell infiltration, driving a pro-inflammatory environment in obese AT (Figure 1.5). The role of immune cells in AT has gained considerable interest as they have been identified to influence systemic inflammation and metabolic pathways (82).

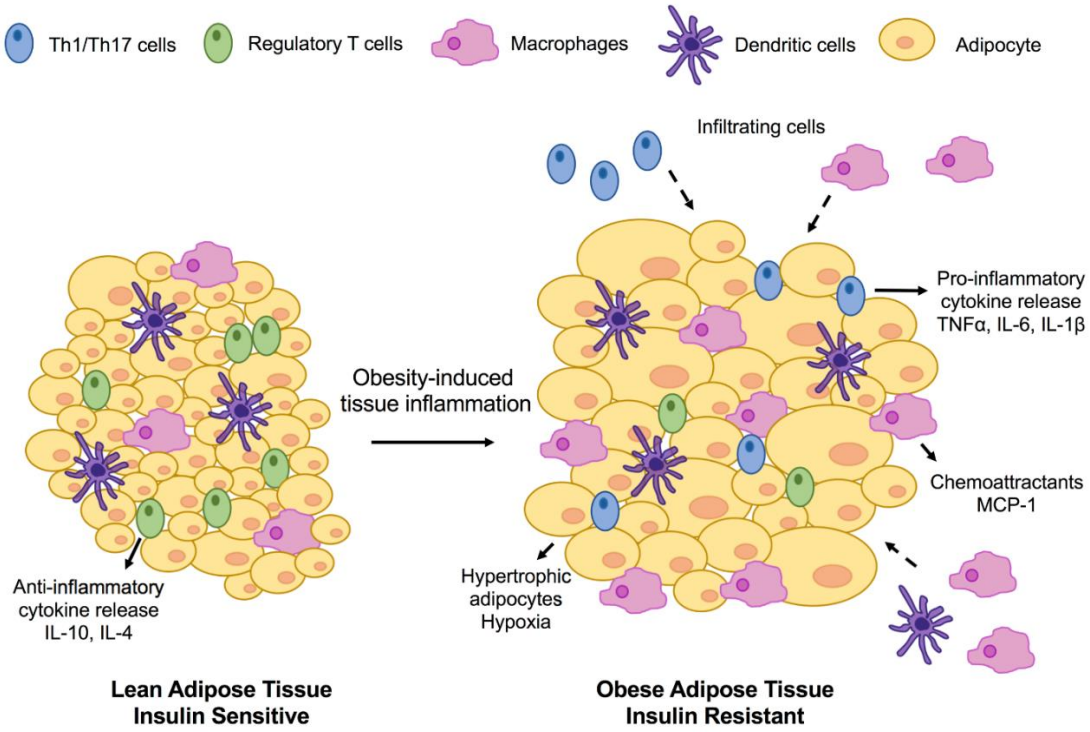

Figure 1.5 Obesity-induced inflammation in adipose tissue
Resident immune cells are critical to maintaining a healthy anti-inflammatory, insulin sensitive phenotype, generating cytokines that prevent inflammation. However, in obesity-induced inflammation, the immune cell composition is altered and reflects a pro-inflammatory state which consequently results in an insulin resistant phenotype.

1.4.1 Myeloid immune populations

Adipose tissue macrophages (ATM) are the most well characterised immune population in the tissue. Derived from circulating monocytes, macrophages are heterogeneous cells widely distributed in peripheral tissues (83). They play key roles in pathogen defence and tissue homeostasis, through their phagocytic capacity. In lean conditions, resident ATM are essential for normal AT function through the clearance of apoptotic adipocytes and cell debris, the control of lipid cytotoxicity by lipid buffering and the production of anti-inflammatory IL-10 (84).

Despite their protecting function in lean tissue, ATM are known to be central players in AT obesity-induced inflammation. A seminal report revealed that the macrophage population significantly increased in AT during obesity (85). The accumulation of ATM is driven by processes such as tissue hypoxia, fibrosis, lipid spillover, adipokine release and ER stress, all of which increases the survival and proliferation of resident ATM, inhibits their emigration from tissue and increases monocyte trafficking to AT. The proportion of ATM increases to 50% of total VAT cells in obesity, accompanied by a recruitment of $F4/80^{+}CD11c^{+}$ inflammatory macrophages (86). Disruption of this macrophage recruitment or their inflammatory activation pathways protects mice from diet-induced IR (87). In addition, obesity promotes a switch in macrophage phenotype, inducing polarisation towards a more pro-inflammatory state (88). PPARγ has demonstrated an important role in this phenotypic shift, modulating lipid accumulation which affects macrophage polarisation (89). These inflammatory ATM are considered the primary source of TNFα, exacerbating AT inflammation (90).

AT dysfunction is defined by adipocyte death from the stress of excessive AT remodelling in obesity (91). Dying adipocytes release cytosolic constituents including damage-associated molecular patterns (DAMPs) which are sensed by pattern recognition receptors (PRRs) such as toll-like receptors (TLRs) on ATM inducing the activation and production of TNFα and IL-1β, exacerbating tissue inflammatory responses (92). The morphology and location of ATM changes during the onset of obesity, often ATM aggregate into crown-like structures surrounding large lipid droplets resulting from apoptotic adipocytes (93).

Other myeloid immune cells populate AT, including neutrophils, mast cells and eosinophils. Neutrophils are short-lived, highly mobile immune cells which comprise of a large number of granules containing diverse, biologically active substances. They are considered the primary effectors of acute inflammatory response and secrete high levels of cytokines and chemokines, recruiting other immune cells. Neutrophils have been observed in lean AT of mice, although in low abundance contributing less than 1 percent of total AT immune cells. They were the first immune population to be recruited after the induction of high fat diet

(HFD) tissue inflammation, suggesting a role during the initial stages (94). Another granulocyte population is the eosinophil, which participates in anti-inflammatory immune responses. Resident eosinophils have been identified in AT and are potent IL-4 producers, however their numbers decrease in obesity (95). IL-4 is known to have insulin-sensitising effects and modulate macrophage polarisation towards anti-inflammatory phenotype. The third granulocyte identified in AT are mast cells, which rapidly degranulate in response to pathogens. Activated mast cells release inflammatory mediators, including prostaglandin PGE2, leukotriene LTB4 and several cytokines. Mast cells are elevated in obese AT of mice and humans, with important roles in ATM infiltration and development of IR (96). Although myeloid populations are fundamental in innate immune responses, they also play roles in the development of adaptive immunity effector cells and cytokine production by macrophages, mast cells and neutrophils are critical for the activation of lymphocytes.

1.4.2 Lymphoid immune populations

T cells are bone-marrow derived lymphocytes that mature in the thymus, which possess vital roles in adaptive immune responses. T cells exist in a naïve state until they encounter antigens recognised by their highly variable T cell receptor (TCR), when they become activated and primed to carry out their effector functions (Figure 1.6). A diverse repertoire of TCR is determined by VDJ gene recombination in the complementary determining region of the antigen recognition site. The T cell population is divided into subtypes by their cell surface markers and roles in immunity. $CD8^+$ cytotoxic T cells produce cytokines and cytotoxic granules and activate caspase cascades through Fas/FasL interactions, to kill tumour cells and cells infected by intracellular pathogens such as viruses. $CD4^+$ T helper (Th) cells are essential for shaping the immune response. They participate in a broad range of functions including assisting B lymphocytes in antibody generation, the activation of innate immune functions and the recruitment of other immune cells. These roles are orchestrated through the production of various cytokines and chemokines from Th cells, which are further categorised by their signature cytokine release; Th1 cells produce IFNγ, IL-2 while Th2 cells release IL-4, IL-5, IL-10, IL-13, IL-25, and the most recently identified Th17 cells produce IL-17A, IL-21, IL-22 (97). These subsets have distinct functions and are involved in specific responses to pathogens. Aberrant

Th cell responses are associated with inflammatory, autoimmune and allergic diseases. Differentiation of Th subsets is dependent on the environment of T cell priming, by the upregulation of specific transcription factors. Another $CD4^+$ T cell subset is regulatory T cells (T regs), which are critical for regulating immune responses and play an important role in immune tolerance. Natural T regs emerge from the thymus, while inducible T regs arise from differentiation of naïve T cells in the periphery. T regs cells exert their suppressive functions through the production of anti-inflammatory cytokine IL-10 and transforming growth factor β (TGF-β). Interestingly, IL-10 production by all Th cells serves as a negative regulatory mechanism for limiting immune responses to prevent tissue damage. Natural killer T (NKT) cells, T follicular helper cells (Tfh) and γδ T cells are other distinct $CD4^+$ T cell populations.

T cells constitute the second largest immune cell population in AT and become increasingly abundant as obesity-induced tissue inflammation develops in mouse and man (98) (99). In lean AT, a unique resident T reg population participates in the maintenance of tissue homeostasis by suppressing immune responses and preserving insulin sensitivity (100) (101). However during AT dysfunction, the number of T regs decreases while Th1, Th17 and cytotoxic effector T cell populations increase generating pro-inflammatory signals in the AT (102) (81). AT-T cells can influence adipokine secretion from adipocytes through CD40/CD40L interactions, and the production of IFNγ drives ATM accumulation (103) (104). A unique feature of T cell populations in AT is their limited TCR repertoire, suggesting that a specific set of antigens drives T cell function during obesity (105). Interestingly, it has been identified in homeostatic conditions that VAT harbours a large population of memory T cells (106). Upon infection these VAT resident memory T cells are sufficient to protect naïve mice from intestinal pathogen re-challenge, indicating VAT as an important site for memory responses with long-term protective functions.

B cells participate in humoral adaptive immunity, producing antigen-specific antibodies. The number of B cells increases in obese AT and B cells are known to mediate tissue inflammation (107) (108). TLRs expressed on AT-resident B cells recognise DAMPs released from dying adipocytes and trigger antibody release during AT dysfunction. Immunoglobulin (Ig)G antibodies induce IR during

diet-induced obesity, with suggested roles in the clearance of apoptotic adipocytes and ATM polarisation (107) (109).

1.4.3 Fat-associated lymphoid clusters

AT contains organised structures referred to as fat-associated lymphoid clusters (FALCs) which expand during inflammation (110). FALCs are considered inducible non-classical lymphoid tissues in direct contact to surrounding adipocytes. The highly vascularised structures are comprised mainly of B cells, with $CD4^+$ T cell and $CD11b^+$ myeloid cell populations also identified (111). It is proposed that FALCs collect peritoneal antigens from AT, contributing to the immune surveillance of the tissue. They are present in heterogeneous size and number within different AT depots (112). Although there is limited understanding of FALCs, it has been suggested that the structures provide immunological niches facilitating adaptive B and T cell immune responses in AT (113). FALCs have also been shown to mediate the recruitment of myeloid cells and express increased levels of Th2 cytokines (110) (111). However much of this work has focused on $CD11c^+$ $F4/80^+$ cells in the FALCs, which is likely to be a mixed population of myeloid cells with varied antigen processing and presenting capacities (114).

1.5 Dendritic cells

Dendritic cells (DCs) are often referred to as ‘sentinels’ for the body, as they sense and respond to their environment and are considered a central component of the immune system. DCs were initially characterised as key antigen presenting cells by Steinman and Cohn in 1973 and have since revealed important functions in innate and adaptive immunity (115). DCs are critical for initiating and modulating immune responses but also for inducing immune tolerance, in order to orchestrate the immune system.

1.5.1 Function of dendritic cells

Migrating from the bone marrow, DC precursors are found in peripheral blood and enter every non-lymphoid tissue where they reside in an immature state.

They are especially abundant in tissues that are exposed to the external stimuli, for example in the skin and gut. These cells are specialised to sample the extracellular milieu for surveillance. They express a repertoire of PRRs, including TLRs on their cell surface to detect and capture antigens including pathogen-associated molecular patterns (PAMPs). Upon PAMP engagement, PRRs trigger signalling cascades in the immature DC that leads to their maturation towards an immunogenic DC phenotype. DCs undergo a complex phenotypical and functional maturation, which involves the stabilisation of the major histocompatibility complex (MHC), the upregulation of cell surface molecules CD86, CD80, CD40 and the secretion of cytokines required for T cell activation. Simultaneously, the chemotactic receptor CCR7 is upregulated, enabling DC migration through the lymphatic system to the draining lymph node. The foreign antigen is processed and presented by the immunogenic DCs to naïve T cells in the lymph nodes through MHC molecules, which in combination with cytokine stimulation and costimulatory signals, induces effector T cell activation and proliferation (Figure 1.6). Different environmental signals to which DCs are exposed to, influence the type of the immune responses initiated, including Th cell polarisation and tolerance induction.

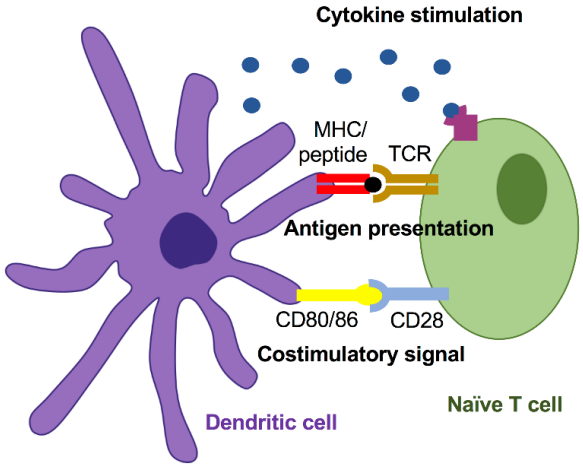

Figure 1.6 Dendritic cell activation of T cell response
Initiation of effector T cell requires three signals from DC. Firstly the stimulation of T cell receptor (TCR) by the major histocompatibility complex (MHC)/peptide complex presented by DC, secondly interactions between costimulatory ligands such as CD80/86 and CD28 and thirdly the secretion of cytokines from DC polarises the T cell response.

Immune tolerance is fundamental for regulating immune homeostasis and depends on two distinct processes; central tolerance occurs in the thymus to

eliminate T cells that detect self-antigens, while peripheral tolerance avoids over-reactivity of the immune system, preventing responses to non-pathogenic organisms or environmental antigens in the tissue and lymph nodes. Tolerogenic DCs are central players in establishing immune tolerance, contributing to both central and peripheral tolerance (116). The tolerogenic DC population is formed of naturally occurring and induced cells, which are viewed together as a subtype of immature-polarised DCs. They are maintained in a tolerogenic state by anti-inflammatory cytokines present in the environment, and only weakly express costimulatory molecules. However, this anti-inflammatory phenotype can be reverted in the presence of pro-inflammatory stimuli. In peripheral and lymphoid tissues, tolerogenic DCs establish T cell tolerance by the induction of anergy, deletion of antigen-specific T cells and stimulation of T reg differentiation and expansion, which collectively suppresses immune responses and is fundamental to the maintenance of tissue immune homeostasis (117). Subsequently, immunogenic and tolerogenic DCs have contrasting effects on T cell responses (Figure 1.7).

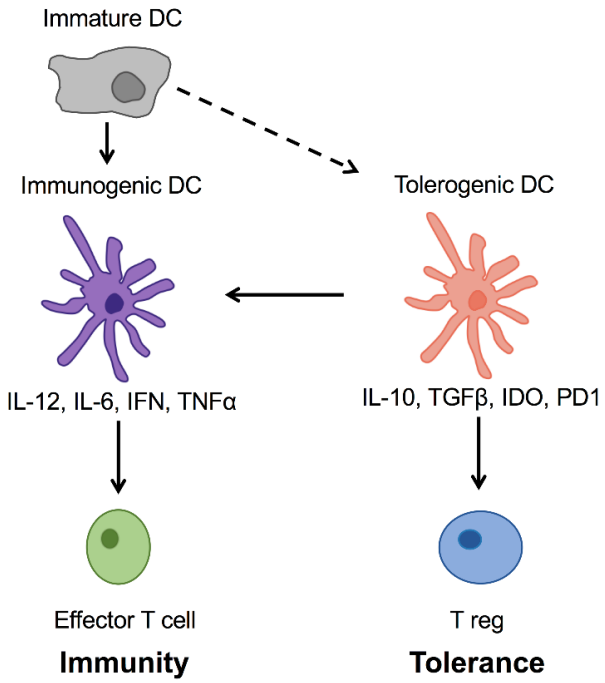

Figure 1.7 Type of dendritic cell affects T cell response
DC sense and respond to their environment. Pro-inflammatory stimuli e.g. PAMPs and DAMPs are recognised by pattern recognition receptors e.g. TLRs on DC cell surface, which leads to the maturation of immunogenic DCs. In the lymph nodes, immunogenic DCs present antigens to naïve T cells and secrete high levels of inflammatory cytokines such as IL-12 and IL-6 which induces effector T cell differentiation and proliferation to shape the adaptive immune response. Under a tolerogenic environment DCs acquire regulatory functions providing signals that enable T reg differentiation and expansion. Tolerogenic DCs are viewed as a subtype of immature-polarised DCs.

1.5.2 Dendritic cell ontogeny and subsets

DCs are a diverse heterogeneous population, characterised by cell surface markers and localisation. DC subsets follow different migratory pathways and provide varied immunological functions (118). Classically DCs are subdivided into two main lineages; myeloid/conventional DCs (cDCs) and plasmacytoid DCs (pDCs). Much research has determined that these cells originate from precursor DC (pre-DCs) progenitors in the bone marrow, in the presence of tyrosine kinase receptor fms-like tyrosine kinase 3 ligand (Flt3L). Tracing back to common myeloid progenitors in the bone marrow, a committed DC progenitor has been identified which gives rise to pre-DC population (119). Before leaving the bone marrow and entering the peripheral blood and lymphoid organs, the development of pDC lineage is committed by the upregulation of transcription factor E2-2 although the mechanism has yet to be fully understood (120) (121). While cDCs differentiate in the periphery from pre-DCs that have migrated from bone marrow into lymphoid and non-lymphoid tissue. cDCs differentiate into two main subsets, cDC1 and cDC2, categorised by their cell surface molecule expression. This differentiation process is controlled by expression of transcription factors including interferon regulatory factor (IRF)-8 and IRF4, which distinguish between cDC1 and cDC2 respectively (118). A recent study has newly identified several other distinct DC subsets using single-cell transcriptome profiling, highlighting DC heterogeneity (122).

DCs have distinct functions that differentially regulate adaptive and innate immune responses. pDCs have decreased antigen presenting capacity due to their lower expression levels of MHCII and CD11c and limited expression of PRRs in steady-state. Yet pDCs play a major role in anti-viral immune responses characterised by the rapid production of type 1 IFN production (123). cDCs populate most lymphoid and non-lymphoid tissues and are identified by high expression levels of MHCII and CD11c (124), hence they have enhanced capability to sense tissue damage, capture and present antigens or to enforce tolerance. The cDC subsets have different transcriptome profiles and lineage markers, with IRF8 and IRF4 required for their development and function (118). $IRF8^+$ cDC1 in lymphoid tissues express CD8 and in non-lymphoid tissue they are characterised by the expression of CD103, while $IRF4^+$ cDC2 express CD11b regardless of tissue (125). In addition to serving as potent antigen presenting

cells, cDC subsets possess distinct roles in innate immune responses against specific type of pathogens (126). cDC1 can efficiently recognise viral and intracellular antigens and have an intrinsic capacity to crosspresent antigens to $CD8^+$ T cells (127). Their non-redundant production of IL-12 is critical to inducing type 1 immune cell responses, including NK cell activation for IFNγ production (128) (129). cDC2 preferentially promote $CD4^+$ T cell responses, such as Th17 cell responses against extracellular bacteria and fungi, through the production of IL-23, IL-6 and TGFβ (130) (131). cDCs are involved in type 2 immune cell responses against parasites, but the exact mechanism by which they regulate Th2 immunity is unclear (126). During inflammation, a distinct population of monocyte derived DCs (moDC) have also been identified in tissues which originate from infiltrating monocytes. These cells can also be differentiated from monocytes *in vitro* using granulocyte-macrophage colony-stimulating factor (GM-CSF) and IL-4.

1.5.3 Dendritic cells in adipose tissue

The distinct contribution of VAT-cDCs in tissue inflammation and tissue immune homeostasis has to date, been poorly understood. Studies have investigated DC populations in VAT, as outlined in Table 1.3. However the phenotypic overlap with other myeloid cells has hampered accurate studies of VAT-cDCs. Although high expression of MHCII and CD11c defines the cDC population, CD11c has also been used to identify inflammatory ATMs (132), thus this promiscuous expression in myeloid cells has rendered the role of VAT-cDCs elusive. For clarity, in studies where the distinction between moDC and cDCs is unclear or contamination with monocytes or macrophages is likely, cells will be referred to as DCs.

1.5.3.1 Adipose tissue dendritic cells in tissue inflammation

A number of studies have demonstrated that the $MHCII^+$ $CD11c^+$ population accumulates in VAT of mouse and man during obesity, although it is unclear if these cells were activated macrophages, moDCs or cDCs (133) (134). The presence of $MHCII^+$ $CD11c^+$ cells has shown to be critical for the recruitment of macrophages into the tissue during diet-induced tissue inflammation. The injection of moDC derived from bone marrow, into mice, boosted immune cell recruitment into VAT, indicating that DCs play a part in regulating immune cell

tissue infiltration (133). A subset of DCs termed 'inflammatory DC' with low expression of F4/80 have been observed in VAT and display enhanced antigen presenting capacity *in vitro*, inducing T cell activation specifically Th17 responses (134). These observations were confirmed by an independent study, which further demonstrated DCs infiltrating VAT secreted higher levels of IL-6 and IL-23 to promote Th17 differentiation (135). Ablating $CD11c^+$ cells, including macrophages, monocytes and DCs, attenuates VAT inflammation in obese mice (132). Although inconclusive, these findings collectively suggest that DCs adopt an activated pro-inflammatory state in obesity and play an important role in the initiation of tissue inflammation. However due to the phenotypic overlap in these studies, the specific role of cDCs in VAT is yet to be revealed.

Key findings	**DC population investigated**	**Model**	**Reference**
• $CD11c^+$ depletion attenuated AT inflammation and restored glucose homeostasis	$CD11c^+$ cells	Mouse	(132)
• Increased numbers of AT-cDCs in HFD, critical for macrophage recruitment • Depletion of cDCs in AT protects from tissue inflammation	$MHCII^{high}$ $CD11c^{high}$ cells	Mouse	(133)
• Inflammatory DC identified in obese AT of mouse and human • DC induced Th17 responses *in vitro*	Inflammatory DC $CD11c^{high}$ $F4/80^{low}$	Mouse and human	(134)
• HFD increases AT-DC recruitment • AT-DCs secreted higher levels of IL-6 and IL-23 to promote Th17 differentiation	$MHCII^{high}$ $CD11c^{high}$ cells	Mouse	(135)
• DC can regulate differentiation of adipocytes via GM-CSF signalling	$F4/80^+$ $CD11b^+$ $CD11c^+$ cells	Mouse	(136)
• DC identified in obese mouse and human AT • CCR7 necessary for AT-DC recruitment	$CD11c^+$ $CD64^-$ cells	Mouse and human	(137)
• DCs take up soluble antigens from lymph nodes, initiating AT inflammation	$CD64^-$ $MertK^-$ $MHCII^{high}$ $CD11c^{high}$ cells	Mouse	(138)

Table 1.3 Key findings on adipose tissue dendritic cells

1.5.3.2 Antigen sampling

In physiological conditions, VAT-cDCs are proposed to participate in antigen sampling, to modulate immune responses. cDCs in VAT surrounding lymph nodes, known as perinodal AT (PAT), are found close to collecting lymphatic vessels (CLVs). This strategic location is suggested in order to 'sense' the tissue environment and contribute to the immune surveillance of neighbouring tissue (138). CLVs have an inherent permeability where the lymph components are released and distributed within the surrounding PAT areas. cDCs closely associate with CLVs to uptake soluble antigens released from leaky CLVs and migrate to the lymph node for antigen presentation to T cells. Vessel permeability can be compromised in obesity, diabetes and infections, facilitating antigen leakage into tissue and VAT-cDC uptake. In addition it has been suggested that the interaction between cDCs and CLVs, a process that is controlled by the chemokine receptor CCR7, contributes to the maintenance of vessel integrity (139).

1.5.3.3 Crosstalk with adipocytes

Pre-adipocytes are predominately adjacent to adipose vasculature where they differentiate to mature adipocytes (140) (141). Interestingly, cDCs are also found in close proximity to AT vessels suggesting a possible interaction with pre-adipocytes. It has been proposed that this crosstalk may be important for tissue homeostasis. A recent study suggested moDCs may play a role in regulating adipocyte expansion and differentiation (136). Interestingly, GM-CSF knockout mice (*Csf2*$^{-/-}$) exhibited greater adipocyte volume and differentiation under physiological conditions compared to control mice, which was accompanied by reduced F4/80^{+} CD11b^{+} CD11c^{+} AT-DCs. However GM-CSF is a growth factor for many myeloid cells including neutrophils, macrophages and moDCs (142). In addition, pre-adipocyte differentiation was inhibited upon incubation with moDC conditioned medium, but not bone marrow-derived macrophage supernatant, through a mechanism mediated by matrix metalloproteinase (MMP)-12 and fibronectin-1 secretion (136).

The interaction between AT-cDCs and adipocytes has the potential to modulate both cell functions. For instance, pathways activated in the adipocyte have been linked with the regulation of cDC function. Such pathways include Xbp1 pathway,

which is upregulated in response to endoplasmic reticulum (ER) stress. It has been suggested that during differentiation, adipocytes upregulate the Xbp1 pathway to counteract the stress associated with protein and lipid biosynthesis. During obesity, increased ER stress leads to pathway upregulation (67). Overexpression of Xbp1 in adipocytes promotes adiponectin multimerisation improving systemic glucose homeostasis *in vivo* (143). Additionally, Xbp1 pathway has been found to be upregulated in tumour-infiltrated DCs resulting in the loss of immunostimulatory activity and inhibition of anti-tumour T cell responses (144). Hypoxia is another pathway associated with adipocyte and cDC dysfunction. Hypoxia is observed in hypertrophic adipocytes, with an accumulation of adipocyte HIF1α detected during chronic over-nutrition. In DCs, HIF1α has been reported to play a crucial role in the activation of inflammation (145) (146). Hypoxic conditions in combination with lipopolysaccharide (LPS) stimulus, modulate the maturation, activation and antigen-presenting capacity of moDCs. Furthermore, CCR7 expression is upregulated on DCs in response to HIF1α, facilitating migration to lymph nodes (147). These results indicate that simultaneous activation of the HIF1α pathway in adipocytes and AT-cDCs during obesity, may exacerbate tissue expansion and inflammation. Collectively these findings open up the possibility that AT immune homeostasis could be modulated by the upregulation of adipocyte-related pathways in cDCs.

1.5.3.4 Lipolysis of adipocytes

Triglycerides (TG) in AT are the major energy reserve in the body. During energy deprivation, adipocytes undergo a switch towards lipolysis resulting in the breakdown of TG into FFA and glycerol. Lipolysis can be initiated not only during starvation but also as a result of infections. This is particularly true for PAT. Adipocytes in PAT exhibit distinct site-specific properties that enable local interactions with the lymph node (148). These local interactions modulate the lipolysis of adipocytes, which is exacerbated by immune stimuli such as TNFα, IL-4 and IL-6 resulting in higher levels of lipolysis in PAT (149). These findings suggest that PAT adipocytes interact directly with lymph nodes, responding to and supporting immunological processes (150). Interestingly, DCs were located preferentially in PAT compared to other AT depots (151). It has been proposed that AT-DCs directly stimulate perinodal adipocyte lipolysis *in vitro* (152). Furthermore, Sadler *et al.* observed that PAT adipocytes elicit higher rates of

lipolysis during low-grade inflammation (152). Therefore, local interactions between VAT-cDCs and PAT may play an important role in maintaining lipid balance and immune responses in AT.

DCs can uptake the fatty acids released from adipocytes, either for use as fuel or to be incorporated into the cell membranes. Alternatively, fatty acids are stored as TGs in lipid droplets (LDs) within the cell, which are increasingly recognised to play important roles in immune regulation. LDs have been shown to facilitate metabolic processes and support immune responses, including antigen crosspresentation, activation of IFN and pathogen clearance (153). LDs are associated with increased DC immunogenicity, in which high levels of LD promote DC activation and enhanced effector T cell stimulation (154). However, the effect of LD accumulation in cDCs is determined by the environmental context. In tumours where there is an increased cellular demand for energy, the accumulation of LDs in DCs induces a dysfunctional phenotype, resulting in defective T cell stimulation and presentation of tumour-associated antigens (155). In addition, oxidised lipids generated in tumour environment were shown to directly abrogate DC crosspresentation of antigens, while in physiological conditions only low levels of oxidised lipids accumulate in DCs (156). Thus, the lipid content of LDs further determines DC function. The lipid-rich environment of AT may increase the lipid uptake of AT-cDCs with higher levels of TG stored in LDs, however the functional consequences of this remains unclear in the context of AT.

1.5.4 Dendritic cell involvement in insulin resistance

Inflammatory immune responses are well recognised to impact metabolic processes. Studies have indicated that the contribution of DCs in AT inflammation affects the development of IR. Depletion of $CD11c^+$ cells in obese mice normalises insulin sensitivity restoring glucose homeostasis (132), although these results are difficult to interpret as CD11c is also expressed on other myeloid cells. Additionally, it has been observed that $CD11c^+$ $CD64^-$ cells in AT contribute to the development of IR in diet-induced obesity (137). Inhibition of dipeptidyl peptidase-4 (DPP4), also known as CD26, on AT moDC has been suggested as a mechanism to attenuate IR (157). Furthermore, it has been proposed that moDC participate in AT mitochondrial metabolism during obesity dysregulating

insulin sensitivity, by a mechanism involving the lysine metabolite 2-aminoadipate (2-AA) (158). These findings collectively suggest that AT-DCs have the capacity to directly or indirectly affect systemic metabolism, by modulating insulin sensitivity during tissue inflammation.

Interestingly, the expression of CD1c, a marker of human cDCs, in SAT has shown to be correlated with homeostasis model assessment-estimated insulin resistance (HOMA-IR) in obese patients (134). Clinical observations remain unclear on the role of DCs in the development of IR. It has been reported that the numbers of circulating cDC1 and pDCs are diminished in T2DM patients with poor metabolic control (159) (160). However in a separate T2DM population study, the number of moDCs were increased in the circulation (161). In the pancreas, the role of cDCs in T1DM autoimmune pathophysiology has been well established. Subsets of cDCs have been identified and demonstrate distinct roles in T1DM islet immunity, such as the cDC1 population which is essential for the recruitment of autoreactive T cells (162) (163). However it is yet to be understood if and how cDCs can directly affect islet inflammation and β-cell insulin secretion in T2DM.

1.6 Wnt/β-catenin signalling

Wnt proteins are secreted signalling molecules that are important during embryonic development and regulate adult tissue homeostasis and remodelling (164). They are fundamental in the control of cell proliferation and differentiation by activating numerous signalling pathways, including the canonical Wnt/β-catenin pathway (165). Although Wnt/β-catenin signalling is required for basic developmental processes, it has recently emerged to play a role in immunity, and in particular in the control of cDC function (166) (167). Additionally, links between the Wnt/β-catenin pathway, adipogenesis and insulin sensitivity are beginning to be identified.

1.6.1 Canonical pathway

β-catenin is constitutively expressed in cells, however in the absence of Wnt ligands it is rendered inactive. Cytoplasmic β-catenin is recruited to a degradation complex containing Axin, adenomatous polyposis coli (APC) and casein kinase I (CKI) and glycogen synthase kinase (GSK)-3β. The kinases phosphorylate β-catenin, targeting it for ubiquination and proteasomal degradation. The Wnt ligand family comprises of 19 Wnt proteins in mammals, which typically act in an autocrine or paracrine manner. Specific Wnt proteins preferentially activate the canonical pathway, including Wnt1, Wnt3a and Wnt10b (168). When Wnt ligands bind to the N-terminal of frizzled receptors (FZD) with the assistance of co-receptor transmembrane low-density lipoprotein receptor-related protein (LRP)-5/6, this leads to the inactivation of the degradation complex. Dishevelled (Dsh) protein is recruited to the cell membrane providing a site for Axin and GSK3β to phosphorylate and bind to the cytoplasmic tail of LRP5/6, rendering them inactive. This results in accumulation of β-catenin in the cytoplasm. After translocation to the nucleus, β-catenin binds to transcription factors lymphoid enhancing factor (LEF) and T cell factor (TCF) to activate gene transcription (Figure 1.8).

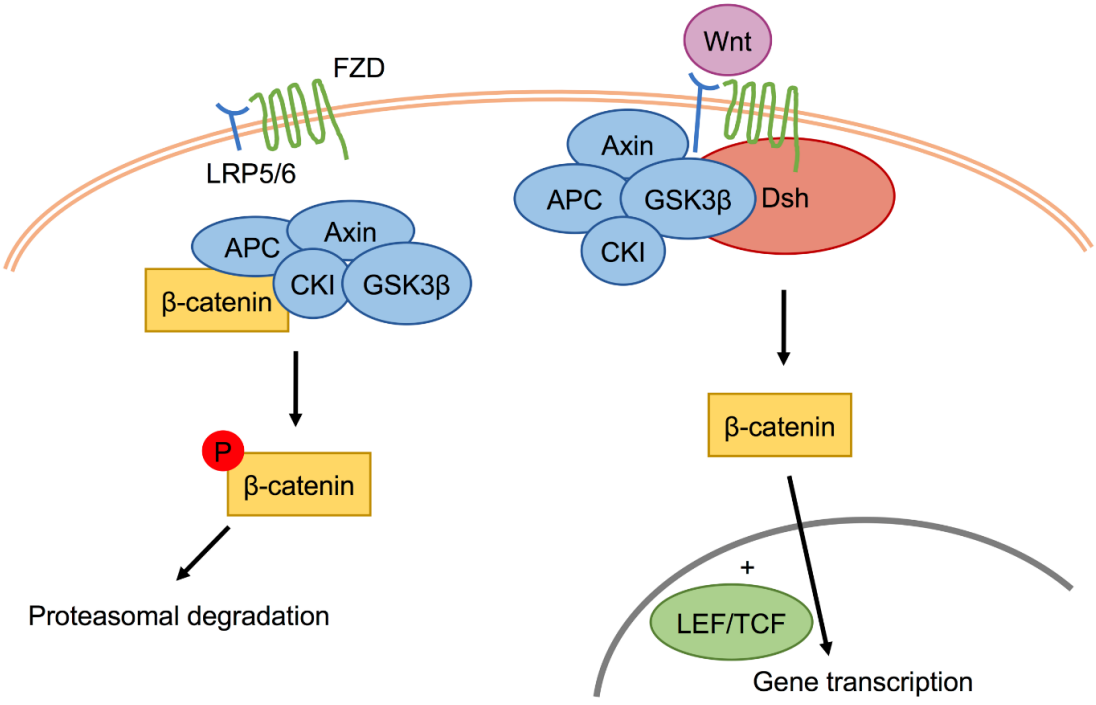

Figure 1.8 Schematic of canonical Wnt/β-catenin signalling pathway
FZD; frizzled receptor, LRP; low-density lipoprotein receptor-related protein, APC; adenomatous polyposis coli, CKI; casein kinase I, GSK3β; glycogen synthase kinase 3β, Dsh; dishevelled; LEF; lymphoid enhancing factor, TCF; T cell factor.

1.6.2 Wnt/β-catenin regulation of gene transcription

β-catenin is an evolutionary conserved protein, with a primary role in cell-cell adhesion but is also critical for gene transcription. β-catenin is the key effector protein in the pathway responsible for signal transduction to the nucleus, where it triggers transcription of Wnt-specific genes mediated by TCF/LEF transcription factors (169). In the absence of β-catenin, TCF/LEF act as transcriptional repressors enabling histone deacetylation however, upon β-catenin binding, co-repressors are displaced, promoting the activation of gene transcription. There is a vast number of diverse Wnt/TCF/β-catenin target genes, which are continuously being discovered. These genes are subject to complex, context-dependent regulation and expressed in a tissue-specific or temporally restricted manner (170). The broad range of processes that Wnt/β-catenin signalling regulates indicates the plethora of target genes. Notably the expression of anti-inflammatory cytokines, IL-10 and IL-27, are the result of Wnt/TCF/β-catenin target gene transcription. Aberrant pathway activation and repression are involved in tumorigenesis.

Relevant to this project, Wnt/β-catenin signalling has been shown to regulate adipogenesis and is associated with insulin sensitivity. Activation of the pathway by glycogen synthase kinase (GSK)-3β inhibitor or Wnt10b ligands, blocks pre-adipocyte differentiation (171) (65). Dysregulation of Wnt/β-catenin signalling has been associated with T2DM susceptibility in mouse and man (172). This was first suggested by the loss of Wnt5b function in humans, which was associated with increased T2DM susceptibility in the absence of obesity (173) (174). Variants of *Tcf7l2*, involved in β-catenin gene transcription, confer higher risk of β-cell dysfunction and the development of T2DM (175). In mice, activation of the pathway *in vivo* by overexpression of Wnt10b in adipocytes showed a significant decrease in total body fat and resistance to developing high-fat diet induced IR (176) (177).

1.6.3 Activation of β-catenin in immune tolerance

Recent studies have shown a further link of the Wnt/β-catenin pathway with the regulation of inflammation, particularly in cDCs where activation of the pathway has emerged to be important for immune tolerance (167). Exposure to Wnt ligands induces a regulatory state of cDCs, producing high levels of IL-10 and

limiting the expression of inflammatory cytokines and in addition Wnt-conditioned DCs promote T reg responses, despite not affecting cDC maturation or expression of costimulatory molecules in response to TLR ligands (178) (179) (180) (181). Activation of β-catenin through various other Wnt-independent mechanisms has also demonstrated a tolerogenic phenotype of cDCs. Disruption of E-cadherin-E-cadherin interactions promotes the activation of β-catenin in DCs, stimulating a high level of IL-10 production *in vitro* and protection against the experimental model of autoimmune encephalomyelitis (EAE) (182). Furthermore, TLR2-mediated signals induce β-catenin activation in DCs through PI3K/Akt pathway, promoting IL-10 production and T reg differentiation to supress chronic inflammation and protection from Th17/Th1 mediated autoimmune neuroinflammation (179). Other pathways activate β-catenin in DCs to promote immune tolerance, including TLR9 (179), Fas signalling (183) and TGF-β (184).

Immune tolerance has shown to be abrogated in a number of mouse models with depletion of β-catenin in the DC population. Using CD11c specific β-catenin knockout mice, intestinal DCs exacerbated inflammatory responses disrupting gut tissue homeostasis (185). The depletion of β-catenin in $CD11c^+$ population decreased production of IL-10, resulting in reduced T reg population and an increased Th17 responses which subsequently rendered mice more susceptible to colitis (185). Similarly, loss of Wnt/β-catenin signalling through deletion of LRP5/6 or β-catenin in $CD11c^+$ population, resulted in increased Th1/Th17 differentiation and reduced T reg response by regulating the expression of pro- and anti-inflammatory cytokines (178). This effect was sufficient to exacerbate the development of EAE, while conversely constitutive activation of β-catenin in $CD11c^+$ cells delayed EAE onset (178). However in another autoimmune model of collagen-induced arthritis (CIA), CD11c specific β-catenin knockout mice exhibited no changes in splenic Th T cell populations but displayed a reduced T reg frequency, although this was not sufficient to alter CIA onset and severity (186). It is proposed that the contrasting results in disease models may in part be explained by tissue-dependent Wnt expression, therefore dependence on Wnt/β-catenin for tolerogenic signalling may be tissue specific.

1.7 Hypothesis and aims

With chronic inflammation playing a key pathogenic role in obesity and the associated development of T2DM, investigating potential immunomodulation mechanisms may provide alternative therapeutic targets. Recent studies have established that activation of the Wnt/β-catenin pathway is important for the tolerogenic activity of cDCs (185) (178). Available transcriptome data indicates that Wnt/β-catenin pathway is upregulated in cDC1 subset present in VAT. Interestingly during obesity, the levels of Wnt10b are known to be supressed implying that the activity of the Wnt/β-catenin pathway is impaired in AT (65). In this thesis, the role of the Wnt/β-catenin pathway in cDCs in VAT and potential therapeutic implications will be investigated. Using cDC-specific mouse models for β-catenin deletion or gain-of-function, this work will explore the effect on VAT-cDC phenotype and VAT homeostasis under steady-state conditions and during diet-induced tissue inflammation. We hypothesise that activation of Wnt/β-catenin pathway in cDCs sustains a tolerogenic phenotype, critical for the maintenance of VAT immune homeostasis. The following aims will be addressed:

- To determine the role of β-catenin in VAT-cDCs, with the use of a mouse model with depletion of β-catenin in cDCs, referred to as β-catenin knockdown
  - Investigate the effect on tissue inflammation
  - Assess the activity of the pathway

- To characterise a mouse model with constitutively active β-catenin in cDCs, referred to as gain-of-function (GOF) in physiological conditions and in a model of diet-induced tissue inflammation
  - Analyse the immune phenotype of the VAT, spleen and lymph nodes
  - Examine the maturation and functional response of the cDC population in VAT
  - Understand the impact on whole-body glucose homeostasis, insulin sensitivity and investigate effects on islet and β-cell biology
  - Explore other metabolic measures, including adipokine and cytokine levels

- To explore targeting the Wnt/β-catenin pathway in cDCs for therapeutic potential
  - Investigate the atherogenic development in *Ldlr*$^{-/-}$ GOF chimera model
  - Test micelle polymer structures for targeted delivery, examine the specificity and affinity of the route

Chapter 2 Materials and Methods

2.1 Mice

C57BL/6 and BALB/c were purchased from Charles River laboratories. *Ctnnb1*^{tmKem} (*Ctnnb1*$^{Fl/Fl}$), *Zbtb46*^{tm1Kmm}/J (*Zbtb46*^{GFP}), B6.Cg-Tg(TcraTcrb) 425Cbn/J (OT-II) and B6.129S7-Ldlr^{tm1Her}/J (*Ldlr* $^{-/-}$) were purchased from Jackson laboratories. *Zbtb46-Cre* mice were kindly provided by M. Nussenzweig (Rockefeller University, USA), *Ctnnb1*$^{lox(ex3)}$ mice were kindly provided by M. M. Taketo (Kyoto University, Japan) (187). *Ctnnb1*$^{Fl/Fl}$ *Zbtb46-Cre* (β-catenin knockdown) mice were generated by crossing *Ctnnb1*$^{Fl/+}$ *Zbtb46-Cre* with *Ctnnb1*$^{Fl/Fl}$. Littermates *Ctnnb1*$^{Fl/+}$ *Zbtb46-Cre* were used as wild type (WT) controls. *Ctnnb1*$^{lox(ex3)/+}$ *Zbtb46-Cre*$^{/+}$ (gain-of-function, GOF) mice were generated by crossing *Ctnnb1*$^{lox(ex3)/+}$ with *Zbtb46-Cre*$^{/+}$. Littermates *Ctnnb1*$^{lox(ex3)/+}$ *Zbtb46*$^{+/+}$ were used as wild type (WT) controls. Mice were housed in temperature- and humidity-controlled rooms at 22°C and 55% humidity, with a 12 hour light/12 hour dark cycle. Mice were fed normal chow diet or AIN-76A Western diet or 58Y1 High fat diet (Test Diet IPS Ltd) and given water *ad libitum*; animals were rehoused in clean cages weekly. Diet composition is detailed in Table 2.1. 15 g of Z-NEST (IPS Ltd) was used as nesting material to help regulate temperature and light levels. Body weight was recorded weekly. All animal work was carried out in accordance with UK government Home Office licensing procedures, under personal licence IC5EB0E35 and project licence 70/7443 and 70/8264.

	Normal diet (ND) Energy: 4.07 kcal/g	**Western diet (WD)** Energy: 4.49 kcal/g	**High fat diet (HFD)** Energy: 5.10 kcal/g
Energy from: Fat Carbohydrate Protein	 13.2% 62.1% 24.7%	 40.1% 44.4% 15.5%	 61.6% 20.3% 18.1%
Additional ingredients	Sucrose - 3.18%	Sucrose - 34.1%	Sucrose - 8.8% Lard - 31.7%

Table 2.1 Diet composition

2.1.1 Genotyping

Genomic DNA was extracted from ear clips and the genotype was determined by PCR. The ear clips were digested using 200 µl DirectPCR lysis buffer (Viagen Biotech) with 0.4 mg/ml proteinase K (Life Technologies) and incubated more than 6 hours at 55°C and then for 1 hour at 85°C. Polymerase chain reaction (PCR) reaction mixes were prepared containing DEPC H_2O, 10 mM dNTP, 10 x PCR buffer (Qiagen), HotStart Taq DNA polyermase (Qiagen), forward and reverse primers (Table 2.2) and DNA template diluted 1:100. PCR reactions were carried out using the thermal cycler (Applied Biosystems) using the following steps; initial activation step at 95°C for 15 min, 35 cycles of denaturation at 94°C for 45 sec, annealing at either 62°C for *Ctnnb1*$^{lox(ex3)}$ or 59°C for *Zbtb46-Cre* or 60°C for *Ctnnb1*$^{Fl/Fl}$ for 45 sec and extension at 72°C for 1 min, after 35 cycles final extension step at 72°C for 10 min. The end products were diluted with 5 x loading dye buffer (BioLine) and analysed on 2% agarose gel run at 60V. Agarose (Sigma) was dissolved into TBE buffer containing 1M Tris base (Sigma), 1M Boric acid (Sigma) and 0.02M EDTA (Sigma) to form a gel including Gel Red (Bioscience) for imaging by UV transilluminator. The presence of a single band at 493 base pairs (bp) was identified as *Zbtb46-Cre*$^{/+}$ or at 300 bp as *Ctnnb1*$^{Fl/Fl}$ and two bands at 600 bp and 700 bp were identified as *Ctnnb1*$^{lox(ex3)/+}$.

Ctnnb1$^{lox(ex3)}$	Forward sequence: AGAATCACGGTGACCTGGGTTAAA
	Reverse sequence: CATTCATAAAGGACTTGGGAGGTGT
Zbtb46-Cre	Forward sequence: GGAGGTGGCGAGGGCTCCCCTGAGG
	Reverse sequence: CCTCACATTGCCAAAAGACGG
Ctnnb1$^{Fl/Fl}$	Forward sequence: AAGGTAGAGTGATGAAAGTTGTT
	Reverse sequence: CACCATGTCCTCTGTCTATTC

Table 2.2 Primer sequences for genotyping

2.1.2 Generation of chimeric mice

Recipient C57BL/6 male or *Ldlr*$^{-/-}$ male or female mice were γ-irradiated twice with a dose of 5 Gγ 3 hours apart. One day later, mice were reconstituted by intravenous (i.v.) injection with either 3 x 10^6 bone marrow cells from GOF or WT mice, or 1 x 10^6 fetal liver cells from β-catenin knockdown mice or relevant WT

control. Recipient mice were maintained on acidified water 1 week before irradiation and during the critical 4 week reconstitution period. Figure 2.1, 2.2 & 2.3 detail the generation of the mouse models.

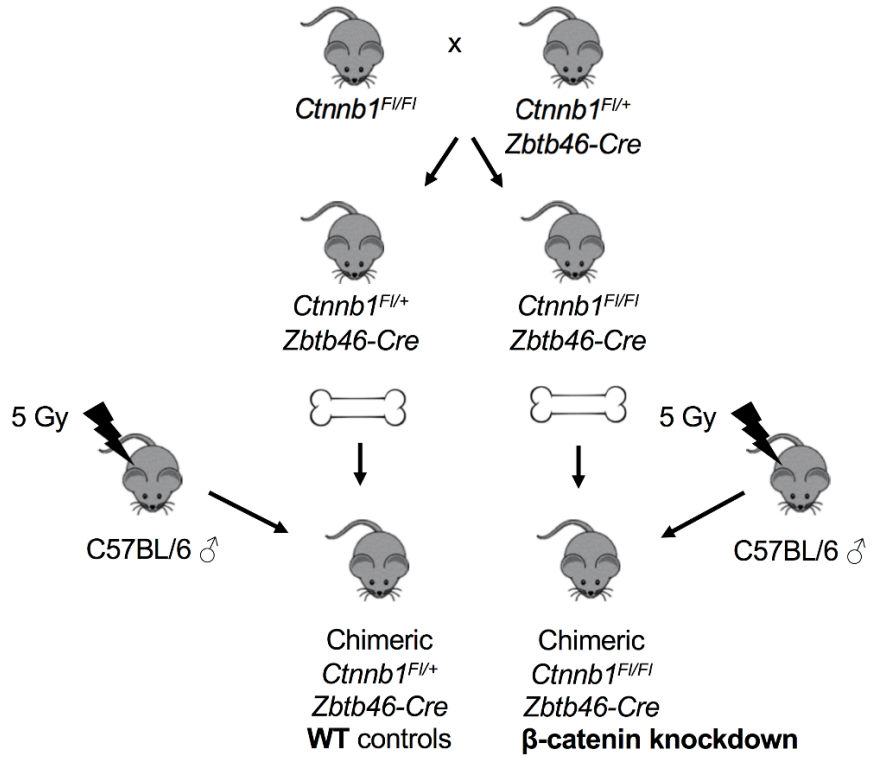

Figure 2.1 Generation of the chimeric β-catenin knockdown model

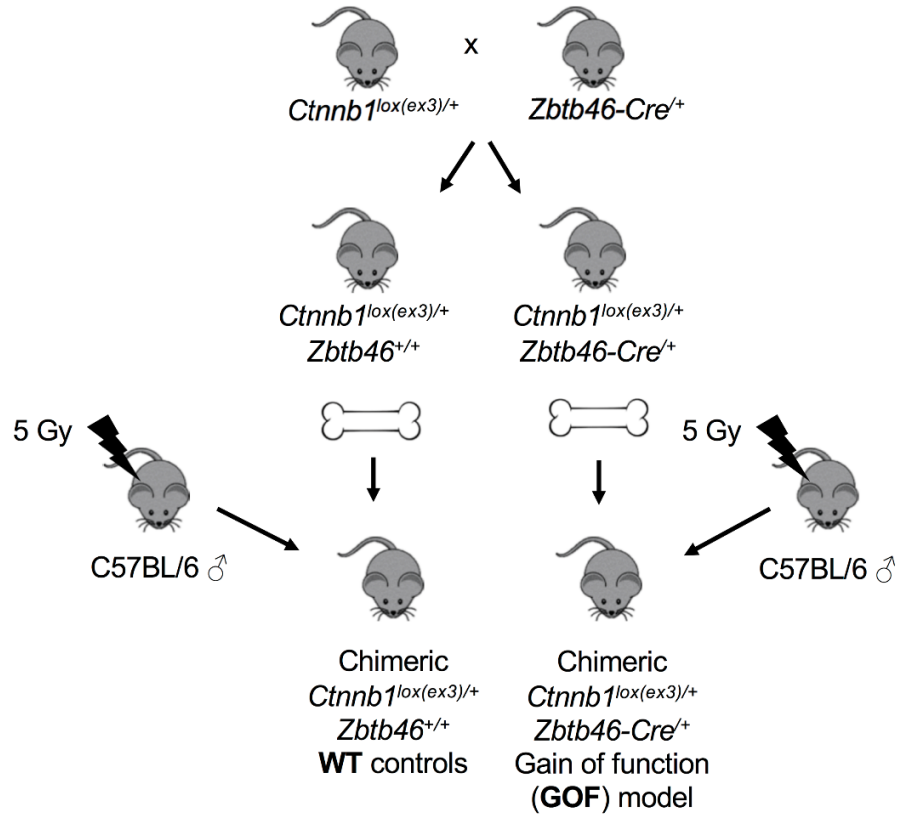

Figure 2.2 Generation of the chimeric GOF model

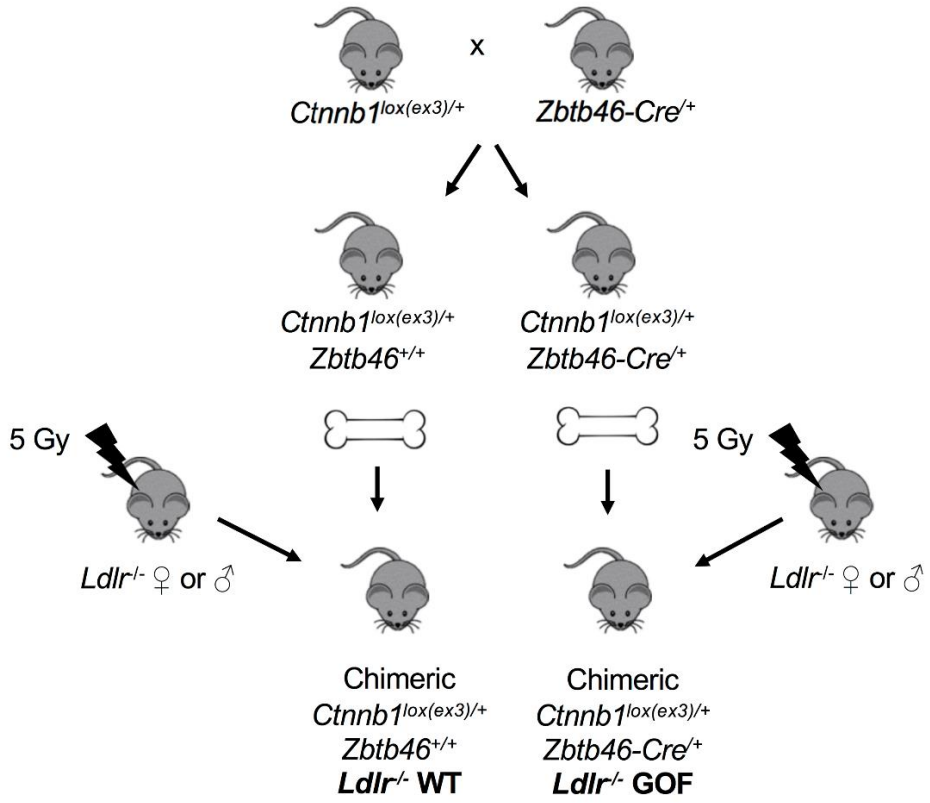

Figure 2.3 Generation of the chimeric *Ldlr*$^{-/-}$ GOF model

2.2 Primary cell culture and isolation

2.2.1 Extraction of mouse bone marrow cells

The femurs and tibias of mice were removed from euthanized animals. The bones were cleaned and sterilised in 70% ethanol. Using MACS buffer containing PBS (Gibco), 2% heat inactivated fetal bovine serum (FBS) (Seralab), 2mM EDTA, the bones were flushed through with 5 ml syringe and 23 G needle (BD Microlance) to liberate the marrow cells. The harvested bone marrow cells were filtered through a 70 µm cell strainer (Fisher) to remove any debris and further washed with MACS buffer, centrifuged at 1600 rpm for 5 min. The supernatant was discarded and cell pellet resuspended in an appropriate volume for counting. To count viable cells, cell suspension was diluted 1:1 ratio with trypan blue (Sigma) for dead cell exclusion and counted using a haemocytometer, visualised by light microscope. The value obtained from one primary 1 mm^2 square was equal to the number of cells x 10^4 in 1 ml. After counting, the cells were resuspended at 3

x 10^7 /ml in sterile PBS for i.v. injections for the generation of chimeras or used for culturing bone marrow dendritic cells.

2.2.2 Culture of bone marrow dendritic cells (BMDC)

The cells harvested from bone marrow were counted as previously described and resuspended to 2.5 x 10^6 /ml in complete R10 media and 0.2 µl/ml Flt3 ligand recombinant protein (Invitrogen). Complete R10 media contained RPMI 1640 (Gibco), 10% FBS, 1% Pen/Strep (Gibco), 1% Glutamine (Gibco), 1% HEPES (Gibco), 1% Sodium Pyruvate (Gibco), 0.1% 2-Mercaptoethanol (Gibco). Cells were seeded at 1 ml/well in a 24 well plate (Costar) and incubated for 9 - 10 days at 37°C, 5% CO_2. On day 5 of culture the media was changed, removing existing media and replacing with fresh complete R10 media and Flt3 ligand.

2.2.3 Immune cell isolation from visceral adipose tissue

Visceral adipose tissue (VAT) was collected from euthanised mice, from the gonadal, epididymal, mesenteric and peri-renal fat depot sites, with care to first remove the lymph nodes. The tissue was weighed and placed into tissue wash buffer containing PBS and 2% FBS and the tissue was diced. The weight was recorded for cell number calculations and to determine the percentage of body weight. To digest the tissue, 5688 U Collagenase II (Sigma) and 0.32 U DNase (Sigma) was added per gram of VAT in 2 ml wash buffer and incubated at 37°C with agitation 220 rpm for 30 min. The digested tissue was passed through 100 µm cell strainer (Fisher) and centrifuged at 2000 rpm for 10 min. If a fatty layer was observed after spinning, the AT was under digested and the layer was collected and re-digested. The supernatant was discarded and the combined pellets of immune cells present in the vascular fraction were isolated. The pellet was lysed for red blood cells using ACK lysis buffer, containing 150mM NH_4Cl (Sigma), 10mM $KHCO_3$ (Sigma), 0.1mM Na_2EDTA (Sigma) dissolved in H_2O and pH adjusted to 7.2 - 7.4. The cells were resuspended in 1 ml ACK lysis buffer for 2 min, and washed with tissue wash buffer and centrifuged at 1800 rpm for 5 min. The resulting cell suspension was filtered through a 70 µm cell strainer and centrifuged at 2000 rpm for 10 min. The supernatant was discarded and the cell pellet was washed with PBS. The immune cell pellet was stained for analysis by flow cytometry or placed in Trizol (Invitrogen) for mRNA analysis.

2.2.4 Immune cell isolation from spleen and lymph nodes

Spleen and mesenteric, inguinal, cervical, axillary, brachial or mediastinal lymph nodes were collected from euthanised mice. The spleen or lymph nodes were placed in serum free DMEM (Gibco) and digested with 400 U/ml Collagenase D (Roche) using 5 ml syringe and 25 G needle (BD Microlance) to balloon the tissue to expel cells, followed by fine dicing of the tissue. The spleen or lymph nodes were incubated with the Collagenase D for 18 min at 37°C and digestion was stopped by adding EDTA. The digested spleen or lymph nodes were passed through 70 µm cell strainer and centrifuged at 1600 rpm for 5 min. The supernatant was discarded and red blood cells in the pellet were lysed using ACK lysis buffer and washed with PBS. The immune cell pellet was stained for analysis by flow cytometry or for further cell isolation.

2.2.5 $CD11c^+$ cell and $CD4^+$ T cell isolation

$CD11c^+$ cells and $CD4^+$ T cells were isolated from spleen or VAT by positive selection using microbeads and LS columns (MACS Miltenyi Biotec). The isolated immune cells were counted and resuspended at 1 x 10^8 /400µl in MACS buffer. The cells were incubated with 40 µl $CD11c^+$ or $CD4^+$ microbeads (MACS Miltenyi Biotec) for 20 min at 4°C. The cells were washed with MACS buffer, centrifuged at 1800 rpm for 5 min and the supernatant was discarded. The cells were then resuspended in 800 µl of MACS buffer and loaded into a pre-washed LS column while being placed in the magnetic field of a MACS separator. The column was washed three times with MACS buffer and the flow through collected was discarded. After the final wash the LS column was removed from the magnet and 5ml MACS buffer was loaded into the column and the cells bound with microbeads within the column were flushed out using the plunger into a new tube. The cells were centrifuged at 1800 rpm for 5 min and the supernatant was discarded. The cells were counted and resuspended in complete R10 media to an appropriate cell concentration for plating.

2.2.6 $CD3^+$ T cell isolation

$CD3^+$ T cells were isolated from spleen and lymph nodes of BALB/c mice by negative selection using Dynabead (Invitrogen). The isolated immune cells were counted and resuspended at 1 x 10^8 /ml in MACS buffer. For an initial blocking

step FBS was added to the cells in a 15 ml tube, followed by the antibody mix. After 20 min incubation at 4°C, the cells were washed twice with MACS buffer, centrifuged at 350 g for 5 min and the supernatant was discarded. The cells were resuspended in MACS buffer and incubated with pre-washed Dynabeads for 15 min at room temperature with agitation. After mixing, the tube was placed in the DynaMag magnet for 2 min to allow for separation and while the tube remained in the magnet the unbound $CD3^+$ T cells were transferred into a new tube. The new tube was placed back into the magnet and the separation was repeated. The $CD3^+$ T cells were washed in MACS buffer, centrifuged at 1800 rpm for 5 min and the supernatant was discarded. The $CD3^+$ T cells were counted ready for CFSE labelling.

2.3 Flow cytometry staining

2.3.1 Extracellular staining

The cells were resuspended in FACS buffer containing PBS, 2% FBS and 2mM EDTA and placed in wells of 96 V-bottom plate (Costar). The cells were stained for surface markers with fluorescently conjugated primary antibodies, see Table 2.3. All the samples were stained with fixable Aqua Dead cell stain (Invitrogen) diluted 1:1000 in PBS, to exclude dead cells from analysis. The samples were stained at 4°C for 30 min and then washed twice with FACS buffer where the plate was centrifuged at 1800 rpm for 5 min and the supernatant discarded. The samples were fixed at 4°C for 30 min with 1% PFA (Sigma) and washed twice with FACS buffer. After staining and fixing the samples were resuspended in FACS buffer and analysed by flow cytometry using a LSR Fortessa (BD Biosciences) and FlowJo version 10 software. A gating strategy was used to identify immune populations through expression of cell surface markers (Figure 2.4).

2.3.2 Intracellular staining

After staining cell surface markers as described previously, the samples were incubated in permeabilization/fixation buffer from intracellular staining kits (eBioscience or BD Bioscience) at 4°C for 30 min. The samples were washed in

permeabilization buffer before staining with fluorescently conjugated primary antibodies (BioLegend), see Table 2.3, at 4°C for 30 min in permeabilization buffer and washed twice with FACS buffer. After staining and fixing the samples were resuspended in FACS buffer and analysed by flow cytometry using a LSR Fortessa and FlowJo version 10 software. A gating strategy was used to identify immune populations through expression of intracellular markers (Figure 2.4).

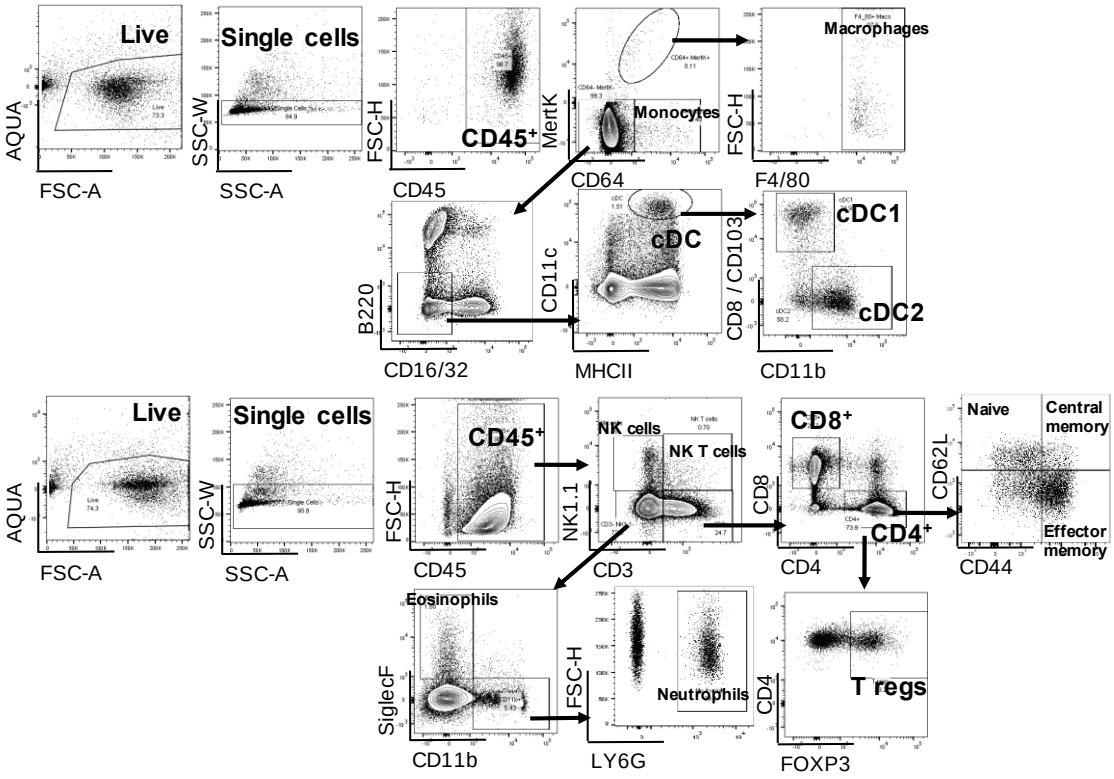

Figure 2.4 Gating strategy for flow cytometry analysis

2.3.3 Fluorescence activated cell sorting of live cells

The cells were stained as previously described with fluorescently conjugated primary antibodies, see Table 2.3 and fixable Aqua Dead cell stain. The cells were counted and resuspended at 2 x 10^7 /ml in FACS buffer in 5 ml polypropylene tube (Falcon). Live sorting was carried out using either an Aria II or Aria Fusion (BD Biosciences) with 85 µm nozzle. $CD11c^+$ $MHCII^+$ $CD103^+$ $CD11b^+$ conventional dendritic cells were collected into pre-coated polypropylene tubes containing 500 µl FBS. Once resuspended in FACS buffer, the cells were centrifuged at 2000 rpm for 10 min and the supernatant was discarded. This wash step was repeated twice. The sorted cells were resuspended in the appropriate media for culture at the specified concentration.

Specificity	Clone	Fluorochrome	Supplier	Dilution
CD16/32	93	FITC	BioLegend	1:200
F4/80	BM8	PerCP	BioLegend	1:200
CD206	C068C2	Brilliant Violet 421™	BioLegend	1:200
CD11c	HL3	Brilliant Violet 605™	BD Biosciences	1:200
CD11c	N418	Brilliant Violet 605™	BioLegend	1:200
CD103	2E7	APC	eBioscience	1:200
MHCII	M5/114.15.2	AlexaFluor®700	BioLegend	1:200
CD11b	M1/70	APC-eFluor®780	eBioscience	1:200
MertK		PE	R&D Systems	1:200
CD45	30-F11	PE-CF594	BioLegend	1:800
CD64	X54-5/7.1	PE-Cy7	BioLegend	1:200
CD8	53-6.7	FITC	eBioscience	1:200
CD8	53-6.7	APC-eFluor®780	eBioscience	1:200
LY6G	IA8	Brilliant Violet 421™	BioLegend	1:200
NK1.1	PK136	Brilliant Violet 605™	BioLegend	1:200
CD3	17A2	AlexaFluor®700	eBioscience	1:200
SiglecF	E50-2440	PE-CF594	BD Biosciences	1:200
CD4	RM4-5	PE-Cy7	BioLegend	1:200
CD4	RM4-5	PerCP	BioLegend	1:200
B220	RA3-6B2	PerCP	BioLegend	1:200
FOXP3	150D/E4	PE	eBioscience	1:200
FOXP3	FJK-16s	PE-Cy7	eBioscience	1:200
CD69	H1.2F3	FITC	BioLegend	1.200
CD44	IM7	eFluor®450	BioLegend	1:200
CD44	IM7	PerCP	BioLegend	1:200
CD62L	MEL-14	Brilliant Violet 605™	BioLegend	1:200
Nkx6.1	R11-560	PE	BD Biosciences	1:50
Nkx6.1	R11-560	AlexaFluor®647	BD Biosciences	1:50
Ki67	16A8	AlexaFluor®700	BioLegend	1:50
TNFα	MP6-XT22	PE-Cy7	BD Biosciences	1:200
IL-17A	eBio17B7	PE	eBioscience	1:200
IFNγ		APC	BD Biosciences	1:200
CCR4	2G12	PE	BioLegend	1:200
TCRVα2	B20.1	PE	BioLegend	1:200

Table 2.3 Antibodies used for flow cytometry staining

2.4 Antigen presentation assays

2.4.1 CFSE labelling of T cells

Isolated $CD3^+$ and $CD4^+$ T cells were labelled with CFSE (Invitrogen). The cells were resuspended at 1 x 10^7 /ml in PBS and incubated with 3 µM CFSE for 9 min at room temperature. Immediately the excess CFSE was quenched by adding an equal volume of FBS and incubating for 1 min before washing with PBS. The cells were centrifuged at 2000 rpm for 10 min and the supernatant was discarded. The cells were washed further once more in PBS and counted. The CFSE labelled $CD3^+$ or $CD4^+$ T cells were resuspended in complete R10 media to an appropriate cell concentration for plating.

2.4.2 *Ex vivo* mixed leukocyte reaction (MLR)

$CD11c^+$ cells or sorted dendritic cells isolated from the spleen or VAT of experimental chimera mice were cultured with CFSE labelled $CD3^+$ T cells, harvested from the spleen and lymph nodes of BALB/c mice. Cells were isolated as previously described and resuspended in complete R5 media. Complete R5 media contained RPMI 1640, 5% FBS, 1% Pen/Strep, 1% Glutamine, 1% HEPES, 1% Sodium Pyruvate, 0.1% 2-Mercaptoethanol. DCs were resuspended at 5 x 10^5 /ml and 100 µl was seeded into a 96 well U-bottom plate (Costar). CFSE labelled $CD3^+$ T cells were resuspended at 2.5 x 10^6 /ml and 100 µl was added into the wells with the DCs. The cells were mixed at a ratio of 1:5 (5 x 10^4 DC: 2.5 x 10^5 $CD3^+$ T cells per well) and incubated for 5 days, after which cells were harvested and CFSE dilution was assessed by flow cytometry. Supernatant was harvested to measure cytokine release from T cells.

2.4.3 *In vivo* antigen presentation

Mice were injected i.v. with ovalbumin (OVA)-specific OT-II $CD4^+$ T cells purified from spleen and lymph nodes of OT-II mice by $CD4^+$ bead positive selection (MACS Miltenyi Biotec) and labelled with 3 µM CFSE (Invitrogen). The next day, mice were immunized with 200 µg of OVA (Sigma) by intraperitoneal (i.p.) injection. Three days later, immune cells were isolated from spleen, lymph nodes and VAT and stained, as described above, for analysis by flow cytometry. The dilution of CFSE in the T cell population was used as an indicator of cell division.

2.5 T cell responses

2.5.1 *Ex vivo* stimulation of cytokines

Immune cells from spleen, lymph nodes and VAT were isolated as previously described. Samples were resuspended in FACS buffer in 5 ml polypropylene tubes and centrifuged at 1800 rpm for 5 min. The supernatant was discarded and the cell pellet was resuspended in 500 µl of complete R5 media containing 20 ng/ml Phorbol 12-myristate 13-acetate (PMA) (Sigma) and 1 µg/ml Ionomycin (Sigma). Unstimulated cells were included as a negative control. After 1 hour incubation at 37°C, 10 µg/ml Brefeldin A (Sigma) was added into all of the tubes +/- stimulation and incubated for a further 4 hours at 37°C. Cells were stained as previously described, to analyse cytokine production by flow cytometry.

2.6 Islets assays

2.6.1 Isolation of islets

Immediately after mice were euthanised, the pancreas was inflated with 1 µg/ml Collagenase V (Sigma) by injecting into the hepatic duct using 30 G needle (BD Microlance), after clamping the ampulla. The inflated pancreas was removed, placed into a tube with 1 ml of 1 µg/ml Collagenase V diluted into additive-free RPMI (Sigma) and incubated in a water bath at 37 °C for 10 min. Cold additive-free RPMI was added followed by centrifugation at 1000 rpm for 1 min. The supernatant was removed before adding about 15 ml of cold additive-free RPMI and the pancreas was resuspended in the media. This pellet was washed three more times. The islets were resuspended in 3 ml of Histopaque 119 (Sigma). A sucrose gradient was made by adding dropwise 3 ml of Histopaque 1083 and 1077 (Sigma) and RPMI was added dropwise up to 12 ml. The gradient was centrifuged at 2500 rpm for 20 min. The islets found just below the RPMI layer were collected and centrifuged at 1000 rpm for 1 min after addition of up to 12 ml RPMI. The supernatant was removed; islets were resuspended and placed in a petri dish containing 15 ml complete R10 media. After a few hours of recovery at 37 °C islets were handpicked. Islets were placed into culture overnight to

measure insulin release or used for co-cultures to measure β-cell proliferation or further processed to isolate immune cells from the islets.

2.6.2 Immune cell isolation from islets

Islets were harvested as previously described and 20 handpicked islets were resuspended in 1 ml of islet digestion buffer containing HBSS (Sigma), 10% FBS and 0.2 mg/ml Collagenase IV (Sigma). Islets were incubated for 30 min at 37°C with agitation 120 rpm and passed through a 30 G needle. The digested islets were passed through 70 µm cell strainer and centrifuged at 1600 rpm for 5 min. The supernatant was discarded and the cell pellet was washed with PBS. The immune cell pellet was stained for analysis by flow cytometry or placed in Trizol for mRNA analysis.

2.6.3 Dendritic cell and islet co-cultures

Islets were harvested as previously described from donor C57BL/6 mice and seeded into a 12 well plate (Costar), 5 handpicked islets were placed into 2 ml complete R10 media per well. The cDC population was sorted from cultured BMDC as previously described and resuspended at 5 x 10^5 /ml and 100 µl was added per well. Islets and DCs were cultured together overnight and treated with or without 1 µg/ml anti-IL-10 (BioLegend). The supernatant was harvested the next day and insulin and IL-10 was measured in the supernatant by ELISA. To measure β-cell proliferation, islets and DCs were cultured together for 5 days. In this set up, 8 islets were seeded into a 48 well plate (Costar) in 500 µl complete R10 media per well. The DC population was resuspended at 1 x 10^5 /ml and 100 µl was added per well. The islets were harvested after 5 day culture and digested as previously described. The cell pellet obtained from the islets was stained for analysis by flow cytometry. Figure 2.5 details the generation of the co-culture experiment.

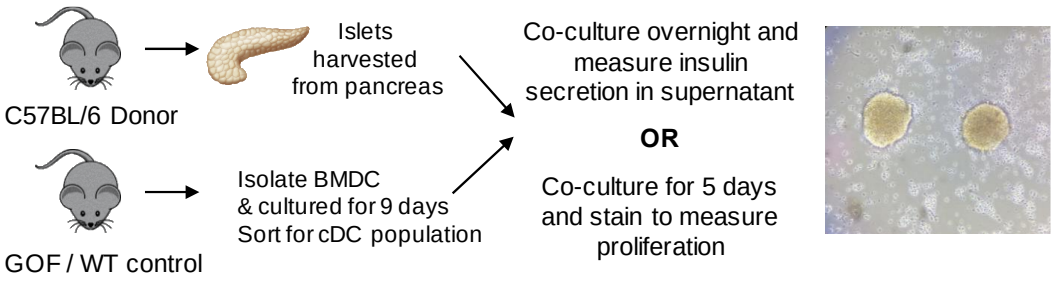

Figure 2.5 Dendritic cell and islet co-culture

2.7 Transcript analysis

2.7.1 Expression profiling

Expression profiling was performed using publicly available raw data (ImmGen GEO: GSE37448) in R (188). Between-array RNA quantile normalization was performed and unmapped or multi-mapping probes removed prior to differential expression analysis with limma (189). Fold change rankings were used in GSEA to identify differentially regulated pathways (FDR < 0.25). Processed data are available at ImmGen data browsers (http://www.immgen.org/).

2.7.2 RNA extraction from visceral adipose tissue and islet immune cells

RNA from 100 mg diced VAT or 20-30 islets was isolated by phase separation and using RNeasy lipid tissue mini kit (Qiagen). The harvested tissue was incubated in Trizol for 5 min at room temperature to allow dissociation of the nucleoprotein complex. The samples were centrifuged at 12,000 g for 10 min at 4°C and the supernatant under the fatty layer was transferred into a new tube. For phase separation, chloroform (Fisher Chemical) was added to the samples and vortexed for 15 sec. After incubation for 2 min at room temperature, the samples were centrifuged at 12,000 g for 15 min at 4°C to separate into layers. Carefully the upper aqueous phase was removed and transferred into a new tube, with care not to disturb the interphase and organic layer. The RNeasy lipid tissue mini kit was used to isolate the RNA, performed to the manufacturer's instructions. An equal volume of 70% ethanol was added to the sample, transferred into spin column placed in 2 ml collection tube and centrifuged at 12,000 g for 15 sec. The flow-through was discarded and the column was washed with buffer RW1, repeating the centrifugation step and discarding the flow-through. The wash step was repeated twice more with buffer RPE. The membrane in the spin column was dried by centrifugation at full speed for 1 min. The column was placed into a new collection tube and RNase-free water was added and centrifuged at 12,000 g for 1 min. The RNA collected in the tube was quantified by LVIS measurement using Spectrostar Omega reader (BMG Labtech).

2.7.3 RNA extraction from immune cells from visceral adipose tissue

RNA from the immune cell pellet from VAT was isolated by phase separation, further precipitated and washed. The pellet was collected in Trizol and processed as previously described. Once the upper aqueous phase was harvested, the RNA was precipitated using 100% Isopropanol (Fisher Chemical). Glyco blue (Life Technologies) was added during this step as a carrier to the aqueous phase. After overnight incubation at 4°C, the sample was centrifuged at 12,000 g for 10 min at 4°C. The supernatant was discarded and the RNA pellet was washed with 75% ethanol, repeating the centrifugation step and carefully discarding all of the supernatant. The pellet was dried by 5 min in the air and resuspended in RNase-free water. The RNA was incubated at 55 - 60°C for 10 min for denaturation. The RNA was quantified by LVIS measurement using Spectrostar Omega reader. In some cases, the RNA purity was improved using RNeasy MinElute cleanup kit (Qiagen), performed to the manufacturer's instructions.

2.7.4 cDNA synthesis

Reverse transcription of RNA to cDNA was performed using High-Capacity RNA-to-cDNA kit (Applied Biosystems). The measured RNA concentration was normalised to the sample with the lowest concentration, the kit can convert up to 2 µg of RNA per reaction. The RT reaction mix was prepared containing; 10 µl of 2 x RT Buffer mix, 1 µl of 20 x RT Enzyme mix and relevant volume of RNA and nuclease- free H_2O to give a total volume of 20 µl per reaction. The RT reaction mixes were added into PCR tubes (Applied Biosystems) and vortexed and centrifuged to spin down the contents and eliminate air bubbles. The RT reactions were carried out using the thermal cycler (Applied Biosystems) with an incubation at 37°C for 60 min and heating to 95°C for 5 min before cooling to 4°C. The cDNA was used for performing quantitative real-time PCR reactions.

2.7.5 Primer design

Forward and reverse primers were either used from the literature, from primer bank or were designed using Primer3 software using NCBI blast generated sequences of mRNA (National Centre for Biotechnology Information). Primers were designed with an amplicon size of 100 - 150 base pairs, the primer size of

18 - 23 base pairs in length, with 40 - 60% GC nucleotide content, a maximum 3' complementarity of 1, a maximum self-complementarity of 2 and a melting temperature between 59.5 and 61°C. Forward and reverse primers were purchased from Invitrogen, see Table 2.4.

2.7.6 Quantitative real-time polymerase chain reactions (qRT-PCR)

Transcripts were analysed by qRT-PCR in 96 well PCR plates (Bio-Rad) by adding to each well 2 µl cDNA, 0.5 µl forward and reverse 10 µM primer stock, 5µl iTaq™ Universal SYBR® green (Bio-Rad) and 2.5 µl nuclease free water (Qiagen). Plates were sealed using adhesive plate sealers (Bio-Rad), gently vortexed and centrifuged at 1800 rpm for 1 min. qRT-PCR was analysed using a CFX connect light cycler (Bio-Rad) with 95°C start for 3 min, then 40 cycles of 95°C for 10 sec and 55°C for 30 sec. Gene-relative expression was calculated using the ΔΔCT method to demonstrate fold-change and normalised to a reference control (GAPDH) with control sample set as 1. The geometric mean was used as a more appropriate representation of ΔΔCT, which does not have a normal data distribution. Data is represented in ΔΔCT format, however statistical analysis was performed on ΔCT data values with a normal distribution.

	Forward sequence	**Reverse sequence**
Gapdh	GGCTCATGACCACAGTCCA	CACATTGGGGGTAGGAACAC
IL-10	AAACAAAGGACCAGCTGGAC	TTCCGATAAGGCTTGGCAAC
TNFα	TCGTAGCAAACCACCAAGTG	TTTGAGATCCATGCCGTTGG
IL-6	TAGTCCTTCCTACCCCAATTTCC	TTGGTCCTTAGCCACTCCTTC
IL-1	AACCTGCTGGTGTGTGACGTTC	CAGCACGAGGCTTTTTTGTTGT
IFNγ	CAGCAACAGCAAGGCGAAA	CTGGACCTGTGGGTTGTTGAC
IL-17A	AAAGCTCAGCGTGTCCAAAC	TTCTGGAGCTCACTTTTGCG
CCL2	GCTGGAGCATCCACGTGTT	ATCTTGCTGGTGAATGAGTAGCA
CCL17	GGATGCCATCGTGTTTCTGA	GCCTTCTTCACATGTTTGTCTTTG
Adipoq	GACGTTACTACAACTGAAGAGC	CATTCTTTTCCTGATACTGGTC
Leptin	TGAGTTTGTCCAAGATGGACC	GCCATCCAGGCTCTCTGG
Tgfβ	CCCGAAGCGGACTACTATGC	ATAGATGGCGTTGTTGCGGT
Wnt1	ATTTTGCGCTGTGACCTCTT	AGCAACCTCCTTTCCCACTT
Wnt2	GGTCAGCTCTTCATGGTGGT	GGAACTGGTGTTGGCACTCT
Wnt3a	TCGGAGATGGTGGTAGAGAAA	CGC AGA AGT TGG GTG AGG
Wnt4	AAGAGGAGACGTGCGAGAAA	CACCACCTTCCCAAAGAACAG
Wnt5a	CTCTCCGAAGTCCATGTCGT	GGACGATACTCCAGGCAGAG
Wnt5b	TCTCCGCCTCACAAAAGTCT	CACAGACACTCTCAAGCCCA
Wnt6	GCGGAGACGATGTGGACTTC	ATGCACGGATATCTCCACGC
Wnt7a	GACAAATACAACGAGGCCGT	GGCTGTCTTATTGCAGGCTC
Wnt8b	CCAGAGTCCCGGGAGGTAG	GAGATGGAGCGGAAGGTGT
Wnt9a	GGACAACCTCAAGTACAGCAG	TCCACTCCAGCCTTTATCACC
Wnt10a	CCACTCCGACCTGGTCTACTTTG	TGCTGCTCTTATTGCACAGGC
Wnt10b	AATGCGGATCCACAACAACA	TTCCATGGCATTTGCACTTC
Wnt11	TGCTTGACCTGGAGAGAGGT	AGCCCGTAGCTGAGGTTGT
Ccr4	ATCGTGCACGCGGTATTCTCC	GACGGGGTTAAGGCAGCAGTGA
Foxp3	GGCCCTTCTCCAGGACAGA	GCTGATCATGGCTGGGTTGT
Myc	GCCACGTCTCCACACATCAG	TCTTGGCAGCAGGATAGTCCTT
Cyclin D1	GCGTACCCTGACACCCCTCTC	CTCCTCTTCGCCTGATCC
Cyclin A	GCCTTCACCATTCATGTGGAT	TTGCTGCGGGTAAAGAGACAG
Cdk4	ACCCTGTCATCTGTTTATGC	AGGTGTTAGTGGGAGATCCT
Fzd1	TGCCCAGTGTCTTTCTCCTT	TCTCTTTAGCCTCTCCCAACC

Table 2.4 Forward and reverse primer sequences

2.8 Metabolic assays

2.8.1 Glucose tolerance test (GTT)

Mice were fasted overnight for approximately 16 hours or 6 hours as stated, in cages with the absence of nesting material. Fasted blood glucose levels were collected from the initial tail bleed using blood glucose meter and test strips (FreeStyle Optium Neo, Abbott). Mice were administered with 1.5 mg D-Glucose /g of body weight (Sigma) by intraperitoneal (i.p.) injection and blood glucose was measured from tail vein blood at 15, 30, 60, 90 and 120 min after injection.

2.8.2 Insulin tolerance test (ITT)

Mice were fasted for 3 hours or 6 hours as stated, in cages with the absence of nesting material. Fasted blood glucose levels were collected from the initial tail bleed using blood glucose meter and test strips. Mice were administered with 0.5 U Insulin /kg of body weight (Actrapid) by i.p. injection with and blood glucose was measured from tails vein bleed at 15, 30, 60, 120 and 180 min after injection.

2.8.3 Collection of plasma

Blood was collected from tail bleed of fasted mice or from terminal cardiac puncture into EDTA-coated capillary blood collection tubes (Sarstedt). The samples were centrifuged at 2000 rpm for 10 min, the cell pellet was discarded and supernatant, the plasma was collected for further analysis.

2.9 Enzyme-linked immunosorbent assay (ELISA)

2.9.1 Cytokine and chemokine ELISA

The concentration of cytokines including TNFα, IL-10, IL-6, IL-12, IL-4, IL-17A, IFNγ and chemokine CCL17, were quantified using ELISA kits (Invitrogen) performed to the manufacturer's instructions. $CD11c^+$ cells were purified from spleen and VAT as described previously, and plated at 1×10^5 cells/ well. Cells were cultured overnight in complete R10 media and supernatant was collected the next day. IL-10, IL-6, IL-12, CCL17 was measured in the harvested $CD11c^+$

supernatant. IL-4, IL-17A, IFNγ was measured in the harvested supernatant from *ex vivo* mixed leukocyte reaction. TNFα was measured in plasma collected from terminal bleed. The wells of a 96 flat-bottom high affinity protein-binding plate (Costar) were coated with purified capture antibody diluted in coating buffer overnight at 4°C. The wells were washed 3 times with PBS + 0.05% Tween-20 (Sigma) (PBS-T) and blocked in assay buffer for 1 hour at room temperature to prevent non-specific antibody binding. The block was aspirated and the standards and samples were added into the wells and incubated for 2 hours at room temperature. Standards were prepared in assay buffer, with a serial 1:2 dilutions performed to generate an 8-point standard curve. Samples were used neat or diluted in assay buffer dependent on the analyte. The wells were washed 3 times with PBS-T and biotin-conjugated detection antibody diluted in assay buffer, was added for 1 hour at room temperature. The wells were washed 3 times with PBS-T and Avidin-HRP enzyme diluted in assay buffer, was added for 30 min at room temperature. The wells were washed 5 times with PBS-T and Tetramethylbenzidine (TMB) substrate solution was added until the standard curve had developed, which ranged between 5 and 20 min depending on the analyte. Once developed, 1M hydrochloric acid was used to stop the reaction, and the plate was read at 450 nm absorbance using Spectrostar Omega reader. The concentrations of the cytokines in the samples were interpolated from the standard curve using Prism 7 (GraphPad software).

2.9.2 Metabolic ELISA

Adiponectin, leptin and insulin from fasted or non-fasted plasma samples were measured using ELISA kits (Merck Millipore) performed to the manufacturer's instructions. The wells of pre-coated plates were washed 3 times with wash buffer and the standards, quality controls and samples were added and incubated for 2 hours at room temperature with agitation with detection antibody. The standards and samples were diluted in assay buffer, dependent on the kit and analyte. The wells were washed 3 times with wash buffer and the enzyme solution was added for 30 min at room temperature with agitation. The wells were washed 5 times with wash buffer and substrate solution was added for 15 min to develop until the stop solution was added. The plate was read at 450nm absorbance using Spectrostar Omega reader and concentrations of analytes in the samples were interpolated from the standard curve using Prism 7.

2.9.3 Cholesterol and free fatty acid quantification

Levels of total cholesterol, HDL and VLDL/LDL from plasma samples were determined using a quantification kit (Abcam) performed to the manufacturer's instructions. HDL and VLDL/LDL fractions were separated from the plasma by mixing with precipitation buffer and incubating for 10 min at room temperature. The sample was centrifuged for 10 min at 2000 g and the HDL fraction supernatant was harvested. The cell pellet was further precipitated to remove all the supernatant and the precipitate was resuspended in PBS to generate the VLDL/ LDL fraction. Total cholesterol was determined from the plasma directly. Standards were prepared in assay buffer to generate a 6-point standard curve from 5 - 0 µg/well. Samples were used neat or diluted in assay buffer dependent on the fraction. The standards and samples were added into a 96 well flat-bottom plate and diluted 1:2 with cholesterol reaction mix containing cholesterol probe, enzyme mix, cholesterol esterase and assay buffer. To measure free cholesterol, cholesterol esterase was absent from the reaction mix. After incubating for 1 hour at 37°C in the dark, the plate was read at 570 nm absorbance using Spectrostar Omega reader and the cholesterol concentration in the samples were interpolated from the standard curve using Prism 7.

2.10 Image staining and analysis

2.10.1 Immunohistochemistry

VAT, heart and pancreas tissue was fixed in 4% PFA and embedded in paraffin by Histopathology core services, QMUL. Sections were mounted onto slides and stained with haematoxylin and eosin. Pancreas sections were immunostained with rabbit polyclonal antibodies for CD3 (Dako), insulin (ICN), Ki67 (Abcam, clone SP6) or cleaved caspase-3 (Cell Signalling Technologies) using Ventana OmniMap DAB- HRP staining system (Discovery XT) performed by Histopathology core services, QMUL. Heart sections were stained with Sirus red for the identification of the aortic sinus. Stained slides were scanned using Pannoramic 250 High Throughput scanner to gain digital images for analysis. Adipocyte size was calculated from H&E stained VAT sections using ImageJ Adiposoft software (190), three fields of view from each image per tissue were

analysed. Islet size was determined from H&E stained pancreas sections using ImageJ software, all islets from five levelled sections per tissue were analysed where the level was set at 25 µm. Ki67$^+$ cells were counted in the islets of Ki67 stained pancreas sections, all islets from three levelled sections per tissue were analysed. All analysis was performed blinded.

2.10.2 Immunofluorescence

Unstained sections from paraffin embedded pancreas tissue were mounted onto slides by Histopathology core services, QMUL. An initial antigen retrieval step was performed before immunofluorescence staining. Slides were incubated in Xylene (Fisher Chemical) for 5 min twice, 100% ethanol for 2 min twice, 90%, 70%, 50% ethanol for 2 min and distilled water for 5 min. Slides were boiled in 10mM Sodium citrate buffer containing 0.05% Tween-20, pH 6, at 100°C for 30 min. After cooling, the slides were washed in PBS-T and blocked with 10% goat serum, 0.3% Triton X-100 (Sigma), 1% BSA buffer for 1 hour at room temperature. Slides were washed three times with PBS-T for 5 min and incubated overnight at 4°C with rabbit anti-mouse Ki67 antibody (Abcam, clone SP6) diluted 1:100 in 10% goat serum, 0.3% Triton X-100, 1% BSA buffer. Slides were washed three times with PBS-T for 5 min and incubated for 1 hour at room temperature with goat anti-rabbit IgG antibody conjugated with AlexaFluor®555 (Life Technologies) diluted 1:1000 in 0.1% goat serum, 0.3% Triton X-100, 0.1% BSA buffer. Slides were washed three times with PBS-T for 5 min and incubated for 1 hour at room temperature with anti-mouse Nkx6.1 antibody conjugated with AlexaFluor®647 (BD Bioscience, clone R11-560) diluted 1:200 and DAPI (Sigma) diluted 1:2000 in 0.1% goat serum, 0.3% Triton X-100, 0.1% BSA buffer. Slides were washed three times with PBS-T for 5 min and covered with mounting media (Vector Laboratories) and coverslip before analysis on Axio Observer Z1 microscope (Zeiss) using AxioVision software (Zeiss). Ki67$^+$ Nkx6.1$^+$ cells were counted in the islets of the stained pancreas sections, all islets from three levelled sections per tissue were analysed. Analysis was performed blinded. Unstained sections from paraffin embedded pancreas tissue from *Zbtb46^{GFP}* were mounted onto slides by Histopathology core services, QMUL. Slides were covered with mounting media containing DAPI (Vector Laboratories) and coverslip, before visualisation on Axio Observer Z1 microscope using AxioVision software to observe GFP signal.

2.10.3 Whole mount aorta staining

Immediately after mice were euthanised, the vasculature was flushed with cold PBS. The aorta was excised, carefully removing the fat deposited on the vessel and aortic arch. The aorta was cut from the heart above the aortic sinus valves and branching vessels were removed in the arch, thorax and abdomen sections. Isolated aortas were placed in a petri dish with PBS and cleaned to remove all external deposits of fat using a dissecting microscope. The aorta were fixed overnight in 4% PFA and stored in 70% ethanol. Carefully the aortas were cut open longitudinally for en face Oil Red O staining. For staining, the aortas were placed into distilled H_2O and transferred into freshly prepared 3 mg/ml Oil Red O solution and incubated for 15 min at room temperature with agitation. The aortas were washed in 60% isopropanol for 5 min, repeated twice more and further transferred into distilled H_2O. Glycerol gelatin (Sigma) was used to mount the aortas onto the slides with coverslips before visualised using M205 FA microscope (Leica). Images of the aortas were analysed blindly using ImageJ to quantify the percentage lesion density.

2.10.4 *Ex vivo* confocal microscopy

Zbtb46^{GFP} mice were injected i.p. with fluorescently conjugated primary antibodies against LYVE-1 (eBioscience) and PECAM-1 (eBioscience) 4 hours prior to surgery. Mice were euthanised and the mesenteric organs including the associated VAT was exteriorised and fixed in 4% PFA for 10 min. The tissue was mounted on a home-built perplex stage and viewed using SP8 confocal microscope (Leica) with 20 x objective. Images were attained with the use of sequential scanning of different channels at every 0.52 µm of tissue depth at a resolution of 1024 x 470 pixels in the x & y plane, respectively and imaged at a zoom factor of x 2. Acquired confocal images were analysed using the 3D imaging analysis software IMARIS™ (bitplane, Switzerland).

2.11 Western blotting

2.11.1 Cell lysis

Cell lysates were generated from $CD11c^+$ isolated cells from spleen, pancreas, VAT and bone marrow using CelLytic M cell lysis reagent (Sigma) and combined phosphatase and proteinase inhibitors (Pierce). The cell pellet was resuspended in lysis buffer and sonicated for 10 sec before incubating on ice for 15 min. The lysed cells were centrifuged at 12,000 g for 15 min and the supernatant containing protein was transferred to a new tube. The protein concentration of the samples were quantified using the Bradford assay.

2.11.2 Bradford assay and sample preparation

The concentration of protein in the cell lysate samples were determined using Bradford reagent (Bio-Rad). BSA standards were prepared in PBS, with a serial 1:2 dilutions performed to generate a 7-point standard curve from 8 - 0.125 mg/ml. The standards and samples were added into a 96 well flat-bottom plate, diluted 1:200 with Bradford reagent. The plate was read at 595 nm absorbance using Spectrostar Omega reader and the protein concentration in the samples were interpolated from the standard curve using Prism 7. The measured cell lysates were normalised to the sample with the lowest protein concentration, to load 10 - 50 µg of protein. The loading mix was prepared containing; 3.75 µl of 4 x NuPAGE™ LDS sample buffer (Invitrogen), 1.5 µl of 10 x NuPAGE™ sample reducing agent (Invitrogen) and relevant volume of cell lysate and nuclease-free H_2O to give a total volume of 15 µl to load per well. The sample mix was heated at 70°C for 10 min.

2.11.3 Gel electrophoresis separation and transfer

The proteins were separated by SDS-PAGE using a mini protean precast gel (Bio-Rad). The gel was assembled into the running tank and a proper seal was ensured. The tank was filled with 1 x running buffer, containing 2.5 mM Tris base, 25 mM Glycine (Sigma) and 0.01% (w/v) SDS (Sigma). The comb from the gel was removed and 15 µl of denatured sample mix and pre-stained ladder (Bio-Rad) were loaded per well. The gel was run at 120V for approximately 1 hour at room temperature, until the blue dye front reached the bottom of the gel cassette.

The nitrocellulose membrane (GE Healthcare) and gel were equilibrated in 1 x transfer buffer, containing 2.5 mM Tris base, 25 mM Glycine and 1% (w/v) Methanol (Fisher). The transfer apparatus was assembled into the running tank and filled with 1 x transfer buffer. The transfer was run at 100V for 1.5 hours at room temperature.

2.11.4 Immunoblotting and visualisation

The membrane was washed in PBS-T for 5 min and blocked for 1 hour at room temperature. The blocking buffer contained PBS-T with 5% (w/v) blotting milk blocker (Bio-Rad). After the blocking step, the buffer was removed and the membrane was incubated with rabbit anti-mouse β-catenin antibody (Cell Signalling Technologies), rabbit anti-mouse non-phospho β-catenin (active) antibody (Cell Signalling Technologies) or rabbit anti-mouse p65 antibody (SantaCruz) overnight at 4°C. The primary antibody was diluted in PBS-T with 5% (w/v) milk, 1:1000 for β-catenin antibody or 1:200 for p65 antibody. After the incubation, the membrane was washed with PBS-T for 10 min and this was repeated twice more. The membrane was incubated with HRP-conjugated donkey anti-rabbit IgG antibody (GE Healthcare) for 1 hour at room temperature. The secondary antibody was diluted 1:2000 in PBS-T with 5% (w/v) milk. After the incubation, the membrane was washed with PBS-T for 10 min and repeated twice more. Blotted proteins were detected using Luminata™ Forte Western HRP substrate (Millipore) and exposed on to Hyperfilm™ photo film (Amersham) for visualisation. The membrane was subsequently probed for β-actin as a loading control following the same method, using rabbit anti-mouse β-actin antibody (Cell Signalling Technologies) diluted 1:1000. Density of the β-catenin or p65 bands was calculated relative to β-actin by ImageJ software.

2.12 Power calculations

The number of mice (sample size) required to obtain statistical difference with 90% of power depended on the assay performed; 5 mice were required for flow cytometry, qRT-PCR and ELISA experiments, 10 mice were required for metabolic assessments by GTT and ITT.

2.13 Statistical analysis

Statistical significance was determined by Student's two-tailed t-test with *p* values of 0.05 or less. For qRT-PCR, Student's t-test established statistical significance from normally distributed ΔCT data values, although data is represented in ΔΔCT format. For GTT, ITT and paired insulin measurements, statistical significance was evaluated with 2-way ANOVA followed by Bonferroni post-test. Data were analysed and charts were generated using Prism 7. Significant differences were denoted as $*p<0.05$, $**p<0.01$, $***p<0.001$ and n.s. not significant.

Chapter 3 Constitutive β-catenin pathway activation in conventional Dendritic cells modulates obesity-induced tissue inflammation

3.1 Introduction

The presence of the MHCII$^+$ CD11c$^+$ DC population in VAT has previously been reported, however a distinct role of cDCs in the tissue has yet to be fully defined. Collectively studies have suggested that MHCII$^+$ CD11c$^+$ DCs adopt an activated pro-inflammatory state in obesity (133) (134) (135). Interestingly, ablating all CD11c$^+$ cells attenuates VAT inflammation and promotes the recovery of glucose homeostasis in obese mice (132). However CD11c is expressed on various myeloid cells including tissue infiltrated macrophages and monocytes. Therefore with this phenotypic overlap the distinct contribution of cDCs in VAT inflammation has been poorly understood. Furthermore, there is limited understanding about the role of cDCs in tissue homeostasis in steady-state conditions. It has been suggested that AT-cDCs participate in antigen sampling to modulate immune responses and have the potential to control adipogenesis and lipogenesis of adipocytes through direct or indirect mechanisms, although this is yet to be clearly established (138) (136) (152). Although these initial findings indicate that cDCs are important in maintaining VAT function, the mechanisms regulating this process have yet to been identified in cDCs.

The Wnt/β-catenin pathway has emerged as an important regulator of adipogenesis and insulin sensitivity (65) (176) (177). Recent studies have shown a further link of Wnt/β-catenin pathway with the regulation of inflammation, particularly in cDCs where activation of the pathway is important for immune tolerance (185) (178). However it has yet to be examined if this dependence on Wnt/β-catenin for tolerogenic signalling is tissue specific. Interestingly, transcriptome data indicates that the Wnt/β-catenin is upregulated in cDC1

subset present in VAT. Transcriptome raw data files are publicly available at http://www.immgen.org/ GEO: GSE37448. Thus we hypothesised that Wnt/β-catenin pathway in cDCs would play role in maintaining VAT homeostasis. Additionally during obesity, the levels of Wnt10b are known to be supressed implying that the activity of the Wnt/β-catenin pathway may be impaired in obese VAT (65). Consequently we further proposed that sustaining Wnt/β-catenin pathway activation in VAT-cDCs could ameliorate the development of obesity-induced tissue inflammation and revert the associated insulin resistance (IR).

In this chapter the role of Wnt/β-catenin signalling in cDCs is investigated to explore the effect on cDC phenotype, immune responses and implications on VAT metabolism during tissue homeostasis and in diet-induced tissue inflammation. Furthermore systemic effects on whole-body glucose homeostasis are assessed in the development of obesity-associated IR.

3.2 Results

3.2.1 cDCs are present in VAT in close proximity to vessels

Overlap of cell surface marker expression has hindered the study of cDCs in VAT. Although high expression of MHCII and CD11c defines the cDC population, CD11c has also been used to identify inflammatory ATMs (132) thus this promiscuous expression in myeloid cells has rendered the role of VAT-cDCs elusive. To understand the distinct contribution of cDCs *in vivo*, new reporter mice have recently been generated based on the expression of the highly cDC-specific *Zbtb46* promoter (191). *Zbtb46* is a transcription factor which is selectively expressed by cDCs and their committed progenitors, but not expressed in pDCs or other myeloid lineages (192). *Zbtb46*^{GFP} and *Zbtb46-Cre* mice have been used to characterise the role of VAT-cDCs in homeostatic conditions and explore the mechanisms that control their immune function (193).

Mesenteric VAT and vessels from *Zbtb46*^{GFP} mice were imaged by *ex vivo* confocal microscopy, showing the close proximity of GFP^{+} cDCs to PECAM-1^{+}

capillary vessels and LYVE-1^{+} initial lymphatic vessel in VAT (Figure 3.1A). This strategic location is consistent with a proposed role of cDCs to sample antigens in VAT (138). Kuan *et al.* observed that collecting lymphatic vessels had an inherent permeability and that cDCs in the surrounding VAT are closely associated with these vessels in order to uptake soluble antigens released from the lymph. These findings support a role for VAT-cDCs for the immune surveillance of neighbouring tissue in homeostatic conditions.

3.2.2 The Wnt/β-catenin pathway is upregulated in VAT-cDC1

cDCs are present in two main subsets in VAT, cDC1 (CD103^{+}) and cDC2 (CD11b^{+}), which vary in function, transcriptome profile and lineage markers (118). Following gene set enrichment pathway analysis (GSEA) it was observed that these populations selectively upregulate distinct adipocyte-specific pathways in VAT, specifically Wnt/β-catenin pathway in cDC1 and PPARγ pathway in cDC2 (193). The protein expression of active β-catenin was increased in *Zbtb46*$^{GFP+}$ sorted VAT-cDC1, while higher levels of PPARγ expression was observed in *Zbtb46*$^{GFP+}$ sorted VAT-cDC2 population (Figure 3.1B). PPARγ is known to regulate lipid accumulation during hypertrophy controlling adipocyte expansion, while the Wnt/β-catenin pathway controls adipocyte hyperplasia (58) (64). Thus, the upregulation of these pathways in cDCs is proposed in order to "sense" changes in tissue homeostasis.

To investigate if, similar to other tissues, activation of the Wnt/β-catenin pathway in cDC1 is important for controlling inflammation, cell-sorted cDC1 isolated from spleen and VAT of *Zbtb46*^{GFP} mice were incubated overnight with TLR4 agonist Glucopyranosyl Lipid A (GLA) in the presence of Wnt/β-catenin pathway agonist SB216763 (SB) (194). Activation of the pathway in cDC1 population suppressed TLR4-induced inflammatory responses, demonstrated by the significant reduction of pro-inflammatory IL-6 release and significant increase in production of anti-inflammatory IL-10 (Figure 3.1C&D). This effect was observed in cDC1 from VAT, but not spleen. Therefore in steady-state, this data supports the hypothesis that activation of the β-catenin pathway in cDC1 sustains a

tolerogenic phenotype in VAT, inhibiting local inflammation and contributing to the maintenance of tissue immune-homeostasis.

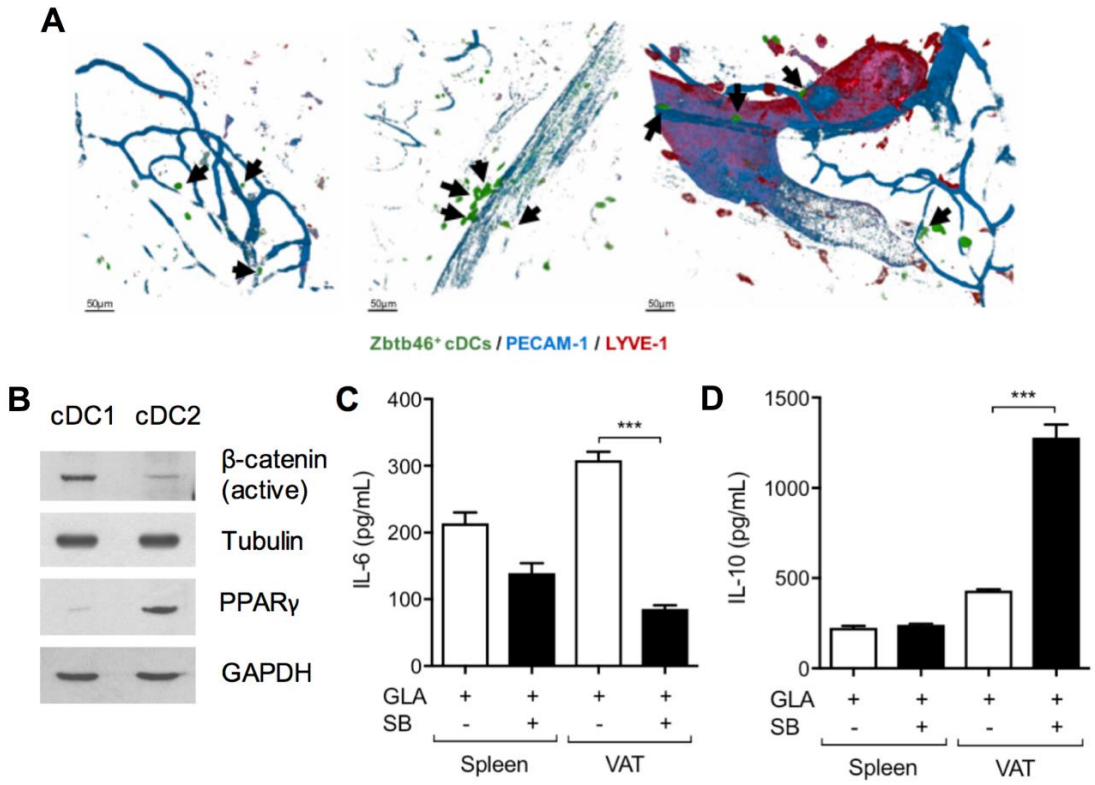

Figure 3.1 VAT-cDCs acquire a tolerogenic phenotype to suppress inflammation
(A) Mesenteric VAT and vessels from *Zbtb46*^{GFP} mice were imaged by *ex vivo* confocal microscopy and visualized using a Leica SP8 confocal microscope. GFP^{+} cDCs (green) located in close proximity (black arrows) to PECAM-1^{+} capillary vessels (blue) in VAT (left and central image) but also close to mesenteric afferent lymphatics (LV, middle picture) and LYVE-1^{+} initial lymphatic vessels (red) near the gut (right image). (B) cDC1 and cDC2 populations were sorted from VAT of *Zbtb46*^{GFP} mice. Expression of active β-catenin and PPARγ was detected by western blot, shown as a representative of three independent experiments. (C) cDC1 cells sorted from VAT and spleen of *Zbtb46*^{GFP} mice, were incubated overnight with 5 µg TLR4 agonist GLA with or without 20 µM β-catenin pathway agonist (SB). Levels of IL-6 (C) and IL-10 (D) in the supernatant were measured by ELISA. Bars represent the mean ± SEM and graphs shown are representative of three independent experiments (n=9). Statistical significance was determined by Student's two-tailed t-test, results not significant unless otherwise denoted as *p<0.05, ***p*<0.01, ****p*<0.001,

3.2.3 Wnt/β-catenin pathway in VAT-cDC1 controls tissue inflammation *in vivo*

To assess the role of Wnt/β-catenin pathway in cDC1 *in vivo*, floxed β-catenin *Ctnnb1*$^{Fl/Fl}$ mice were crossed with transgenic *Zbtb46-Cre* mice to generate a knockdown model. Unexpectedly, β-catenin deletion was lethal due to *Zbtb46* off-target expression in non-hematopoietic cells. To bypass this issue, chimeric mice

were generated using fetal liver cells from conditional cDC-specific β-catenin knockdown mice or littermate control mice, hence forth referred to as β-catenin knockdown mice or WT control mice respectively (Figure 2.1). Thus, in this model only cDCs express *Zbtb46* and therefore β-catenin was only knocked down in cDCs. To understand the effect on VAT immune homeostasis, mRNA expression in VAT from β-catenin knockdown mice and WT control mice was measured by qRT-PCR. In steady state conditions where mice were fed normal chow diet (ND) and in the absence of tissue inflammation, the levels of IL-10 were significantly decreased in β-catenin knockdown mice compared to the WT (Figure 3.2A). This suggests that deletion of β-catenin in cDCs decreases anti-inflammatory phenotype in homeostatic conditions, supporting previous data that β-catenin prevents the onset of inflammation through IL-10 production. Interestingly, IL-10 is known to supress cDC maturation (195).

The association between obesity and low-grade chronic inflammation has been well described. Inflammatory responses in VAT are known to play a causal role in obesity-induced IR (35). To understand the effect the β-catenin in cDCs in the control of obesity-induced VAT inflammation, β-catenin knockdown mice and WT control mice were fed western diet (WD) for 12 weeks. WD is formulated to represent typical Western nutrition, including increased levels of cholesterol, saturated fats, salt and sugar (Table 2.1). This enables the translation of mouse models for diet-induced obesity research. qRT-PCR analysis of VAT from mice fed WD, demonstrated a significant decrease in IL-10 mRNA levels in β-catenin knockdown mice compared to WT mice (Figure 3.2B). This was accompanied by a significant increase in the T cell chemoattractant CCL17 production, reduction in IFNγ and a switch to IL-17A T cell responses in VAT of β-catenin knockdown mice. This suggests that cDC-specific deletion of β-catenin alters T cell responses in VAT, which is associated with increased inflammation. Furthermore levels of the pro-inflammatory cytokine IL-6 was increased in line with previous data, suggesting that β-catenin pathway activation in cDCs is important for delaying the onset of pro-inflammatory responses in obesity. In addition, the mRNA expression of adiponectin, which is expressed by adipocytes, was significantly reduced, indicating some degree of adipocyte dysfunction in VAT of β-catenin knockdown mice. These findings were replicated in the mRNA analysis of the stromal vascular fraction (SVF), the compartment of VAT where immune

cells reside (Figure 3.2C). These observations strongly support that β-catenin abrogation in cDC population exacerbates obesity-induced VAT inflammation.

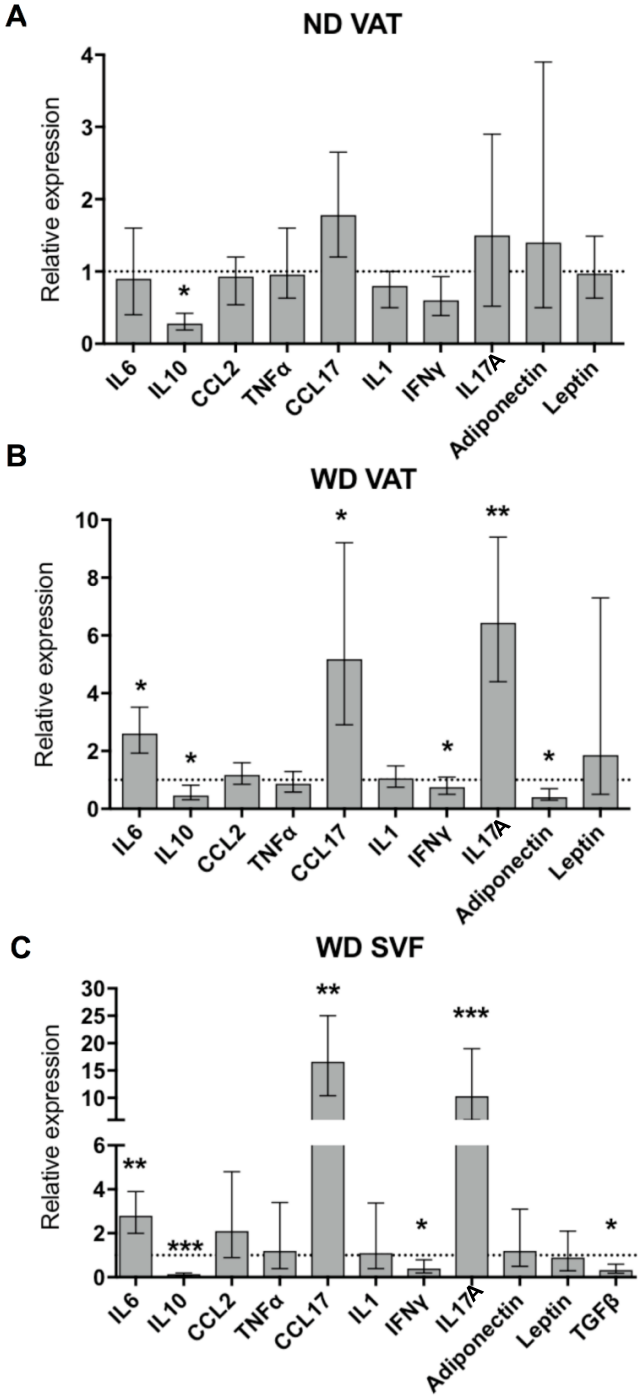

Figure 3.2 Deletion of β-catenin in cDCs modulates the inflammatory state of VAT qRT-PCR analysis for the mRNA expression in VAT of β-catenin knockdown and WT mice fed ND (A) or 12 weeks of WD (B). Similarly mRNA expression was analysed in SVF of β-catenin knockdown and WT mice fed 12 weeks of WD (C). Expression levels of all mRNA were normalised to GAPDH expression. Bars represent ΔΔCT data values, the expression in β-catenin knockdown mice compared to WT, set at 1 indicated by the dotted line. Error bars show the geometric mean of ten biological replicates for VAT and five for SVF. Statistical significance of ΔCT data values was determined by Student's two-tailed t-test, results not significant unless otherwise denoted as *p<0.05, ***p*<0.01, ****p*<0.001.

3.2.4 Impaired Wnt/β-catenin pathway in cDC1 in obese VAT

A single nucleotide polymorphism in the human *Wnt10b* gene has been associated with early-onset familial obesity (196). During obesity it is proposed that Wnt ligand availability diminishes in VAT, specifically Wnt10b levels are suppressed in obesity, which inhibits preadipocyte differentiation enabling adipocyte hyperplasia (65). Significant reduction of Wnt10b was confirmed at the transcriptional level in VAT from mice fed WD (Figure 3.3A). This suggests that the activity of the Wnt/β-catenin pathway could be impaired in cDC1, in part contributing to the development of VAT inflammation after long-term chronic nutrition. Indeed, reduced active β-catenin protein expression was observed in *Zbtb46*$^{GFP+}$ sorted VAT-cDC1 from WD compared to ND fed mice (Figure 3.3B). This was not due to a defective pathway, as VAT-cDC1 were still able to respond to β-catenin pathway agonist SB when cultured *ex vivo*, albeit at lower levels reflecting the activated-state of cDCs in VAT. A significant reduction of IL-6 and increase in IL-10 levels were measured from the supernatants of incubated VAT-cDC1 (Figure 3.3C&D). Hence during obesity, activation of the β-catenin pathway is reduced, fuelling cDC activation and VAT inflammation.

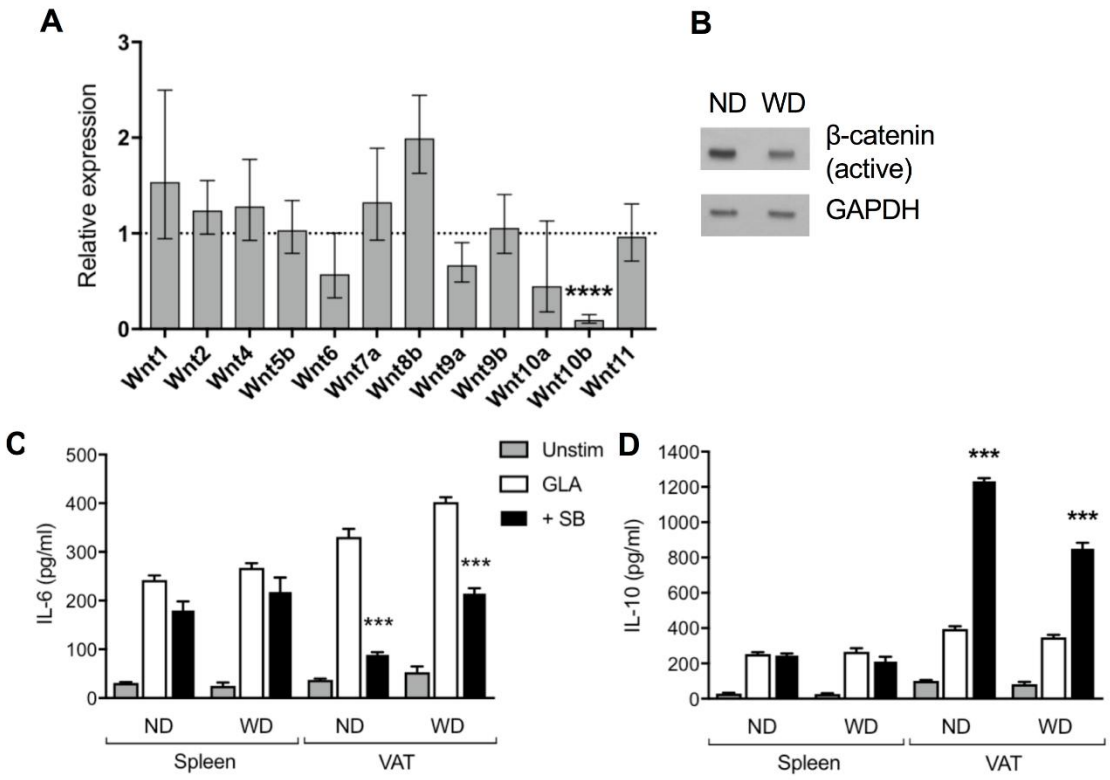

Figure 3.3 Chronic over-nutrition reduces Wnt/β-catenin pathway activation in VAT-cDCs

Zbtb46^{GFP} mice were fed ND or WD for 12 weeks. (A) qRT-PCR analysis for the mRNA expression of Wnt ligands in VAT of mice fed ND compared to WD. Expression levels of all mRNA were normalised to GAPDH expression. Bars represent ΔΔCT data values, the expression in WD fed mice compared to mice fed ND, set at 1 indicated by the dotted line. Error bars show the geometric mean of five biological replicates. Statistical significance of ΔCT data values was determined by Student's two-tailed t-test, results not significant unless otherwise denoted as *p<0.05, **p<0.01, ***p<0.001. (B) cDC1 cells were sorted from VAT of *Zbtb46*^{GFP} mice fed ND or WD. Expression of active β-catenin was detected by western blot, shown as a representative of three independent experiments. (C) cDC sorted from VAT and spleen of *Zbtb46*^{GFP} mice fed ND or WD, were incubated overnight with 5 µg TLR4 agonist GLA with or without 20 µM β-catenin pathway agonist (SB) or DMSO control (Unstim). Levels of IL-6 (C) and IL-10 (D) in the supernatant were measured by ELISA. Bars represent the mean ± SEM and graphs shown are representative of three independent experiments (n=9). Statistical significance was determined by Student's two-tailed t-test, results not significant unless otherwise denoted as *p<0.05, **p<0.01, ***p<0.001.

3.2.5 Generation of a mouse model with constitutive activation of the β-catenin pathway in cDCs

The previous data suggests that sustained activation of β-catenin signalling in cDCs could ameliorate the development of tissue inflammation and IR during obesity. To investigate this, a mouse model was generated with constitutive expression of degradable resistant form of active β-catenin (*Ctnnb1*$^{lox(ex3)/+}$) (187) in the cDCs (*Zbtb46-Cre*$^{+}$) (191). *Zbtb46-Cre*$^{/+}$ mice were crossed with *Ctnnb1*$^{lox(ex3)/+}$ mice, where Lox/Cre-dependent deletion of exon 3 prevents the phosphorylation and degradation of β-catenin, rendering the Wnt/β-catenin pathway constitutively active. Due to expression of *Zbtb46* in non-hematopoietic cells, mice died between 3-4 weeks of birth. Thus bone marrow chimeras were generated, where bone marrow cells from *Ctnnb1*$^{lox(ex3)/+}$ *Zbtb46-Cre*$^{/+}$ (gain-of-function, GOF) or littermate controls *Ctnnb1*$^{lox(ex3)/+}$ *Zbtb46*$^{+/+}$ (wild type, WT) were transferred into irradiated C57BL/6 recipient mice, hence forth referred to as GOF mice or WT mice respectively (Figure 2.2). In the GOF mice, only cDCs express *Zbtb46* and hence specifically express constitutively active β-catenin. Increased expression of β-catenin in cDCs was confirmed in VAT and bone marrow of the GOF mice by western blot and densitometry analysis (Figure 3.4A&B).

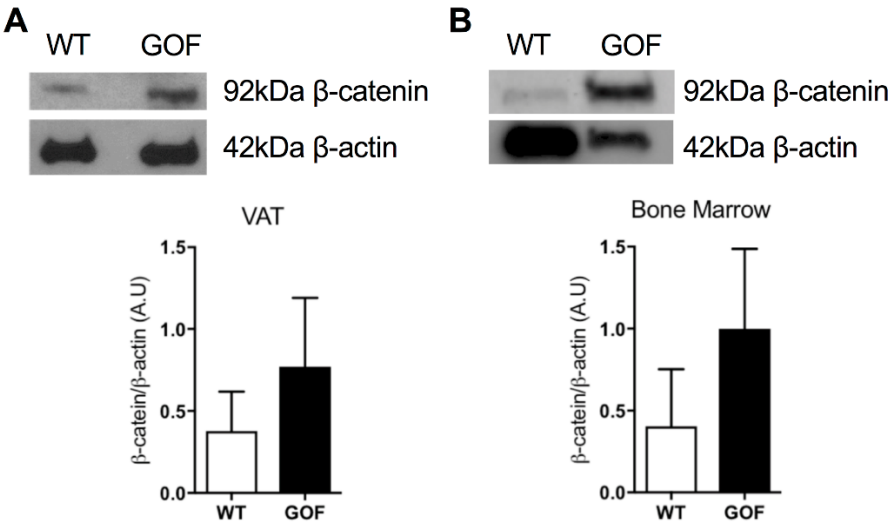

Figure 3.4 Overexpression of β-catenin in the GOF model
CD11c^{+} DCs were isolated from VAT (A) and from Flt3L-bone marrow cultures (B) of WT and GOF mice. Expression of β-catenin was detected by western blot, shown as a representative of three independent experiments. Expression of β-catenin was normalised to β-actin expression by densitometry analysis, mean ± SEM (n=3). Statistical significance was determined by Student's two-tailed t-test, results not significant.

3.2.6 Constitutive β-catenin activation in cDCs modulates the immune phenotype in homeostatic conditions

Activation of β-catenin signalling has emerged as a mechanism for inducing tolerogenic DCs. To understand the effects of constitutive β-catenin activation in cDCs in homeostatic conditions, chimeric GOF and WT control mice were fed ND. Both groups of mice increased in body weight at the same rate over time (Figure 3.5A). Similarly, there was no difference observed in total (Figure 3.5B) or percentage (Figure 3.5C) of VAT weight between GOF and WT mice fed ND. Constitutive activation of β-catenin in cDCs does not impact body and VAT weight in steady state, which is not surprising as VAT inflammation would be minimal and locally restrained by the resident anti-inflammatory immune network.

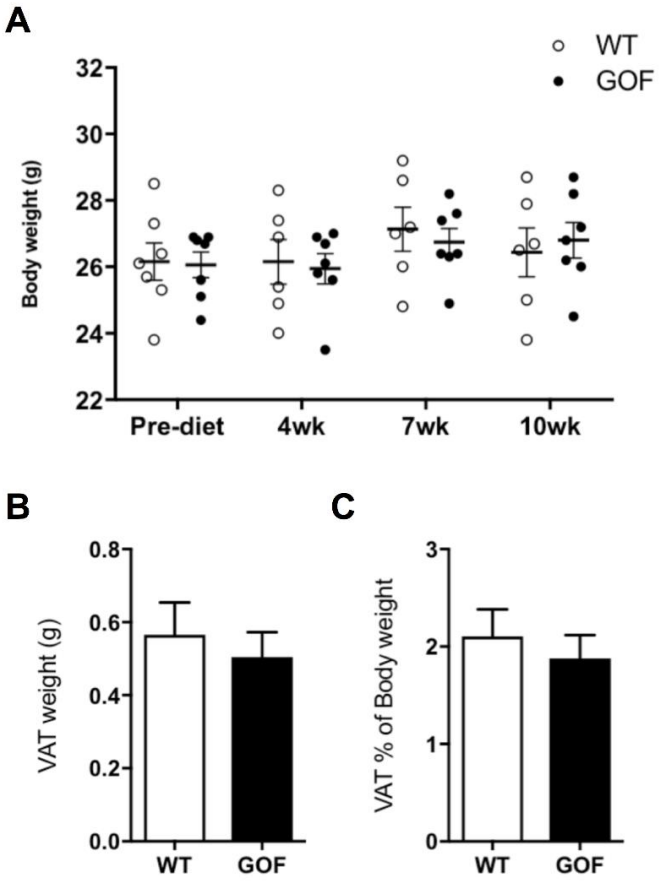

Figure 3.5 Body and VAT weight measures in the GOF model in homeostatic conditions
GOF and WT mice were fed ND. (A) Body weight was measured over the duration of 10 weeks, mean ± SEM (n=6/7). (B) Total VAT from GOF and WT mice was harvested and weighed, mean ± SEM (n=6/7). (C) VAT content was calculated as percentage of body weight, mean ± SEM (n=6/7). Statistical significance was determined by Student's two-tailed t-test, results not significant.

To examine the impact of constitutive β-catenin activation in cDCs on the steady state immune phenotype, flow cytometry staining was used to quantify immune cell numbers in the VAT, spleen, mesenteric draining lymph nodes and inguinal non-draining lymph nodes of GOF and WT mice. The gating strategy detailed previously was used to analyse the immune populations (Figure 2.4). In addition, the mRNA expression of cytokines, chemokines and adipokines were measured in VAT and SVF by qRT-PCR.

The spleen is an important lymphoid organ, it is the site for the initiation of the immune responses by lymphocytes in response to DCs presenting antigens found circulating in the blood. By measuring immune populations in the spleen this provides an understanding of systemic immune health of the whole organism. Furthermore a caveat of the GOF model is that constitutively active β-catenin in cDCs is expressed systemically, not exclusively in VAT where it was initially observed to maintain tissue inflammation. Similar systemic effects would be observed during therapeutic drug treatments. Constitutive activation of β-catenin in cDCs induced a significant increase in total number of NK cells and a decrease in total macrophage numbers, albeit not significant, in the spleen (Figure 3.6A). Interestingly the ratio of T reg cells in $CD4^+$ T cell population was significantly increased in the GOF mice compared to WT mice, implicating a wider change in T reg cell homeostasis (Figure 3.6A). However, there were no changes in the cytokine expression of $CD4^+$ T cell population, indicative of helper T cell subsets, nor in the production of T cell chemoattractant CCL17 from cDCs *ex vivo* between the GOF and WT mice in steady state (Figure 3.6B&C). The production of IL-6 from splenic cDCs cultured *ex vivo* was decreased and the levels of IL-10 secreted were marginally elevated in the GOF mice indicating a potential tolerogenic phenotype of cDC, although these observations were not significant (Figure 3.6D&E). The numbers of immune populations in the mesenteric draining lymph nodes and inguinal lymph nodes were not significantly altered between the GOF and WT mice in steady state (Figure 3.7 & Figure 3.8).

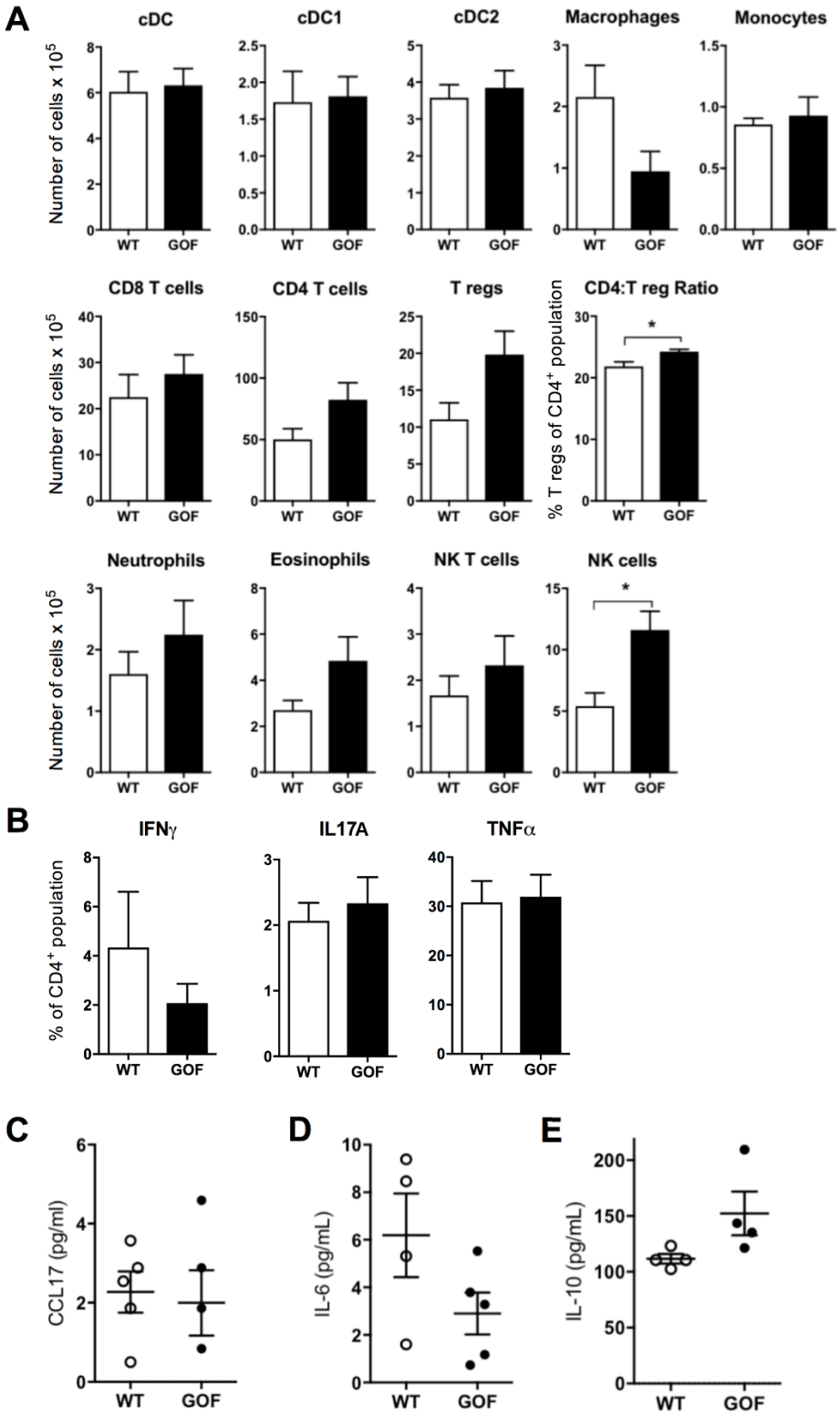

Figure 3.6 Immune phenotype in the spleen of the GOF model in homeostatic conditions

Spleens from GOF and WT mice fed ND, were digested. (A) Total numbers of immune populations in the spleen were quantified by flow cytometry, mean ± SEM (n=4). (B) Percentage of IFNγ, IL-17A, TNFα -expressing $CD4^+$ T cells were quantified by flow cytometry, mean ± SEM (n=5). $CD11c^+$ DCs were isolated from the spleen of GOF and WT mice and cultured overnight. (C) CCL17, (D) IL-6 and (E) IL-10 were measured in supernatant by ELISA, mean ± SEM (n=3). Statistical significance was determined by Student's two-tailed t-test, results not significant unless otherwise denoted as *p<0.05.

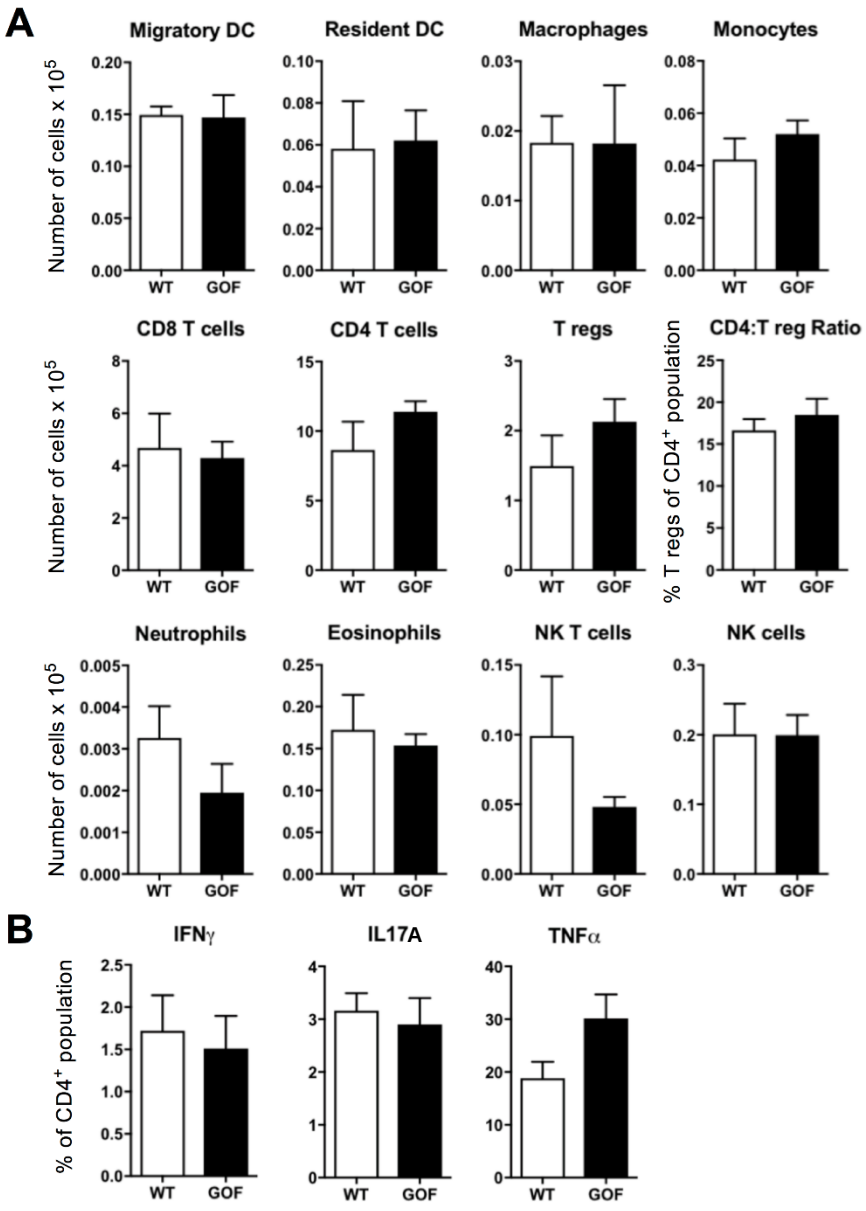

Figure 3.7 Immune phenotype in the draining lymph nodes of the GOF model in homeostatic conditions

Mesenteric draining lymph nodes from GOF and WT mice fed ND, were digested. (A) Total numbers of immune populations in the draining lymph nodes were quantified by flow cytometry, mean ± SEM (n=3). (B) Percentage of IFNγ, IL-17A, TNFα -expressing $CD4^+$ T cells were quantified by flow cytometry, mean ± SEM (n=3). Statistical significance was determined by Student's two-tailed t-test, results not significant.

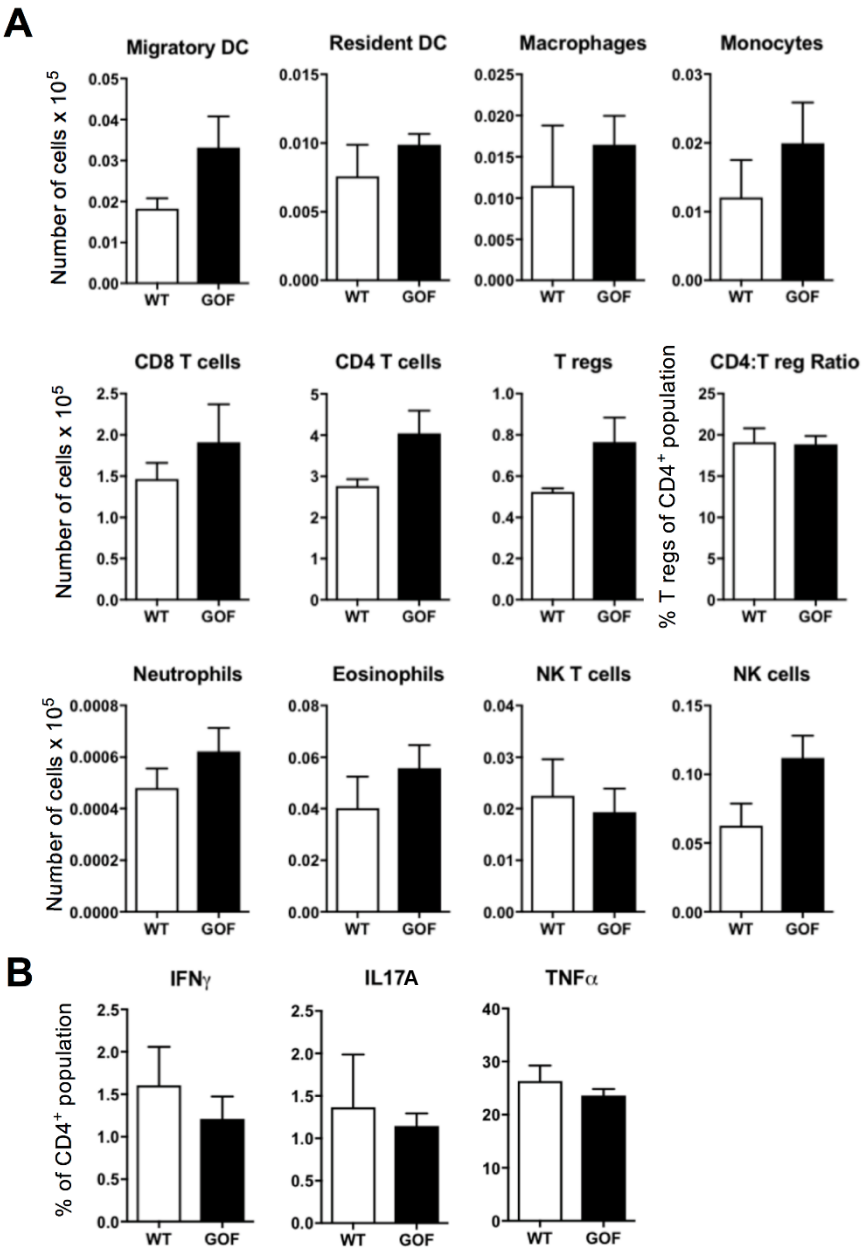

Figure 3.8 Immune phenotype in the non-draining lymph nodes of the GOF model in homeostatic conditions

Inguinal non-draining lymph nodes from GOF and WT mice fed ND, were digested. (A) Total numbers of immune populations in the non-draining lymph nodes were quantified by flow cytometry, mean ± SEM (n=4). (B) Percentage of IFNγ, IL-17A, TNFα -expressing $CD4^+$ T cells were quantified by flow cytometry, mean ± SEM (n=3). Statistical significance was determined by Student's two-tailed t-test, results not significant.

Interestingly there is a suggestion that constitutive β-catenin activation in cDCs modulates the T cell composition in VAT during homeostatic conditions. The total numbers of $CD4^+$ T cells and T reg cells were significantly increased in GOF mice compared to WT, despite no difference in the ratio (Figure 3.9A-C). Furthermore, in the GOF mice there was a significant decrease in T cell chemoattractant CCL17 production in VAT and increase in FOXP3 expression in SVF, as measured by qRT-PCR analysis (Figure 3.9D&E). The chemokine CCL17 is known to recruit $CCR4^+$ inflammatory T cells and restrict the recruitment of T reg cells (197) (198) (199). This suggests an altered recruitment of T cell populations in VAT of GOF mice at steady state. In addition mRNA levels of IL-17A, but not IFNγ, were also significantly increased in the SVF of GOF mice (Figure 3.9E), which has been recently linked with the accumulation of T reg cells in AT by tissue-resident population of γδ T cells (200). Overall these findings suggest that constitutive β-catenin activation in cDCs enables a T cell driven immunosuppressive phenotype in VAT in homeostatic conditions.

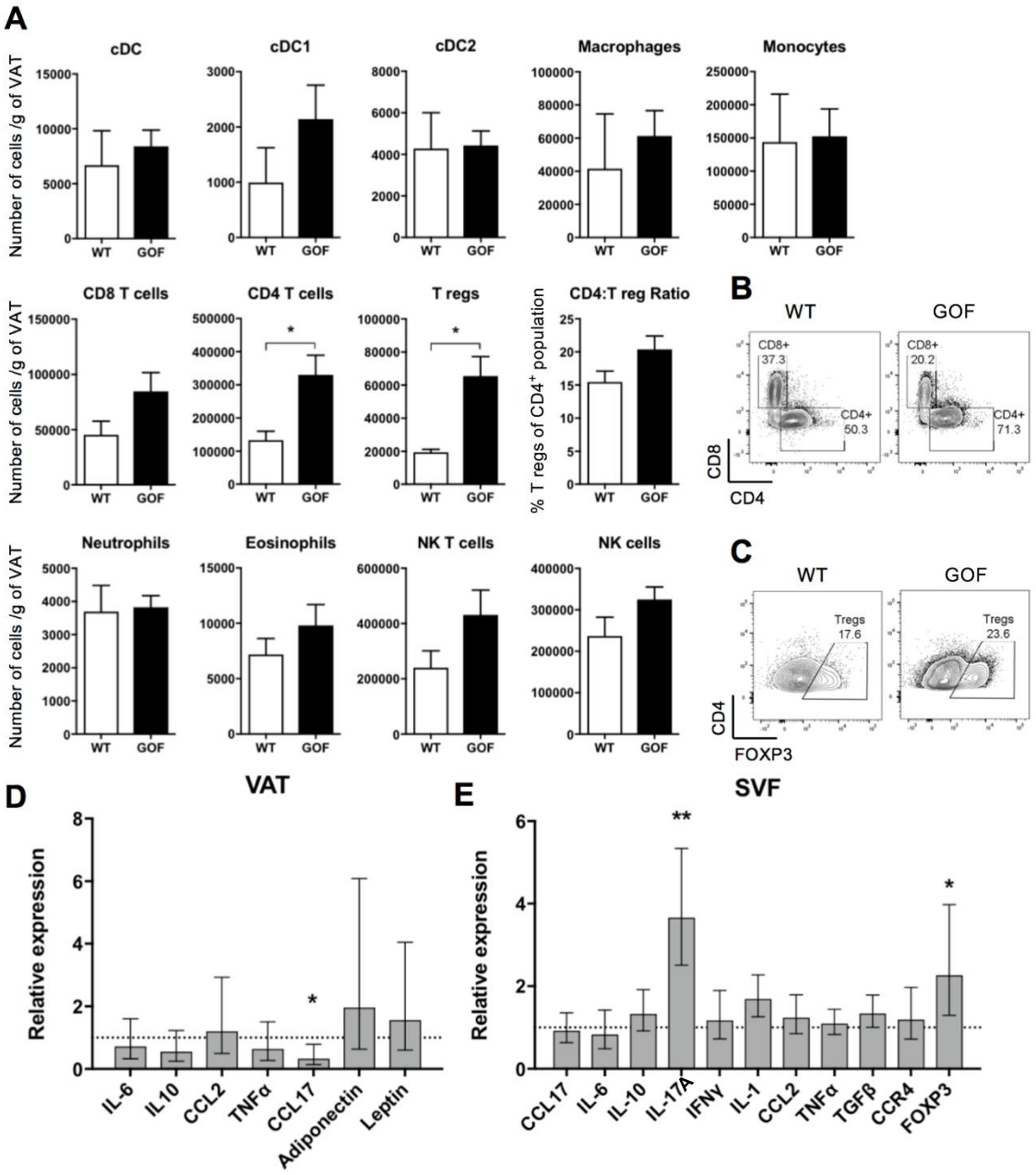

Figure 3.9 Immune phenotype in the VAT of the GOF model in homeostatic conditions

VAT was digested from GOF and WT mice fed ND. (A) Total numbers of immune populations in the VAT were quantified by flow cytometry, mean ± SEM (n=4). Representative dot plots of $CD3^+$ T cell population with gates on $CD8^+$ and $CD4^+$ T cells (B) and T reg cells (C), from VAT of GOF and WT mice. Statistical significance was determined by Student's two-tailed t-test, results not significant unless otherwise denoted as *p<0.05. qRT-PCR analysis for mRNA expression in VAT (D) and SVF (E) of GOF and WT mice. Expression levels of all mRNA were normalised to GAPDH expression. Bars represent ΔΔCT data values, the expression in GOF mice compared to WT, set at 1 indicated by the dotted line. Error bars show the geometric mean of six biological replicates. Statistical significance of ΔCT data values was determined by Student's two-tailed t-test, results not significant unless otherwise denoted as *p<0.05, **p<0.01.

3.2.7 Constitutive β-catenin activation in cDCs modulates the immune phenotype in Western diet-induced tissue inflammation

To investigate the hypothesis that constitutive β-catenin pathway activation in cDCs could revert the development of tissue inflammation during obesity, GOF and WT mice were fed WD for 16 weeks. WD induces chronic inflammation in VAT and enables translation of mouse models for diet-induced obesity research. Body weight of both groups of mice increased at the same rate over time (Figure 3.10A). The VAT harvested from mice fed 16 weeks of WD demonstrated no difference in weight between the GOF and WT (Figure 3.10B), additionally this remained unchanged when calculated as percentage of the body weight (Figure 3.10C).

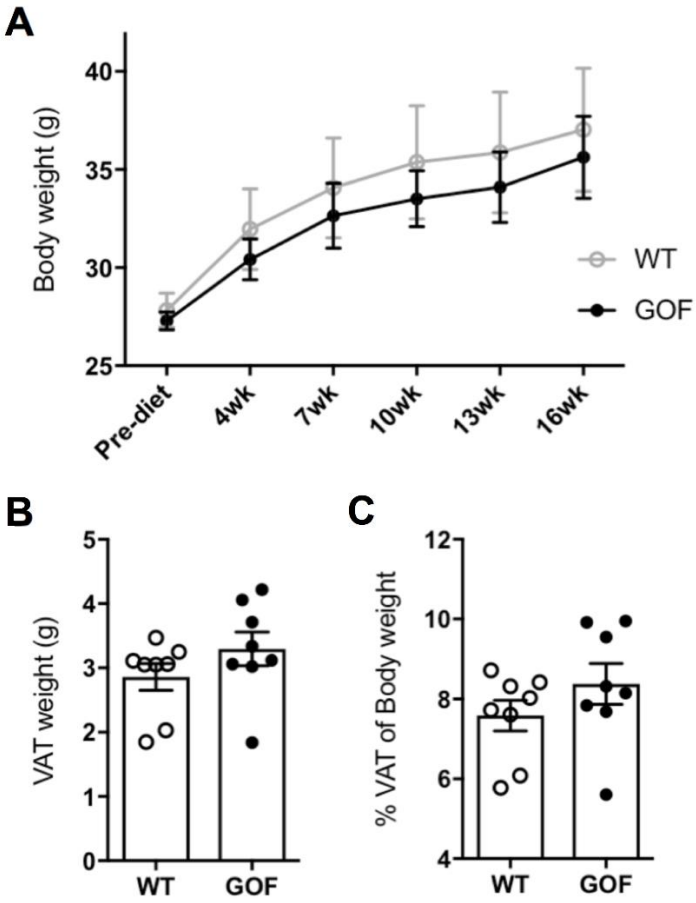

Figure 3.10 Body and VAT weight measure of the GOF model in inflammation
GOF and WT mice were fed WD. (A) Body weight was measured over the duration of 16 weeks, mean ± SEM (n=8). (B) Total VAT from GOF and WT mice was harvested and weighed, mean ± SEM (n=8). (C) VAT content was calculated as percentage of body weight, mean ± SEM (n=8). Statistical significance was determined by Student's two-tailed t-test, results not significant.

To assess the effect of constitutive β-catenin activation in cDCs on the immune phenotype during inflammation, the mRNA expression of cytokines, chemokines and adipokines were measured in VAT and SVF by qRT-PCR. During obesity, a shift in $CD4^+$ T cell subsets has been well described, with the expansion of activated Th1, Th17 populations and a reduction of Th2 cells and T reg cells (201). The expression of FOXP3 was significantly increased in the SVF of GOF mice, as measured by qRT-PCR analysis (Figure 3.11A) indicating a greater T reg population. This was accompanied by a significant decrease in the T cell chemoattractant CCL17 production in VAT of GOF mice (Figure 3.11B). Interestingly, cDC-derived CCL17 has been shown to promote tissue inflammation by restricting T reg cell recruitment (198). A significant reduction in IFNγ mRNA expression in VAT of GOF mice further confirmed a modulation of VAT-T cell responses by constitutive β-catenin activation in cDCs (Figure 3.11B). In the GOF model, an immunosuppressive environment in the tissue is clearly induced as evidenced by the significant increase in IL-10 and adiponectin expression in the SVF and VAT of the GOF mice respectively (Figure 3.11A&B). These results echo the observations in steady state that constitutive β-catenin activation in cDCs promotes a trend towards a T cell driven immunosuppressive phenotype, to restore the anti-inflammatory immune network in VAT in GOF mice.

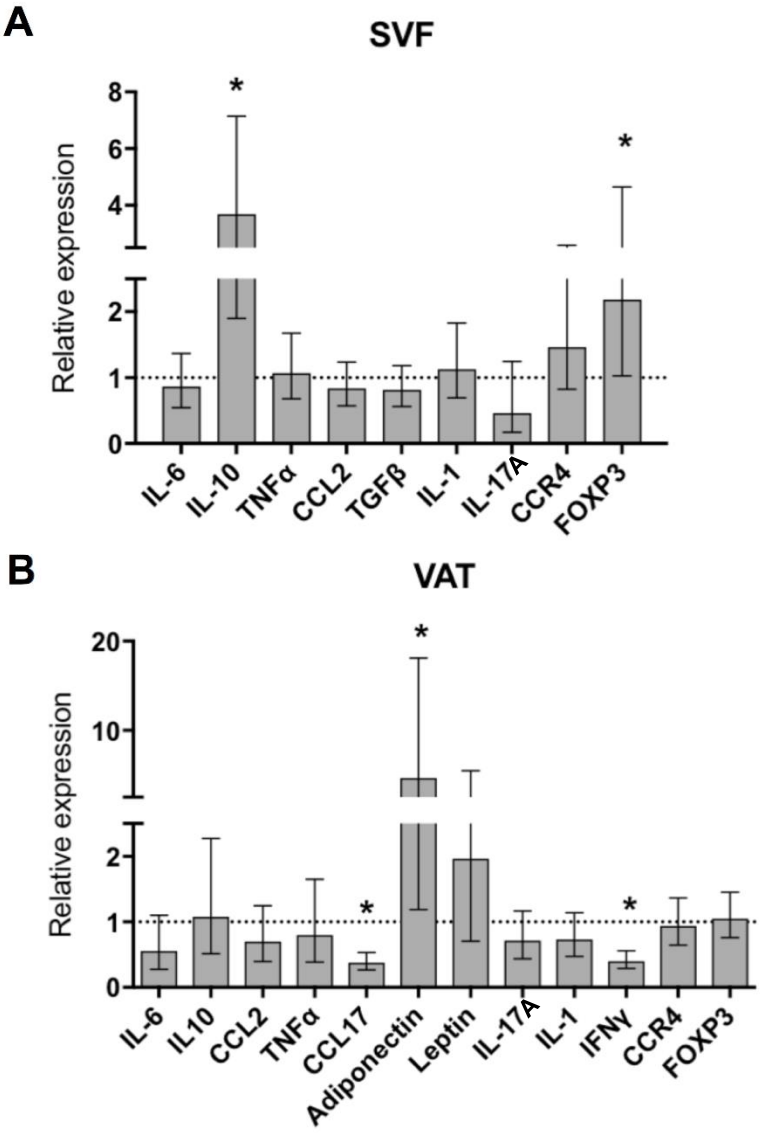

Figure 3.11 mRNA expression in the VAT of the GOF model in inflammation
VAT was digested from GOF and WT mice fed 16 weeks of WD, to induce chronic low-grade tissue inflammation. qRT-PCR analysis for mRNA expression in SVF (A) and VAT (B) of GOF and WT mice. Expression levels of all mRNA were normalised to GAPDH expression. Bars represent ΔΔCT data values, the expression in GOF mice compared to WT, set at 1 indicated by the dotted line. Error bars show the geometric mean of six biological replicates. Statistical significance of ΔCT data values was determined by Student's two-tailed t-test, results not significant unless otherwise denoted as *p<0.05.

The previous data indicates at the mRNA level the T cell phenotype is modulated in the GOF model. Immune cell populations in the VAT, spleen, mesenteric draining lymph nodes, inguinal non-draining lymph nodes and blood of GOF and WT mice, were analysed by flow cytometry staining. The gating strategy detailed previously was used to analyse the immune populations (Figure 2.4). In VAT, there is a suggestion that cDCs with constitutively activated β-catenin drives a T cell driven immunosuppressive phenotype. The ratio of T reg cells in the $CD4^+$ T cell population showed a trend towards an increase in the GOF mice compared to the WT, although there were no significant changes in the abundance of $CD4^+$ T cells or T reg cells (Figure 3.12A). Trends towards an increase in naïve T cell population and decrease in the percentage of IFNγ, IL-17A, TNFα -expressing $CD4^+$ T cells were also observed in the GOF mice compared to WT (Figure 3.12A&B). Furthermore, there was a suggestion that the population of central memory T cells was increased in VAT of the GOF mice (Figure 3.12A). In fact this population may simply be maintained in the GOF model, as it has recently been reported that VAT harbours a large population of memory T cells with long-term protective functions during homeostasis (106). While in VAT of WT mice the numbers of memory T cells may potentially decrease during the development of tissue inflammation. Modulation of the innate immune populations were also observed in VAT of the GOF mice. Constitutive activation of β-catenin in cDCs reduced the infiltration of macrophages, neutrophils and monocytes, albeit not significantly (Figure 3.12A). Interestingly there was a trend towards an increase of total numbers of the cDC1 population in VAT of GOF mice, despite no differences in total numbers of cDCs or the cDC2 population (Figure 3.12A). These observations were in concordance with previous models of constitutive expression of active β-catenin in $CD11c^+$ populations, where β-catenin has shown to direct the development of cDC1 by activating IRF8 (202).

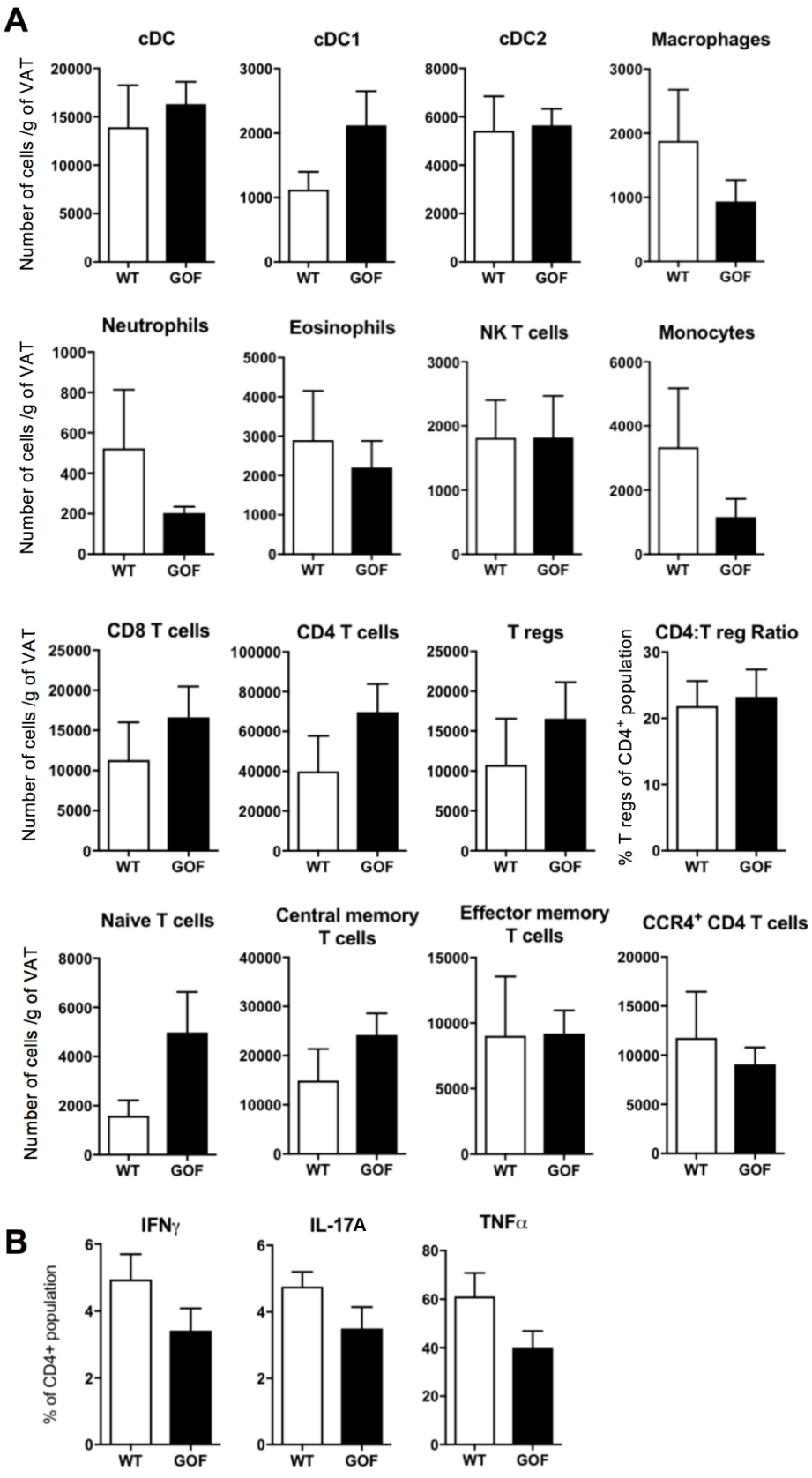

Figure 3.12 Immune phenotype of the VAT in the GOF model in inflammation
VAT was digested from GOF and WT mice fed 16 weeks of WD, to induce chronic low-grade tissue inflammation. (A) Total numbers of immune populations in the VAT were quantified by flow cytometry, mean ± SEM (n=4). (B) Percentage of IFNγ, IL-17A, TNFα -expressing $CD4^+$ T cells were quantified by flow cytometry, mean ± SEM (n=5). Statistical significance was determined by Student's two-tailed t-test, results not significant.

The spleen of GOF mice fed WD reflected similar modulations of immune cell populations as observed in VAT. Total numbers of neutrophils were significantly reduced, indicating a decrease in systemic inflammation in the GOF mice (Figure 3.13A&C). A significant increase in the total number of cDC1 cells was observed in the spleen of GOF mice (Figure 3.13A&B), confirming previous observations in similar models (202). In addition the splenic T reg population was significantly expanded in the GOF mice compared to WT (Figure 3.13A&D). Although there was no difference in the ratio of T reg cells in the $CD4^+$ T cell population between GOF and WT mice, nor in the abundance of other T cell populations (Figure 3.13A&B). Interestingly, the production of IL-12 from splenic DCs derived from GOF mice was significantly decreased, in the presence or absence of LPS indicating that constitutive activation of β-catenin in cDCs promotes a potential tolerogenic responses upon an inflammatory challenge (Figure 3.13F).

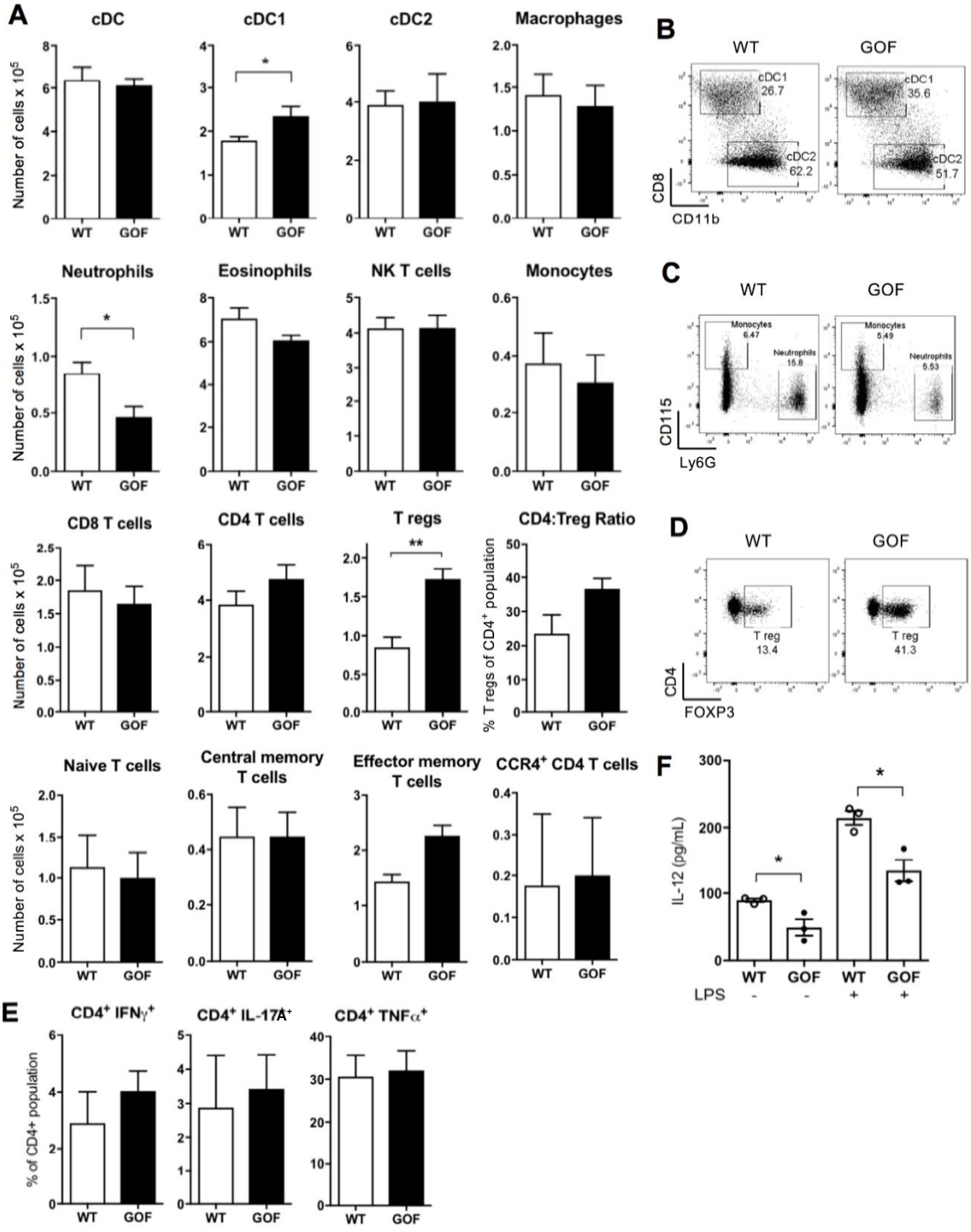

Figure 3.13 Immune phenotype of the spleen in the GOF model in inflammation
Spleen from GOF and WT mice fed WD, were digested. (A) Total numbers of immune populations in the spleen were quantified by flow cytometry, mean ± SEM (n=4). Representative dot plots of cDC populations (B), Ly6G$^+$ neutrophils (C), and T reg cells (D) from the spleen of GOF and WT mice. (E) Percentage of IFNγ, IL-17A, TNFα - expressing CD4$^+$ T cells were quantified by flow cytometry, mean ± SEM (n=6). (F) CD11c$^+$ DCs were isolated from the spleen of GOF and WT mice and cultured overnight with and without 1 μg/ml LPS. Levels of IL-12 were measured in supernatant by ELISA, mean ± SEM (n=3). Statistical significance was determined by Student's two-tailed t-test, results not significant unless otherwise denoted as *p<0.05, **p<0.01.

Lymphatic vessels in VAT drain into the mesenteric lymph nodes, with the primary function to filter lymph collected from the tissue. Antigens collected by cDCs or other antigen presenting cells, initiate adaptive immune responses in the lymph nodes. It has been shown during obesity, CLVs encased in VAT are remodelled and develop increased permeability which exacerbates tissue inflammation due to antigen infiltration in VAT (138). Thus, investigating the immune cell populations of the draining lymph nodes and control non-draining lymph nodes, was important to understand the immune responses instigated during the onset of tissue inflammation. The abundance and ratio of T reg cells in the $CD4^+$ T cell population of the mesenteric lymph node were significantly increased in the GOF mice fed WD compared to WT mice (Figure 3.14A-C). A trend towards a decrease in the percentage of IFNγ -expressing $CD4^+$ T cells was observed between the GOF and WT mice, although this was not significant (Figure 3.14D). These findings reflect the changes observed in VAT of GOF mice. The numbers of immune populations in the inguinal non-draining lymph nodes were not significantly altered between the GOF and WT mice during inflammation (Figure 3.15A & B).

Immune cells originate from the bone marrow and circulate and mature in the blood, before migrating to peripheral tissues. Analysing immune populations in the blood indicates the systemic modulation of immune responses and inflammatory state. Interestingly, there was a significant decrease in total number of $CD45^+$ leukocytes, $CD3^+$ and $CD8^+$ T cell populations and neutrophils in the blood of the GOF mice fed WD compared to WT (Figure 3.16A-C), indicating a reduction in systemic inflammation by constitutive β-catenin activation in cDCs.

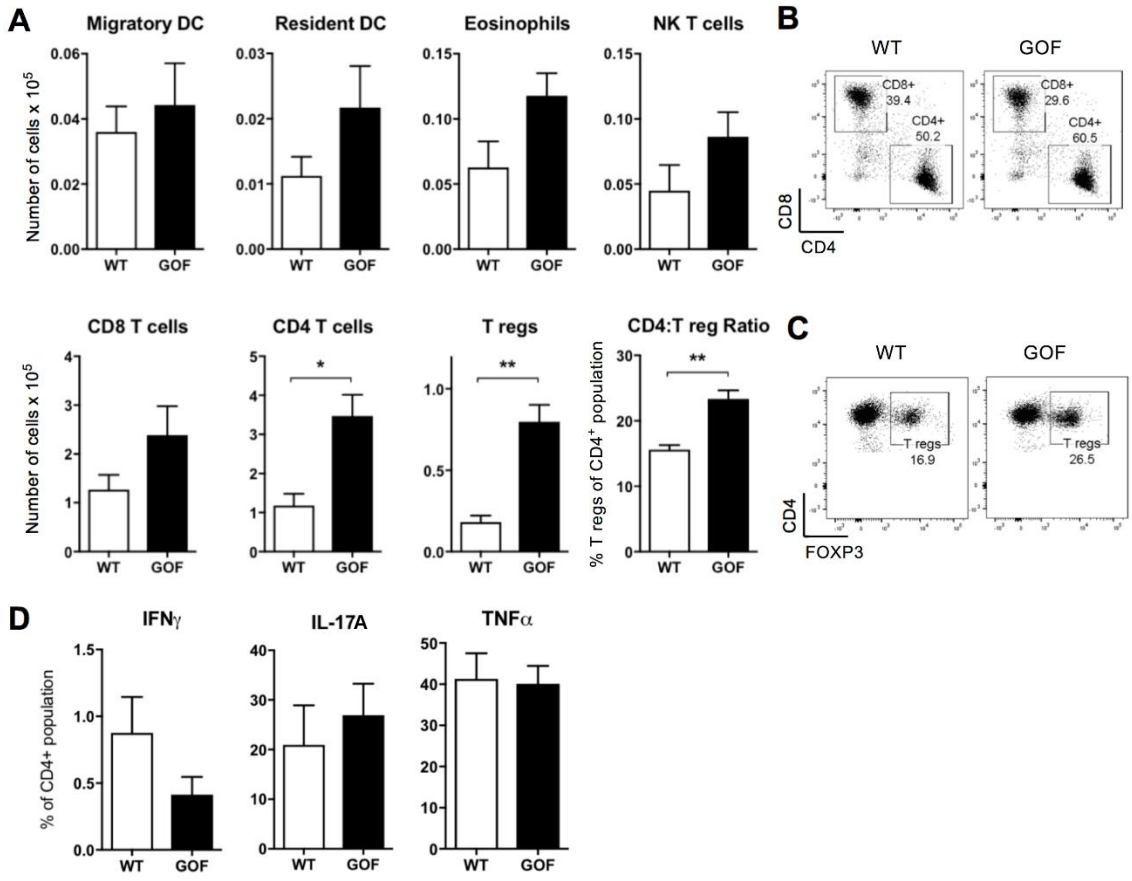

Figure 3.14 Immune phenotype of the draining lymph nodes in the GOF model in inflammation

Mesenteric draining lymph nodes from GOF and WT mice fed WD, were digested. (A) Total numbers of immune populations in the draining lymph nodes were quantified by flow cytometry, mean ± SEM (n=4). Representative dot plots of $CD3^+$ T cell population with gates on $CD8^+$ and $CD4^+$ T cells (B) and T reg cells (C), from draining lymph nodes of GOF and WT mice. (D) Percentage of IFNγ, IL-17A, TNFα -expressing $CD4^+$ T cells were quantified by flow cytometry, mean ± SEM (n=4). Statistical significance was determined by Student's two-tailed t-test, results not significant unless otherwise denoted as *p<0.05, **p<0.01.

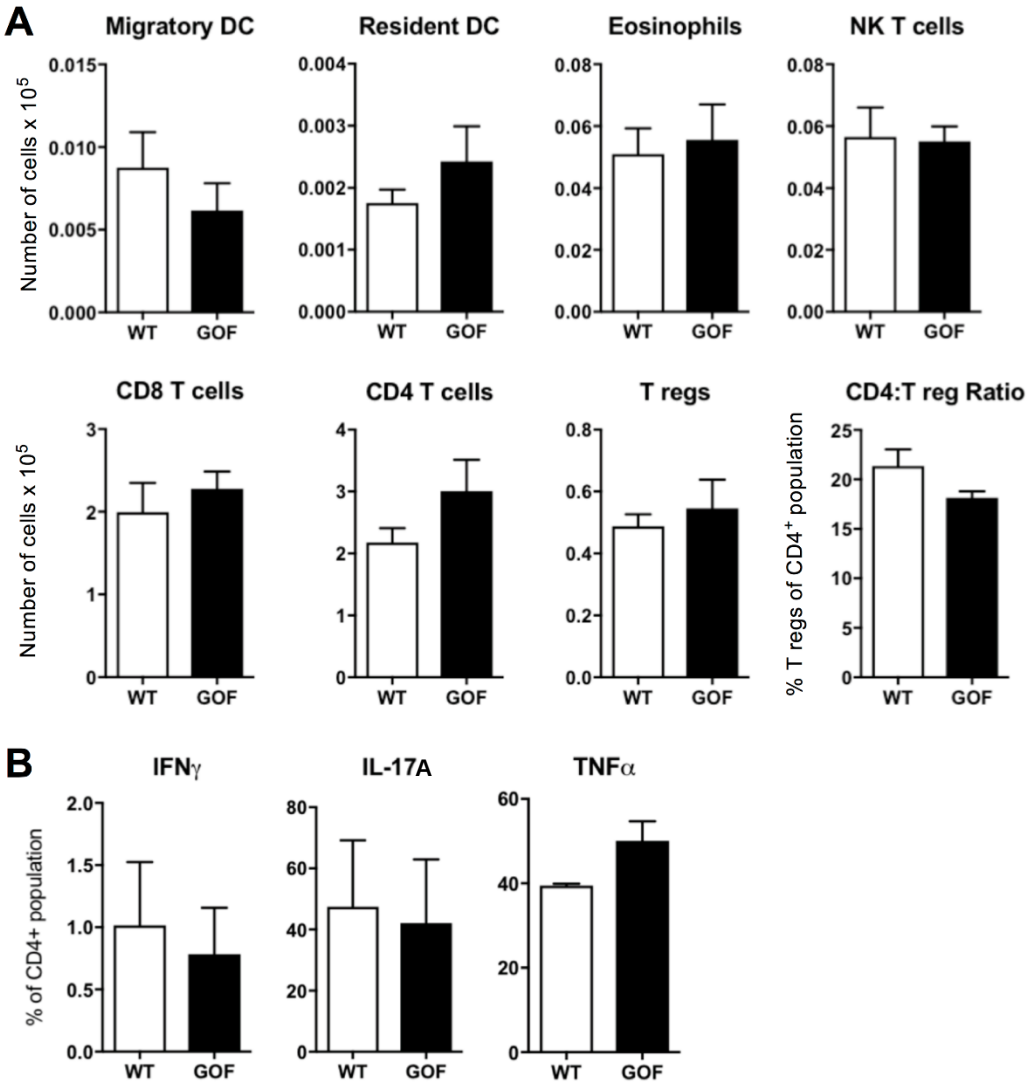

Figure 3.15 Immune phenotype of the non-draining lymph nodes in the GOF model in inflammation

Inguinal non-draining lymph nodes from GOF and WT mice fed ND, were digested. (A) Total numbers of immune populations in the non-draining lymph nodes were quantified by flow cytometry, mean ± SEM (n=4). (B) Percentage of IFNγ, IL-17A, TNFα -expressing $CD4^+$ T cells were quantified by flow cytometry, mean ± SEM (n=3). Statistical significance was determined by Student's two-tailed t-test, results not significant.

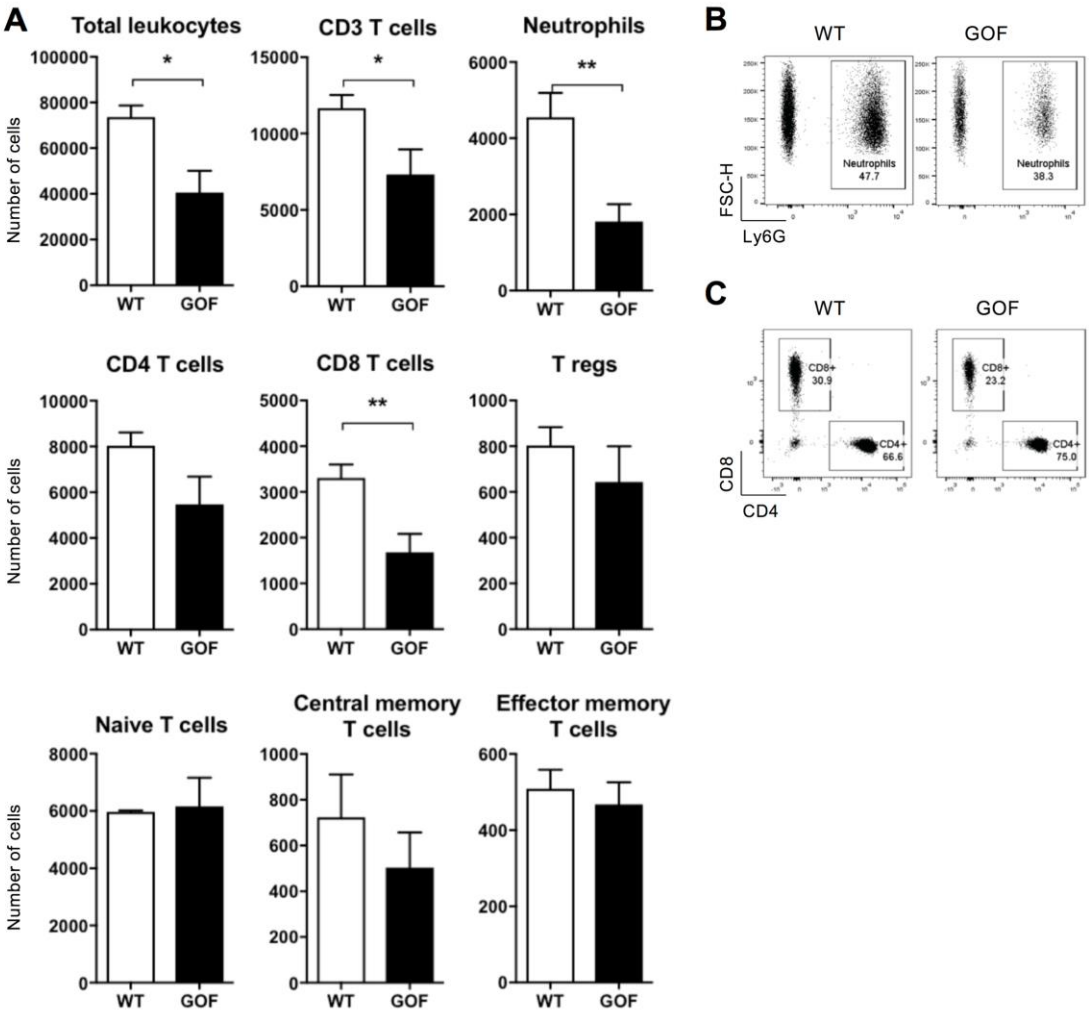

Figure 3.16 Immune phenotype of the blood in the GOF model in inflammation
(A) Total numbers of immune populations in the blood were quantified by flow cytometry, mean ± SEM (n=4). Representative dot plots of Ly6G$^+$ neutrophils (B) and CD3$^+$ T cell population with gates on CD8$^+$ and CD4$^+$ T cells (C) from the blood of GOF and WT mice. Statistical significance was determined by Student's two-tailed t-test, results not significant unless otherwise denoted as *p<0.05, **p<0.01.

3.2.8 VAT-cDCs function and phenotype are modulated by constitutive β-catenin activation

cDCs orchestrate the immune system, with a central role in initiating T cell immune responses. The maturation state of cDCs further shapes the T cell response. We proposed previously that cDCs in VAT of the GOF mice have a less activated phenotype, through the reduction in pro-inflammatory cytokine production. Thus, the antigen presenting capacity of cDCs was measured *ex vivo* with mixed leukocyte reactions (MLR) and *in vivo* with ovalbumin (OVA) immunisation. The ability of cDCs to initiate CD4$^+$ T cell responses, was directly

assessed by analysing $CD4^+$ T cell proliferation. In these assays $CD4^+$ T cells were labelled with CFSE, a stable fluorescent cell dye which covalently binds to intracellular lysine residues. The CFSE signal dilutes during cell division, enabling easy tracking of cell proliferation. MLR use allogenic populations to initiate mismatch polyclonal T cell responses, while OT-II $CD4^+$ T cells, which express transgenic OVA-specific αβ-TCRs, were utilised to observe antigen specific T cell activation after OVA immunisation.

As expected, VAT-cDCs purified from GOF mice fed WD showed a decreased allo-stimulatory capacity indicated by a reduction in CFSE dilution, thus decreased $CD4^+$ T cell proliferation (Figure 3.17A&B). This difference was not observed between spleen cDCs from GOF and WT mice (Figure 3.17A&B). Cytokines measured from the harvested supernatant of the MLR cultures, indicate a modulation in the $CD4^+$ T cell helper subsets activated by the cDCs. IFNγ, produced by Th1 cells was significantly decreased and IL-4, produced by Th2 cells was significantly increased in the MLR cultures of VAT-cDCs from the GOF mice compared to the WT (Figure 3.17C). There was no difference in IL-17A, produced by Th17 cells. This confirms the previous results that constitutive β-catenin activation in cDCs promotes an altered T cell phenotype *in vivo*, with moderate decreases in IFNγ, but not IL-17A. Furthermore, VAT-cDCs displayed reduced antigen specific T cell activation *in vivo* in response to OVA immunisation, shown by a decrease in CFSE dilution of OT-II $CD4^+$ TCR $V\alpha2^+$ cells (Figure 3.17D&E). This difference was not observed in the spleen (Figure 3.17D&E). These findings suggest VAT-cDCs in GOF mice exhibit reduced antigen-presenting capacity, suggesting a less immunogenic phenotype and improved tolerogenic responses.

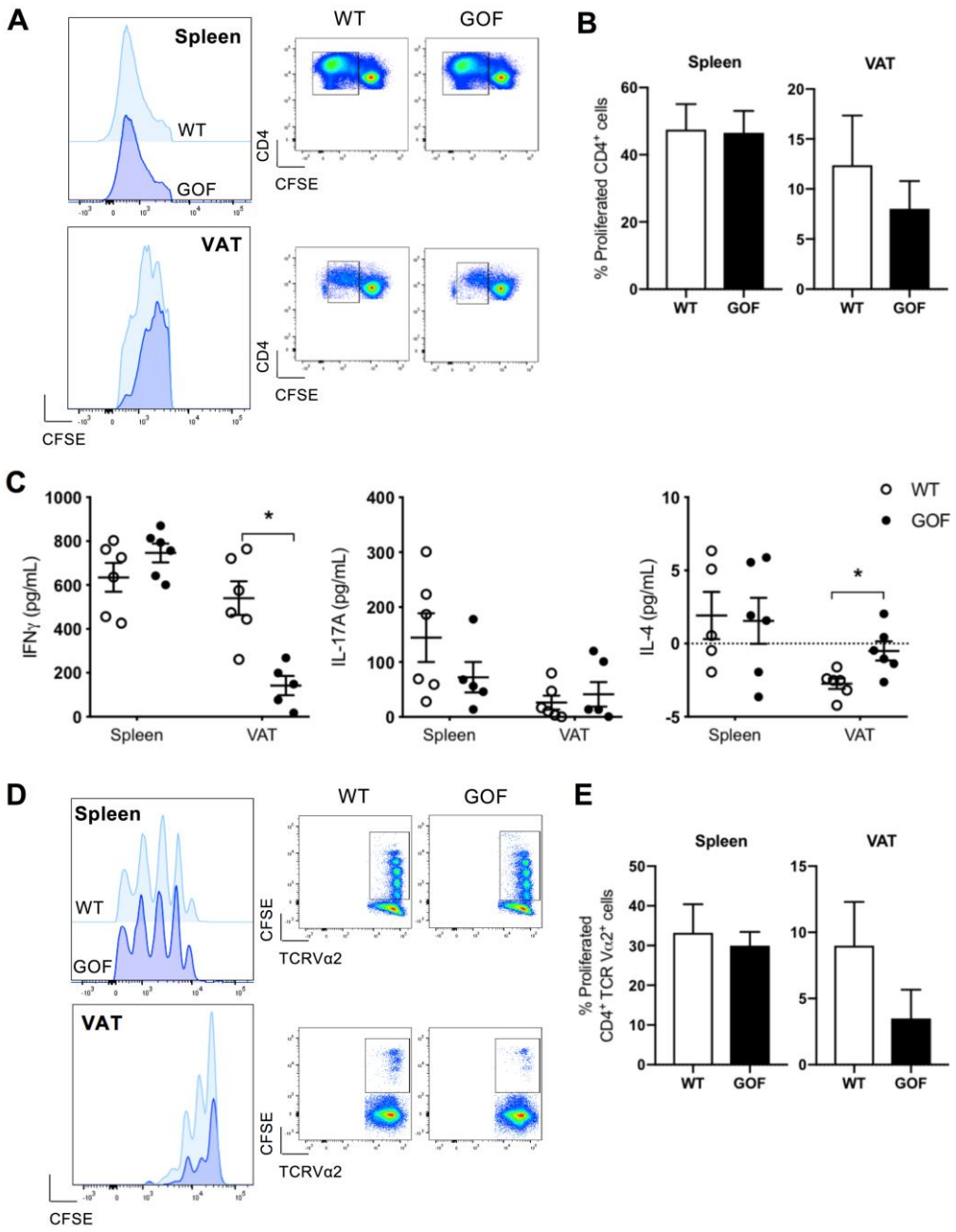

Figure 3.17 Decreased antigen presenting capacity of VAT-DC in the GOF model in inflammation

(A) *Ex vivo* antigen presentation capacity of cDCs from VAT and spleen of WT and GOF mice were evaluated by mixed leukocyte reaction (MLR). $CD4^+$ T cell proliferation was assessed by CFSE dilution. Histogram and dot plots were gated on the $CD4^+$ T cell population and are representative of three independent experiments. (B) Percentage of proliferated $CD4^+$ T cells in MLR cultures with cDCs from VAT and spleen of WT and GOF mice, mean ± SEM (n=3). (C) Levels of IFNγ, IL-17A and IL-4 secreted from MLR cultures, were measured in the supernatant by ELISA, mean ± SEM (n=6). (D) For *in vivo* antigen presentation, CFSE labelled OT-II cells were transferred intravenously 1 day before immunisation with 200 µg OVA intraperitoneally. Three days later, cell division of proliferating OT-II T cells were analysed in VAT and spleen from GOF and WT mice by flow cytometry. CFSE dilution was analysed on gated $CD45^+$ $CD3^+$ $CD4^+$ TCR $Vα2^+$ cells. Histogram and dot plots are representative of three independent experiments. (E) Percentage of proliferated $CD4^+$ TCR $Vα2^+$ cells from VAT and spleen of immunised WT and GOF mice, mean ± SEM (n=3). Statistical significance was determined by Student's two-tailed t-test, results not significant unless otherwise denoted as *p<0.05.

To further assess the VAT-cDC phenotype, cell surface activation markers and production of cytokines were measured. Interestingly, the levels of secreted CCL17 from VAT-cDCs cultured *ex vivo* was significantly decreased in the GOF mice, while the levels of IL-6 and IL-10 only showed minimal changes (Figure 3.18A-C). As CCL17 is associated with the recruitment of $CCR4^+$ inflammatory T cell recruitment, this suggest that modulation of cDC activation and CCL17 production by constitutive activation of β-catenin may not necessarily alter the total number of $CD4^+$ T cells but may modulate the phenotype of the recruited $CD4^+$ T cells. In response to inflammation, cDCs upregulate costimulatory molecules including CD40, CD80 and CD86 on their surface to enable antigen presentation. The VAT-cDC *in vivo* from GOF mice displayed a trend towards a decreased expression of CD40 compared to VAT-cDCs from WT mice (Figure 3.18D). However, there was no overall significant differences in co-stimulatory molecules, as the expression of CD80 and CD86 remained unchanged. Combined, these findings suggest that constitutive activation of β-catenin improves tolerogenic responses of VAT-cDCs by influencing the T cell immune phenotype in diet-induced tissue inflammation.

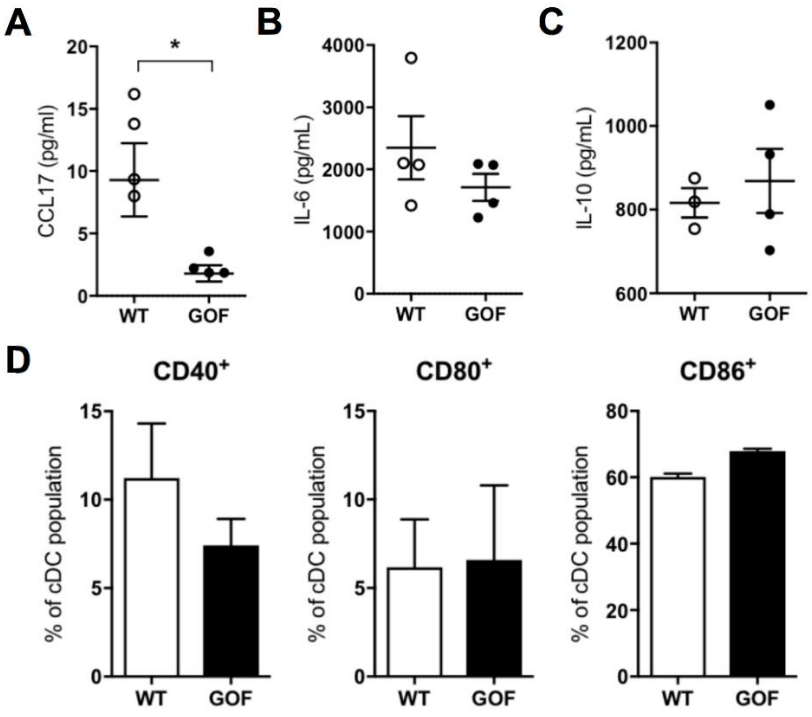

Figure 3.18 VAT-DC phenotype of the GOF model in inflammation
VAT-DCs were isolated from GOF and WT mice fed 16 weeks of WD. $CD11c^+$ DCs were isolated from VAT of GOF and WT mice and cultured overnight. (A) CCL17, (B) IL-6 and (C) IL-10 were measured in supernatant by ELISA, mean ± SEM (n=4). (D) Percentage of $CD40^+$, $CD80^+$, $CD86^+$ -expressing DCs were quantified by flow cytometry, mean ± SEM (n=3). Statistical significance was determined by Student's two-tailed t-test, results not significant unless otherwise denoted as *p<0.05.

3.2.9 Constitutive β-catenin activation in cDCs modulates the systemic adiponectin levels in Western diet-induced tissue inflammation

Obesity is a prominent cause of metabolic dysfunction, including the dysregulation of systemic lipid metabolism. Excess energy is stored as TG in adipocytes and mobilised through lipolysis to be released as FFA when required. However during adipocyte dysfunction in obesity, levels of FFA and TG are increased in the plasma as lipid are redirected in the body. Despite a significant decrease in systemic levels of TNFα in the plasma of the GOF mice fed WD compared to WT, there was no difference in levels of FFA or TG measured in the plasma (Figure 3.19A-C). This implies that although constitutive β-catenin activation in cDC modulates the systemic inflammatory state, it has no observable effect on lipid regulation during tissue inflammation.

Mature adipocytes secrete adipokines, such as leptin and adiponectin, to regulate tissue homeostasis and energy metabolism (76) (57). The dysregulation of adipokines has been recognised in obesity; excess adiposity and adipocyte dysfunction causes an increase in adipokine release, often which possess pro-inflammatory properties (203). The systemic levels of leptin in the plasma of GOF and WT mice fed WD were not different (Figure 3.19D), in agreement with no change in mRNA expression of leptin measured by qRT-PCR in VAT (Figure 3.11B). Adiponectin levels are important biomarkers for metabolic syndrome, low levels of adiponectin are inversely correlated with body mass index in patient populations (204). As previously reported, the concentration of adiponectin decreases during obesity, as observed in WT mice (Figure 3.19E) (205). However in concordance with increased mRNA levels in VAT (Figure 3.11B), the systemic plasma concentration of adiponectin was significantly increased in the GOF mice fed WD compared to WT (Figure 3.19E).

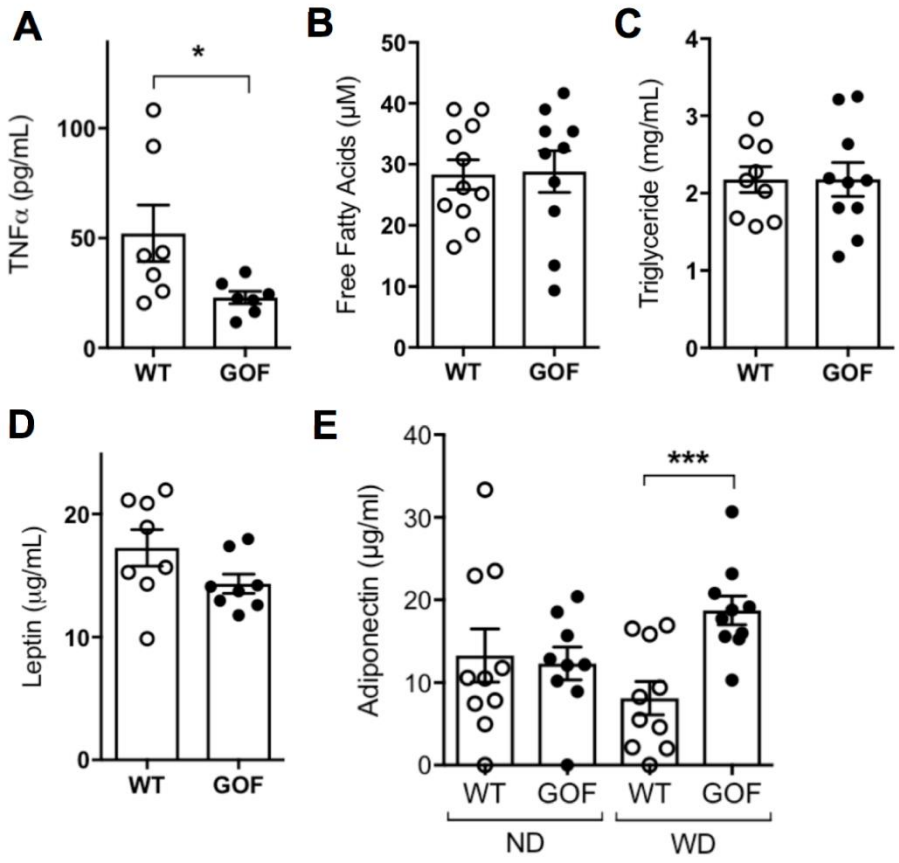

Figure 3.19 Metabolic measures of the GOF model in inflammation
Plasma was harvested from the GOF and WT mice fed 16 weeks of WD. (A) TNFα was measured in the plasma collected from terminal cardiac bleed by ELISA, mean ± SEM (n=7). Mice were fasted overnight and plasma was collected from tail bleeds. (B) Levels of free fatty acid and (C) triglycerides were quantified in the fasted plasma using commercial kits, mean ± SEM (n=10). (D) Leptin was measured in the fasted plasma by ELISA, mean ± SEM (n=8). (E) Adiponectin was measured in the fasted plasma by ELISA, from GOF and WT mice fed ND or WD, mean ± SEM (n=10). Statistical significance was determined by Student's two-tailed t-test, results not significant unless otherwise denoted as *p<0.05, ***p*<0.01, ****p*<0.001.

The observed increase in adiponectin indicates an improved adipocyte function in VAT of the GOF mice fed WD. This can be the result of decreased adipocyte hypertrophy, which is known to occur during chronic over-nutrition. However, there was no difference in adipocyte size between the GOF and WT mice fed WD (Figure 3.20A&B). In addition, during metabolic overload adipocyte dysfunction results in ectopic fat deposits in the liver and other tissues. Fat deposition was observed in the liver of WD fed mice and visually appears not to be altered between the GOF and WT mice (Figure 3.20C), however further analysis and quantification would be required to determine if there was a difference.

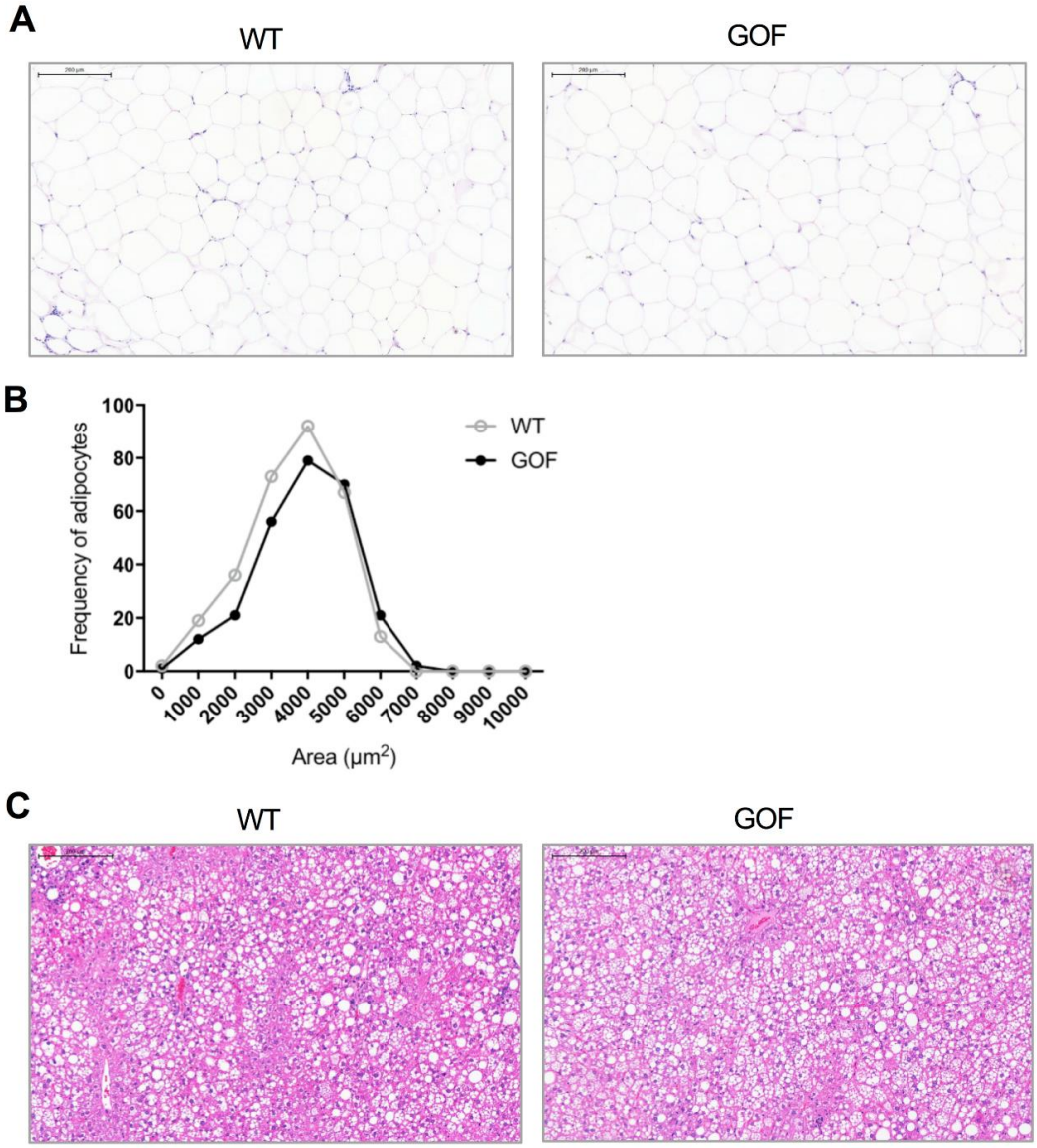

Figure 3.20 Tissue structure of the GOF model in inflammation
(A) Representative images of H&E stained sections of adipose tissue from GOF and WT mice fed 16 weeks of WD. (B) Frequency distribution of adipocyte area in GOF and WT mice fed WD. Frequency of cell area is expressed in number of cells per area bin, from measurements using ImageJ Adiposoft software. Statistical significance was determined by Student's two-tailed t-test, results not significant (C) Representative images of H&E stained sections of liver from GOF and WT mice fed WD.

3.2.10 Constitutive β-catenin activation in cDCs in High fat diet-induced tissue inflammation

Majority of mouse models of obesity rely on high fat diet (HFD) to induce chronic tissue inflammation, which has further elevated levels of saturated fat, more than 60% energy from fat compared to 40% in WD and no extra sugars (Table 2.1). Consequently, the inflammatory response in VAT from HFD fed mice is instigated predominately by tissue infiltrating inflammatory macrophages due to the increase in lipid content (86). Therefore, it was of interest to investigate if the effects of immune modulation by constitutive β-catenin activation in cDC were also observed in an alternative inflammatory setting, such as HFD fed mice. GOF and WT mice were fed HFD for 16 weeks and body weight increased at the same rate over time (Figure 3.21A). Immune modulation in VAT of the GOF mice fed HFD demonstrated similar results to WD fed GOF mice, specifically significant increases in the mRNA expression of adiponectin and IL-10 and the ratio of T reg cells in $CD4^+$ T cell population was significantly increased (Figure 3.21B&C). This suggests that constitutive activation of β-catenin in cDCs enables a T cell driven immunosuppressive phenotype in HFD fed mice, therefore also possess the potential to revert tissue inflammation. Furthermore, the increase in the cDC1 population in the spleen of GOF mice was also observed, although no differences in numbers of neutrophils or T reg cells (Figure 3.21D). The numbers of immune populations in the mesenteric draining lymph nodes and inguinal non-draining lymph nodes were not significantly altered between the GOF and WT mice fed HFD (Figure 3.21E&F).

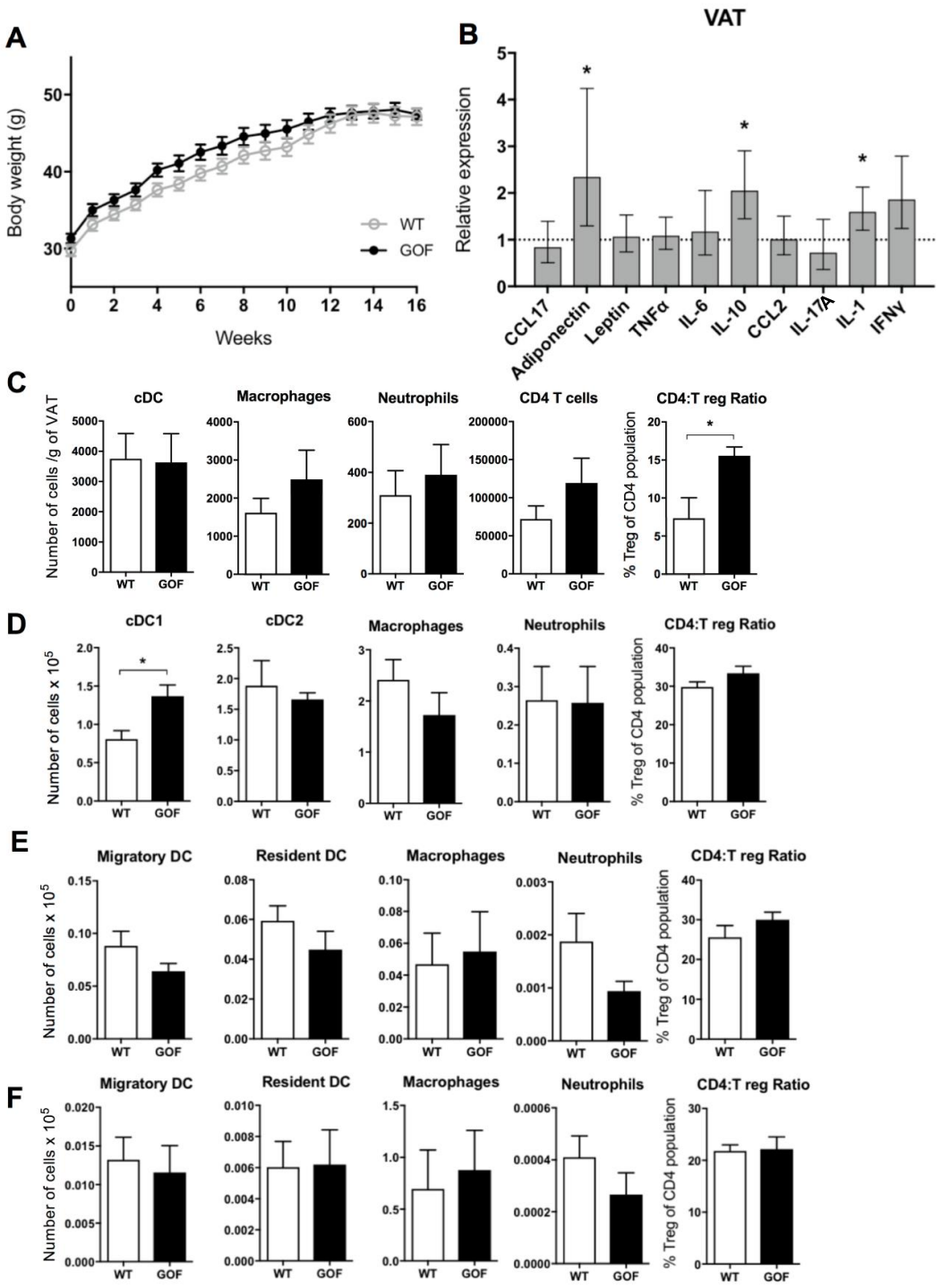

Figure 3.21 Immune phenotype in the GOF model in High fat diet-induced inflammation

GOF and WT mice were fed HFD to induce chronic low-grade tissue inflammation. (A) Body weight was measured over the duration of 16 weeks. (B) qRT-PCR analysis for mRNA expression in VAT of GOF and WT mice fed HFD. Expression levels of all mRNA were normalised to GAPDH expression. Bars represent ΔΔCT data values, the expression in GOF mice compared to WT, set at 1 indicated by the dotted line. Error bars show the geometric mean of six biological replicates. Statistical significance of ΔCT data values was determined by Student's two-tailed t-test, results not significant unless otherwise denoted as *p<0.05. Total numbers of immune populations in the (C) VAT, (D) spleen, (E) mesenteric draining lymph nodes and (F) inguinal non-draining lymph nodes were quantified by flow cytometry, mean ± SEM (n=4). Statistical significance was determined by Student's two-tailed t-test, results not significant unless otherwise denoted as *p<0.05.

3.2.11 Constitutive β-catenin activation in cDCs improves the glucose homeostasis in Western diet-induced tissue inflammation

The previous data suggests that constitutive activation of β-catenin pathway in cDCs plays a role in reverting the development of VAT inflammation during obesity. Modulation of tissue inflammation has long been proposed to restore insulin sensitivity. Studies have demonstrated that neutralisation of pro-inflammatory adipose cytokines and ablation of inflammatory cells in VAT, promotes the recovery of glucose homeostasis in obese mice (10) (132). Thus, we hypothesised that constitutive β-catenin activation in cDCs would prevent the development of IR during WD-induced tissue inflammation.

To assess the effects on whole-body glucose sensitivity and the response to insulin, mice were fasted to remove the effects of nutritional glucose. Intraperitoneal glucose tolerance tests (GTT) and insulin tolerance tests (ITT) were used to evaluate the glucose homeostasis in GOF and WT mice. The clearance of intraperitoneally (i.p) injected glucose load was measured in the GTT, whereby the ability of pancreatic β-cells to release insulin, was assessed in response to high blood glucose levels. The ITT determined the insulin sensitivity; an insulin bolus was injected i.p. to induce hypoglycaemia and blood glucose concentrations were measured over time to detect insulin resistance in the peripheral tissues, as blood glucose levels were restored to normal. There were no differences in the ITT response between the GOF and WT mice fed ND and WD (Figure 3.22). This absence of effect suggests that although constitutive β-catenin activation in cDCs was able to revert the development of tissue inflammation in part, this was not sufficient to improve insulin sensitivity in obesity.

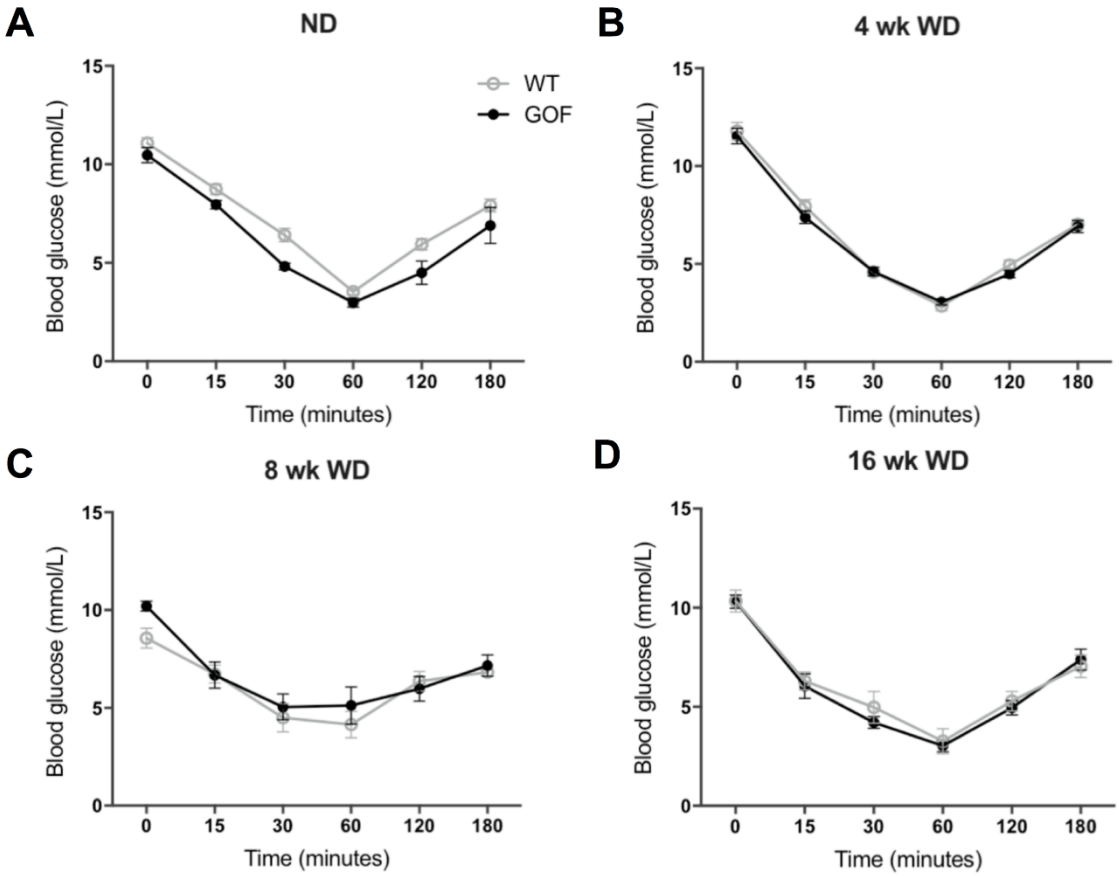

Figure 3.22 Insulin sensitivity of the GOF model in inflammation is not altered
Systemic insulin sensitivity was measured by insulin tolerance test (ITT) in GOF and WT mice fed ND (A), 4 weeks of WD (B), 8 weeks of WD (C) or 16 weeks of WD (D), mean ± SEM (n=10). Statistical significance at different time points was analysed by two-way ANOVA with Bonferroni's post-test, results not significant unless otherwise denoted as *p<0.05, **p<0.01, ***p<0.001.

As expected there was no observable difference in GTT response between GOF and WT mice fed ND (Figure 3.23A). However, as diet-induced tissue inflammation developed over time, the response to glucose deteriorated in WT mice (Figure 3.23B-D). There was no differential response between the GOF and WT mice fed 4 or 8 weeks of WD (Figure 3.23B&C). Although, by 16 weeks of diet-induced tissue inflammation, the GTT response of the GOF mice was significantly different than the response by WT mice demonstrating improved whole-body glucose sensitivity (Figure 3.23D). The basal levels of blood glucose were lower in the GOF mice fed 16 weeks of WD after fasting, indicating prior to glucose challenge the GOF mice have not developed the diet-induced hyperglycaemia to the same extent as the WT mice (Figure 3.23D). This metabolic modulation represents a key observation for the GOF model, specifically that constitutive β-catenin activation in cDCs has the ability to alter

insulin secretion. Interestingly, systemic insulin levels measured from the plasma of fasted mice demonstrated a significant increase in GOF mice fed WD for 12 weeks, although no change was observed in mice fed ND (Figure 3.24A). In addition to the increased basal level of insulin in the plasma of the GOF mice, these levels remained significantly higher 15 min post administration of glucose i.p. compared to the WT mice (Figure 3.24B). Thus, as constitutive activation of β-catenin in cDCs improved whole-body glucose response but not insulin sensitivity, this suggested that the elevation in insulin was due to a modulation in the insulin secretion of the β-cells in the pancreas.

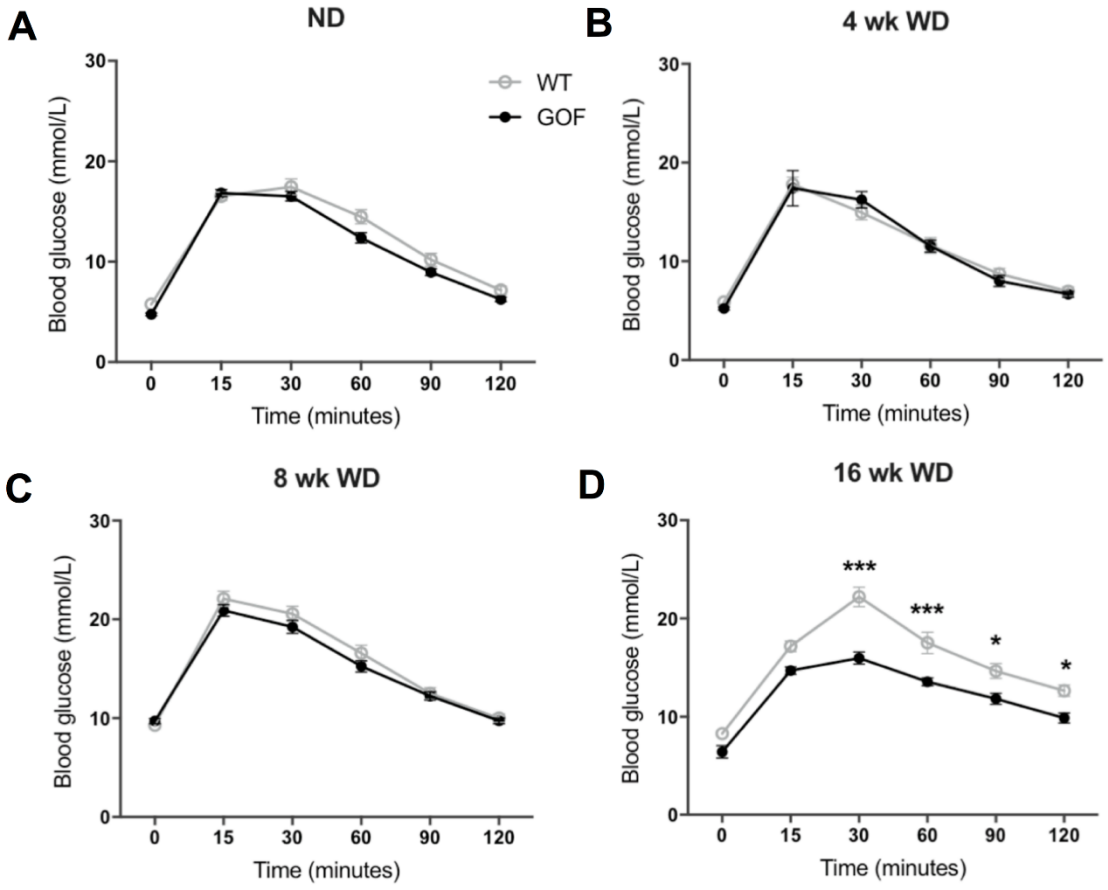

Figure 3.23 Improved glucose sensitivity of the GOF model in inflammation
Systemic glucose homeostasis was measured by glucose tolerance test (GTT) in GOF and WT mice fed ND (A), 4 weeks of WD (B), 8 weeks of WD (C) or 16 weeks of WD (D), mean ± SEM (n=10). Statistical significance at different time points was analysed by two-way ANOVA with Bonferroni's post-test, results not significant unless otherwise denoted as *p<0.05, **p<0.01, ***p<0.001.

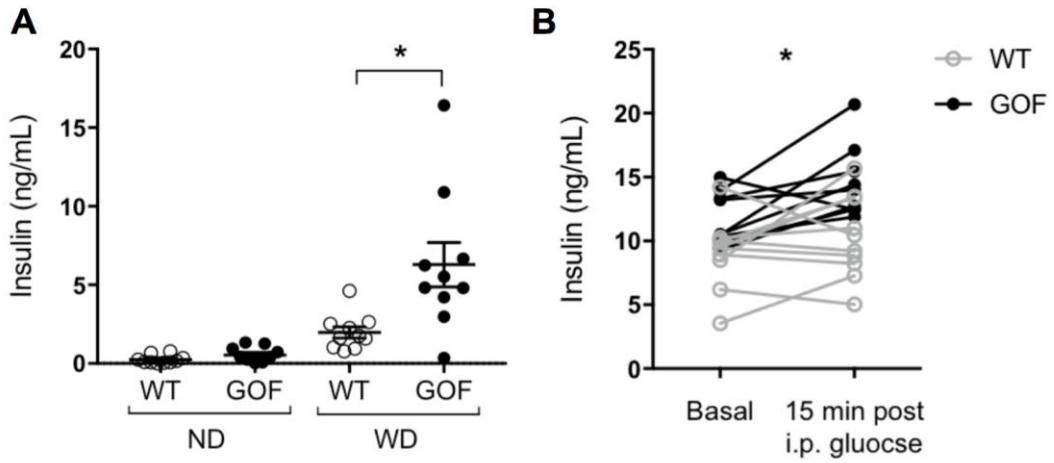

Figure 3.24 Systemic insulin production increased in the GOF model
(A) Insulin was measured by ELISA in the plasma of fasted GOF and WT mice fed either ND or WD, mean ± SEM (n=10). Statistical significance was determined by Student's two-tailed t-test, results not significant unless otherwise denoted as *p<0.05. (B) Insulin was measured by ELISA in the plasma collected after fast and 15 min post intraperitoneal injection with 1.5 mg glucose /g of body weight of GOF and WT mice, mean ± SEM (n=10). Statistical significance was analysed by two-way ANOVA with Bonferroni's post-test, denoted as *p<0.05.

3.3 Discussion

Studies have demonstrated a clear link between the Wnt/β-catenin pathway and the immune function of cDCs, contributing to the switch in phenotype to promote tolerogenic responses. This chapter has evaluated the role of β-catenin in cDCs in the context of VAT homeostasis and obesity-induced tissue inflammation.

In VAT, cDCs acquire a tolerogenic phenotype during homeostatic conditions by upregulating adipocyte related pathways to maintain tissue homeostasis. Activation of Wnt/β-catenin pathway in cDC1 subset promoted an anti-inflammatory milieu in the tissue through enhanced IL-10 production (Figure 3.1D). This highlights that tissue microenvironment influences cDC phenotype. Wnt ligands are produced by preadipocytes to regulate adipogenesis. Preadipocytes are predominately located adjacent to adipose vasculature where they also differentiate to mature adipocytes (140) (141). Interestingly, cDCs are also found in close proximity to AT vessels (138) (Figure 3.1A), suggesting a possible crosstalk with pre-adipocytes to activate Wnt/β-catenin pathway in VAT-cDCs. The depletion of β-catenin pathway in cDCs exacerbates VAT inflammatory response *in vivo* through the loss of a tolerogenic phenotype (Figure

3.2), further detailed in Table 3.1 (193). The alteration of T cell responses in the inflamed VAT of β-catenin knockdown mice, align with previous observations that abrogation of β-catenin expression promotes Th17 T cell responses and inhibits T reg cell induction (185) (178) (186). Due to the high specificity of the Zbtb46 promoter used for generating β-catenin knockdown mice, the contribution of this T-cell mediated phenotype in modulating VAT inflammation is likely to be due to the action of β-catenin on cDC, rather than through an effect on macrophage populations, which reportedly modulates the innate pro-inflammatory profile in VAT. These findings confirm the importance of cDCs in controlling T cell responses *in vivo* and identify a novel mechanism by which cDCs maintain tissue immune homeostasis during steady state and obesity-induced inflammation.

Chronic inflammation promotes cDC recruitment in VAT, where they adopt an activated pro-inflammatory state. In addition to obesity-induced tissue inflammation overriding suppressive pathways, inhibition of the β-catenin pathway in cDCs also plays a role in promoting the switch to immunogenic phenotype in VAT. In line with previous reports, Wnt ligand availability was diminished in obese VAT, specifically the levels of Wnt10b, which resulted in impaired Wnt/β-catenin pathway activation in VAT-cDCs (Figure 3.3). Thus, we investigated if constitutive activation of β-catenin in cDCs in obese VAT could revert the development of tissue inflammation and associated IR.

In homeostatic conditions with mice fed ND, constitutive activation of β-catenin in cDCs exhibited minimal changes in the immune phenotype however there were indications of a possible T cell driven immunosuppressive phenotype in VAT. Increased T reg cell infiltration and reduction in the T cell chemoattractant CCL17 expression suggests that constitutive activation of β-catenin in cDCs played a role in steady state conditions to promote anti-inflammatory T cell responses in VAT (Figure 3.9). Despite this, there was no increase of IL-10 production in VAT, which several studies have shown activation of β-catenin in DCs produces high levels of IL-10 (206) (182) (179). However, it is important to note that Wnt/β-catenin pathway is active in steady-state VAT-DCs (Figure 3.4A) and the GOF model only increases the level of activation which may account for only marginal changes observed under ND, in the absence of VAT inflammation. Modulation of T reg cell induction was also observed in the spleen in homeostatic conditions,

indicating a wider systemic change in T reg cell homeostasis by constitutive active β-catenin in cDCs (Figure 3.6A). Although β-catenin is not normally active in splenic cDCs, in the GOF model constitutive activation is induced in all cDCs in every tissue having a systemic effect and not just restrained to VAT, where expression is normally observed. However, this caveat of systemic β-catenin activation in cDCs, more accurately represents a therapeutic drug strategy, for example GSK3β inhibitors, where similar systemic effects may be observed. Surprisingly the number of splenic NK cells increased with active β-catenin in cDCs (Figure 3.6A), despite no change in other tissues in homeostatic conditions. This could suggest β-catenin may affect cDC activation of innate effector functions, however further characterisation would be required.

Restoring β-catenin activation in cDCs demonstrated signs of reduced local obesity-induced inflammation. VAT-cDCs were modulated to induce a tolerogenic phenotype by constitutive β-catenin activation in concordance with previous reports, where similar phenotypes of DCs were exhibited in other tissues such as the gut. This change in cDC function is responsible for the altered T cell phenotype in VAT of GOF mice. Although only limited differences were observed in the abundance of T cells in VAT, the modulation of mRNA expression and increased numbers of naïve T cells suggested there was a change in phenotype of recruited T cells (Figure 3.11 & 3.12A). This was further confirmed by *ex vivo* analysis of VAT-cDCs from GOF mice, where reduced T cell responses were observed (Figure 3.17). Thus, the subtle but important change in T cell phenotype affects local inflammation by modulating the VAT immune network. However, the distribution of immune populations in VAT is heterogenous. It is widely reported that perinodal AT (PAT) is enriched with immune cells and lymphocytes especially, locate in FALCs which suggests that inflammatory responses are in very localised parts of the tissue. In these *in vivo* experiments, immune cell populations were analysed in total VAT from pooled depots in each mouse and consequently the effects by constitutive β-catenin activation in cDCs on inflammatory responses may have been diluted. This explains why potentially only minimal differences were observed in VAT of the GOF model and therefore localised responses in PAT may have revealed more striking effects by constitutive β-catenin activation in cDCs. While indications suggested local inflammation was in part reduced, the level of systemic inflammation was also

affected in GOF mice fed WD. Effects on the systemic immune populations may have arisen as a consequence of local changes in VAT immune populations or resulting from the systemic nature of the GOF model, where constitutive β-catenin activation is induced in all cDCs from every tissue including the spleen and lymph nodes. The exact mechanism by which β-catenin in cDCs modulates systemic inflammation will be difficult to decipher. However local and systemic inflammation was not completely restrained, suggesting that constitutive β-catenin activation in cDCs was not sufficient to fully overcome established inflammatory processes. As detailed in Table 3.1, the GOF model did not completely restore the results observed in the β-catenin knockdown mice (193). A maximal tolerogenic effect of β-catenin activity in cDCs may have been reached, which could not limit the development of tissue inflammation. Furthermore, residual β-catenin expression was still detectable in VAT-cDCs from obese control mice indicating that activation of the Wnt/β-catenin was not entirely impaired (Figure 3.4A). Thus, this may explain why constitutive β-catenin activation in cDCs does not induce highly significant changes, if activity however minimal was still present in obese VAT-cDCs of control mice.

β-catenin knockdown mice	β-catenin gain-of-function mice
In ND fed mice, reduction of IL-10 mRNA expression and T reg infiltrate in VAT. Antigen-specific T cell activation increased in VAT with and without inflammatory stimulus. No change in metabolic parameters- including body and VAT weight, glucose and insulin sensitivity. **Decreased anti-inflammatory state of VAT in homeostatic conditions**	In ND fed mice, increase in $CD4^+$ T cells and T regs and mRNA expression of IL-17A, FOXP3 in VAT. Reduction in CCL17 and no change in IL-10 mRNA expression. No change in metabolic parameters- including body and VAT weight, glucose and insulin sensitivity. **Anti-inflammatory state of VAT maintained in homeostatic conditions**
In WD fed mice, reduction of IL-10 and adiponectin mRNA expression and increase in CCL17, IL17, IL6 mRNA expression in VAT and SVF. Decrease in T reg infiltrate in VAT. Elevated antigen-specific T cell activation and cDC stimulatory capacity. **Exacerbated obesity-induced VAT inflammation**	In WD fed mice, elevation of IL-10, FOXP3 and adiponectin mRNA expression and decrease in CCL17 and IFNγ mRNA expression in VAT and SVF. No change in T reg numbers in VAT although possible change in T cell phenotype. Reduction in antigen-specific T cell activation and cDC stimulatory capacity. **Reduced diet-induced VAT inflammation in part**
In WD fed mice, decreased glucose and insulin sensitivity and reduction of insulin-stimulated AKT phosphorylation in VAT and liver. **Increased obesity-induced IR**	In WD fed mice, increased glucose sensitivity and elevated systemic insulin secretion. **Improved control of obesity-induced hyperglycaemia**

Table 3.1 Comparison of phenotypes in β-catenin knockdown and GOF mice
Summary of data in this thesis and published in Macdougall *et al*. (193)

The results of the GOF model mimic the effect of pharmacological inhibition of upstream GSK3β which renders β-catenin active. GSK3β inhibitors result in DC maturation and acquisition of tolerogenic potential (182). In view of this, other signalling pathways that inactivate GSK3β could supply Wnt-independent mechanisms to promote tolerance. Interestingly, activation of TLRs which

respond to pathogenic antigens, may simultaneously activate genes controlled by GSK3β while also stimulating the production of immunogenic DCs. This poses a feedback mechanism that could attenuate T cell activation by DCs. Hence pathways that β-catenin interacts with, need to be further investigated to understand the complete functional effect of constitutive β-catenin activation in cDCs.

Obesity-induced inflammation plays a crucial role in the development of insulin resistance and consequently T2DM (207). A decrease in insulin sensitivity initiates in VAT, where modulation of adipokines promotes chronic systemic exposure of pro-inflammatory mediators. These mediators disrupt insulin signalling in peripheral tissues, promoting insulin resistance and resulting in reduced glucose uptake from the blood and subsequently hyperglycaemia develops. In this context, β-cells increase the production of insulin in an attempt to counteract high glucose levels. Thus, elevated systemic insulin levels are ordinarily associated with the development of IR. Interestingly, constitutive β-catenin activation in cDCs induced an improvement in whole-body glucose homeostasis, although this was not caused by an improvement in peripheral insulin sensitivity (Figure 3.22 & 3.23). Rather increased levels of circulating insulin were observed paradoxically (Figure 3.24), not as an indication of increased IR but as a result of enhanced insulin secretion and an improved ability to control hyperglycaemia. Consequently, the effect of constitutive β-catenin activation in cDCs on metabolic control is further investigated in Chapter 4, specifically examining the impact on β-cells in the islets. Thus, in the GOF model where all cDCs are systemically targeted for sustained β-catenin activation, cDCs may have varying tissue-dependent effects including in the pancreas. Therefore β-catenin activity in cDCs may not be confined to VAT and could regulate other metabolic processes.

In summary, this chapter has demonstrated a novel mechanism to induce a tolerogenic phenotype of cDCs in VAT through activation of Wnt/β-catenin pathway, which was responsible for reverting, in part, systemic and local adipose tissue inflammation in a model of diet-induced obesity.

Chapter 4 Metabolic changes induced by constitutive β-catenin pathway activation in conventional dendritic cells

4.1 Introduction

In obesity, the inability of adipocytes to store excess lipids causes dysregulation of lipid and glucose metabolism leading to ectopic fat deposition, hyperglycaemia, insulin resistance (IR) and dyslipidaemia (66). The pancreas responds to obesity through the expansion of β-cell mass, in order to compensate for the increased IR of the peripheral tissues and to restrain hyperglycaemia, by increasing insulin production (31). Understanding what regulates β-cell proliferation in obesity is a complex picture with many factors playing a role, including nutrients, insulin, incretins and growth factors (208). During the development of T2DM, β-cell mass and function are dramatically reduced and thus stimulating β-cell proliferation could provide therapeutic potential to revert β-cell failure.

The dysregulation of Wnt/β-catenin pathway has been associated with IR and the development of T2DM in mouse and man (172). Loss of Wnt5b function and variants of *Tcf7l2* confer increased T2DM susceptibility in humans (173) (175). In mice, overexpression of Wnt10b in adipocytes prevented the development of HFD induced insulin resistance (176). Interestingly, Wnt/β-catenin pathway has been shown to have a direct effect on β-cells. *Tcf7l2*-deficient mice exhibit reduced β-cell mass and decreased insulin secretion (209). In addition, a recent study detailed further that during pre-diabetic state, β-catenin was activated in islets during compensatory β-cell hyperplasia in mice (210). The low-density lipoprotein receptor-related proteins (LRP) are co-receptors critical for transducing Wnt signals for canonical β-catenin signalling. Loss of LRP5 modulates systemic cholesterol and glucose metabolism, specifically impairing the glucose-induced insulin secretion of islets (211). Wnt ligands have also been shown to stimulate insulin secretion and induce β-cell proliferation *in vitro* (212),

while SFRP5, a secreted Wnt inhibitor blocks rat β-cell proliferation (213). Furthermore in primary mouse islets and *in vivo*, increasing β-catenin expression expands β-cell mass (214). However the source of Wnt ligands to induce β-catenin activation for β-cell expansion remains unknown.

Modulation of tissue inflammation has long been proposed to restore peripheral insulin sensitivity. However results from Chapter 3 indicated that despite restraining obesity-induced systemic and local inflammation, constitutive activation of β-catenin in cDCs was not sufficient to improve peripheral insulin sensitivity. Interestingly, constitutive β-catenin activation in cDCs improved whole-body glucose homeostasis as a result of enhanced insulin production. Combined, these results indicated that constitutive activation of β-catenin in cDCs could have the potential to modulate islet biology and β-cell secretory responses through reverting inflammatory responses in the pancreas, although the mechanisms remain unclear.

In this chapter the role of Wnt/β-catenin signalling in cDCs is investigated to evaluate the metabolic effect on insulin secretion and islet inflammation in the context of obesity-induced insulin resistance and the development of T2DM.

4.2 Results

4.2.1 Constitutive β-catenin activation in cDCs induces the expansion of islet size

Islets are distributed through the pancreas and contain endocrine cells that secrete hormones, predominately comprised of insulin secreting β-cells. Using H&E and insulin counterstained sections (Figure 4.1C&D), the islet size was assessed in the pancreas of the GOF and WT mice. There was a trend towards an increase in mean size of the islets in the GOF mice compared to WT fed ND, however in mice fed WD there was a significant expansion of islet size (Figure 4.1A). In addition the distribution of islet size was modulated, indicating a significant decrease of smaller islets in the GOF model (Figure 4.1B). To confirm

that the increased insulin production observed in the plasma of GOF mice (Figure 3.24) was a result of the increased islet size, sized-matched islets from mice fed WD were cultured overnight. A significant increase in insulin secretion could be detected from cultured islets from GOF mice compared to WT (Figure 4.1E). This suggests that, despite changes in VAT inflammation, the improved whole-body glucose metabolism observed in GOF mice was due to a modulation of insulin secretion in the pancreas.

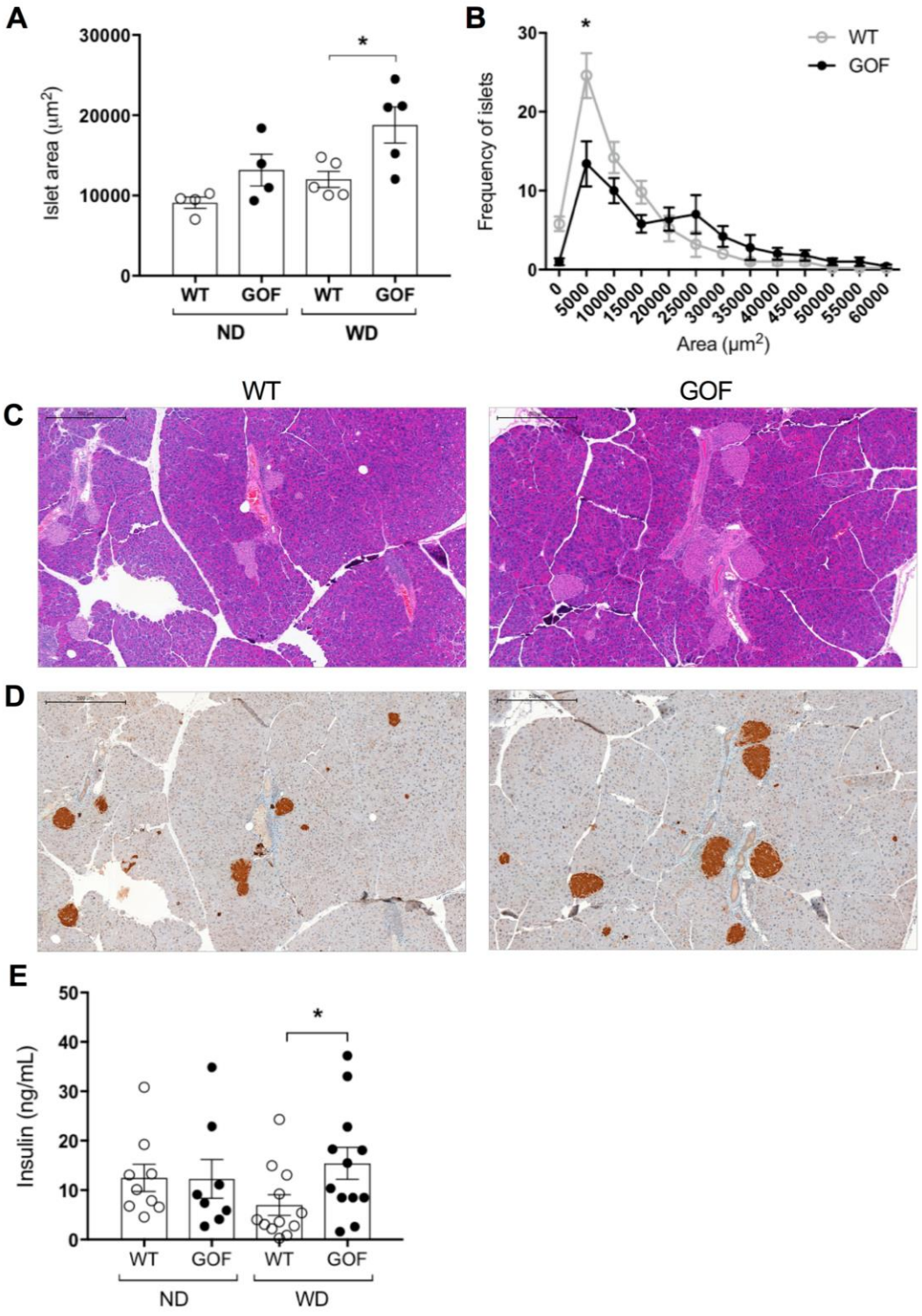

Figure 4.1 Increased size of islets in the GOF model
(A) Quantification of islet size from levelled sections of pancreas tissues from GOF and WT mice fed ND or WD was determined using ImageJ software, mean ± SEM (n= 4/5). (B) Frequency distribution of islets size in pancreas sections of GOF and WT mice. Frequency of cell area is expressed in number of cells per area bin, mean ± SEM (n= 5). Representative images of (C) H&E and (D) insulin counter-stained sections of pancreas from GOF and WT mice fed WD. (E) Sized-matched islets isolated from GOF and WT mice fed ND or WD, were cultured overnight and insulin was measured by ELISA from the supernatant harvested the next day to measure basal secretion, mean ± SEM (n=9/12). Statistical significance was determined by Student's two-tailed t-test, results not significant unless otherwise denoted as *p<0.05.

Insulin regulation of blood glucose concentration, is correlated with β-cell mass. The processes that regulate β-cell mass are highly complex and balanced between β-cell differentiation, replication and death. To understand the mechanism of islet expansion in the GOF model, cell proliferation was investigated. To do so, islets from donor B6 mice were co-cultured with Flt3L-bone marrow derived cDCs from GOF or WT mice (Figure 2.5). After 5 days of culture, a clear increase in $Ki67^+$ cells could be observed in the islets incubated with GOF cDCs (Figure 4.2A). Ki67 is a widely used marker for cell proliferation. When cells undergo mitosis, levels of Ki67 increase which can be easily detected by antibody staining. Proliferation markers at the mRNA level showed a trend towards an increase in cMyc and CyclinD1 expression in the islets from GOF mice fed WD (Figure 4.2B), confirming previous reports *in vitro* (214). Furthermore, immunohistochemistry staining demonstrated a significant increase in $Ki67^+$ cells in the islets of the GOF mice compared to WT (Figure 4.2C&D). No changes in apoptosis in the islets visually appears between the GOF and WT mice as measured by cleaved caspase-3 immunohistochemistry staining (Figure 4.2E), however further analysis and quantification would be required to determine if there was a difference. These results indicate that constitutive activation of β-catenin in cDCs induces expansion of islets by increasing cell proliferation.

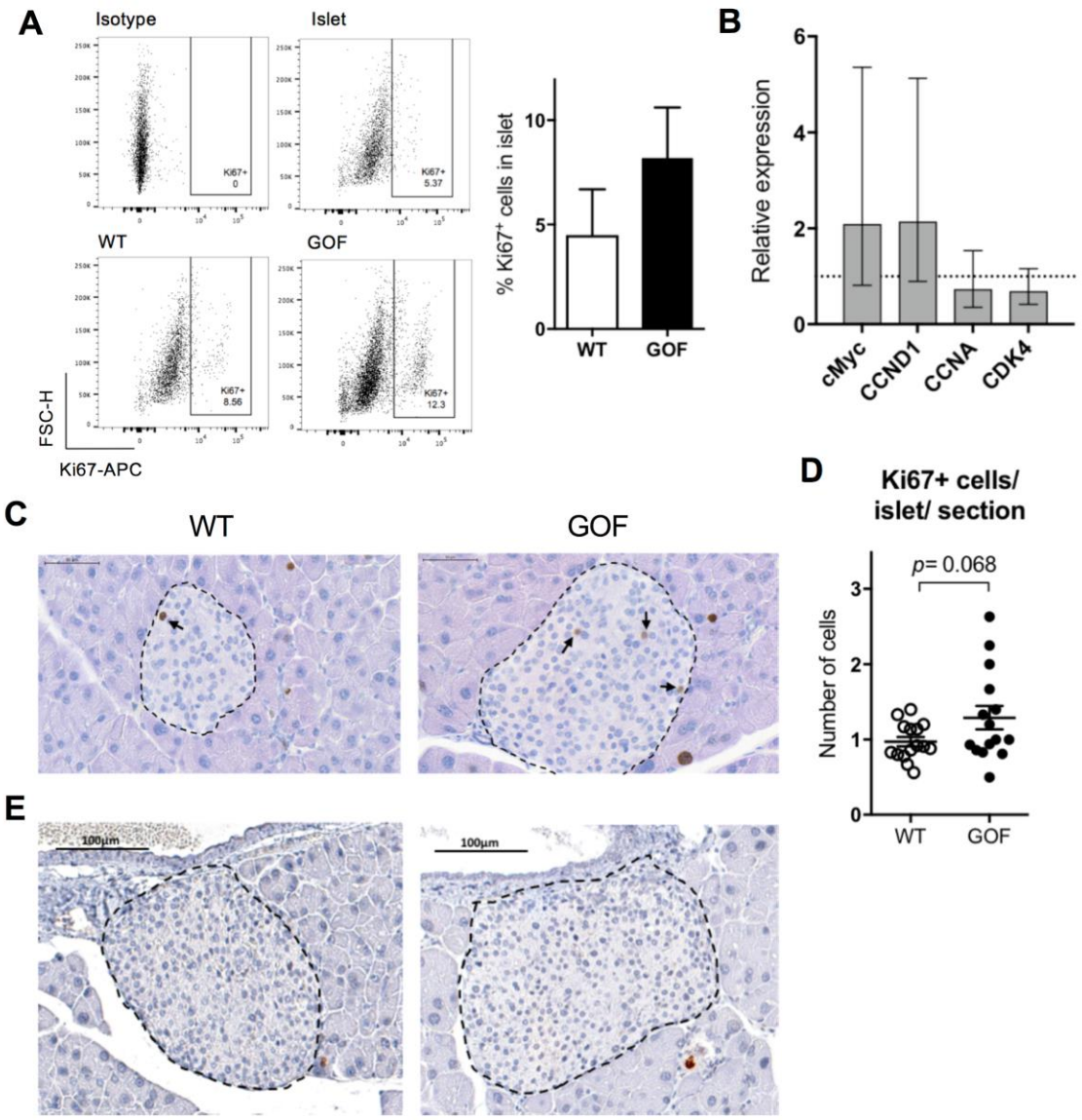

Figure 4.2 Increased proliferation in the islets of the GOF model
(A) cDCs isolated from GOF and WT mice fed WD were co-cultured with islets from donor mice for 5 days. Proliferation in the islets was analysed by flow cytometry to measure the $Ki67^+$ cells, represented as a percentage of $CD45^-$ population, mean ± SEM (n=3). (B) qRT-PCR analysis for mRNA expression of proliferation markers in islets of GOF and WT mice. Expression levels of all mRNA were normalised to GAPDH expression. Bars represent ΔΔCT data values, the expression in GOF mice compared to WT, set at 1 indicated by the dotted line. Error bars show the geometric mean of five biological replicates. Statistical significance of ΔCT data values was determined by Student's two-tailed t-test, results not significant. (C) Representative images of Ki67-stained sections of pancreas from GOF and WT mice. Islets are indicated by the dotted line, arrows indicate $Ki67^+$ cells. (D) $Ki67^+$ cells in islets counted and number per islet per section determined, mean ± SEM (n=15). (E) Representative images of cleaved caspase-3 -stained sections of pancreas from GOF and WT mice, islets are indicated by the dotted line. Statistical significance was determined by Student's two-tailed t-test, results not significant.

Islets are comprised of five main endocrine cell types, which produce specific hormones. To investigate the proliferating cell type, islets were analysed by immunofluorescence staining which revealed a significant increase in the proliferation of Nkx6.1^{+} β-cells (Figure 4.3A&B). This was supported by an increase in the number of Nkx6.1^{+} β-cells in the islets co-cultured with GOF cDCs for 5 days (Figure 4.3C). The primary source of new pancreatic β-cells in adult mice is through replication of existing β-cells (215). Therefore harnessing mechanisms that regulate β-cell proliferation has the potential to restore insulin secretion in diabetes.

The processes that trigger endogenous β-cell proliferation have been widely studied, with several pathways implicated. Wnt signalling in the pancreas has been reported to be necessary and sufficient for β-cell proliferation (214) (212). Wnt proteins are known to affect cell growth, the expression of these are tightly regulated during development. Interestingly, in the GOF mice there was an increase, though not significant, in islet Wnt3a expression by RT-PCR analysis (Figure 4.3D), which supports previous observations (214). Furthermore, the production of Wnt ligands from Flt3L-bone marrow derived cDCs was altered in the GOF mice, with elevated mRNA expression certain Wnt ligands (Figure 4.4). Collectively from these results we hypothesise that the constitutive activation of β-catenin in cDCs produces an increase in Wnt ligand expression and availability, which enables the expansion of islet size by increasing β-cell proliferation.

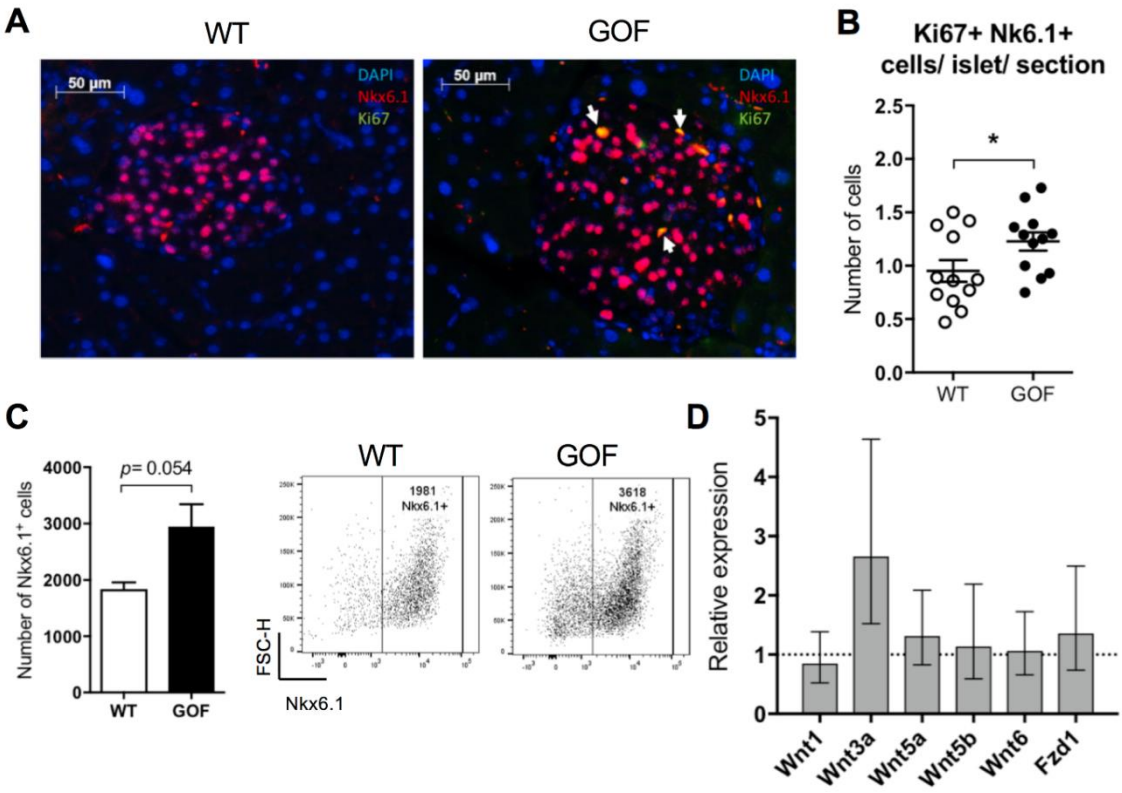

Figure 4.3 β-cell proliferation is increased in the islets of the GOF model
(A) Representative images of immunofluorescence stained sections of pancreas from GOF and WT mice. Arrows indicate Ki67$^+$ Nkx6.1$^+$ β-cells. (B) Ki67$^+$ Nkx6.1$^+$ β-cells in islets counted and number per islet per section determined, mean ± SEM (n=12). Statistical significance was determined by Student's t-test with two-tailed *P* values, results not significant unless otherwise denoted as *p<0.05. (C) cDCs isolated from GOF and WT mice fed WD were co-cultured with islets from donor mice for 5 days. Number of Nkx6.1$^+$ β-cells was determined in these islets by flow cytometry, mean ± SEM (n=3). (D) qRT-PCR analysis for mRNA expression of Wnt ligands in islets of GOF and WT mice. Expression levels of all mRNA were normalised to GAPDH expression. Bars represent ΔΔCT data values, the expression in GOF mice compared to WT, set at 1 indicated by the dotted line. Error bars show the geometric mean of five biological replicates. Statistical significance of ΔCT data values was determined by Student's two-tailed t-test, results not significant.

Dysregulation of Wnt/β-catenin pathway has been implicated with T2DM susceptibility, for example variants of *Tcf7l2* gene are strongly associated with T2DM (175). In addition, single nucleotide polymorphisms in *Wnt5b* gene are associated with the risk of T2DM in the absence of obesity (173) (174). Interestingly, levels of Wnt5b were elevated in cDCs from the GOF mice compared to WT (Figure 4.4). Expression of Wnt7a and Fzd1, which is a Wnt signalling receptor, were also significantly increased in cDCs from the GOF mice, while production of Wnt10a expression was reduced compared to WT (Figure 4.4).

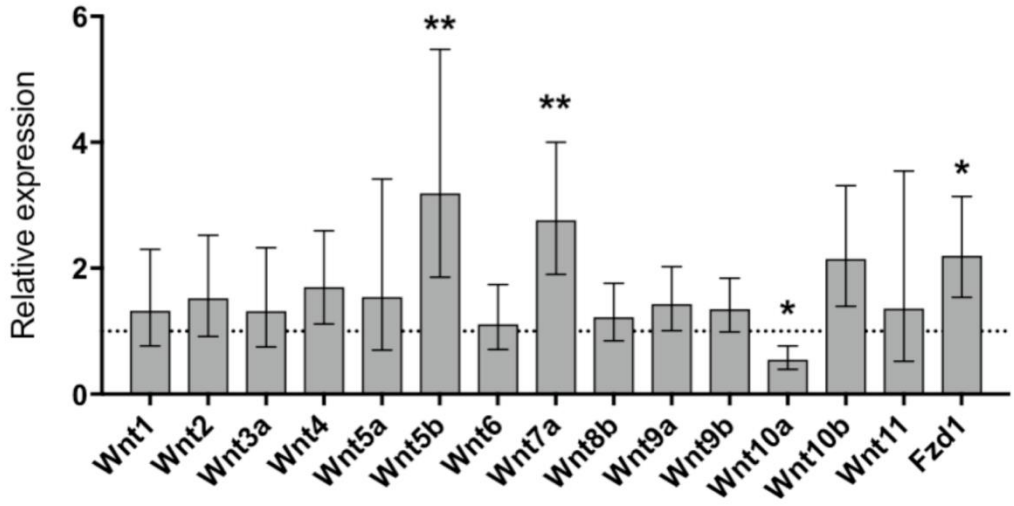

Figure 4.4 Wnt profile in the GOF model
qRT-PCR analysis for mRNA expression of Wnt ligands in Flt3L-bone marrow derived cDCs from GOF and WT mice. Expression levels of all mRNA were normalised to GAPDH expression. Bars represent ΔΔCT data values, the expression in GOF mice compared to WT, set at 1 indicated by the dotted line. Error bars show the geometric mean of six biological replicates. Statistical significance of ΔCT data values was determined by Student's t-test with two-tailed *P* values, results not significant unless otherwise denoted as *p<0.05, **p<0.01.

4.2.2 Modulation of islet immune phenotype by constitutive β-catenin activation in cDCs

The link between the development of T2DM and chronic low-grade inflammation is well reported (207). It has been shown that infiltrating $CD68^+$ macrophages are present in islets of T2DM human tissue (37), producing high levels of IL-1β which plays a role in the early pathology of T2DM through inflammasome activation in islets (50) (38). However, there remains a limited understanding of if and how cDCs can directly affect β-cell insulin secretion in T2DM.

To evaluate if differences in the activated cDC phenotype of GOF and WT mice could directly influence insulin release by β-cells, co-cultures were set up with islets from donor B6 mice and Flt3L-bone marrow derived cDCs from GOF or WT mice (Figure 2.5). The acute overnight incubation was designed to analyse the effects on insulin release in a size independent manner, separate from the previous observations on β-cell proliferation. To note, manipulation of cDCs by pipetting or co-culturing is known to induce a certain level of cell activation which consequently is expected to affect β-cell function. Insulin measured from GOF

cDC co-cultures was increased compared to WT cDC co-cultures (Figure 4.5A), suggesting that WT cDC exhibit a more activated phenotype than GOF cDC and subsequently inhibit insulin release. Furthermore, when neutralising IL-10 in the co-cultures, insulin secretion was significantly decreased in the GOF co-cultures (Figure 4.5B). This effect on insulin release can be in part explained by the increase in IL-10 produced from GOF cDC (Figure 4.5C), which could contribute towards a generating an immunosuppressive environment in the islets preventing deleterious effects on β-cell insulin secretion.

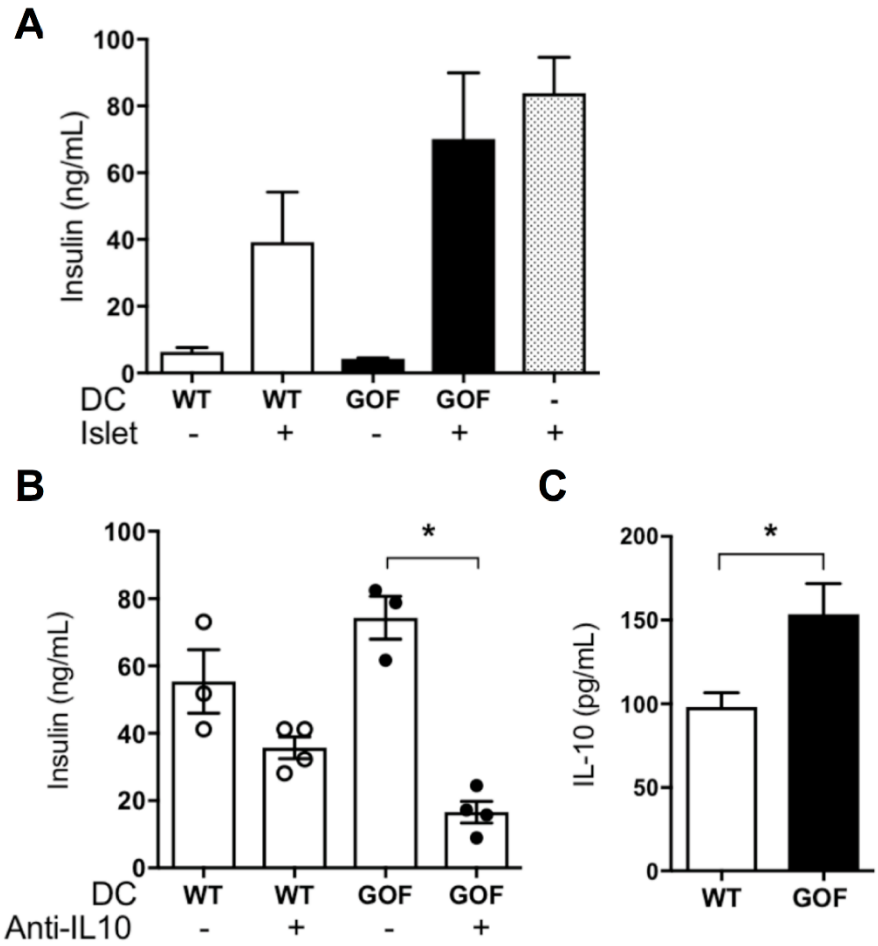

Figure 4.5 GOF cDCs alter the insulin release from islets independent of size
(A) cDCs isolated from GOF and WT mice fed WD were co-cultured overnight with and without islets from donor mice. Insulin was measured by ELISA from the supernatant harvested the next day to measure secretion, mean ± SEM (n=4) representative of three independent experiments. (B) IL-10 was neutralised in the co-cultures with 1 µg/ml anti-IL-10 and insulin was measured by ELISA from the supernatant harvested the next day, mean ± SEM (n=3/4) representative of three independent experiments. (C) Concentration of IL-10 measured by ELISA from supernatant of WT and GOF cDC cultured overnight, mean ± SEM (n=6). Statistical significance was determined by Student's two-tailed t-test, results not significant unless otherwise denoted as *p<0.05.

The phenotype of cDCs in the pancreas during chronic inflammation and T2DM has yet to be fully characterised, in contrast to the well-studied autoimmune T1DM where subsets of cDCs have been identified in islets (163). Indeed, using *Zbtb46*^{GFP} mice the presence of cDCs were confirmed in both the pancreas and islets (Figure 4.6A&B). Increased expression of β-catenin in cDCs from the pancreas was observed in the GOF mice by western blot and densitometry analysis (Figure 4.6C). To assess the pancreas cDC phenotype and abundance, expression of co-stimulatory molecules was analysed by flow cytometry. There were no differences in the percentage of cDCs or subsets in the pancreas between the GOF and WT mice fed WD (Figure 4.6D). In addition, the expression of costimulatory molecules CD40, CD80 and CD86 remain unchanged on the pancreas cDC surface, indicating no effect on co-stimulation of pancreas cDC in mice with diet-induced tissue inflammation (Figure 4.6E). These findings suggest that the observed effect by of constitutive β-catenin activation in cDCs on insulin secretion is likely due to functional differences, such as IL-10 production.

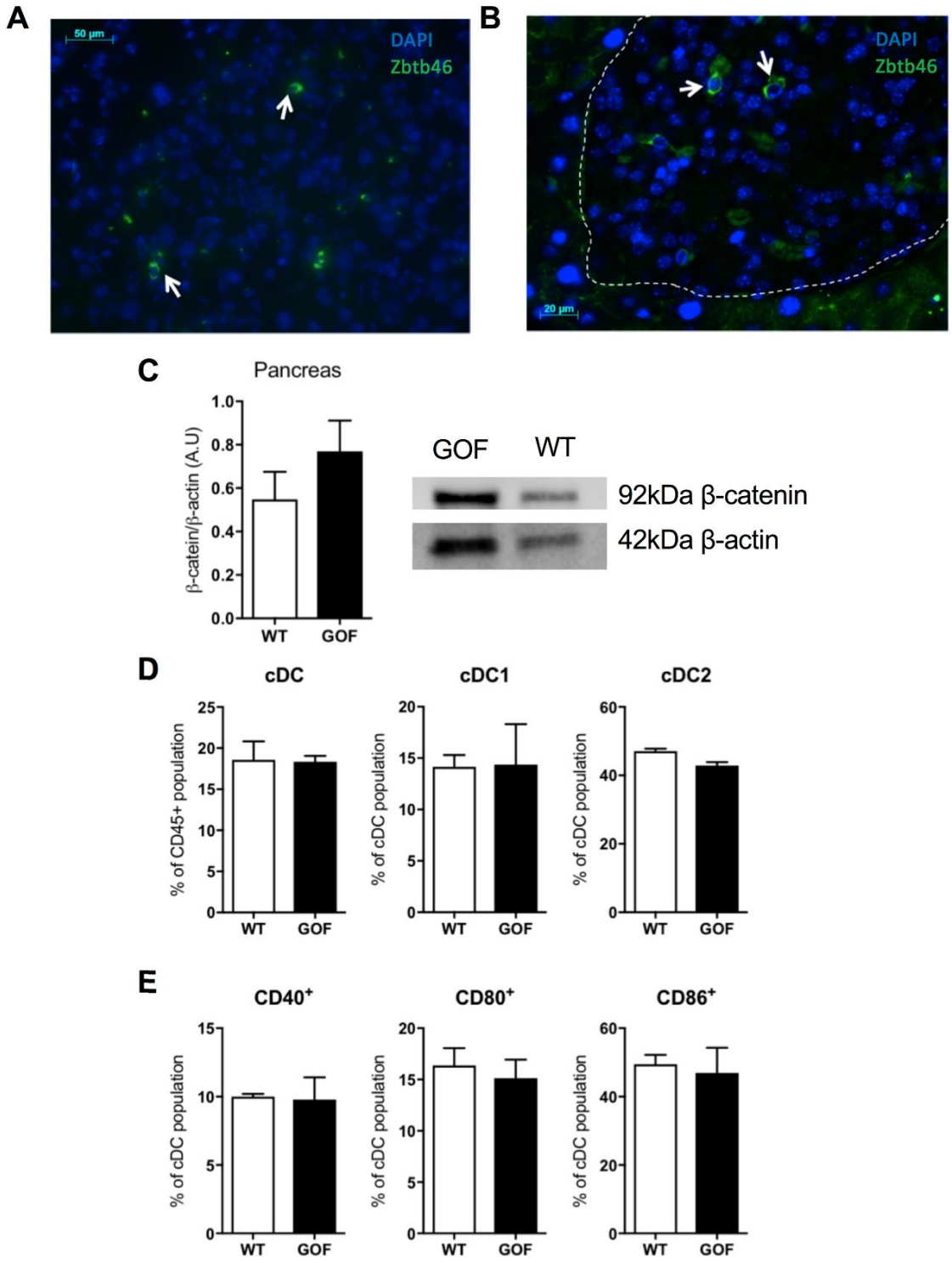

Figure 4.6 Pancreas DC phenotype in the GOF model
(A) Representative images of immunofluorescence stained sections of pancreas from *Zbtb46*^{GFP} mice. Islet is indicated by the dotted line, arrows indicate cDCs in pancreas tissue and (B) in islet. (C) CD11c^{+} DCs were isolated from pancreas of WT and GOF mice. Expression of β-catenin was detected by western blot, shown as a representative of three independent experiments. Expression of β-catenin was normalised to β-actin expression by densitometry analysis, mean ± SEM (n=3). (D) Islets from GOF and WT mice fed WD were digested and cDC populations were analysed by flow cytometry, presented as percentage of parent population, mean ± SEM (n=3). (E) Percentage of CD40^{+}, CD80^{+}, CD86^{+} -expressing cDCs were quantified by flow cytometry, mean ± SEM (n=3). Statistical significance was determined by Student's two-tailed t-test, results not significant.

The previous results suggest that modulation of *in vivo* insulin secretion in the GOF mice can be controlled by local inflammation. To investigate this possibility, immune cell responses in the islets of GOF and WT mice fed WD were assessed. Immune cell populations in the islets were analysed by flow cytometry. The gating strategy detailed previously was used to analyse the immune populations (Figure 2.4). A trend towards a reduction in the percentage of $CD3^+$ T cells and a significant increase in the percentage of T reg cells was observed in the GOF mice compared to WT (Figure 4.7A&B). The percentage of T cell memory subsets were unchanged, however in the GOF mice there was a significant reduction in the percentage of IFNγ-producing $CD4^+$ T cells (Figure 4.7C). The overall reduction in $CD3^+$ T cells suggests less lymphocytes infiltrate into the islets of the GOF mice fed WD, which was also confirmed by immunohistochemistry staining of $CD3^+$ T cells (Figure 4.7D). Furthermore, the expression of T cell chemoattractant CCL17 was significantly decreased in the islets of GOF mice fed WD compared to WT, as measured by qRT-PCR analysis (Figure 4.7E). This corroborates previous findings in Chapter 3, that constitutive β-catenin activation in cDCs modulates T cell recruitment and promotes a T cell driven immunosuppressive phenotype. Despite this, the CCR4 expression in the islets of the GOF mice was not decreased, which is the cognate chemokine receptor for CCL17. In addition, the mRNA expression of IL-10 in the islets was not significantly increased in the GOF mice fed WD. Although unexpected, the absence of difference in IL-10 expression could be the result of low cDC abundance in the islet or rather a localised effect which was diluted in whole islet mRNA expression analysis. However, a significant reduction was observed in the expression of NFkB p65 subunit as measured by western blot, suggesting a decrease in activation of immune cells and consequently as an indicator of less inflammation in the islets of the GOF mice (Figure 4.7F). Therefore, constitutive β-catenin activation in cDCs promotes a healthier immune phenotype in the islets which in combination with an increased islet size, enables the islets to provide a greater insulin reserve in response to diet-induced inflammation.

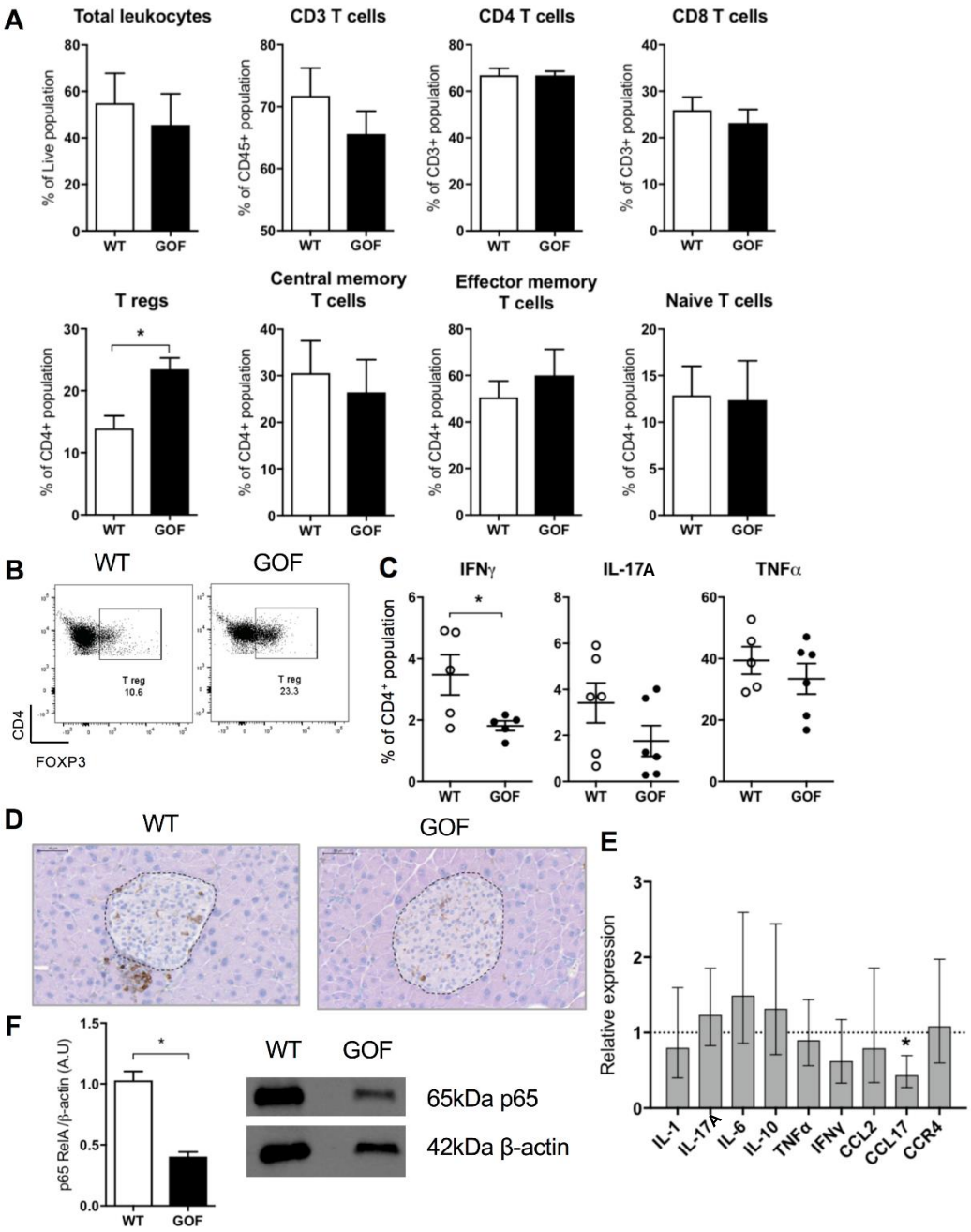

Figure 4.7 Modulation of the T cell phenotype in the islets of the GOF model
(A) Immune cell populations from islets of GOF and WT mice fed WD were analysed by flow cytometry, presented as percentage of parent population, as determined in gating strategy (Figure 2.4), mean ± SEM (n=5). (B) Representative dot plots of T reg cells from the islets of GOF and WT mice. (C) Intracellular cytokine expression of islet infiltrated $CD4^+$ T cells was analysed by flow cytometry, presented as percentage of $CD4^+$ population, mean ± SEM (n=5/6). (D) Representative images of CD3-stained sections of pancreas from GOF and WT mice, islets are indicated by the dotted line. (E) qRT-PCR analysis for mRNA expression in islets of GOF and WT mice. Expression levels of all mRNA were normalised to GAPDH expression. Bars represent ΔΔCT data values, the expression in GOF mice compared to WT, set at 1 indicated by the dotted line. Error bars show the geometric mean of five biological replicates. Statistical significance of ΔCT data values was determined by Student's two-tailed t-test, results not significant unless otherwise denoted as *p<0.05. (F) Expression of p65 RelA protein in islets from GOF and WT mice fed WD, measured by western blot, mean ± SEM (n=4). Statistical significance was determined by Student's two-tailed t-test, results not significant unless otherwise denoted as *p<0.05.

4.3 Discussion

Metabolic control is tightly entwined with the immune system. Studies are beginning to explore the effect of immune cells in the development of T2DM. This chapter has discovered a novel role of β-catenin activation in cDCs to enhance β-cell insulin secretion and modulate islet inflammation, thus generating a greater insulin reserve in response to diet-induced obesity and providing an increased ability to control hyperglycaemia.

While investigating the pancreas function, an unexpected observation was uncovered in relation to islet size (Figure 4.1). Constitutive activation of β-catenin in cDCs induced the expansion of islets, which was attributed to increased β-cell proliferation (Figure 4.3). The number of functional β-cells is the main factor that contributes to the amount of insulin secreted in response to metabolic demand. A decrease in β-cell number and function contributes to the pathophysiology of T2DM. Interestingly, a modulation of Wnt ligands was observed in the islets of GOF mice. The Wnt/β-catenin pathway has been previously linked to expansion of β-cell mass and improved insulin secretory function (211) (209). Specifically Wnt3a signalling in the pancreas has been shown to induce β-cell proliferation (214). Wnt3a is an activator of the canonical Wnt/β-catenin pathway and is present in the developing pancreas and in adult human islets (216). Wnt3a stimulates the expression of multiple β-cell cycle regulators including *c-Myc*, *cyclin D1* and *CDK4*, to promote cell proliferation (214). It has also been proposed that Wnt signalling may crosstalk with other pathways within the β-cell to induce proliferation, for example with the incretin, glucagon-like peptide-1 (GLP-1) signalling (172). As well as stimulating insulin secretion, GLP-1 is also known to promote β-cell proliferation (217). Thus, Wnt ligands may act directly or indirectly to initiate β-cell proliferation. An increase, although not significant, of Wnt3a, cMyc and Cyclin D1 expression was observed in the islets of GOF mice (Figure 4.2 & 4.3), suggesting constitutive β-catenin activation in cDCs may contribute locally to an increase β-cell proliferation. Additionally, the Wnt ligand profile produced by Flt3L-bone marrow derived cDCs was significantly altered in the GOF mice (Figure 4.4), indicating a potential local increase in ligand availability. It has been observed previously that cDCs produce Wnt ligands in the gut (185). Thus, we propose that constitutive activation of β-catenin may directly induce a

feedforward loop for initiating and producing Wnt ligands from cDCs, which could act in a paracrine manner on β-cells to induce proliferation. Indeed, Wnt ligands have poor solubility implying this interaction may happen locally in the islets, in close proximity. Therefore, cDCs with constitutive β-catenin activation, which are present in the pancreas and islets, may potentially act as a source for tissue-specific Wnt ligands. This increase in Wnt ligand expression and availability in the pancreas, may act as a local system promoting β-cell proliferation and increasing β-cell mass. However, the exact mechanism requires further investigation. Interestingly, the proliferative potential of human β-cells has been shown to rely on Wnt ligand receptor activation, through crosstalk of multiple signalling pathways (218). Thus, activation of Wnt/β-catenin pathway in cDCs, may have the potential to translate in humans as a possible strategy to restore the loss of β-cell mass in T2DM, as well as in T1DM.

Although β-cell proliferation from pre-existing β-cells is increased in the GOF islets, this may not entirely account for the expansion of β-cell population in the islets. β-cell neogenesis also occurs in the pancreas, through activation of β-cell progenitor cells or transdifferentiation, which may additionally increase the number of β-cells. Transdifferentiation is a process whereby a differentiated cell is converted into another cell type. It has been shown that functional insulin secreting β-cells have arisen from pre-existing α-cells in the islet and exocrine cells including acinar ductal cells (219). The Wnt/β-catenin pathway is known to be important for regulating cell differentiation. Interestingly, the pathway is activated during the differentiation of adipose-derived stem cells into functional β-cells (220), suggesting another possible mechanism by which the β-cell population expands in response to increased Wnt ligand exposure. Although prolonged activation of Wnt/β-catenin pathway has also shown to affect the differentiation state of β-cells (221). Consequently the local levels of Wnt expression in the islets may be critical to determine their beneficial effect on β-cell population. Thus, further investigation of alternative mechanisms by which β-cell expansion can occur in the islet, in response to constitutive β-catenin activation in cDCs, will be required.

Islet inflammation has been associated with T2DM and is known to contribute to the onset and progression of β-cell failure (39). Increased numbers of leukocytes

and pro-inflammatory mediators have been observed in the islets of individuals with T2DM, specifically an elevation of $CD68^+$ macrophages, increased B lymphocyte infiltration and greater absolute numbers of T cells and $CD11b^+$ $CD11c^+$ myeloid cells (37) (36). However less is known about the infiltration and pathological consequence of cDCs in the islets in T2DM. A size-independent effect was observed by cDCs with constitutively active β-catenin, to generate an immunosuppressive environment in the islet through increased IL-10 production and infiltration of T reg cells (Figure 4.5 & 4.7). IL-10 has well characterised anti-inflammatory properties, and emerging evidence suggests the cytokine can exert direct effects on β-cell function and viability (222) (223). In addition T reg cells are known to promote systemic insulin sensitivity, demonstrated in the inhibition of diabetes induced through the adoptive transfer of diabetogenic T cells in immunocompromised NOD mice (224). At an islet-specific level the action of T reg cells are yet to be explored in T2DM but it is known their numbers and function are decreased in the inflamed islets of T1DM patients (225). Interestingly, islet antigen-specific T reg cells, expanded *in vitro* by cDCs, were able to expand the endogenous T reg population *in vivo*, restoring insulin secretion and further reverting diabetes in the NOD mouse (226). Therefore, the reduction of islet inflammation by constitutive activation of β-catenin in cDCs may provide a potential mechanism to prevent the deleterious effects on β-cell insulin secretion. Despite the beneficial effects on β-cell health, the immunosuppressive environment generated by constitutively active β-catenin in cDCs should be cautious to consider the development of pancreatic cancer. Tumour development favours immune suppression, including the recruitment of T reg cells and tolerogenic DCs. Furthermore overexpression of β-catenin promotes pancreatic cancer (227).

In summary, this chapter has demonstrated a novel mechanism by which cDCs promote a healthier immune phenotype in the islets, which in combination with an increased islet size, enables the islets to provide a greater insulin reserve in response to diet-induced inflammation. Furthermore, this work suggests a possible new compensatory mechanism to prevent hyperglycaemia in the development of T2DM. Although we have shown the Wnt/β-catenin signalling as a novel pathway in cDCs to modulate islet inflammation, investigations of other immunosuppressive pathways in cDCs may also provide beneficial effects on

islet immune health during T2DM. Ultimately, these findings highlight the potential of immune modulation to improve β-cell mass and function and opens up the possibility of targeting cDCs for the treatment of T2DM.

Chapter 5 Translational impact of Wnt/β-catenin pathway activation in conventional dendritic cells

5.1 Introduction

Adiponectin is known to regulate a number of metabolic processes including glucose regulation and fatty acid oxidation, thus suppressing the metabolic derangements that result in the development of T2DM and obesity (205). Adiponectin has also been shown to have a beneficial role in cardiovascular disease, specifically anti-inflammatory and anti-atherogenic effects in the development of atherosclerosis (228). Results in Chapter 3 demonstrated significant increases in adiponectin mRNA expression in VAT, as measured by qRT-PCR and elevated levels of adiponectin protein in the plasma of the GOF model in diet-induced tissue inflammation (Figure 3.11B & 3.19E). Additionally, it has been shown that CCL17-expressing cDCs drive atherosclerosis by restraining T reg cell recruitment into the aortic vessel (198). In line with this, results in Chapter 3 also showed a significant decrease in CCL17 mRNA expression in VAT, as well as reduced protein level produced by VAT-cDCs from the GOF mice during diet-induced tissue inflammation (Figure 3.11B & 3.18A). Furthermore, the T reg cell phenotype is modulated in the GOF model, suggesting a decrease in CCL17 may enable an expansion of the T reg population in the aorta. Combined, these results indicated that constitutive activation of β-catenin in cDCs may have the potential to reduce atheroprogression by reverting inflammatory responses in the aortic vessel.

Atherogenesis is a process of atheroma plaque formation in the intima layer of arteries, causing vessel remodelling. The luminal of the artery becomes narrowed and arterial walls stiffen as the plaque develops over time, which results in an increased risk of cardiovascular complications including coronary artery disease, stroke and kidney disorders. A number of contributory factors that exacerbate atheroprogression include obesity and T2DM. The progressive development of

atherosclerosis occurs predominately due to endothelial dysfunction, lipid accumulation and chronic inflammation (229). Macrophages and oxidised low-density lipoprotein (LDL) are well-established players in the initiation of atheroma development (230). Cholesterol lipids are required for cell membranes and are transported in the blood by lipoproteins, which are categorised by their density including LDL, high-density lipoprotein (HDL) and very low-density lipoprotein (VLDL). HDL is responsible for scavenging cholesterol from peripheral tissues to the liver for their removal, while LDL exerts opposite functions carrying cholesterol from towards cells where it binds to LDL receptors (LDL-R) for cholesterol absorption. However, during chronic overnutrition when cells reach their limit of cholesterol uptake from the blood, the synthesis of LDL-R is blocked resulting in elevated blood cholesterol levels (hypocholesterolaemia) (229). Free LDL is oxidised in the blood and phagocytosed by macrophages, which are recruited to the arterial wall and transform into high-lipid carrying “foam cells” (231). These cells are a hallmark of the early atherosclerotic plaque and secrete pro-inflammatory cytokines to amplify local inflammatory responses at the arterial site (232). Recruitment of other inflammatory immune cells, increased ROS generation and production of matrix metalloproteinases (MMP) and growth factors contribute to the atherosclerotic plaque formation, where smooth muscle cell deposition of extracellular matrix accumulates, increasing the plaque size (233). Inflammation is key in the pathophysiology of atherosclerosis and has been the focus of therapeutic interventions to ameliorate disease progression. Although macrophages are well characterised in atherogenesis, adaptive immune responses also contribute to the regulation of aortic inflammation (232). T cells are present in atherosclerotic plaques and depending on the balance of T helper cell subsets, exacerbate or limit inflammation to influence atheroma formation (234). cDCs have also been identified in atherosclerosis, participating in lipid uptake and inflammation resolution (235). Thus, we proposed that cDCs with constitutive β-catenin activation may have the potential to attenuate the systemic inflammation developed in VAT as a result of dyslipidaemia and/or directly affect local inflammation in the plaque. Therefore we hypothesised that GOF mice could have a potential cardio-protective phenotype, reducing plaque development in an atherosclerosis model.

In this chapter the role of Wnt/β-catenin signalling in cDCs is investigated, to assess the effect on the development of atherosclerosis and explore the therapeutic potential of targeting of the Wnt/β-catenin pathway in cDCs.

5.2 Results

5.2.1 Constitutive β-catenin activation in cDCs reduces free fatty acids in an atherosclerosis model

To investigate the effect of constitutive β-catenin activation in cDCs on atherogenic development, bone marrow chimeric mice were generated using the *Ldlr* $^{-/-}$ mouse model. The *Ldlr* $^{-/-}$ mouse model is commonly used for atherosclerotic studies due to the deficiency of functional LDL-R, consequently cholesterol cannot be efficiently cleared from the blood accelerating the development of atherosclerotic plaques during WD feeding. Bone marrow cells from β-catenin$^{Fl/+}$ Zbtb46-Cre^{+} (GOF) or β-catenin$^{+/+}$ Zbtb46-Cre^{+} (WT) were transferred into irradiated B6.129S7-Ldlr^{tm1Her}/J (*Ldlr*$^{-/-}$) recipient mice, hence forth referred to as *Ldlr* $^{-/-}$ GOF mice or *Ldlr* $^{-/-}$ WT mice respectively (Figure 2.3). In the *Ldlr* $^{-/-}$ GOF model, only cDCs express Zbtb46 and hence, exclusively express constitutively active β-catenin. Mice were fed 12 weeks of WD to induce atherogenic development. There was no difference in body weight between *Ldlr* $^{-/-}$ GOF and *Ldlr* $^{-/-}$ WT mice fed WD (Figure 5.1A). Free fatty acids (FFA) are elevated in the plasma during obesity and contribute to the development of atherosclerotic plaques. Encouragingly, there was a significant decrease of plasma FFA levels in *Ldlr* $^{-/-}$ GOF mice compared to *Ldlr* $^{-/-}$ WT mice (Figure 5.1B), suggesting that constitutive β-catenin activation in cDCs may limit FFA generation from inflamed VAT and thus promote a beneficial effect on lipid regulation. Despite this, there was no difference in total cholesterol, HDL or LDL/VLDL levels in the plasma between *Ldlr* $^{-/-}$ GOF and *Ldlr* $^{-/-}$ WT mice (Figure 5.1C-E). Furthermore the adipokine leptin, which has a well-established role in the metabolic control of lipids, was unchanged in the plasma of *Ldlr* $^{-/-}$ GOF mice (Figure 5.1F). Unexpectedly, the level of circulating adiponectin in the plasma of

Ldlr $^{-/-}$ GOF mice was not significantly increased compared to *Ldlr* $^{-/-}$ WT mice (Figure 5.1G).

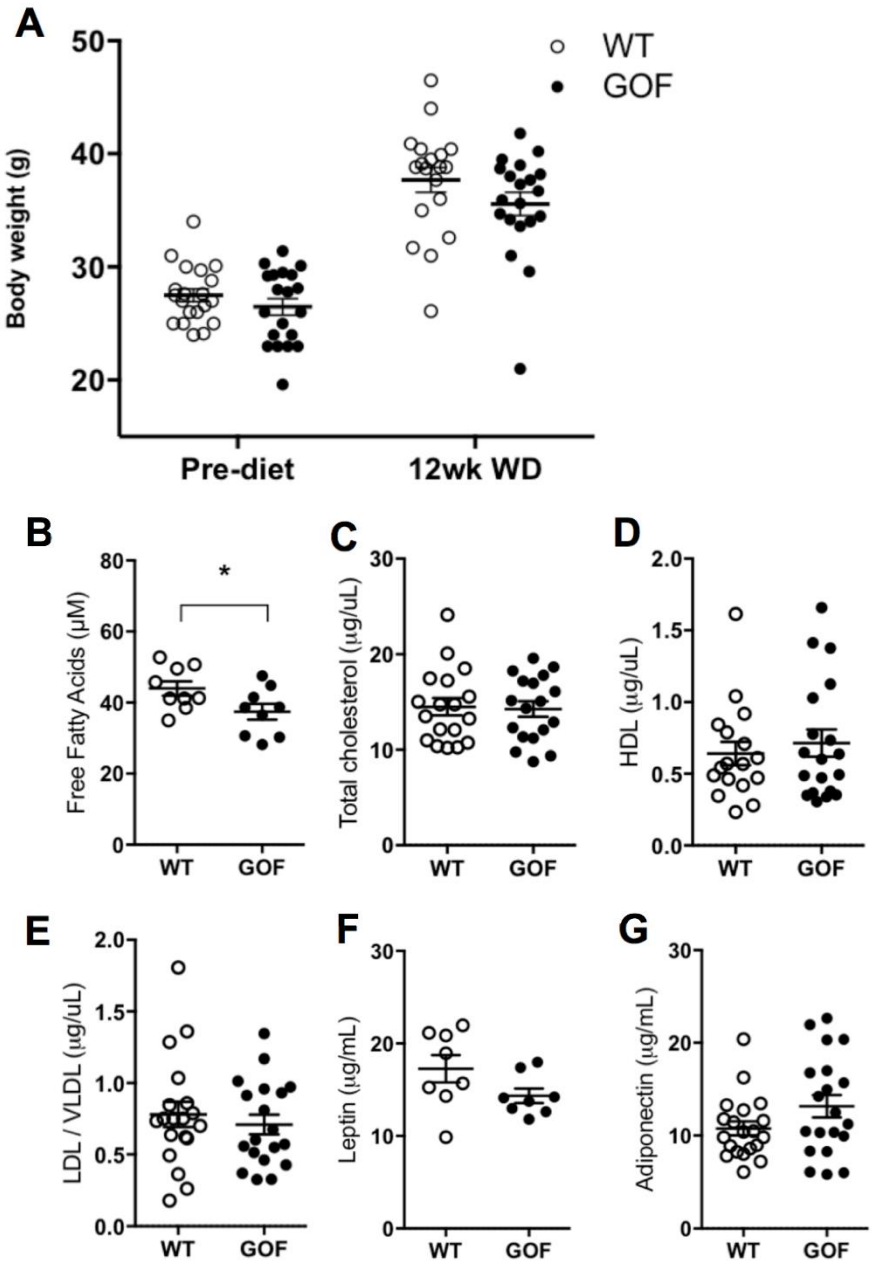

Figure 5.1 Metabolic phenotype of the *Ldlr* $^{-/-}$ GOF model
(A) Body weight was measured pre-diet and after 12 weeks of WD of *Ldlr* $^{-/-}$ GOF and *Ldlr* $^{-/-}$ WT mice, mean ± SEM (n=20). (B) Levels of free fatty acid and (C) total cholesterol, (D) HDL, (E) VLDL /LDL, (F) leptin and (G) adiponectin were quantified in the fasted plasma of *Ldlr* $^{-/-}$ GOF and *Ldlr* $^{-/-}$ WT mice, using ELISA and commercial kits, mean ± SEM B. (n=9) F. (n=8) C-E, G. (n=20). Statistical significance was determined by Student's two-tailed t-test, results not significant.

5.2.2 Constitutive activation of β-catenin in cDCs affects the immune phenotype in an atherosclerosis model

To explore the impact of constitutive β-catenin activation in cDCs on the immune phenotype in the *Ldlr* $^{-/-}$ model, flow cytometry staining was used to quantify immune cell numbers in the spleen, mediastinal draining lymph nodes and inguinal non-draining lymph nodes of *Ldlr* $^{-/-}$ GOF and *Ldlr* $^{-/-}$ WT mice. The gating strategy detailed previously, was used to analyse the immune populations (Figure 2.4). Constitutive activation of β-catenin in cDCs did not impact the numbers of immune cells in the spleen (Figure 5.2). Interestingly, however when analysing the immune populations in the mediastinal draining lymph nodes and inguinal non-draining lymph nodes, the neutrophil populations were observed to be significantly reduced in the *Ldlr* $^{-/-}$ GOF mice compared to *Ldlr* $^{-/-}$ WT (Figure 5.3 & 5.4). A decrease in the number of neutrophils suggests a decrease in systemic inflammation, although this effect was not detected in the spleen. Constitutive activation of β-catenin in cDCs did not significantly affect the numbers of other immune cell populations in the mediastinal draining lymph nodes and inguinal non-draining lymph nodes (Figure 5.3 & 5.4). However there was an indication that migratory cDCs were increased in the draining lymph nodes of the *Ldlr* $^{-/-}$ GOF mice, while a trend towards a decrease in numbers of migratory cDCs was observed in the non-draining lymph nodes. This distribution infers that constitutively activated β-catenin in cDCs may preferentially locate to the site of inflammation in the aorta.

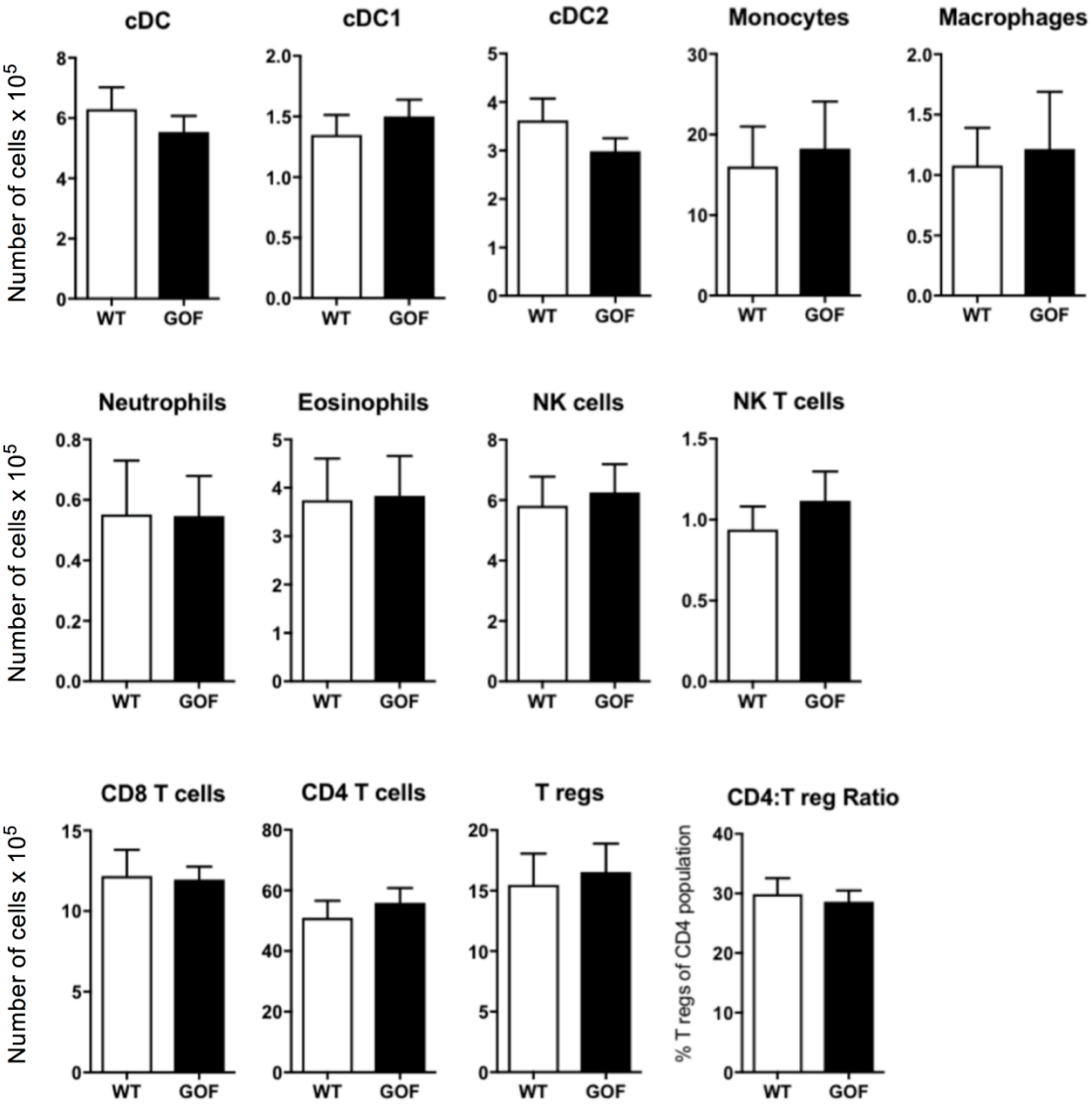

Figure 5.2 Immune phenotype in the spleen of the *Ldlr* $^{-/-}$ GOF model
Spleen from *Ldlr* $^{-/-}$ GOF and *Ldlr* $^{-/-}$ WT mice were digested. Total numbers of immune populations were quantified by flow cytometry, mean ± SEM (n=10). Statistical significance was determined by Student's two-tailed t-test, results not significant.

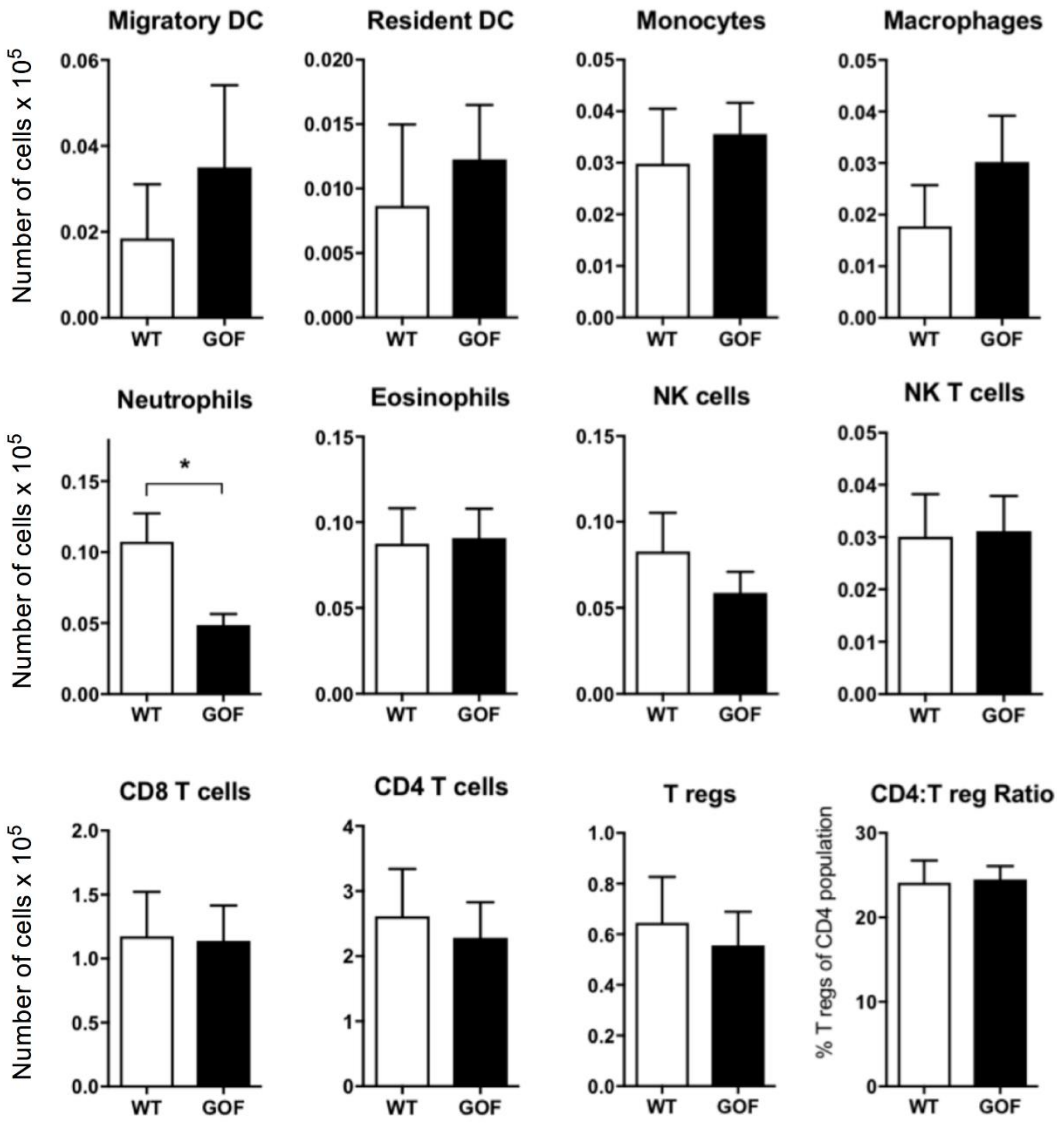

Figure 5.3 Immune phenotype in the draining lymph nodes of the *Ldlr*$^{-/-}$ GOF model

Mediastinal draining lymph nodes from *Ldlr*$^{-/-}$ GOF and *Ldlr*$^{-/-}$ WT mice were digested. Total numbers of immune populations were quantified by flow cytometry, mean ± SEM (n=8). Statistical significance was determined by Student's two-tailed t-test, results not significant.

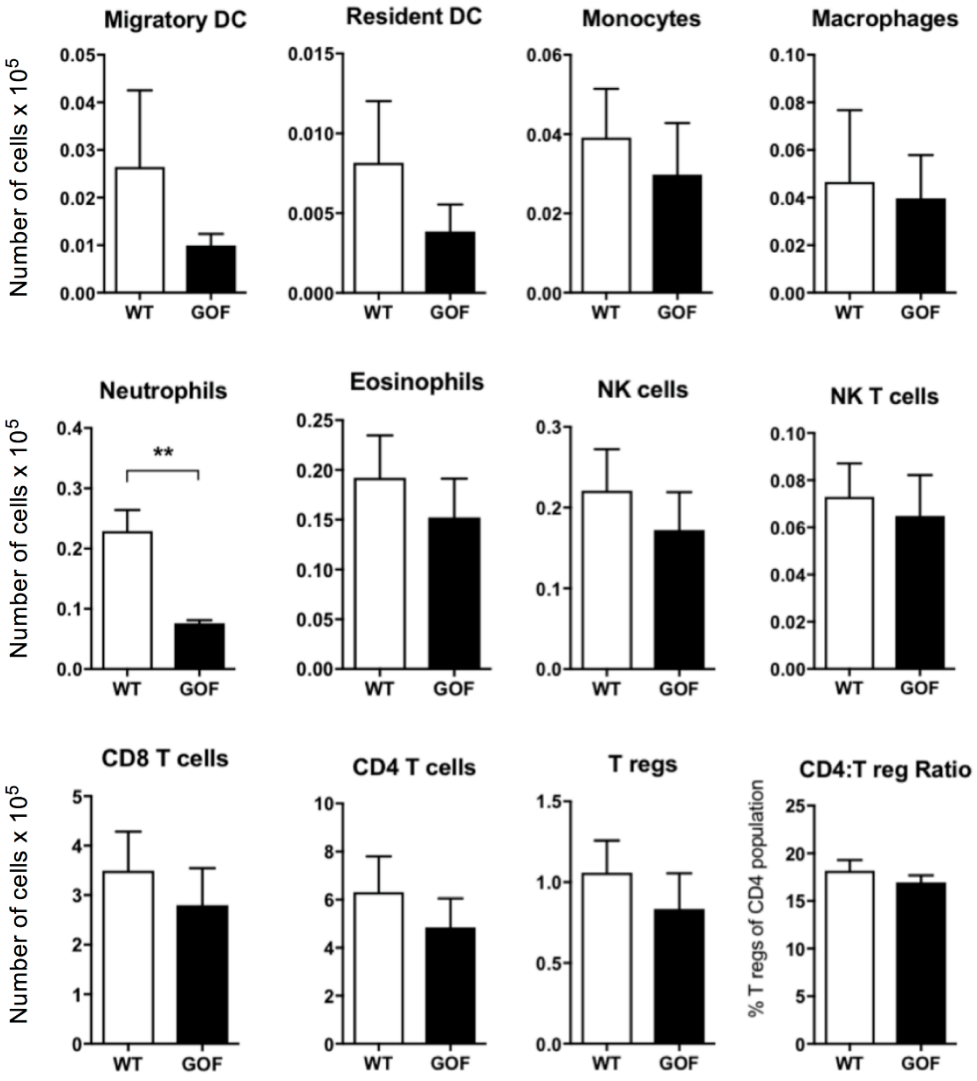

Figure 5.4 Immune phenotype in the non-draining lymph nodes of the *Ldlr*$^{-/-}$ GOF model
Inguinal non-draining lymph nodes from *Ldlr*$^{-/-}$ GOF and *Ldlr*$^{-/-}$ WT mice were digested. Total numbers of immune populations were quantified by flow cytometry, mean ± SEM (n=7). Statistical significance was determined by Student's two-tailed t-test, results not significant.

Immune populations could not be analysed in the aorta of *Ldlr*$^{-/-}$ GOF and *Ldlr*$^{-/-}$ WT mice as the whole aortas were required for plaque density measurements. However in previous experiments, immune cells in the aorta of WT and GOF mice fed WD to induce inflammation, were analysed to indicate potential changes in the *Ldlr*$^{-/-}$ model. There were no differences in the percentage of total leukocytes in the aorta, neither in the percentage of the $CD3^+$, $CD8^+$, $CD4^+$ T cell or T reg cell populations (Figure 5.5). This indicates there was no change of immune cell recruitment in the aorta of GOF and WT mice suggesting that constitutive β-

catenin activation in cDCs may not have affected the aortic inflammation in the *Ldlr*$^{-/-}$ atherosclerosis model.

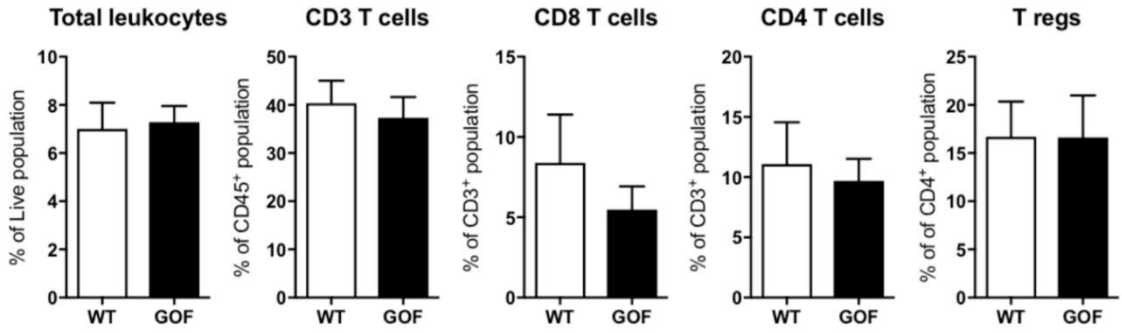

Figure 5.5 Immune populations in the aorta of the GOF model in inflammation
Aortic cells were isolated from GOF and WT mice and immune cell populations were analysed by flow cytometry. Presented as percentage of parent population, as determined in gating strategy (Figure 2.4), mean ± SEM (n=5). Statistical significance was determined by Student's two-tailed t-test, results not significant.

5.2.3 Constitutive activation of β-catenin in cDCs improves the immune phenotype of the adipose tissue in an atherosclerosis model

To further assess the immune phenotype of *Ldlr* $^{-/-}$ GOF mice, mRNA expression of cytokines, chemokines and adipokines was measured in the SVF and pericardial AT by qRT-PCR. Similarly to previous observations in a model of diet-induced obesity (Figure 3.11), the expression of T cell chemoattractant CCL17 was significantly reduced in SVF of *Ldlr* $^{-/-}$ GOF compared to *Ldlr* $^{-/-}$ WT mice (Figure 5.6A). This suggests that constitutive activation of β-catenin in cDCs may have modulated the T cell recruitment in VAT to reduce inflammation. Although there was no change in expression of T cell immunosuppressive cytokines such as IL-10 and TGFβ between *Ldlr* $^{-/-}$ GOF and *Ldlr* $^{-/-}$ WT mice, there was a trend towards an increase in FOXP3 expression suggesting a potential expansion of T reg cell population in VAT of *Ldlr* $^{-/-}$ GOF mice. Additionally the production of pro-inflammatory TNFα was significantly reduced, indicating a potential reduction in TNFα -expressing $CD4^+$ T cells (Figure 5.6A). Furthermore in pericardial AT located around the aorta vessel, there was also a significant reduction in CCL17 and TNFα and an increase in FOXP3 expression in *Ldlr* $^{-/-}$ GOF mice (Figure 5.6B). This suggests a local modulation of T cell phenotype near the vessel,

potentially promoting an immunosuppressive environment. IL-6 was significantly decreased in the pericardial AT of *Ldlr* $^{-/-}$ GOF mice indicating there was a possible reduction in inflammation (Figure 5.6B). Despite previous results showing no change in circulating adiponectin levels (Figure 5.1G), there was a significant increase in the adiponectin expression locally in the pericardial AT of *Ldlr* $^{-/-}$ GOF mice (Figure 5.6B). This suggests an improved local adipocyte function, although local production was not sufficient to affect systemic concentrations. Therefore, the beneficial effects of adiponectin on supressing inflammation may have occurred locally and not systemically in the *Ldlr*$^{-/-}$ GOF atherosclerosis model.

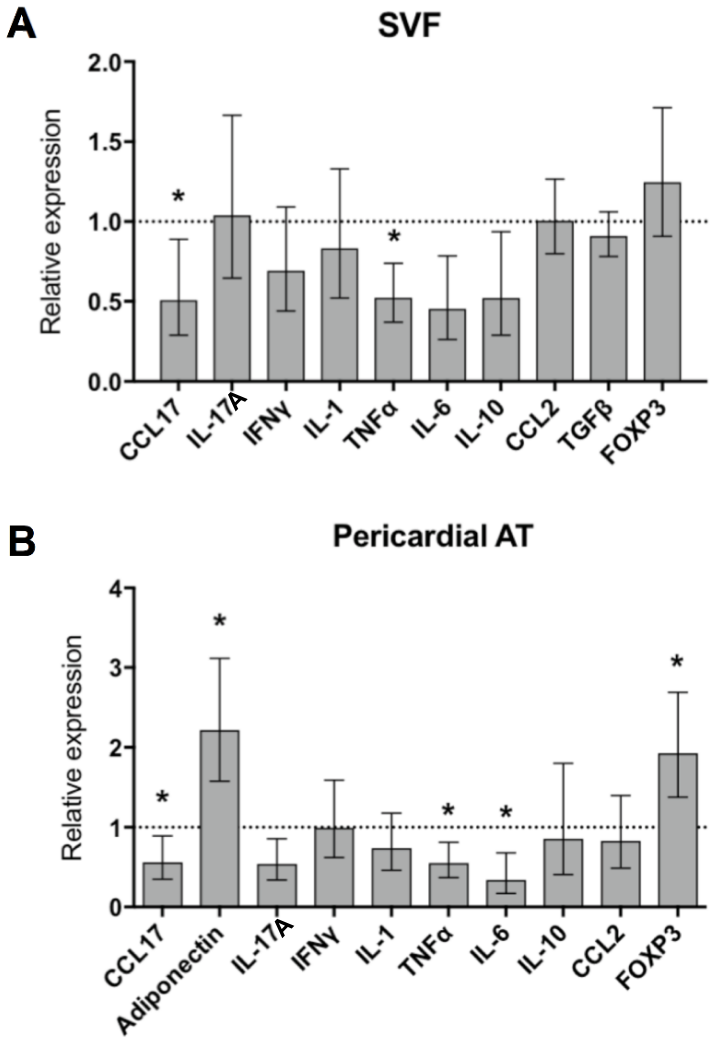

Figure 5.6 Immune phenotype in the VAT and pericardial AT of the *Ldlr* $^{-/-}$ GOF model

qRT-PCR analysis for mRNA expression in SVF (A) and pericardial AT (B) of *Ldlr* $^{-/-}$ GOF and *Ldlr* $^{-/-}$ WT mice. Expression levels of all mRNA were normalised to GAPDH expression. Bars represent ΔΔCT data values, the expression in GOF mice compared to WT, set at 1 indicated by the dotted line. Error bars show the geometric mean of eight biological replicates. Statistical significance of ΔCT data values was determined by Student's two-tailed t-test, results not significant unless otherwise denoted as *p<0.05.

5.2.4 Constitutive β-catenin activation in cDCs does not revert the development of atherosclerosis

Atherogenic development can be assessed in mouse models by measuring atherosclerotic plaque size in the aorta. Oil Red O solution is fat soluble, staining TG, cholesteryl esters and lipoproteins but not biological membranes. Oil Red O is commonly used to stain lipid-rich regions such as plaques, in aortic vessels. Whole mount en face aortas from *Ldlr* $^{-/-}$ GOF and *Ldlr* $^{-/-}$ WT mice were stained with Oil Red O (Figure 5.7A). The Oil Red O^{+} stained plaque area was analysed blindly to determine the lesion density as a percentage of total aorta area. The percentage aortic lesion density was not significantly different between *Ldlr* $^{-/-}$ GOF and *Ldlr* $^{-/-}$ WT mice (Figure 5.7B), demonstrating that constitutive activation of β-catenin in cDCs could not revert the development of atherosclerosis. Furthermore, there was no improvement in collagen deposition in the aortic sinus of *Ldlr* $^{-/-}$ GOF mice compared to the *Ldlr* $^{-/-}$ WT mice (Figure 5.8), suggesting that the atherogenic process was not impacted by constitutive activation of β-catenin in cDCs.

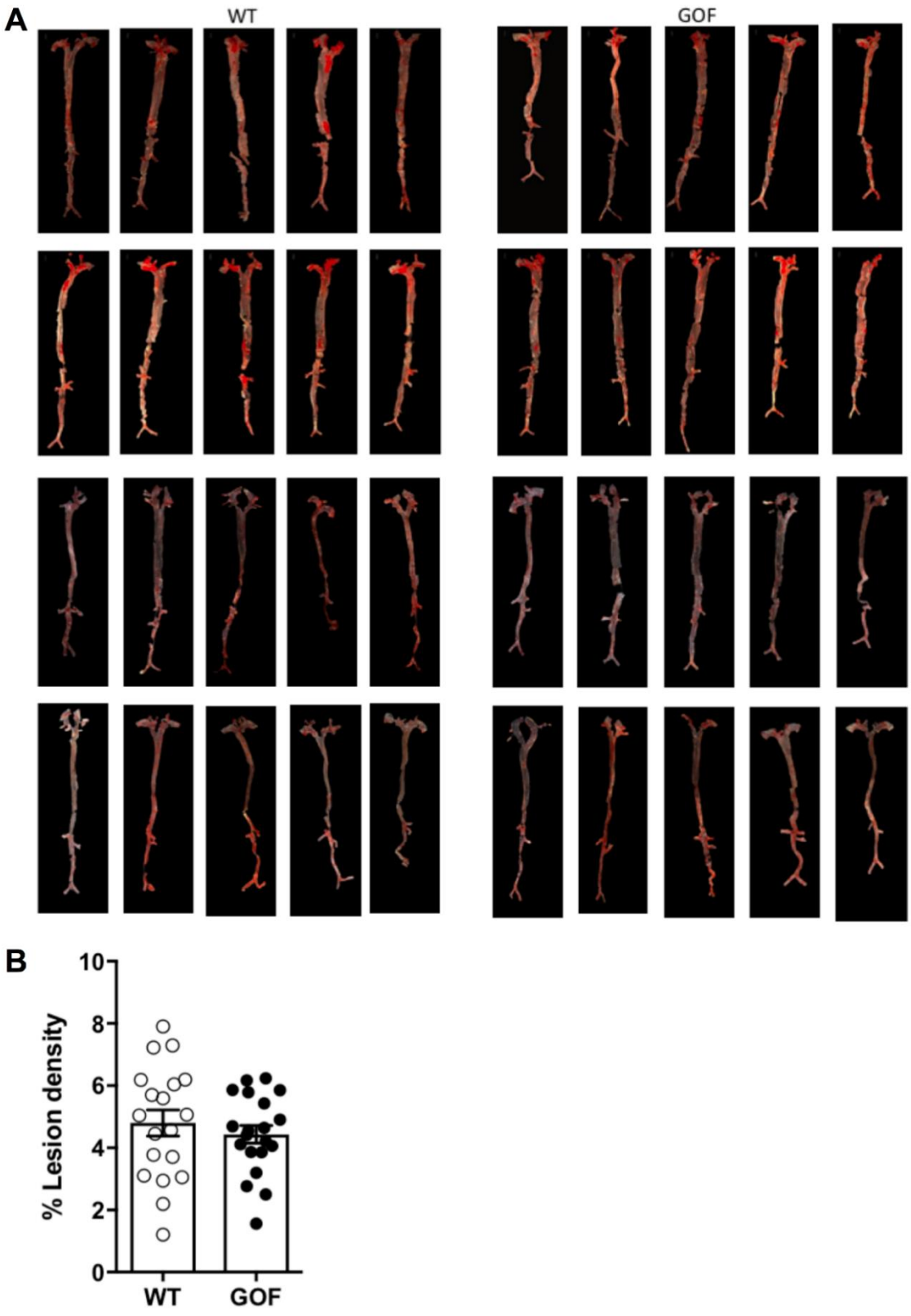

Figure 5.7 Lesion density in the aorta of the *Ldlr*$^{-/-}$ GOF model
(A) Whole mount en face aortas stained with Oil Red O from *Ldlr*$^{-/-}$ GOF and *Ldlr*$^{-/-}$ WT mice. (B) Lesion density calculated as Oil Red O^{+} stained plaque area as a percentage of total aorta area, mean ± SEM (n=20). Statistical significance was determined by Student's two-tailed t-test, results not significant.

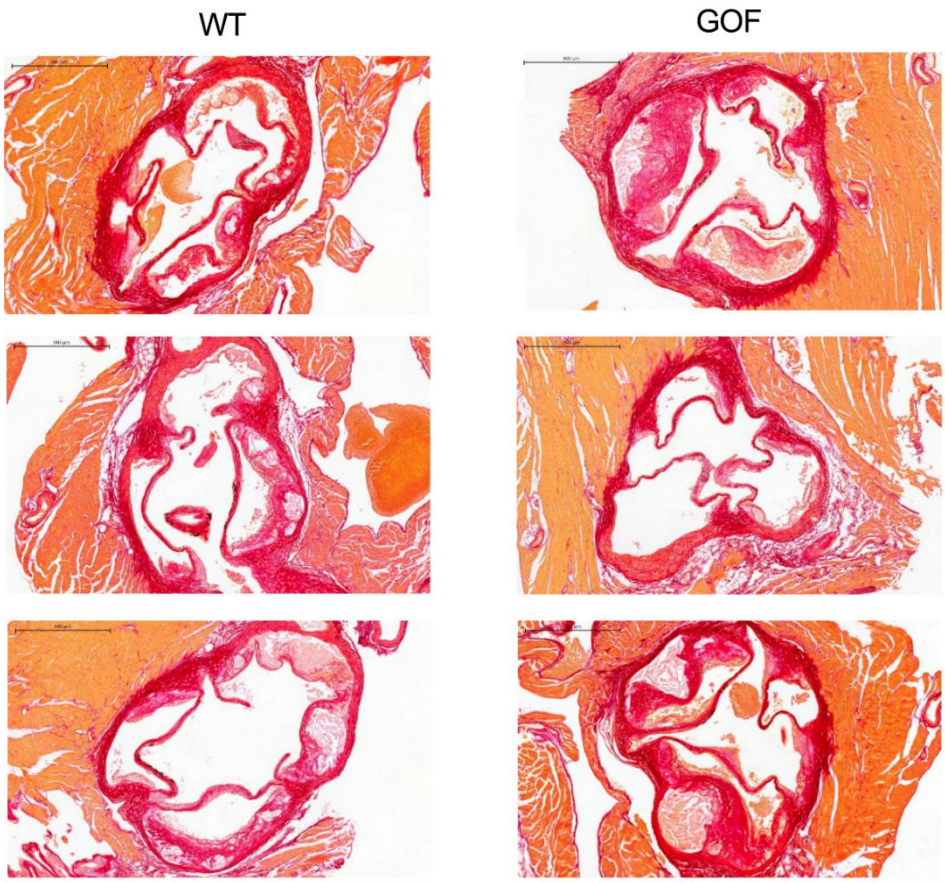

Figure 5.8 Histopathology of the aortic sinus of the *Ldlr*$^{-/-}$ GOF model
Representative images of sirus red stained aortic sinus sections of the heart from *Ldlr*$^{-/-}$ GOF and *Ldlr*$^{-/-}$ WT mice.

5.2.5 Translation of constitutive β-catenin activation in cDCs for therapeutic use

Despite not ameliorating atherogenic development in the *Ldlr*$^{-/-}$ model, constitutive β-catenin activation in cDCs has demonstrated beneficial effects in reducing VAT inflammation and improving whole-body glucose metabolism in Chapters 3 and 4. Thus we proposed that activation of Wnt/β-catenin pathway in cDCs could hold therapeutic potential. Since the Wnt/β-catenin pathway modulates many biological processes, non-specific activation of the pathway has significant wide-ranging effects. Pharmacological inhibitors of GSK3β have failed to have successful clinical use due to the lack of selectivity, high toxicity and adverse side effects (236). Additionally the stabilisation and nuclear translocation of β-catenin, induced by GSK3β inhibitors also holds oncogenic potential (237). Therefore a targeted method of activating the Wnt/β-catenin pathway in cDCs

could provide increased specificity, while requiring lower dosage, avoiding unwanted responses and reducing toxicity. Furthermore, targeting cDCs in vaccinations is widely accepted as a successful concept for protective immunity (238).

To investigate the specificity and affinity of such targeted delivery, multi-polymer micelle structures were kindly generated by Dr. Remzi Becer (School of Engineering and Materials Science, QMUL). The micelles encapsulate drugs for intracellular delivery, such as Wnt/β-catenin pathway agonist SB216763 (SB) and are formed of polymers which have high affinity to lectins. Lectins are glycoproteins, highly expressed on the surface of cDCs and macrophages. To measure the selectivity of micelles to cDCs, FITC conjugated micelles were utilised to determine their binding by flow cytometry. The gating strategy detailed previously was used to analyse the immune populations (Figure 2.4). A mixed splenocyte single cell population was treated with FITC conjugated micelles and the number of FITC labelled cells of immune populations were determined. The cDC population showed the greatest number of FITC labelled cells compared to other immune cells, suggesting the lectin binding provided specificity for targeted delivery (Figure 5.9A&B). An advantage of targeted delivery is the reduced drug dosage required, therefore micelles containing SB were titrated and IL-10 production from cDCs was analysed as a functional response. The dose response curve demonstrated that treatment of 1 µg/ml of micelle containing SB was the concentration which had maximal effect on β-catenin activity (Figure 5.9C). This concentration of micelle containing SB was used to compare with SB alone, as a measure of targeted versus untargeted β-catenin activation in cDCs. The concentration of SB used previously in initial experiments (20 µM, 7.42 µg/ml), was used in these experiments to ensure cDC response was achieved. The IL-10 response was significantly increased in VAT-cDCs treated with micelle containing SB compared to untreated (Figure 5.9D). Interestingly, this response was greater than the treatment of VAT-cDCs with SB alone, suggesting the micelle enhanced delivery for β-catenin activity while requiring a lower concentration of SB. Control treatment with micelle alone in the absence of SB showed an unexpected level of IL-10 production from VAT-cDCs, indicating that micelles alone may have a non-specific effect on β-catenin activity. Thus, this

method of delivery will need to be further investigated to understand how micelles affect pathways in cDCs.

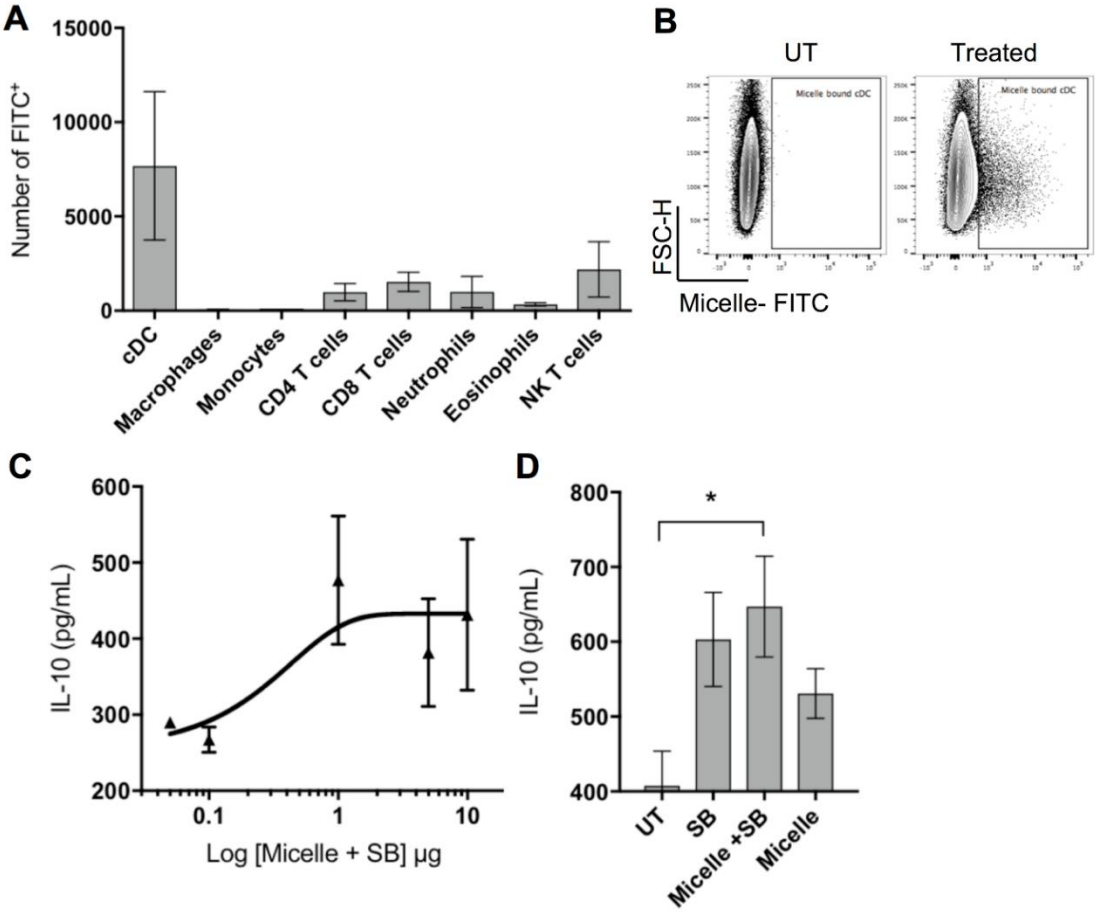

Figure 5.9 Targeted micelle delivery of Wnt/β-catenin pathway agonists to cDCs
(A) Spleen from C57BL/6 mice were digested and single cell mixed splenocyte population was treated with 1 µg/ml FITC conjugated micelles for 1 hour. After washing, immune cell populations were permeabilised and stained to analyse micelle binding by flow cytometry, mean ± SEM (n=3). (B) Representative dot plots of micelle binding from cDC population treated and untreated. (C) VAT-cDCs were isolated from C57BL/6 mice and treated with increasing concentrations of micelle containing β-catenin pathway agonist (SB) overnight. IL-10 was measured in the supernatant by ELISA, mean ± SD (n=2). (D) VAT-cDCs were treated with 1 µg/ml Micelle with or without SB, 20 µM (7.42 µg/ml) SB alone or untreated overnight. IL-10 was measured in the supernatant by ELISA, mean ± SEM (n=3). Statistical significance was determined by Student's two-tailed t-test, results not significant unless otherwise denoted as *p<0.05.

5.3 Discussion

Chronic inflammation underlies many metabolic-related diseases including atherogenesis. As cDCs play a critical role in the initiation of inflammatory responses, modulating their function has been proposed as a mechanism to ameliorate chronic inflammation and the development of cardiovascular disease.

In this chapter, we have shown that constitutive β-catenin activation in cDCs was not sufficient to revert the atherogenic process. Nevertheless, activation of Wnt/β-catenin pathway contributes to the regulation of inflammatory responses by for example, improving whole-body glucose metabolism. Thus, initial findings suggest that targeted delivery to activate Wnt/β-catenin pathway in cDCs could hold therapeutic potential.

Chemokines are crucial regulators of leukocyte trafficking during immune surveillance and inflammation. CCL17 has been previously reported to play a role in the recruitment of DCs to atherosclerotic plaques (198). DCs which express CCL17, accumulate in the arterial intima of atherosclerotic-susceptible regions of mice and recruitment of cDCs is also observed in advanced human plaques (239) (240). CCL17-expressing DCs have been shown to exacerbate inflammation during atheroma formation, recruiting circulating T cells and limiting T reg population expansion (198). Despite constitutive activation of β-catenin in cDCs resulting in the reduction of CCL17 expression, the numbers of T cell populations, specifically T reg cells, were not changed systemically in the *Ldlr* $^{-/-}$ GOF model (Figure 5.2). Thus the local mechanism in the aorta proposed by Weber *et al*. may not correlate in other tissues or systemically as observed in the spleen. Although there was a suggestion that T cell phenotype was modulated in the mesenteric AT and pericardial AT of *Ldlr* $^{-/-}$ GOF mice, this may imply that the decreased CCL17 induced by constitutive β-catenin activation in cDCs promotes local T cell changes in the tissue (Figure 5.6). Yet there were no differences in T cell populations in the aorta of GOF mice fed WD (Figure 5.5), however due to experimental constraints, immune cells could not be analysed in the aorta of the *Ldlr* $^{-/-}$ chimera mice. Thus, the aortic immune populations measured in previous experiments of diet-induced obesity, may not have been exposed to the same level of inflammation in the aorta as in the *Ldlr* $^{-/-}$ model, caused by the higher lipid conditions in the absence of LDL-R.

Despite previous observations in Chapter 3 that constitutive β-catenin activation in cDCs, in part, reverted systemic inflammation, there was less of an indication that systemic inflammation was controlled in the *Ldlr*$^{-/-}$ GOF mice. The immune cell populations remained unchanged in the spleen (Figure 5.2), in contrast to previous observations in Chapter 3 in diet-induced obesity model, where there

was an increased number of cDC1 and reduced neutrophil count in the GOF mice (Figure 3.13). The absence of these differences in the spleen of *Ldlr* $^{-/-}$ GOF mice could be due to changes in the stroma environment in *Ldlr* $^{-/-}$ model and/or the high lipid conditions in the absence of LDL-R. Indeed, it has been observed that the capacity of tolerogenic cDCs is altered by high cholesterol, in respect to the lipid droplet (LD) content (154). However there was a significant decrease in the number of neutrophils in the lymph nodes (Figure 5.3 & 5.4). Neutrophils are the first immune cells recruited to the site of inflammation, hence the reduction suggests a decrease of inflammation in the peripheral tissues. Additionally, it is known that neutrophils participate in atherogenesis (241), thus it is possible that if there are less neutrophils present in the aorta-draining lymph nodes of the *Ldlr* $^{-/-}$ GOF mice, constitutive β-catenin activation in cDCs may decrease aortic inflammatory responses. Although neutrophils are also important for the resolution of inflammation, suggesting that with less neutrophils, there may be greater inflammation-induced damage. Despite this, a reduction of pro-inflammatory cytokines and an increase in FOXP3 was observed in the pericardial AT of the *Ldlr* $^{-/-}$ GOF mice indicating a possible immunosuppressive phenotype in the tissue (Figure 5.6). As pericardial AT is in close contact with the aorta, restraining the local tissue inflammation could revert inflammatory responses in the vessel.

In addition to inflammation, dyslipidaemia plays a key role in the pathophysiology of atherosclerosis. The total cholesterol and lipoprotein plasma concentrations remained unchanged in the GOF mice. However the circulating levels of FFA were decreased in the *Ldlr* $^{-/-}$ GOF mice (Figure 5.1), which could suggest that adipocytes have a reduced capacity to buffer the excess of lipids, although the exact mechanism is unclear. The dyslipidaemia associated with the *Ldlr* $^{-/-}$ model, is known to activate skin murine DCs, paradoxically inhibiting their migration to lymph nodes and suppressing immunological priming (242). Interestingly, the migratory cDC population was increased in the mediastinal draining lymph nodes of the *Ldlr* $^{-/-}$ GOF mice (Figure 5.3), suggesting that the cDCs with constitutive β-catenin activation were less affected by the high lipid inhibition on their migration. Improved VAT function was further suggested by a local increase in adiponectin in the pericardial AT (Figure 5.6). Yet this elevated adiponectin was not observed in circulating levels in the *Ldlr* $^{-/-}$ GOF mice, as previously demonstrated in GOF

mice in diet-induced obesity model (Figure 3.19E). Despite constitutive β-catenin activation in cDCs promoting local improvement of adiponectin expression, systemic differences may have been lost in *Ldlr* $^{-/-}$ GOF mice due to the contribution of bone marrow AT (BMAT) to circulating levels of adiponectin. BMAT is a rich source of adiponectin (243), thus in the higher lipid *Ldlr* $^{-/-}$ model BMAT production of adiponectin may have disguised the local changes in white AT depots. Further investigation will be required to assess VAT and pericardial AT function in this model, however these results indicate that constitutive β-catenin activation in cDCs improves adipocyte function during tissue inflammation sufficiently to improve local adiponectin levels and decrease systemic FFA levels.

Additionally these results suggest that constitutive β-catenin activation in cDCs may induce less inflammatory responses locally in the aorta during atheroprogression. Although there was a reduction of CCL17-expressing cDCs and possible modulation of systemic and local inflammation in the *Ldlr* $^{-/-}$ GOF mice, constitutive β-catenin activation in cDCs did not affect the plaque development. Weber *et al*. investigated the role of CCL17-expressing DCs in *ApoE*$^{-/-}$ model of atherosclerosis using a knockout of CCL17 (198). While expression of CCL17 in our model was significantly reduced, it was not totally abrogated thus expression of CCL17, albeit at low levels still permits the development of atherosclerosis.

The translational impact of modulating the Wnt/β-catenin pathway has been highlighted by the generation of GSK3β inhibitors. However due to off-target effects, progress in the pharmaceutical modulation of the Wnt/β-catenin pathway has been hampered. By targeting β-catenin agonists to cDCs, these issues could be bypassed. Initial results suggest that multi-polymer micelle structures demonstrate specificity and affinity for cDCs and can activate β-catenin activity as measured by IL-10 production. Thus, delivery of β-catenin pathway agonist through micelle structures has demonstrated a potential route for therapeutic use. Further investigations are required to evaluate the selectivity and efficacy of micelle-drug delivery *in vivo*.

In summary, this chapter has demonstrated that constitutive β-catenin activation in cDCs does not confer a cardio-protective phenotype in this model. Activation of Wnt/β-catenin pathway in cDCs in the *Ldlr* $^{-/-}$ atherosclerotic model did not reduce systemic or local inflammation enough to ameliorate plaque development. Interestingly, initial findings indicate the delivery of β-catenin pathway agonists through micelle structures could hold a potential route for therapeutic use.

Chapter 6 General discussion

This thesis has examined the role of the Wnt/β-catenin pathway in cDCs, particularly in the context of VAT inflammation and obesity-associated T2DM. Activation of the Wnt/β-catenin pathway has recently been described to influence cDC function and limit inflammatory responses (167), however this had yet to be explored in VAT, where β-catenin plays a critical role in adipogenesis (65). Therefore, we aimed to evaluate the effect of Wnt/β-catenin pathway activation on VAT-cDC phenotype and on VAT immune and metabolic homeostasis, under steady-state conditions and during diet-induced tissue inflammation.

From transcriptome data, we initially discovered that the Wnt/β-catenin pathway was selectively upregulated in VAT-cDC1 subset. This was expected since β-catenin is known to target the *Irf8* promoter specific for cDC1 differentiation (202). Although stabilisation of β-catenin was not observed in splenic cDCs, active β-catenin was demonstrated in cDCs in the pancreas as well as in VAT. This revealed that activation of Wnt/β-catenin pathway in cDCs potentially had pleiotropic effects dependent on tissue. In VAT, we proposed that activation of β-catenin in cDCs is due to a possible crosstalk with pre-adipocytes in order to maintain tissue homeostasis. However, how this pathway is activated in pancreas cDCs and not in splenic cDCs remains unclear. It may be due to tissue specificity of Wnt ligand expression, which are key extracellular regulators of β-catenin stabilisation. Regulation of Wnt ligands in adult tissue is complex and varies dependent on tissue in a temporal and spatially restricted manner. Wnt ligands are also key signalling molecules for maintaining stem cell niches in tissues (244), hence similar to in VAT, crosstalk of stem cell populations with cDCs in tissues such as the pancreas, may offer a possible means of how β-catenin activation in cDCs occurs. Independent of Wnt, β-catenin can also become activated in cDCs through various other signalling pathways including TLR (179), TGF-β (184) and inflammatory cytokines such as TNFα and IFNγ. Therefore the stromal environment in tissues may also indirectly regulate activation of β-catenin in cDCs.

A number of studies have reported that activation of Wnt/β-catenin pathway induces tolerogenic responses by cDCs (185) (178). Results from our β-catenin knockdown mice supports this, demonstrating that β-catenin in VAT-cDCs plays a role in modulating T cell responses and tissue homeostasis. Furthermore abrogation of Wnt/β-catenin pathway in VAT-cDCs exposed the potential for manipulating cDC function in VAT, to control the initiation of tissue inflammation and obesity-associated IR. This highlights the concept of immunomodulation in VAT, which can have significant impact locally in the tissue and systemically in whole body glucose metabolism. Indeed, systemic immunotherapy targeting T or B cells for depletion, suppresses VAT inflammation and reverses IR in diet-induced obesity mice models (105) (107). In addition, cytotoxic T lymphocyte antigen (CTLA)-4Ig immunotherapy exploits ATM polarisation to ameliorate inflammation and IR in HFD fed mice (245). In our GOF mouse model, we have shown that constitutive β-catenin activation in cDCs offers a novel mechanism to induce tolerogenic VAT-cDCs, which promotes an immunosuppressive VAT phenotype in steady-state and reverts in part, systemic and local tissue inflammation in diet-induced obesity. These findings open up the possibility that VAT immune homeostasis could be modulated by other adipocyte-related pathways regulating cDC function, including the Xbp1 and HIF1α pathways.

We have shown that β-catenin activity in cDCs is not exclusive to VAT and in addition, plays a non-redundant role in the pancreas. Constitutive activation of the Wnt/β-catenin pathway in cDCs demonstrated an improvement of whole-body glucose homeostasis, as a result of enhanced β-cell insulin secretion and modulation of islet inflammation in response to diet-induced obesity. Our data revealed an increase in islet size in GOF mice, which we propose is due to increased Wnt ligands produced by cDCs with constitutively active β-catenin. It has been observed previously that cDCs produce Wnt ligands in the gut (185). β-catenin or associated proteins may directly regulate Wnt ligand expression, inducing a feedforward circuit of the Wnt/β-catenin pathway by cDCs. Interestingly, it has emerged that components of the Wnt/β-catenin pathway, such as FZD receptors, Axin, LRP6, TCF/LEF and pathway agonist R-spondin (Rspo) are regulated by β-catenin (170), suggesting that self-regulatory loops of the pathway do exist. Indeed, induction of Rspo and TCF/LEF gene transcription by Wnt/β-catenin pathway activation has shown to reinforce Wnt signalling,

driving a feedforward mechanism (246) (247). However, whether Wnt gene transcription is self-regulated directly or indirectly by β-catenin remains to be explored. Wnt biogenesis and secretion is a highly regulated process, involving several post-translational modifications (170) (248). A multitude of proteins are required to glycosylate, palmitoylate and escort the synthesised Wnt ligands from the ER to membrane. Thus, active β-catenin may play a role in promoting these processes to enhance Wnt production in cDCs.

Aberrant Wnt/β-catenin pathway activation occurs in disease (249). Interestingly, modulation of Wnt ligand expression has been identified in pathological conditions. High expression of Wnt ligands are reported in cancers and inflammatory diseases, such as arthritis (250), psoriasis (251) and neuroinflammation (252). Furthermore, in the intestine, Wnt ligand expression increases with the development of inflammation (253) (185). On the contrary, in VAT inflammation, we have shown that chronic overnutrition decreases the availability of Wnt ligands in obese VAT, in order to promote adipocyte hyperplasia. These results support previous findings that loss of Wnt10b function is associated with obesity (196) (176), while loss of Wnt5b function confers susceptibility to T2DM (173). Wnt5b represses the canonical Wnt/β-catenin pathway, thus suggesting pathway activation occurs in T2DM. Indeed it has been shown that activation of Wnt/β-catenin pathway in the islet is important for the β-cell adaptive stage early in the pre-diabetic state (254) (214). During the initial stages of hyperglycaemia in obesity or pre-diabetes, compensatory β-cell expansion occurs to fulfil the insulin requirement of peripheral tissues. Wnt/β-catenin pathway has been suggested to regulate this β-cell adaption, supporting cell growth and proliferation (214) (172) (255). β-catenin is activated in islets during compensatory β-cell hyperplasia in pre-diabetic mice (210). However the transition from pre-diabetes to the onset of T2DM, when β-cells can no longer compensate and their mass and function declines, correlates with reduced canonical Wnt expression and loss of Wnt/β-catenin pathway activation. In a recent study, modulation of Wnt expression was demonstrated during the progression of HFD-induced T2DM, specifically canonical Wnt activator Wnt3a and canonical Wnt suppressor Wnt4 (254). In pre-diabetic rats Wnt3 increased in VAT, skeletal muscle and plasma, while expression reduced later on in the development of T2DM as Wnt4 levels elevated, resulting in dysfunctional

pancreatic islet function (256). Similarly, the expression of Wnt4 has shown to be significantly upregulated in IR mouse models particularly in the islets, and furthermore in the islets of T2DM patients (257) (254). Since Wnt4 suppresses canonical β-catenin pathway activation, exogenous Wnt4 antagonises Wnt3a action in islets, inhibiting the Wnt3a stimulated β-cell proliferation and insulin secretion (255). What controls this modulation of Wnt expression in the islets, during the transition from pre-diabetes to the onset of T2DM remains unknown. Wnt ligand expression can be regulated in response to nutritional and metabolic changes, thus potentially as hyperglycaemia increases and β-cell adaption can no longer compensate, high glucose or low insulin levels could trigger a change in Wnt ligand expression. Another possible mechanism may involve epigenetic changes in the promoter regions of Wnt genes. As changes occur in lipid metabolism in obesity and subsequently T2DM, it has been reported that palmitate metabolism modulates DNA methylation and hence altering gene expression (258). Wnt crosstalk may also occur between IR tissues and the pancreas (256). However we have shown that constitutive β-catenin activation in cDCs appears to elevate Wnt3a expression in the islets of a diet-induced obesity model, suggesting a potential mechanism to induce sustained expression of Wnt3a in order to revert the decrease observed during the onset of T2DM. Wnt4 expression was not examined in the islets of the GOF mice, although it would be of interest to understand how constitutive β-catenin activation in cDCs affects Wnt4 levels in particular during T2DM. Thus, these findings reveal a previously unreported role for cDCs in the pancreas and opens up the possibility that cDCs, and potentially other Wnt-producing immune cells, could restore Wnt/β-catenin pathway activation in β-cells.

β-cell adaption involves the expansion of β-cell mass, by increasing proliferation, replication and hypertrophy to compensate for the increased demand of insulin secretion (259). This occurs in obesity and in pre-diabetes when IR of peripheral tissues initiates, in order to conserve glucose homeostasis. β-cell adaption can successfully prevent the development of T2DM in many obese individuals, however in a fraction of the obese population β-cell function and mass cannot sufficiently compensate resulting in hyperglycaemia and β-cell failure (260). Many factors are thought to contribute to this loss of β-cell adaption, including ageing, genetic variants, metabolic insults such as glucotoxicity, lipotoxicity and

ER stress and inflammation, and in addition changes in Wnt ligand exposure as discussed above (32) (34) (35). These contributors are not mutually exclusive and it is widely accepted that multiple signalling systems and pathways act synergistically to exacerbate β-cell dysfunction. Our findings have demonstrated that modulating cDC function has had multifaceted effects on β-cell mass and function, to potentially prevent islet failure. However it is unclear how these compensatory effects would maintain long-term health of β-cells and prevent the development of T2DM. It is possible that other factors and signalling events may override the potential beneficial effects that constitutive β-catenin activation in cDC may serve in the islet.

Interestingly, we have observed different responses in different tissues in the GOF model. Constitutively active β-catenin was induced systemically in cDCs, not exclusively to VAT where it was initially observed to maintain tissue inflammation. While our results suggest that inflammation was, in part, reverted in VAT and in the islets of the GOF mice in a diet-induced obesity model, there was less of an indication that inflammation was controlled in the atherosclerosis model. An anatomical reason that could explain this, is the lack of epicardial AT in mice, which sits in close contact with the heart and aortic vessel in humans and is considered a potential regulator of vessel inflammation. Therefore in the *Ldlr*$^{-/-}$ mice, constitutively active β-catenin in cDCs may not have had the opportunity to influence aortic inflammation due to the absence of epicardial AT, although in humans there may be a greater effect on atherosclerosis. Despite constitutively active β-catenin in cDCs revealing an increase in β-cell proliferation in the pancreas to elevate insulin secretion, it was not sufficient to revert the atherogenic process. The differences in tissue responses may have been due to the abundance of cDCs in these tissues, hence varying the tolerogenic effect on tissue inflammation. In addition, the influence of cDCs is likely to be tissue-specific and differ in pathological processes. Other immune cells such as macrophages predominate in atherosclerotic inflammation, thus cDCs may have had less impact. These findings in the GOF mice indicate that modulating cDC function in the pancreas has a notable consequence, greater than in the aorta. As we have suggested, Wnt ligands produced by cDCs control β-cell proliferation, thus it is also possible that Wnt ligands were produced by cDCs in the aorta of the GOF mice. However in vessels these Wnt ligands may play a detrimental role,

promoting plaque growth. Indeed, the Wnt/β-catenin pathway is known to control the expression of several extracellular matrix components and assist in the proliferation and survival of smooth muscle cells (261). Thus our proposed mechanism of Wnt production by cDCs with constitutively active β-catenin, may provide differing effects dependent on tissue. Furthermore, this study reveals that immune modulation does not promote consistent responses systemically, tissues have varied stromal environments and hence different outcomes are observed.

The GOF model represents a therapeutic drug strategy, whereby systemically all cDCs are targeted for Wnt/β-catenin pathway activation. Targeted delivery by for example, micelles could be an effective method with the advantages of a lower drug dosage, reduced side effects and toxicity, but with greater specificity compared to current options of β-catenin activation such as GSK3β inhibitors. cDCs have been successfully targeted for therapeutic vaccination strategies, to deliver antigens for the priming of T cell and B cell responses for protective and anti-tumour immunity. Multiple delivery systems to cDCs have been explored including ligand based, antibody based and nanoparticles such as liposomes, to offer the potential for co-delivery (262). Hence targeting cDCs with Wnt/β-catenin pathway agonist could promote tolerogenic responses to reduce inflammation and provide beneficial effects on β-cell health. However, the immunosuppressive environment generated by constitutively active β-catenin in cDCs, should be considered in respect to the development of cancer. Tumour development favours immune suppression, including the recruitment of T reg cells and tolerogenic DCs. Furthermore overexpression of β-catenin holds oncogenic potential and promotes tumour development.

Research limitations of this study include power for statistical tests. Improved power calculations and increased sample sizes would have generated more robust data conclusions. Although irradiated chimeras were used to analyse the effects of solely donor bone marrow immune cells, resident irradiation-resistant immune cells in recipient tissue may not have been fully eradicated and hence could have interfered with immune responses. Sampling of VAT in mice as discussed previously, did not consider the distribution of immune cells and thus may have diluted the effect of localised immune responses.

6.1 Future work

Although we have established that constitutive Wnt/β-catenin pathway activation in cDCs has the potential to revert VAT inflammation, co-activation of other complementary suppressive pathways in VAT-cDCs such as PPARγ would be of interest, since PPARγ signalling is also impaired in obesity (263) (264). Similarly restoring PPARγ activity in cDCs could also revert VAT inflammation. In addition, gender and age are factors which will need to be considered in the effects on inflammatory immune response in VAT. Sex differences are known to exist in VAT deposition and influence inflammatory and metabolic status of the tissue (265).

Our findings in the pancreas will require further characterisation to determine the mechanisms by which constitutive activation of β-catenin in cDCs can enhance insulin secretion. It will be critical to understand the production of Wnt ligands from pancreas cDCs and how this can be altered during the development of diet-induced obesity and T2DM. As the GOF model systemically affects cDCs, the Wnt-specific effects in other tissues such as the liver, should also be further explored. Although innate immune cells have been well established in islet inflammation in T2DM, the contribution of adaptive immune responses are less clear. It would be of interest to further investigate the action of cDCs and T cells in the islets during pre-diabetes and progression of T2DM, specifically focusing on the tolerogenic effects beneficial for islet immune health.

The interaction between cDC chemokine CCL17 and $CCR4^+$ T cells has been discussed in this thesis, however the exact mechanisms of homing in the VAT and how this affects VAT homeostasis are still yet to be explored. Specifically, how activation of β-catenin in cDCs modifies CCL17 expression remains to be clarified. In addition, CCR4 has another cognate chemokine, CCL22 which is also expressed by cDCs. It would be interesting to understand the effect of constitutive β-catenin activation on CCL22 expression and the impact on $CCR4^+$ T cell recruitment.

6.2 Conclusion

This thesis has demonstrated the significance of modulating the Wnt/β-catenin pathway in cDCs, with the potential to control VAT inflammation and metabolic dysfunction in obesity and in the development of T2DM. While depletion of β-catenin in cDCs exacerbated diet-induced tissue inflammation, constitutive activation of β-catenin pathway in cDCs was able to revert, in part, the development of systemic and local tissue inflammation in a model diet-induced obesity. By inducing a tolerogenic phenotype in VAT-cDCs, constitutive β-catenin activation modulates T cell responses generating an immunosuppressive phenotype in VAT. However activation of Wnt/β-catenin pathway in cDCs did not reduce systemic or local inflammation enough to ameliorate plaque development in the *Ldlr* $^{-/-}$ atherosclerotic model. Interestingly, despite no change in peripheral insulin sensitivity, whole-body glucose homeostasis was improved due to enhanced β-cell insulin secretion and reduction of islet inflammation. We demonstrated a novel finding by which cDCs with constitutive β-catenin activation induce β-cell proliferation and suggest a potential mechanism through the production of Wnt3a. Further investigation will be required to decipher if cDCs act as a source of Wnt ligands in the pancreas and if this holds the potential to restore β-cell mass and function in T2DM. This work proposes a unique compensatory mechanism driven by cDCs to generate a greater insulin reserve in response to obesity-induced IR, highlighting the potential of immune modulation in the development of T2DM.

References

1. Trends in adult body-mass index in 200 countries from 1975 to 2014: a pooled analysis of 1698 population-based measurement studies with 19.2 million participants. *Lancet*. 2016;387(10026):1377-96.

2. Hruby A, Hu FB. The Epidemiology of Obesity: A Big Picture. *PharmacoEconomics*. 2015;33(7):673-89.

3. Obesity: preventing and managing the global epidemic. Report of a WHO consultation. *World Health Organization technical report series*. 2000;894:i-xii, 1-253.

4. Heymsfield SB, Wadden TA. Mechanisms, Pathophysiology, and Management of Obesity. *The New England Journal of Medicine*. 2017;376(3):254-66.

5. Walley AJ, Blakemore AI, Froguel P. Genetics of obesity and the prediction of risk for health. *Human molecular genetics*. 2006;15 Spec No 2:R124-30.

6. Frayling TM, Timpson NJ, Weedon MN, Zeggini E, Freathy RM, Lindgren CM, et al. A common variant in the FTO gene is associated with body mass index and predisposes to childhood and adult obesity. *Science*. 2007;316(5826):889-94.

7. Lopomo A, Burgio E, Migliore L. Epigenetics of Obesity. *Progress in molecular biology and translational science*. 2016;140:151-84.

8. Backhed F, Manchester JK, Semenkovich CF, Gordon JI. Mechanisms underlying the resistance to diet-induced obesity in germ-free mice. *Proceedings of the National Academy of Sciences*. 2007;104(3):979-84.

9. Redinger RN. The pathophysiology of obesity and its clinical manifestations. *Gastroenterology & hepatology*. 2007;3(11):856-63.

10. Hotamisligil GS, Shargill NS, Spiegelman BM. Adipose expression of tumor necrosis factor-α: direct role in obesity-linked insulin resistance. *Science*. 1993;259(5091):87-91.

11. Uysal KT, Wiesbrock SM, Marino MW, Hotamisligil GS. Protection from obesity-induced insulin resistance in mice lacking TNF-α function. *Nature*. 1997;389(6651):610-4.

12. Ventre J, Doebber T, Wu M, MacNaul K, Stevens K, Pasparakis M, et al. Targeted disruption of the tumor necrosis factor-α gene: metabolic consequences in obese and nonobese mice. *Diabetes*. 1997;46(9):1526-31.

13. Kaur J. A comprehensive review on metabolic syndrome. *Cardiology research and practice*. 2014;2014:943162.

14. Grundy SM. Metabolic syndrome: a multiplex cardiovascular risk factor. *Journal of clinical endocrinology and metabolism*. 2007;92(2):399-404.

15. Rocha VZ, Libby P. Obesity, inflammation, and atherosclerosis. *Nature reviews Cardiology*. 2009;6(6):399-409.

16. Alberti KG, Eckel RH, Grundy SM, Zimmet PZ, Cleeman JI, Donato KA, et al. Harmonizing the metabolic syndrome: a joint interim statement of the International Diabetes Federation Task Force on Epidemiology and Prevention; National Heart, Lung, and Blood Institute; American Heart Association; World Heart Federation; International Atherosclerosis Society; and International Association for the Study of Obesity. *Circulation*. 2009;120(16):1640-5.

17. Grundy SM. Drug therapy of the metabolic syndrome: minimizing the emerging crisis in polypharmacy. *Nature reviews Drug discovery*. 2006;5(4):295-309.

18. Cho NH, Shaw JE, Karuranga S, Huang Y, da Rocha Fernandes JD, Ohlrogge AW, et al. IDF Diabetes Atlas: Global estimates of diabetes prevalence for 2017 and projections for 2045. *Diabetes research and clinical practice*. 2018;138:271-81.

19. DeFronzo RA, Ferrannini E, Groop L, Henry RR, Herman WH, Holst JJ, et al. Type 2 diabetes mellitus. *Nature reviews Disease primers.* 2015;1:15019.

20. Chawla A, Chawla R, Jaggi S. Microvasular and macrovascular complications in diabetes mellitus: Distinct or continuum? *Indian journal of endocrinology and metabolism*. 2016;20(4):546-51.

21. Schernthaner G. Cardiovascular mortality and morbidity in type-2 diabetes mellitus. *Diabetes research and clinical practice*. 1996;31 Suppl:S3-13.

22. Xue A, Wu Y, Zhu Z, Zhang F, Kemper KE, Zheng Z, et al. Genome-wide association analyses identify 143 risk variants and putative regulatory mechanisms for type 2 diabetes. *Nature communications*. 2018;9(1):2941.

23. Roder PV, Wu B, Liu Y, Han W. Pancreatic regulation of glucose homeostasis. *Experimental & molecular medicine*. 2016;48:e219.

24. Aronoff SL, Berkowitz K, Shreiner B, Want L. Glucose Metabolism and Regulation: Beyond Insulin and Glucagon. *Diabetes Spectrum*. 2004;17(3):183-90.

25. Martin BC, Warram JH, Krolewski AS, Bergman RN, Soeldner JS, Kahn CR. Role of glucose and insulin resistance in development of type 2 diabetes mellitus: results of a 25-year follow-up study. *Lancet*. 1992;340(8825):925-9.

26. Guo S. Insulin signaling, resistance, and the metabolic syndrome: insights from mouse models into disease mechanisms. *The Journal of endocrinology*. 2014;220(2):T1-t23.

27. Yu C, Chen Y, Cline GW, Zhang D, Zong H, Wang Y, et al. Mechanism by which fatty acids inhibit insulin activation of insulin receptor substrate-1 (IRS-1)-associated phosphatidylinositol 3-kinase activity in muscle. *The Journal of biological chemistry*. 2002;277(52):50230-6.

28. Shoelson SE, Lee J, Goldfine AB. Inflammation and insulin resistance. *The Journal of clinical investigation*. 2006;116(7):1793-801.

29. Kulkarni RN. The islet β-cell. *The international journal of biochemistry & cell biology*. 2004;36(3):365-71.

30. Hodson DJ, Mitchell RK, Bellomo EA, Sun G, Vinet L, Meda P, et al. Lipotoxicity disrupts incretin-regulated human β-cell connectivity. *The Journal of clinical investigation*. 2013;123(10):4182-94.

31. Prentki M, Nolan CJ. Islet β-cell failure in type 2 diabetes. *The Journal of clinical investigation*. 2006;116(7):1802-12.

32. Nolan CJ, Damm P, Prentki M. Type 2 diabetes across generations: from pathophysiology to prevention and management. *Lancet*. 2011;378(9786):169-81.

33. Jurczyk A, Bortell R, Alonso LC. Human β-cell regeneration: progress, hurdles, and controversy. *Current opinion in endocrinology, diabetes, and obesity*. 2014;21(2):102-8.

34. Marchetti P, Bugliani M, Boggi U, Masini M, Marselli L. The pancreatic β-cells in human type 2 diabetes. *Advances in experimental medicine and biology*. 2012;771:288-309.

35. Donath MY, Dalmas E, Sauter NS, Boni-Schnetzler M. Inflammation in obesity and diabetes: islet dysfunction and therapeutic opportunity. *Cell metabolism*. 2013;17(6):860-72.

36. Butcher MJ, Hallinger D, Garcia E, Machida Y, Chakrabarti S, Nadler J, et al. Association of proinflammatory cytokines and islet resident leucocytes with islet dysfunction in type 2 diabetes. *Diabetologia.* 2014;57(3):491-501.

37. Richardson SJ, Willcox A, Bone AJ, Foulis AK, Morgan NG. Islet-associated macrophages in type 2 diabetes. *Diabetologia.* 2009;52(8):1686-8.

38. Masters SL, Dunne A, Subramanian SL, Hull RL, Tannahill GM, Sharp FA, et al. Activation of the NLRP3 inflammasome by islet amyloid polypeptide provides a mechanism for enhanced IL-1β in type 2 diabetes. *Nature immunology*. 2010;11(10):897-904.

39. Marchetti P. Islet inflammation in type 2 diabetes. *Diabetologia.* 2016;59(4):668-72.

40. Johnston NR, Mitchell RK, Haythorne E, Pessoa MP, Semplici F, Ferrer J, et al. β-cell Hubs Dictate Pancreatic Islet Responses to Glucose. *Cell metabolism*. 2016;24(3):389-401.

41. D'Alessio D. The role of dysregulated glucagon secretion in type 2 diabetes. *Diabetes, obesity & metabolism.* 2011;13 Suppl 1:126-32.

42. Guilherme A, Virbasius JV, Puri V, Czech MP. Adipocyte dysfunctions linking obesity to insulin resistance and type 2 diabetes. *Nature reviews Molecular cell biology.* 2008;9(5):367-77.

43. Nguyen NQ, Debreceni TL, Bambrick JE, Chia B, Wishart J, Deane AM, et al. Accelerated intestinal glucose absorption in morbidly obese humans: relationship to glucose transporters, incretin hormones, and glycemia. *The Journal of clinical endocrinology and metabolism.* 2015;100(3):968-76.

44. Wilding JP. The role of the kidneys in glucose homeostasis in type 2 diabetes: clinical implications and therapeutic significance through sodium glucose co-transporter 2 inhibitors. *Metabolism: clinical and experimental.* 2014;63(10):1228-37.

45. Shpakov AO, Derkach KV, Berstein LM. Brain signaling systems in the Type 2 diabetes and metabolic syndrome: promising target to treat and prevent these diseases. *Future science*. 2015;1(3):Fso25.

46. Meek TH, Morton GJ. Leptin, diabetes, and the brain. *Indian journal of endocrinology and metabolism*. 2012;16(Suppl 3):S534-42.

47. Kusminski CM, Bickel PE, Scherer PE. Targeting adipose tissue in the treatment of obesity-associated diabetes. *Nature reviews Drug discovery.* 2016;15(9):639-60.

48. Tuomilehto J, Lindstrom J, Eriksson JG, Valle TT, Hamalainen H, Ilanne-Parikka P, et al. Prevention of type 2 diabetes mellitus by changes in lifestyle among subjects with impaired glucose tolerance. *The New England journal of medicine*. 2001;344(18):1343-50.

49. Inzucchi SE, Bergenstal RM, Buse JB, Diamant M, Ferrannini E, Nauck M, et al. Management of hyperglycemia in type 2 diabetes: a patient-centered approach: position statement of the American Diabetes Association (ADA) and the European Association for the Study of Diabetes (EASD). *Diabetes care*. 2012;35(6):1364-79.

50. Larsen CM, Faulenbach M, Vaag A, Volund A, Ehses JA, Seifert B, et al. Interleukin-1-receptor antagonist in type 2 diabetes mellitus. *The New England journal of medicine.* 2007;356(15):1517-26.

51. Herder C, Dalmas E, Boni-Schnetzler M, Donath MY. The IL-1 Pathway in Type 2 Diabetes and Cardiovascular Complications. *Trends in endocrinology and metabolism.* 2015;26(10):551-63.

52. Goldfine AB, Fonseca V, Jablonski KA, Chen YD, Tipton L, Staten MA, et al. Salicylate (salsalate) in patients with type 2 diabetes: a randomized trial. *Annals of internal medicine.* 2013;159(1):1-12.

53. Di Prospero NA, Artis E, Andrade-Gordon P, Johnson DL, Vaccaro N, Xi L, et al. CCR2 antagonism in patients with type 2 diabetes mellitus: a randomized, placebo-controlled study. *Diabetes, obesity & metabolism.* 2014;16(11):1055-64.

54. Hocking S, Samocha-Bonet D, Milner KL, Greenfield JR, Chisholm DJ. Adiposity and insulin resistance in humans: the role of the different tissue and cellular lipid depots. *Endocrine reviews.* 2013;34(4):463-500.

55. Suchacki KJ, Cawthorn WP, Rosen CJ. Bone marrow adipose tissue: formation, function and regulation. *Current opinion in pharmacology.* 2016;28:50-6.

56. Hassan M, Latif N, Yacoub M. Adipose tissue: friend or foe? *Nature reviews Cardiology.* 2012;9(12):689-702.

57. Coelho M, Oliveira T, Fernandes R. Biochemistry of adipose tissue: an endocrine organ. *Archives of medical science*. 2013;9(2):191-200.

58. Wang F, Mullican SE, DiSpirito JR, Peed LC, Lazar MA. Lipoatrophy and severe metabolic disturbance in mice with fat-specific deletion of PPARγ. *Proceedings of the National Academy of Sciences*. 2013;110(46):18656-61.

59. Olefsky JM. Treatment of insulin resistance with peroxisome proliferator-activated receptor γ agonists. *The Journal of clinical investigation*. 2000;106(4):467-72.

60. Rosen ED, Sarraf P, Troy AE, Bradwin G, Moore K, Milstone DS, et al. PPAR γ is required for the differentiation of adipose tissue in vivo and in vitro. *Molecular cell*. 1999;4(4):611-7.

61. Siersbaek R, Nielsen R, Mandrup S. PPARγ in adipocyte differentiation and metabolism--novel insights from genome-wide studies. *FEBS letters*. 2010;584(15):3242-9.

62. Linhart HG, Ishimura-Oka K, DeMayo F, Kibe T, Repka D, Poindexter B, et al. C/EBPα is required for differentiation of white, but not brown, adipose tissue. *Proceedings of the National Academy of Sciences*. 2001;98(22):12532-7.

63. Wu Z, Rosen ED, Brun R, Hauser S, Adelmant G, Troy AE, et al. Cross-regulation of C/EBPα and PPARγ controls the transcriptional pathway of adipogenesis and insulin sensitivity. *Molecular cell*. 1999;3(2):151-8.

64. Christodoulides C, Lagathu C, Sethi JK, Vidal-Puig A. Adipogenesis and WNT signalling. *Trends in endocrinology and metabolism*. 2009;20(1):16-24.

65. Ross SE, Hemati N, Longo KA, Bennett CN, Lucas PC, Erickson RL, et al. Inhibition of adipogenesis by Wnt signaling. *Science*. 2000;289(5481):950-3.

66. Rutkowski JM, Stern JH, Scherer PE. The cell biology of fat expansion. *The Journal of cell biology*. 2015;208(5):501-12.

67. Cho YM, Kim DH, Kwak SN, Jeong SW, Kwon OJ. X-box binding protein 1 enhances adipogenic differentiation of 3T3-L1 cells through the downregulation of Wnt10b expression. *FEBS letters*. 2013;587(11):1644-9.

68. Gregor MF, Misch ES, Yang L, Hummasti S, Inouye KE, Lee AH, et al. The role of adipocyte XBP1 in metabolic regulation during lactation. *Cell reports*. 2013;3(5):1430-9.

69. Osborn O, Olefsky JM. The cellular and signaling networks linking the immune system and metabolism in disease. *Nature medicine.* 2012;18(3):363-74.

70. Sun K, Tordjman J, Clement K, Scherer PE. Fibrosis and adipose tissue dysfunction. *Cell metabolism.* 2013;18(4):470-7.

71. Krishnan J, Danzer C, Simka T, Ukropec J, Walter KM, Kumpf S, et al. Dietary obesity-associated Hif1α activation in adipocytes restricts fatty acid oxidation and energy expenditure via suppression of the Sirt2-NAD+ system. *Genes & development*. 2012;26(3):259-70.

72. Lee YS, Kim JW, Osborne O, Oh DY, Sasik R, Schenk S, et al. Increased adipocyte O2 consumption triggers HIF-1α, causing inflammation and insulin resistance in obesity. *Cell*. 2014;157(6):1339-52.

73. Sun K, Halberg N, Khan M, Magalang UJ, Scherer PE. Selective inhibition of hypoxia-inducible factor 1α ameliorates adipose tissue dysfunction. *Molecular and cellular biology*. 2013;33(5):904-17.

74. Hosogai N, Fukuhara A, Oshima K, Miyata Y, Tanaka S, Segawa K, et al. Adipose tissue hypoxia in obesity and its impact on adipocytokine dysregulation. *Diabetes*. 2007;56(4):901-11.

75. Ohashi K, Shibata R, Murohara T, Ouchi N. Role of anti-inflammatory adipokines in obesity-related diseases. *Trends in endocrinology and metabolism*. 2014;25(7):348-55.

76. Galic S, Oakhill JS, Steinberg GR. Adipose tissue as an endocrine organ. *Molecular and cellular endocrinology.* 2010;316(2):129-39.

77. Lord GM, Matarese G, Howard JK, Baker RJ, Bloom SR, Lechler RI. Leptin modulates the T-cell immune response and reverses starvation-induced immunosuppression. *Nature.* 1998;394:897-901.

78. Verma S, Li SH, Wang CH, Fedak PW, Li RK, Weisel RD, et al. Resistin promotes endothelial cell activation: further evidence of adipokine-endothelial interaction. *Circulation.* 2003;108(6):736-40.

79. Ouchi N, Parker JL, Lugus JJ, Walsh K. Adipokines in inflammation and metabolic disease. *Nature reviews Immunology.* 2011;11(2):85-97.

80. Dodson MV, Mir PS, Hausman GJ, Guan LL, Du M, Jiang Z, et al. Obesity, metabolic syndrome, and adipocytes. *Journal of lipids.* 2011;2011:721686.

81. Mraz M, Haluzik M. The role of adipose tissue immune cells in obesity and low-grade inflammation. *The Journal of endocrinology.* 2014;222(3):R113-27.

82. Lolmede K, Duffaut C, Zakaroff-Girard A, Bouloumie A. Immune cells in adipose tissue: key players in metabolic disorders. *Diabetes & metabolism*. 2011;37(4):283-90.

83. Gordon S, Pluddemann A. Tissue macrophages: heterogeneity and functions. *BMC biology.* 2017;15(1):53.

84. Castoldi A, Naffah de Souza C, Camara NO, Moraes-Vieira PM. The Macrophage Switch in Obesity Development. *Frontiers in immunology.* 2015;6:637.

85. Weisberg SP, McCann D, Desai M, Rosenbaum M, Leibel RL, Ferrante AW, Jr. Obesity is associated with macrophage accumulation in adipose tissue. *The Journal of clinical investigation.* 2003;112(12):1796-808.

86. Lumeng CN, Deyoung SM, Bodzin JL, Saltiel AR. Increased inflammatory properties of adipose tissue macrophages recruited during diet-induced obesity. *Diabetes.* 2007;56(1):16-23.

87. Neels JG, Olefsky JM. Inflamed fat: what starts the fire? *The Journal of clinical investigation.* 2006;116(1):33-5.

88. Lumeng CN, Bodzin JL, Saltiel AR. Obesity induces a phenotypic switch in adipose tissue macrophage polarization. *The Journal of clinical investigation.* 2007;117(1):175-84.

89. Bassaganya-Riera J, Misyak S, Guri AJ, Hontecillas R. PPARγ is highly expressed in F4/80(hi) adipose tissue macrophages and dampens adipose-tissue inflammation. *Cellular immunology.* 2009;258(2):138-46.

90. Xu H, Barnes GT, Yang Q, Tan G, Yang D, Chou CJ, et al. Chronic inflammation in fat plays a crucial role in the development of obesity-related insulin resistance. *The Journal of clinical investigation.* 2003;112(12):1821-30.

91. Kuroda M, Sakaue H. Adipocyte Death and Chronic Inflammation in Obesity. *The journal of medical investigation*. 2017;64(3.4):193-6.

92. Grant RW, Dixit VD. Adipose tissue as an immunological organ. *Obesity*. 2015;23(3):512-8.

93. Cinti S, Mitchell G, Barbatelli G, Murano I, Ceresi E, Faloia E, et al. Adipocyte death defines macrophage localization and function in adipose tissue of obese mice and humans. *Journal of lipid research.* 2005;46(11):2347-55.

94. Ferrante AW, Jr. The immune cells in adipose tissue. *Diabetes, obesity & metabolism.* 2013;15 Suppl 3:34-8.

95. Wu D, Molofsky AB, Liang HE, Ricardo-Gonzalez RR, Jouihan HA, Bando JK, et al. Eosinophils sustain adipose alternatively activated macrophages associated with glucose homeostasis. *Science*. 2011;332(6026):243-7.

96. Liu J, Divoux A, Sun J, Zhang J, Clement K, Glickman JN, et al. Genetic deficiency and pharmacological stabilization of mast cells reduce diet-induced obesity and diabetes in mice. *Nature medicine.* 2009;15(8):940-5.

97. Raphael I, Nalawade S, Eagar TN, Forsthuber TG. T cell subsets and their signature cytokines in autoimmune and inflammatory diseases. *Cytokine*. 2015;74(1):5-17.

98. Wu H, Ghosh S, Perrard XD, Feng L, Garcia GE, Perrard JL, et al. T-cell accumulation and regulated on activation, normal T cell expressed and secreted upregulation in adipose tissue in obesity. *Circulation*. 2007;115(8):1029-38.

99. Duffaut C, Zakaroff-Girard A, Bourlier V, Decaunes P, Maumus M, Chiotasso P, et al. Interplay between human adipocytes and T lymphocytes in obesity: CCL20 as an adipochemokine and T lymphocytes as lipogenic modulators. *Arteriosclerosis, thrombosis, and vascular biology*. 2009;29(10):1608-14.

100. Feuerer M, Hill JA, Mathis D, Benoist C. Foxp3+ regulatory T cells: differentiation, specification, subphenotypes. *Nature immunology*. 2009;10(7):689-95.

101. Cipolletta D, Feuerer M, Li A, Kamei N, Lee J, Shoelson S, et al. PPARγ is a major driver of the accumulation and phenotype of adipose-tissue Treg cells. *Nature*. 2012;486(7404):549-53.

102. Feuerer M, Herrero L, Cipolletta D, Naaz A, Wong J, Nayer A, et al. Lean, but not obese, fat is enriched for a unique population of regulatory T cells that affect metabolic parameters. *Nature medicine*. 2009;15(8):930-9.

103. Poggi M, Jager J, Paulmyer-Lacroix O, Peiretti F, Gremeaux T, Verdier M, et al. The inflammatory receptor CD40 is expressed on human adipocytes: contribution to crosstalk between lymphocytes and adipocytes. *Diabetologia*. 2009;52(6):1152-63.

104. Rocha VZ, Folco EJ, Sukhova G, Shimizu K, Gotsman I, Vernon AH, et al. Interferon-γ, a Th1 cytokine, regulates fat inflammation: a role for adaptive immunity in obesity. *Circulation research*. 2008;103(5):467-76.

105. Winer S, Chan Y, Paltser G, Truong D, Tsui H, Bahrami J, et al. Normalization of obesity-associated insulin resistance through immunotherapy. *Nature medicine*. 2009;15(8):921-9.

106. Han SJ, Glatman Zaretsky A, Andrade-Oliveira V, Collins N, Dzutsev A, Shaik J, et al. White Adipose Tissue Is a Reservoir for Memory T Cells and Promotes Protective Memory Responses to Infection. *Immunity.* 2017;47(6):1154-68.e6.

107. Winer DA, Winer S, Shen L, Wadia PP, Yantha J, Paltser G, et al. B cells promote insulin resistance through modulation of T cells and production of pathogenic IgG antibodies. *Nature medicine*. 2011;17(5):610-7.

108. DeFuria J, Belkina AC, Jagannathan-Bogdan M, Snyder-Cappione J, Carr JD, Nersesova YR, et al. B cells promote inflammation in obesity and type 2 diabetes through regulation of T-cell function and an inflammatory cytokine profile. *Proceedings of the National Academy of Sciences*. 2013;110(13):5133-8.

109. Duffaut C, Galitzky J, Lafontan M, Bouloumie A. Unexpected trafficking of immune cells within the adipose tissue during the onset of obesity. *Biochemical and biophysical research communications.* 2009;384(4):482-5.

110. Moro K, Yamada T, Tanabe M, Takeuchi T, Ikawa T, Kawamoto H, et al. Innate production of T_H2 cytokines by adipose tissue-associated c-Kit$^+$Sca-1$^+$ lymphoid cells. *Nature.* 2010;463(7280):540-4.

111. Benezech C, Luu NT, Walker JA, Kruglov AA, Loo Y, Nakamura K, et al. Inflammation-induced formation of fat-associated lymphoid clusters. *Nature immunology.* 2015;16(8):819-28.

112. Cruz-Migoni S, Caamano J. Fat-Associated Lymphoid Clusters in Inflammation and Immunity. *Frontiers in immunology.* 2016;7:612.

113. Rangel-Moreno J, Moyron-Quiroz JE, Carragher DM, Kusser K, Hartson L, Moquin A, et al. Omental milky spots develop in the absence of lymphoid tissue-inducer cells and support B and T cell responses to peritoneal antigens. *Immunity.* 2009;30(5):731-43.

114. Morris DL, Cho KW, Delproposto JL, Oatmen KE, Geletka LM, Martinez-Santibanez G, et al. Adipose tissue macrophages function as antigen-presenting cells and regulate adipose tissue CD4+ T cells in mice. *Diabetes.* 2013;62(8):2762-72.

115. Steinman RM, Cohn ZA. Identification of a novel cell type in peripheral lymphoid organs of mice. I. Morphology, quantitation, tissue distribution. *The journal of experimental medicine*. 1973;137:1142-62.

116. Steinman RM, Hawiger D, Nussenzweig MC. Tolerogenic dendritic cells. *Annual review of immunology*. 2003;21:685-711.

117. Maldonado RA, von Andrian UH. How tolerogenic dendritic cells induce regulatory T cells. *Advances in immunology.* 2010;108:111-65.

118. Merad M, Sathe P, Helft J, Miller J, Mortha A. The dendritic cell lineage: ontogeny and function of dendritic cells and their subsets in the steady state and the inflamed setting. *Annual review of immunology*. 2013;31:563-604.

119. Liu K, Nussenzweig MC. Origin and development of dendritic cells. *Immunology review*. 2010;234(1):45-54.

120. Cisse B, Caton ML, Lehner M, Maeda T, Scheu S, Locksley R, et al. Transcription factor E2-2 is an essential and specific regulator of plasmacytoid dendritic cell development. *Cell.* 2008;135(1):37-48.

121. Reizis B, Bunin A, Ghosh HS, Lewis KL, Sisirak V. Plasmacytoid dendritic cells: recent progress and open questions. *Annual review of immunology*. 2011;29:163-83.

122. Villani AC, Satija R, Reynolds G, Sarkizova S, Shekhar K, Fletcher J, et al. Single-cell RNA-seq reveals new types of human blood dendritic cells, monocytes, and progenitors. *Science*. 2017;356(6335).

123. Siegal FP, Kadowaki N, Shodell M, Fitzgerald-Bocarsly PA, Shah K, Ho S, et al. The nature of the principal type 1 interferon-producing cells in human blood. *Science*. 1999;284:1835-7.

124. Metlay JP, Witmer-Pack MD, Agger R, Crowley MT, Lawless D, Steinman RM. The distinct leukocyte integrins of mouse spleen dendritic cells as identified with new hamster monoclonal antibodies. *Journal of experimental medicine*. 1990;171:1753-71.

125. Guilliams M, Ginhoux F, Jakubzick C, Naik SH, Onai N, Schraml BU, et al. Dendritic cells, monocytes and macrophages: a unified nomenclature based on ontogeny. *Nature reviews Immunology*. 2014;14(8):571-8.

126. Durai V, Murphy KM. Functions of Murine Dendritic Cells. *Immunity*. 2016;45(4):719-36.

127. den Haan JM, Lehar SM, Bevan MJ. $CD8^+$ but not $CD8^-$ dendritic cells cross-prime cytotoxic T cells in vivo. *Journal of experimental medicine*. 2000;192:1685-96.

128. Mashayekhi M, Sandau MM, Dunay IR, Frickel EM, Khan A, Goldszmid RS, et al. CD8α(+) dendritic cells are the critical source of interleukin-12 that controls acute infection by Toxoplasma gondii tachyzoites. *Immunity*. 2011;35(2):249-59.

129. Askenase MH, Han SJ, Byrd AL, Morais da Fonseca D, Bouladoux N, Wilhelm C, et al. Bone-Marrow-Resident NK Cells Prime Monocytes for Regulatory Function during Infection. *Immunity*. 2015;42(6):1130-42.

130. Schlitzer A, McGovern N, Teo P, Zelante T, Atarashi K, Low D, et al. IRF4 transcription factor-dependent CD11b+ dendritic cells in human and mouse control mucosal IL-17 cytokine responses. *Immunity*. 2013;38(5):970-83.

131. Satpathy AT, Briseno CG, Lee JS, Ng D, Manieri NA, Kc W, et al. Notch2-dependent classical dendritic cells orchestrate intestinal immunity to attaching-and-effacing bacterial pathogens. *Nature immunology*. 2013;14(9):937-48.

132. Patsouris D, Li PP, Thapar D, Chapman J, Olefsky JM, Neels JG. Ablation of CD11c-positive cells normalizes insulin sensitivity in obese insulin resistant animals. *Cell metabolism*. 2008;8(4):301-9.

133. Stefanovic-Racic M, Yang X, Turner MS, Mantell BS, Stolz DB, Sumpter TL, et al. Dendritic cells promote macrophage infiltration and comprise a substantial proportion of obesity-associated increases in CD11c+ cells in adipose tissue and liver. *Diabetes*. 2012;61(9):2330-9.

134. Bertola A, Ciucci T, Rousseau D, Bourlier V, Duffaut C, Bonnafous S, et al. Identification of adipose tissue dendritic cells correlated with obesity-associated insulin-resistance and inducing Th17 responses in mice and patients. *Diabetes*. 2012;61(9):2238-47.

135. Chen Y, Tian J, Tian X, Tang X, Rui K, Tong J, et al. Adipose tissue dendritic cells enhances inflammation by prompting the generation of Th17 cells. *PloS one*. 2014;9(3):e92450.

136. Pamir N, Liu NC, Irwin A, Becker L, Peng Y, Ronsein GE, et al. Granulocyte/Macrophage Colony-stimulating Factor-dependent Dendritic Cells Restrain Lean Adipose Tissue Expansion. *The Journal of biological chemistry*. 2015;290(23):14656-67.

137. Cho KW, Zamarron BF, Muir LA, Singer K, Porsche CE, DelProposto JB, et al. Adipose Tissue Dendritic Cells Are Independent Contributors to Obesity-Induced Inflammation and Insulin Resistance. *Journal of immunology*. 2016;197(9):3650-61.

138. Kuan EL, Ivanov S, Bridenbaugh EA, Victora G, Wang W, Childs EW, et al. Collecting lymphatic vessel permeability facilitates adipose tissue inflammation and distribution of antigen to lymph node-homing adipose tissue dendritic cells. *Journal of immunology*. 2015;194(11):5200-10.

139. Ivanov S, Scallan JP, Kim KW, Werth K, Johnson MW, Saunders BT, et al. CCR7 and IRF4-dependent dendritic cells regulate lymphatic collecting vessel permeability. *The Journal of clinical investigation*. 2016;126(4):1581-91.

140. Tran KV, Gealekman O, Frontini A, Zingaretti MC, Morroni M, Giordano A, et al. The vascular endothelium of the adipose tissue gives rise to both white and brown fat cells. *Cell metabolism*. 2012;15(2):222-9.

141. Hong KY, Bae H, Park I, Park DY, Kim KH, Kubota Y, et al. Perilipin+ embryonic preadipocytes actively proliferate along growing vasculatures for adipose expansion. *Development*. 2015;142(15):2623-32.

142. Ushach I, Zlotnik A. Biological role of granulocyte macrophage colony-stimulating factor (GM-CSF) and macrophage colony-stimulating factor (M-CSF) on cells of the myeloid lineage. *Journal of leukocyte biology*. 2016;100(3):481-9.

143. Sha H, Yang L, Liu M, Xia S, Liu Y, Liu F, et al. Adipocyte spliced form of X-box-binding protein 1 promotes adiponectin multimerization and systemic glucose homeostasis. *Diabetes*. 2014;63(3):867-79.

144. Cubillos-Ruiz JR, Silberman PC, Rutkowski MR, Chopra S, Perales-Puchalt A, Song M, et al. ER Stress Sensor XBP1 Controls Anti-tumor Immunity by Disrupting Dendritic Cell Homeostasis. *Cell*. 2015;161(7):1527-38.

145. Jantsch J, Chakravortty D, Turza N, Prechtel AT, Buchholz B, Gerlach RG, et al. Hypoxia and hypoxia-inducible factor-1α modulate lipopolysaccharide-induced dendritic cell activation and function. *Journal of immunology*. 2008;180(7):4697-705.

146. Hammami A, Charpentier T, Smans M, Stager S. IRF-5-Mediated Inflammation Limits CD8+ T Cell Expansion by Inducing HIF-1α and Impairing Dendritic Cell Functions during Leishmania Infection. *PLoS pathogens*. 2015;11(6):e1004938.

147. Kohler T, Reizis B, Johnson RS, Weighardt H, Forster I. Influence of hypoxia-inducible factor 1α on dendritic cell differentiation and migration. *European journal of immunology*. 2012;42(5):1226-36.

148. Pond CM. Physiological specialisation of adipose tissue. *Progress in lipid research*. 1999;38(3):225-48.

149. Mattacks CA, Pond CM. Interactions of noradrenalin and tumour necrosis factor-α, interleukin 4 and interleukin 6 in the control of lipolysis from adipocytes around lymph nodes. *Cytokine*. 1999;11(5):334-46.

150. Pond CM, Mattacks CA. The activation of the adipose tissue associated with lymph nodes during the early stages of an immune response. *Cytokine*. 2002;17(3):131-9.

151. Mattacks CA, Sadler D, Pond CM. The effects of dietary lipids on dendritic cells in perinodal adipose tissue during chronic mild inflammation. *The British journal of nutrition*. 2004;91(6):883-92.

152. Sadler D, Mattacks CA, Pond CM. Changes in adipocytes and dendritic cells in lymph node containing adipose depots during and after many weeks of mild inflammation. *Journal of anatomy*. 2005;207(6):769-81.

153. den Brok MH, Raaijmakers TK, Collado-Camps E, Adema GJ. Lipid Droplets as Immune Modulators in Myeloid Cells. *Trends in immunology*. 2018;39(5):380-92.

154. Ibrahim J, Nguyen AH, Rehman A, Ochi A, Jamal M, Graffeo CS, et al. Dendritic cell populations with different concentrations of lipid regulate tolerance and immunity in mouse and human liver. *Gastroenterology*. 2012;143(4):1061-72.

155. Herber DL, Cao W, Nefedova Y, Novitskiy SV, Nagaraj S, Tyurin VA, et al. Lipid accumulation and dendritic cell dysfunction in cancer. *Nature medicine*. 2010;16(8):880-6.

156. Ramakrishnan R, Tyurin VA, Veglia F, Condamine T, Amoscato A, Mohammadyani D, et al. Oxidized lipids block antigen cross-presentation by dendritic cells in cancer. *Journal of immunology*. 2014;192(6):2920-31.

157. Zhong J, Rao X, Deiuliis J, Braunstein Z, Narula V, Hazey J, et al. A potential role for dendritic cell/macrophage-expressing DPP4 in obesity-induced visceral inflammation. *Diabetes*. 2013;62(1):149-57.

158. Plubell DL, Fenton AM, Wilmarth PA, Bergstrom P, Zhao Y, Minnier J, et al. GM-CSF driven myeloid cells in adipose tissue link weight gain and insulin resistance via formation of 2-aminoadipate. *Scientific reports*. 2018;8(1):11485.

159. Seifarth CC, Hinkmann C, Hahn EG, Lohmann T, Harsch IA. Reduced frequency of peripheral dendritic cells in type 2 diabetes. *Experimental and clinical endocrinology & diabetes*. 2008;116(3):162-6.

160. Blank SE, Johnson EC, Weeks DK, Wysham CH. Circulating dendritic cell number and intracellular TNF-α production in women with type 2 diabetes. *Acta diabetologica.* 2012;49 Suppl 1:S25-32.

161. Musilli C, Paccosi S, Pala L, Gerlini G, Ledda F, Mugelli A, et al. Characterization of circulating and monocyte-derived dendritic cells in obese and diabetic patients. *Molecular immunology*. 2011;49(1-2):234-8.

162. Ferris ST, Carrero JA, Mohan JF, Calderon B, Murphy KM, Unanue ER. A minor subset of Batf3-dependent antigen-presenting cells in islets of Langerhans is essential for the development of autoimmune diabetes. *Immunity*. 2014;41(4):657-69.

163. Yin N, Xu J, Ginhoux F, Randolph GJ, Merad M, Ding Y, et al. Functional specialization of islet dendritic cell subsets. *Journal of immunology*. 2012;188(10):4921-30.

164. Komiya Y, Habas R. Wnt signal transduction pathways. *Organogenesis.* 2008;4(2):68-75.

165. Logan CY, Nusse R. The Wnt signaling pathway in development and disease. *Annual review of cell and developmental biology.* 2004;20:781-810.

166. Staal FJ, Luis TC, Tiemessen MM. WNT signalling in the immune system: WNT is spreading its wings. *Nature reviews immunology*. 2008;8(8):581-93.

167. Swafford D, Manicassamy S. Wnt signaling in dendritic cells: its role in regulation of immunity and tolerance. *Discovery medicine.* 2015;19(105):303-10.

168. Fuster JJ, Zuriaga MA, Ngo DT, Farb MG, Aprahamian T, Yamaguchi TP, et al. Noncanonical Wnt signaling promotes obesity-induced adipose tissue inflammation and metabolic dysfunction independent of adipose tissue expansion. *Diabetes.* 2015;64(4):1235-48.

169. Valenta T, Hausmann G, Basler K. The many faces and functions of β-catenin. *The EMBO journal.* 2012;31(12):2714-36.

170. MacDonald BT, Tamai K, He X. Wnt/β-catenin signaling: components, mechanisms, and diseases. *Developmental cell*. 2009;17(1):9-26.

171. Bennett CN, Ross SE, Longo KA, Bajnok L, Hemati N, Johnson KW, et al. Regulation of Wnt signaling during adipogenesis. *The Journal of biological chemistry.* 2002;277(34):30998-1004.

172. Welters HJ, Kulkarni RN. Wnt signaling: relevance to β-cell biology and diabetes. *Trends in endocrinology and metabolism*. 2008;19(10):349-55.

173. Kanazawa A, Tsukada S, Sekine A, Tsunoda T, Takahashi A, Kashiwagi A, et al. Association of the gene encoding wingless-type mammary tumor virus integration-site family member 5B (WNT5B) with type 2 diabetes. *American journal of human genetics*. 2004;75(5):832-43.

174. Salpea KD, Gable DR, Cooper JA, Stephens JW, Hurel SJ, Ireland HA, et al. The effect of WNT5B IVS3C>G on the susceptibility to type 2 diabetes in UK Caucasian subjects. *Nutrition, metabolism, and cardiovascular diseases*. 2009;19(2):140-5.

175. Grant SF, Thorleifsson G, Reynisdottir I, Benediktsson R, Manolescu A, Sainz J, et al. Variant of transcription factor 7-like 2 (TCF7L2) gene confers risk of type 2 diabetes. *Nature genetics*. 2006;38(3):320-3.

176. Wright WS, Longo KA, Dolinsky VW, Gerin I, Kang S, Bennett CN, et al. Wnt10b inhibits obesity in ob/ob and agouti mice. *Diabetes*. 2007;56(2):295-303.

177. Longo KA, Wright WS, Kang S, Gerin I, Chiang SH, Lucas PC, et al. Wnt10b inhibits development of white and brown adipose tissues. *The Journal of biological chemistry*. 2004;279(34):35503-9.

178. Suryawanshi A, Manoharan I, Hong Y, Swafford D, Majumdar T, Taketo MM, et al. Canonical wnt signaling in dendritic cells regulates Th1/Th17 responses and suppresses autoimmune neuroinflammation. *Journal of immunology*. 2015;194(7):3295-304.

179. Manoharan I, Hong Y, Suryawanshi A, Angus-Hill ML, Sun Z, Mellor AL, et al. TLR2-dependent activation of β-catenin pathway in dendritic cells induces regulatory responses and attenuates autoimmune inflammation. *Journal of immunology*. 2014;193(8):4203-13.

180. Oderup C, LaJevic M, Butcher EC. Canonical and noncanonical Wnt proteins program dendritic cell responses for tolerance. *Journal of immunology*. 2013;190(12):6126-34.

181. Valencia J, Hernandez-Lopez C, Martinez VG, Hidalgo L, Zapata AG, Vicente A, et al. Wnt5a skews dendritic cell differentiation to an unconventional phenotype with tolerogenic features. *Journal of immunology*. 2011;187(8):4129-39.

182. Jiang A, Bloom O, Ono S, Cui W, Unternaehrer J, Jiang S, et al. Disruption of E-cadherin-mediated adhesion induces a functionally distinct pathway of dendritic cell maturation. *Immunity*. 2007;27:610-24.

183. Qian C, Qian L, Yu Y, An H, Guo Z, Han Y, et al. Fas signal promotes the immunosuppressive function of regulatory dendritic cells via the ERK/β-catenin pathway. *The Journal of biological chemistry*. 2013;288(39):27825-35.

184. Vander Lugt B, Beck ZT, Fuhlbrigge RC, Hacohen N, Campbell JJ, Boes M. TGF-β suppresses β-catenin-dependent tolerogenic activation program in dendritic cells. *PloS one*. 2011;6(5):e20099.

185. Manicassamy S, Reizis B, Ravindran R, Nakaya H, Salazar-Gonzalez RM, Wang YC, et al. Activation of β-catenin in dendritic cells regulates immunity versus tolerance in the intestine. *Science*. 2010;329(5993):849-53.

186. Alves CH, Ober-Blobaum JL, Brouwers-Haspels I, Asmawidjaja PS, Mus AM, Razawy W, et al. Dendritic Cell-Specific Deletion of β-catenin Results in Fewer Regulatory T-Cells without Exacerbating Autoimmune Collagen-Induced Arthritis. *PloS one*. 2015;10(11):e0142972.

187. Harada N, Tamai Y, Ishikawa T, Sauer B, Takaku K, Oshima M, et al. Intestinal polyposis in mice with a dominant stable mutation of the β-catenin gene. *The EMBO journal*. 1999;18(21):5931-42.

188. R Core Team. R: A language and environment for statistical computing. Vienna, Austria 2016.

189. Ritchie ME, Phipson B, Wu D, Hu Y, Law CW, Shi W, et al. limma powers differential expression analyses for RNA-sequencing and microarray studies. *Nucleic acids research*. 2015;43(7):e47.

190. Galarraga M, Campion J, Munoz-Barrutia A, Boque N, Moreno H, Martinez JA, et al. Adiposoft: automated software for the analysis of white adipose tissue cellularity in histological sections. *Journal of lipid research*. 2012;53(12):2791-6.

191. Loschko J, Schreiber HA, Rieke GJ, Esterhazy D, Meredith MM, Pedicord VA, et al. Absence of MHC class II on cDCs results in microbial-dependent intestinal inflammation. *Journal of experimental medicine*. 2016;213(4):517-34.

192. Satpathy AT, Kc W, Albring JC, Edelson BT, Kretzer NM, Bhattacharya D, et al. Zbtb46 expression distinguishes classical dendritic cells and their committed progenitors from other immune lineages. *Journal of experimental medicine*. 2012;209(6):1135-52.

193. Macdougall CE, Wood EG, Loschko J, Scagliotti V, Cassidy FC, Robinson ME, et al. Visceral Adipose Tissue Immune Homeostasis Is Regulated by the Crosstalk between Adipocytes and Dendritic Cell Subsets. *Cell metabolism*. 2018;27(3):588-601.e4.

194. Coghlan MP, Culbert AA, Cross DA, Corcoran SL, Yates JW, Pearce NJ, et al. Selective small molecule inhibitors of glycogen synthase kinase-3 modulate glycogen metabolism and gene transcription. *Chemistry & biology*. 2000;7(10):793-803.

195. Corinti S, Albanesi C, la Sala A, Pastore S, Girolomoni G. Regulatory activity of autocrine IL-10 on dendritic cell functions. *Journal of immunology*. 2001;166:4312-8.

196. Christodoulides C, Scarda A, Granzotto M, Milan G, Dalla Nora E, Keogh J, et al. WNT10B mutations in human obesity. *Diabetologia*. 2006;49(4):678-84.

197. Heiseke AF, Faul AC, Lehr HA, Forster I, Schmid RM, Krug AB, et al. CCL17 promotes intestinal inflammation in mice and counteracts regulatory T cell-mediated protection from colitis. *Gastroenterology*. 2012;142(2):335-45.

198. Weber C, Meiler S, Doring Y, Koch M, Drechsler M, Megens RT, et al. CCL17-expressing dendritic cells drive atherosclerosis by restraining regulatory T cell homeostasis in mice. *Journal of clinical investigation*. 2011;121(7):2898-910.

199. Andrew DP, Ruffing N, Kim CH, Miao W, Heath H, Li Y, et al. C-C chemokine receptor 4 expression defines a major subset of circulating nonintestinal memory T cells of both Th1 and Th2 potential. *Journal of immunology*. 2001;166(1):103-11.

200. Kohlgruber AC, Gal-Oz ST, LaMarche NM, Shimazaki M, Duquette D, Nguyen HN, et al. γδ T cells producing interleukin-17A regulate adipose regulatory T cell homeostasis and thermogenesis. *Nature immunology*. 2018;19(5):464-74.

201. Schipper HS, Prakken B, Kalkhoven E, Boes M. Adipose tissue-resident immune cells: key players in immunometabolism. *Trends in endocrinology and metabolism*. 2012;23(8):407-15.

202. Cohen SB, Smith NL, McDougal C, Pepper M, Shah S, Yap GS, et al. β-catenin signaling drives differentiation and proinflammatory function of IRF8-dependent dendritic cells. *Journal of immunology*. 2015;194(1):210-22.

203. Kwon H, Pessin JE. Adipokines mediate inflammation and insulin resistance. *Frontiers in endocrinology*. 2013;4:71.

204. Arita Y, Kihara S, Ouchi N, Takahashi M, Maeda K, Miyagawa J, et al. Paradoxical decrease of an adipose-specific protein, adiponectin, in obesity. 1999. *Biochemical and biophysical research communications*. 2012;425(3):560-4.

205. Nigro E, Scudiero O, Monaco ML, Palmieri A, Mazzarella G, Costagliola C, et al. New insight into adiponectin role in obesity and obesity-related diseases. *BioMed research international*. 2014;2014:658913.

206. Fu C, Liang X, Cui W, Ober-Blobaum JL, Vazzana J, Shrikant PA, et al. β-catenin in dendritic cells exerts opposite functions in cross-priming and maintenance of CD8+ T cells through regulation of IL-10. *Proceedings of the National Academy of Sciences*. 2015;112(9):2823-8.

207. Donath MY, Shoelson SE. Type 2 diabetes as an inflammatory disease. *Nature reviews immunology*. 2011;11(2):98-107.

208. Linnemann AK, Baan M, Davis DB. Pancreatic β-cell proliferation in obesity. *Advances in nutrition*. 2014;5(3):278-88.

209. Mitchell RK, Mondragon A, Chen L, McGinty JA, French PM, Ferrer J, et al. Selective disruption of Tcf7l2 in the pancreatic β-cell impairs secretory function and lowers β-cell mass. *Human molecular genetics*. 2015;24(5):1390-9.

210. Maschio DA, Oliveira RB, Santos MR, Carvalho CP, Barbosa-Sampaio HC, Collares-Buzato CB. Activation of the Wnt/β-catenin pathway in pancreatic β-cells during the compensatory islet hyperplasia in prediabetic mice. *Biochemical and biophysical research communications*. 2016;478(4):1534-40.

211. Fujino T, Asaba H, Kang MJ, Ikeda Y, Sone H, Takada S, et al. Low-density lipoprotein receptor-related protein 5 (LRP5) is essential for normal cholesterol metabolism and glucose-induced insulin secretion. *Proceedings of the National Academy of Sciences*. 2003;100(1):229-34.

212. Schinner S, Ulgen F, Papewalis C, Schott M, Woelk A, Vidal-Puig A, et al. Regulation of insulin secretion, glucokinase gene transcription and β-cell proliferation by adipocyte-derived Wnt signalling molecules. *Diabetologia*. 2008;51(1):147-54.

213. Rebuffat SA, Oliveira JM, Altirriba J, Palau N, Garcia A, Esteban Y, et al. Downregulation of Sfrp5 promotes β-cell proliferation during obesity in the rat. *Diabetologia.* 2013;56(11):2446-55.

214. Rulifson IC, Karnik SK, Heiser PW, ten Berge D, Chen H, Gu X, et al. Wnt signaling regulates pancreatic β-cell proliferation. *Proceedings of the National Academy of Sciences*. 2007;104(15):6247-52.

215. Dor Y, Brown J, Martinez OI, Melton DA. Adult pancreatic β-cells are formed by self-duplication rather than stem-cell differentiation. *Nature*. 2004;429(6987):41-6.

216. Heller RS, Dichmann DS, Jensen J, Miller C, Wong G, Madsen OD, et al. Expression patterns of Wnts, Frizzleds, sFRPs, and misexpression in transgenic mice suggesting a role for Wnts in pancreas and foregut pattern formation. *Developmental dynamics*. 2002;225(3):260-70.

217. Buteau J, Foisy S, Joly E, Prentki M. Glucagon-like peptide 1 induces pancreatic β-cell proliferation via transactivation of the epidermal growth factor receptor. *Diabetes*. 2003;52(1):124-32.

218. Aly H, Rohatgi N, Marshall CA, Grossenheider TC, Miyoshi H, Stappenbeck TS, et al. A novel strategy to increase the proliferative potential of adult human β-cells while maintaining their differentiated phenotype. *PloS one*. 2013;8(6):e66131.

219. Kim HS, Lee MK. β-cell regeneration through the transdifferentiation of pancreatic cells: Pancreatic progenitor cells in the pancreas. *Journal of diabetes investigation*. 2016;7(3):286-96.

220. Wang H, Ren Y, Hu X, Ma M, Wang X, Liang H, et al. Effect of Wnt Signaling on the Differentiation of Islet β-cells from Adipose-Derived Stem Cells. *BioMed research international*. 2017;2017:2501578.

221. Heiser PW, Lau J, Taketo MM, Herrera PL, Hebrok M. Stabilization of β-catenin impacts pancreas growth. *Development*. 2006;133(10):2023-32.

222. Russell MA, Morgan NG. The impact of anti-inflammatory cytokines on the pancreatic β-cell. *Islets.* 2014;6(3):e950547.

223. Dirice E, Kahraman S, Jiang W, El Ouaamari A, De Jesus DF, Teo AK, et al. Soluble factors secreted by T cells promote β-cell proliferation. *Diabetes.* 2014;63(1):188-202.

224. Mukherjee R, Chaturvedi P, Qin HY, Singh B. $CD4^+CD25^+$ regulatory T cells generated in response to insulin B:9-23 peptide prevent adoptive transfer of diabetes by diabetogenic T cells. *Journal of autoimmunity*. 2003;21(3):221-37.

225. Kornete M, Sgouroudis E, Piccirillo CA. ICOS-dependent homeostasis and function of Foxp3+ regulatory T cells in islets of nonobese diabetic mice. *Journal of immunology*. 2012;188(3):1064-74.

226. Tarbell KV, Petit L, Zuo X, Toy P, Luo X, Mqadmi A, et al. Dendritic cell-expanded, islet-specific, $CD4^+$ $CD25^+$ $CD62L^+$ regulatory T cells restore normoglycemia in diabetic NOD mice. *Journal of experimental medicine*. 2007;204:191-201.

227. Heiser PW, Cano DA, Landsman L, Kim GE, Kench JG, Klimstra DS, et al. Stabilization of β-catenin induces pancreas tumor formation. *Gastroenterology*. 2008;135(4):1288-300.

228. Shimada K, Miyazaki T, Daida H. Adiponectin and atherosclerotic disease. *Clinica chimica acta*. 2004;344(1-2):1-12.

229. Kher N, Marsh JD. Pathobiology of atherosclerosis--a brief review. *Seminars in thrombosis and hemostasis*. 2004;30(6):665-72.

230. Libby P. Inflammation in atherosclerosis. *Nature*. 2002;420(6917):868-74.

231. Yu XH, Fu YC, Zhang DW, Yin K, Tang CK. Foam cells in atherosclerosis. *Clinica chimica acta*. 2013;424:245-52.

232. Libby P. Inflammation in atherosclerosis. *Arteriosclerosis, thrombosis, and vascular biology*. 2012;32(9):2045-51.

233. Singh RB, Mengi SA, Xu YJ, Arneja AS, Dhalla NS. Pathogenesis of atherosclerosis: A multifactorial process. *Experimental and clinical cardiology.* 2002;7(1):40-53.

234. Tse K, Tse H, Sidney J, Sette A, Ley K. T cells in atherosclerosis. *International immunology.* 2013;25(11):615-22.

235. Subramanian M, Tabas I. Dendritic cells in atherosclerosis. *Seminars in immunopathology*. 2014;36(1):93-102.

236. Meijer L, Flajolet M, Greengard P. Pharmacological inhibitors of glycogen synthase kinase 3. *Trends in pharmacological sciences.* 2004;25(9):471-80.

237. Wang Y, Krivtsov AV, Sinha AU, North TE, Goessling W, Feng Z, et al. The Wnt/β-catenin pathway is required for the development of leukemia stem cells in AML. *Science*. 2010;327(5973):1650-3.

238. Steinman RM. Dendritic cells and vaccines. *Proceedings (Baylor University Medical Centre)*. 2008;21(1):3-8.

239. Liu P, Yu YR, Spencer JA, Johnson AE, Vallanat CT, Fong AM, et al. CX3CR1 deficiency impairs dendritic cell accumulation in arterial intima and reduces atherosclerotic burden. *Arteriosclerosis, thrombosis and vascular biology*. 2008;28:243-50.

240. Bobryshev YV. Dendritic cells in atherosclerosis: current status of the problem and clinical relevance. *European heart journal*. 2005;26:1700-4.

241. Weber C, Zernecke A, Libby P. The multifaceted contributions of leukocyte subsets to atherosclerosis: lessons from mouse models. *Nature review immunology*. 2008;8(10):802-15.

242. Angeli V, Llodra J, Rong JX, Satoh K, Ishii S, Shimizu T, et al. Dyslipidemia associated with atherosclerotic disease systemically alters dendritic cell mobilization. *Immunity*. 2004;21(4):561-74.

243. Cawthorn WP, Scheller EL, Learman BS, Parlee SD, Simon BR, Mori H, et al. Bone marrow adipose tissue is an endocrine organ that contributes to increased circulating adiponectin during caloric restriction. *Cell metabolism*. 2014;20(2):368-75.

244. Mills KM, Szczerkowski JLA, Habib SJ. Wnt ligand presentation and reception: from the stem cell niche to tissue engineering. *Open biology*. 2017;7(8).

245. Fujii M, Inoguchi T, Batchuluun B, Sugiyama N, Kobayashi K, Sonoda N, et al. CTLA-4Ig immunotherapy of obesity-induced insulin resistance by manipulation of macrophage polarization in adipose tissues. *Biochemical and biophysical research communications*. 2013;438(1):103-9.

246. Arce L, Yokoyama NN, Waterman ML. Diversity of LEF/TCF action in development and disease. *Oncogene*. 2006;25(57):7492-504.

247. Hoppler S, Kavanagh CL. Wnt signalling: variety at the core. *Journal of cell science*. 2007;120(Pt 3):385-93.

248. Tian Q, Jin H, Cui Y, Guo C, Lu X. Regulation of Wnt gene expression. *Development, growth & differentiation*. 2005;47(5):273-81.

249. Clevers H, Nusse R. Wnt/β-catenin signaling and disease. *Cell.* 2012;149(6):1192-205.

250. Rabelo Fde S, da Mota LM, Lima RA, Lima FA, Barra GB, de Carvalho JF, et al. The Wnt signaling pathway and rheumatoid arthritis. *Autoimmunity reviews*. 2010;9(4):207-10.

251. Gudjonsson JE, Johnston A, Stoll SW, Riblett MB, Xing X, Kochkodan JJ, et al. Evidence for altered Wnt signaling in psoriatic skin. *The Journal of investigative dermatology*. 2010;130(7):1849-59.

252. Marchetti B, Pluchino S. Wnt your brain be inflamed? Yes, it Wnt! *Trends in molecular medicine.* 2013;19(3):144-56.

253. Hughes KR, Sablitzky F, Mahida YR. Expression profiling of Wnt family of genes in normal and inflammatory bowel disease primary human intestinal myofibroblasts and normal human colonic crypt epithelial cells. *Inflammatory bowel diseases*. 2011;17(1):213-20.

254. Lee SH, Demeterco C, Geron I, Abrahamsson A, Levine F, Itkin-Ansari P. Islet specific Wnt activation in human type II diabetes. *Experimental diabetes research.* 2008;2008:728763.

255. Bowen A, Kos K, Whatmore J, Richardson S, Welters HJ. Wnt4 antagonises Wnt3a mediated increases in growth and glucose stimulated insulin secretion in the pancreatic β-cell line, INS-1. *Biochemical and biophysical research communications.* 2016;479(4):793-9.

256. Kozinski K, Jazurek M, Dobrzyn P, Janikiewicz J, Kolczynska K, Gajda A, et al. Adipose- and muscle-derived Wnts trigger pancreatic β-cell adaptation to systemic insulin resistance. *Scientific reports.* 2016;6:31553.

257. Krutzfeldt J, Stoffel M. Regulation of wingless-type MMTV integration site family (WNT) signalling in pancreatic islets from wild-type and obese mice. *Diabetologia.* 2010;53(1):123-7.

258. Malodobra-Mazur M, Dziewulska A, Kozinski K, Dobrzyn P, Kolczynska K, Janikiewicz J, et al. Stearoyl-CoA desaturase regulates inflammatory gene expression by changing DNA methylation level in 3T3 adipocytes. *The international journal of biochemistry & cell biology*. 2014;55:40-50.

259. Weir GC, Laybutt DR, Kaneto H, Bonner-Weir S, Sharma A. β-cell adaptation and decompensation during the progression of diabetes. *Diabetes*. 2001;50 Suppl 1:S154-9.

260. Alejandro EU, Gregg B, Blandino-Rosano M, Cras-Meneur C, Bernal-Mizrachi E. Natural history of β-cell adaptation and failure in type 2 diabetes. *Molecular aspects of medicine*. 2015;42:19-41.

261. Mill C, George SJ. Wnt signalling in smooth muscle cells and its role in cardiovascular disorders. *Cardiovascular research.* 2012;95(2):233-40.

262. Chen P, Liu X, Sun Y, Zhou P, Wang Y, Zhang Y. Dendritic cell targeted vaccines: Recent progresses and challenges. *Human vaccines & immunotherapeutics*. 2016;12(3):612-22.

263. Choi JH, Banks AS, Estall JL, Kajimura S, Bostrom P, Laznik D, et al. Anti-diabetic drugs inhibit obesity-linked phosphorylation of PPARγ by Cdk5. *Nature.* 2010;466(7305):451-6.

264. Cipolletta D, Cohen P, Spiegelman BM, Benoist C, Mathis D. Appearance and disappearance of the mRNA signature characteristic of Treg cells in visceral adipose tissue: age, diet, and PPARγ effects. *Proceedings of the National Academy of Sciences*. 2015;112(2):482-7.

265. Macotela Y, Boucher J, Tran TT, Kahn CR. Sex and depot differences in adipocyte insulin sensitivity and glucose metabolism. *Diabetes.* 2009;58(4):803-12.